



HAL
open science

Functional reorganization of the yeast genome during the cell cycle

Luciana Lazar-Stefanita

► **To cite this version:**

Luciana Lazar-Stefanita. Functional reorganization of the yeast genome during the cell cycle. Genetics. Université Pierre et Marie Curie - Paris VI, 2017. English. NNT : 2017PA066400 . tel-01756973

HAL Id: tel-01756973

<https://theses.hal.science/tel-01756973>

Submitted on 3 Apr 2018

HAL is a multi-disciplinary open access archive for the deposit and dissemination of scientific research documents, whether they are published or not. The documents may come from teaching and research institutions in France or abroad, or from public or private research centers.

L'archive ouverte pluridisciplinaire **HAL**, est destinée au dépôt et à la diffusion de documents scientifiques de niveau recherche, publiés ou non, émanant des établissements d'enseignement et de recherche français ou étrangers, des laboratoires publics ou privés.

Sorbonne Universités – Pierre et Marie Curie
Ecole doctorale Complexité du Vivant

Functional reorganization of the yeast genome during the cell cycle

Ph.D. thesis presented on 26 September 2017 by:

Luciana Lazar-Stefanita

Jury composition:

Frederic Devaux	President
Armelle Lengronne	Rapporteur
Olivier Gadai	Rapporteur
Marie-Noelle Prioleau	Examiner
Stephane Marcand	Examiner
Romain Koszul	Ph.D. Director

Acknowledgments

Firstly, I would like to thank all the readers of this PhD manuscript for their patience, advice and support. I am particularly grateful to my supervisor, Romain, for the opportunity to work on such a challenging and fascinating topic and for all his patience and understanding whilst I slowly mastered the many methods in this work.

It has been a unique and particularly rich learning experience. Above all, the freedom and the guidance I received during the past four years has taught me autonomy and confidence, and has hopefully made me a better person/scientist.

It has not always been a smooth path and I could have not made it without the help of many exceptional people. In particular, I would like to thank Julien Mozziconacci for co-supervising part of this work, which would also not have been possible without the contributions of Vittore and Guillaume. I also wish to thank Angela Taddei and Antoine Hocher for motivating and productive collaborations during this PhD.

A big thank you to all the members of the RSG lab (past and present), for their motivation and fruitful scientific and non-scientific discussions, usually accompanied by long coffee breaks. I wish to thank Heloise for sharing her wisdom on budding yeast and for guiding me through many troubleshooting sessions. Thank you Charlie and Aurèle for the invaluable help during the drafting of this manuscript. I also thank Axel for the assiduous weekend discussions on condensins, Martial for being the Swiss army man of the lab, Lyam for (how many?) croissants, the “minion” Théo and Agnes for buying us all of the fanciest lab tools .

Among all of the many amazing people in Pasteur, I wish to thank Cosmin Saveanu, for his patience and precious advice during my first internship and for directing me towards Romain’s lab.

Finally, thank you *Saccharomyces cerevisiae* for teaching me more about life.

Grazie Matteo per essere una roccaforte nella mia esistenza.

Va multumesc parinti pentru toate sacrificiile care le-ati facut pentru mine. Iti multumesc tata pentru toti kilometrii pe jos, iti multumesc mama pentru bunul sfat. Va multumesc pentru incredere.

Dedico questo manoscritto a mia sorella Cristiana.

Table of Contents

Table of figures.....	7
Abstract.....	9
1. Introduction.....	13
1.1 Investigating the eukaryotic cell cycle	13
1.1.1 Cytogenetic studies.....	13
1.1.2 Genomic studies.....	14
1.1.3 Yeasts as convenient model organisms	19
1.1.4 Yeast genetics.....	19
1.1.4.1 Identification of cell-division cycle (<i>cdc</i>) genes.....	20
1.1.4.2 Cell-cycle control system.....	22
1.1.4.3 Checkpoints.....	22
1.1.5 Cell cycle synchronization methods in <i>S. cerevisiae</i>	24
1.1.5.1 Genetic synchronization	24
1.1.5.2 Chemical synchronization.....	26
1.1.5.3 Mechanical synchronization	26
1.2 Investigate genome organization in eukaryotes.....	27
1.2.1 Imaging approaches	27
1.2.2 Multiscale genome-wide approaches	31
1.3 Integrating genome organization and cell cycle in <i>S. cerevisiae</i>.....	34
1.3.1 Quiescent (G0) state.....	37
1.3.2 Chromosome replication during S phase.....	38
1.3.2.1 Spatial-temporal organization of the replication program	40
1.3.2.2 DNA damage response at replication forks.....	43
1.3.2.3 Sister chromatid cohesion during replication.....	46
1.3.3 Chromosome segregation during M phase	49
1.3.3.1 Mitotic entry: spindle assembly and pericentromeric chromatin.....	49
1.3.3.2 Metaphase to anaphase transition	53
1.3.3.3 Mitotic exit: early to late anaphase	55
1.3.3.4 Mitotic exit: rDNA condensation and segregation in anaphase.....	57
2. Results	61
2.1 Chromosome dynamics during the cell cycle.....	63
2.2 Organization and maintenance of silenced chromatin.....	95

2.3 Investigating the influence of genome architecture and dynamics on genomic stability during replication in <i>S. cerevisiae</i>	121
3. Conclusion and discussion	149
4. Bibliography	157

Table of figures

Chapter 1

Figure 1 Illustration of mitotic cell division of salamander embryo.	15
Figure 2 Schematic representation of the cell cycle.	17
Figure 3 Cell cycle progression in unicellular yeast microorganisms.	21
Figure 4 View on the cell-cycle control system.	23
Figure 5 Cell cycle analysis of <i>S. cerevisiae</i> by flow cytometry.	25
Figure 6 Chromosome territories (CTs) by <i>in situ</i> hybridization.	28
Figure 7 Folding of the DNA fibre into a chromosome.	30
Figure 8 Schematic representation of the Chromosome Conformation Capture.	32
Figure 9 Rabl-like organization of <i>S. cerevisiae</i> 's chromosomes.	35
Figure 10 Assembly of the pre-replication and pre-initiation complexes.	39
Figure 11 Origin firing and replication profile.	41
Figure 12 Mechanisms of replication fork restart.	45
Figure 13 Architecture of cohesin and condensin complexes.	47
Figure 14 Bioriented attachment of mitotic chromosomes.	50
Figure 15 A spring of pericentromeric chromatin in metaphase.	52
Figure 16 Chromosome segregation occurs at metaphase to anaphases transition.	54
Figure 17 Temporal and spatial regulation of mitotic exit.	56
Figure 18 Cdc14 is required for rDNA segregation in late anaphase.	58
Figure 19 Condensin is required for rDNA segregation in late anaphase.	60

Chapter 2.1 Article.

Chapter 2.2

Figure 1 Structure of yeast telomeres.	98
Figure 2 Telomeres: from no cluster to hypercluster.	100
Figure 3 Telomere clusters are Sir3 dependent.	103
Figure 4 Telomere-proximal <i>FLO</i> genes interact independently of Sir3.	104
Figure 5 Genomic structural differences in metabolic different cells.	106
Figure 6 Sir3 binds and spreads in the telomere's proximity.	108
Figure 7 Structural differences between silenced and non-silenced hyperclusters.	109
Figure 8 Reorganization of telomere hyperclusters in G2/M arrested cells.	112
Figure 9 Contacts between telomere-distal Sir3 binding sites.	115
Figure 10 Dynamics of a telomere-distal Sir3 binding site.	116

Chapter 2.3

Figure 1 Spatial-temporal organization of the DNA replication program.	125
Figure 2 Replication fork block (RFB) by <i>Ter</i> -Tus system.	130
Figure 3 Bidirectional <i>Ter</i> -Tus replication block is persistent.	131
Figure 4 Bidirectional <i>Ter</i> -Tus block induces fork regression and resection.	134
Figure 5 Replication pause arises after the activation of the origin.	136
Figure 6 Detecting rearrangements at multiple RFBs.	138
Figure 7 High-throughput method to detect rearrangements at multiple RFBs.	140

Chapter 3

Figure 1 An interplay between condensins and topoisomerase 2 in anaphase.	151
Figure 2 The formation of a mega-sized loop.	153

Abstract

Decades of studies have shown that the structure and organization of chromatin is tightly linked to DNA related metabolic processes, through the dynamic regulation of a myriad of molecular factors. The proper structuration of chromosomes is notably important to ensure the maintenance of DNA integrity during cell cycle progression. Using the model *Saccharomyces cerevisiae*, the aim of my PhD project was to characterize the extent that chromatin reorganization during the cell cycle may influence chromosome stability. To do so, we first generated a comprehensive genome-wide study of the reorganization of budding yeast's chromosomes during an entire cell cycle. This work, besides recapitulating and/or generalizing expected chromosomal features of the replication and mitotic stages, led to the characterization of peculiar chromosome structures such as a DNA loop bridging the rDNA and the centromere clusters. The role of structural maintenance of chromosomes (SMC) complexes and of microtubules were also quantified, both globally and locally.

A second part of my PhD work focused on describing features of chromatin organization in cells that have exited the proliferative cell cycle and entered into quiescence. Using Hi-C, we characterized the dense status of silenced heterochromatin at specific loci, such as telomeres, in relation to the silent information regulator (SIR). We found that the spreading-mediated silencing activity of Sir3 is a key component in the establishment of the heterochromatic status.

Finally, we tried to achieve a better understanding of the functional interplay between chromosome stability and the 3D genome architecture during replication. The bacterial replication termination (*Tus/Ter*) system was introduced at various sites in the *S. cerevisiae* genome. We then used 2D gel electrophoresis and genome-wide approaches to investigate potential chromosomal instability introduced by replication pausing at *Ter*. Overall, these results point at a striking plasticity and adaptability of replication structures to different stresses. Future work aims to map replication-dependent chromosomal rearrangements on the genomic-scale.

Living things were generated by water being evaporated by the sun.

Humans, in the beginning, were similar to another animal, namely to fish.

Anaximenes 585 – 528 BC

1. Introduction

Life on Earth is amazingly complex and diverse. Yet, this diversity is built upon the same essential molecules, the ubiquitous nucleic acids DNA and RNA, as the propagation of all living organisms from generation to generation requires the proper transmission of the genetic information encoded in the DNA molecule. This is accomplished through the duplication of the genetic material and its segregation into daughter cells during the cell division process. The succession of DNA-related events, taking place during cell division, are evolutionary conserved and present important similarities between single-celled and multicellular organisms.

In the following sections, I will provide an historical perspective and a brief overview of the general principles underlying the series of events that accompany the duplication and segregation of the DNA material during the cell cycle.

1.1 Investigating the eukaryotic cell cycle

One can argue that the discovery of cellular division marked the birth of cell cycle studies (Nurse, 2000). This research involved the joint efforts of scientists from different fields, such as Cytology, Embryology, Physics, Biochemistry and Genetics, for more than a century. As typical of scientific progress, the development of new methods has accompanied this exploration, while research and comparisons between different organisms has been key in the discovery of the regulatory mechanisms involved in these processes.

1.1.1 Cytogenetic studies

In 1838, approximately two centuries after Robert Hook first description of the cell in 1665, Theodor Schwann and Matthias Schleiden formulated the cell theory. Based on their observations of plant and animal tissues, it postulated that cells are the basic units of life. The proposition that cells appear and propagate through divisions was mostly promoted later by Robert Remak, Albert Kolliker and formally formulated by Rudolph Virchow in 1855 with the powerful dictum, *Omnis cellula e cellula*: "All cells only arise from pre-existing cells". In 1880, Walther Flemming, a pioneer of cytogenetics, identified the chromatin structure in the nucleus from its peculiar response and absorption to basophilic dye exposure. While investigating cell division in salamander cells, he was able to associate chromatin to the episodic presence of threadlike structures in some of

the cells, which were later dubbed chromosomes. He suggested that chromosomes were related to chromatin, and called mitosis their segregation into daughter cell during the cell division, from the Greek word for thread (Figure 1) (Flemming, 1882).

Improvements in microscopy techniques kept bringing new insights into the changes occurring to chromosomes during mitosis. In 1885, the anatomist Carl Rabl found that, in salamander epithelial cells, chromosomes were constant in number and occurred in similar arrangements before and after division. He proposed that chromosomes were permanent entities, whose centromeres and telomeres were located at opposite sides of the nucleus, an organization called "Rabl" today (RABL, 1885). A few years later Theodor Boveri observed chromosome splitting (e.g. the separation of sister chromatids) during the maturation of the fertilized sea urchin egg. In 1902, he described the detrimental effect of the unequal segregation of chromosomes in these cells, suggesting that missegregation could result in tumours and birth defects (Boveri, 1902). Shortly after, Walter Sutton (1903) and Boveri (1904) presented the idea that chromosomes may function as hereditary vehicles.

Remarkably, Boveri was also the first to describe the mitotic spindle, as an astral array of filaments extending between the chromosomes (Boveri, 1907). Continuing improvements in fixation protocols, microscopy, and later in the development of electron microscopy led to the structural characterization of the mitotic spindle. A complex array of microtubules - polymers of tubulin proteins - employed by the cells to segregate the chromosomes during division (see section 1.3.3.1) (Peterson and Ris, 1976).

1.1.2 Genomic studies

In the early 1910's, thanks to the rediscovery of Mendel's work and theories on biological inheritance in 1865, several scientists started to work on the hypothesis that chromosomes might be the key of the heredity of phenotypic traits. Experiments on mitotic and meiotic chromosomes from Boveri (1889 - 1904), Bateson (1902), Sutton (1902, 1903), Farmer and Moore (1905) have led Frans Janssens to make a connection between his observations of chiasma between chromosomes during meiosis prophase I with the segregation of Mendelian characters during meiosis (1909). These evidences encouraged Hunt Morgan to start his experiments on the fruit fly. And in 1915, he proved that genetic material was carried on chromosomes (Morgan, 1915). Chromosomes are the ubiquitous structures adopted by the DNA molecules associated with proteins in all genomes. Although, the nucleic acid was isolated in 1870 by Johann Friedrich Miescher, the first experimental evidence leading to the identification of DNA

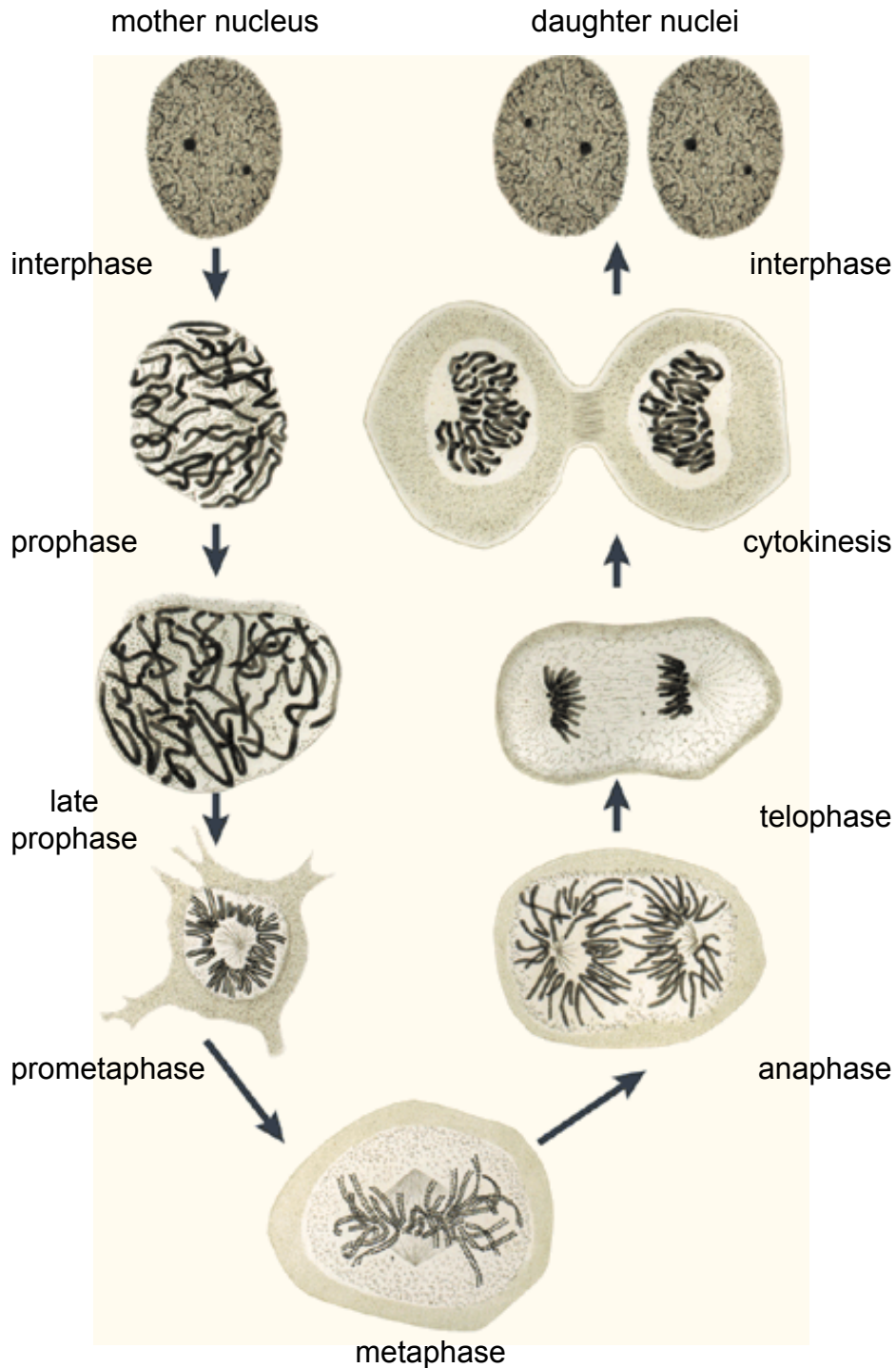


Figure 1 Illustration of mitotic cell division of salamander embryo. Mitosis starts with the formation of nuclear threads in prophase, which change into the aster (star-like configuration of the threads) at prometaphase. This stage moves into the equatorial plate in metaphase, which then immediately forms the double star in anaphase. When the threads have reached the position of the daughter-cell nucleus, the telophase can be observed. A fixative solution called “Flemming’s solution” (a mixture of chromic, osmic and glacial acetic acids) has been used to fix and stain living cells. Adapted from: Flemming, W. *Zellsubstanz, Kern und Zelltheilung* (F. C. W. Vogel, Leipzig, 1882)

as the genetic material came only in late 1930s and 1940s (Avery et al., 1944). The following two decades saw many scientists focused on understanding the structure and the function associated with this molecule, paving the way of today's molecular biology (Jacob et al., 1960; Leder and Nirenberg, 1964; Watson and Crick, 1953).

Eventually, the discovery of the double-helical base-paired structure of DNA (Watson and Crick, 1953) provided a hint on how chromosomes could be duplicated through semi-conservative mechanisms, which was demonstrated by Meselson and Stahl later, in 1958. Studies on DNA duplication showed that replication occurs during a limited part of interphase called S phase (Swift, 1950).

These results led to the division of the cell cycle into phases interposed by gaps (Figure 2) (Prestige, 1972). The commonly accepted program of eukaryotic cell division consists of four stages: first, the first gap phase (G1; un-replicated chromosomes), where cells from the former division decide whether or not to commit to a new round of cell division; second, the synthetic (S) phase, during which the DNA is replicated; third, the second gap phase (G2; replicated chromosomes), where cells grow further and get ready for division; and finally the mitotic (M) phase, during which duplicated chromosome(s) are segregated (mitosis) and the cytoplasmic division (cytokinesis) physically splits the two daughter cells. In prokaryotes, chromosome replication and partition are not necessarily temporally separated. For instance, in some bacterial species, under fast growing conditions, chromosome replication and cell division are uncoupled, so that chromosomes in a same cell can display different stages at the same time (Kuzminov, 2013). The temporal regulation in the typical eukaryotic cell cycle that insulates these different stages from one another may have emerged as a regulatory mechanism concomitant to the increase in DNA content (which even appear sometimes completely unregulated) in eukaryotes.

More recent advancements in understanding DNA-related processes are directly associated with the emergence of sequencing in the late 1970s, and of PCR in 1983. Walter Gilbert and Fred Sanger were first to report efficient sequencing methods, providing a remarkable contribution to the field of genomics (Maxam and Gilbert, 1977; Sanger and Coulson, 1975). At first, these methods were employed to sequence the small bacteriophages (MS2 and ϕ X174 (Fiers et al., 1976; Sanger et al., 1977)). The genomes of the bacteria *Haemophilus influenza* (Fleischmann et al., 1995) and the archaea *Methanococcus jannaschii* (Bult et al., 1996) were then sequenced and published almost concomitantly to the full genome of a eukaryote, *Saccharomyces cerevisiae* (Goffeau et al., 1996). This later project, a coordinated effort by dozens of European laboratories,

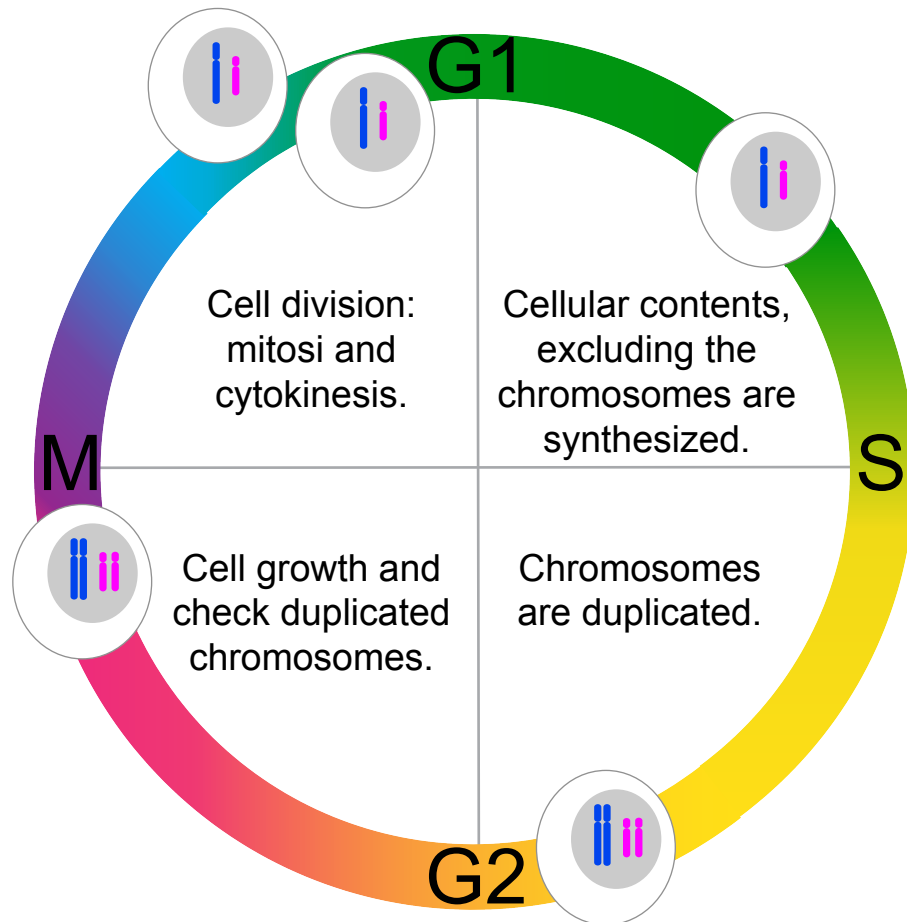


Figure 2 Schematic representation of the different gaps and phases of the cell cycle. During the first gap 1 (G1) cells grow and prepare to enter the synthetic (S) phase, in which chromosomes are duplicated. During the second gap 2 (G2) cells continue growing and check the replicated chromosomes before entering mitotic (M) phase. In mitosis chromosomes are equally divided and it is followed by cytokinesis, during which cell's content divides to form two daughter cells.

paved the way to the assembly of large consortiums aimed at tackling ambitious genomic projects. The most well-known is, of course, the human genome project, which led to the publication of the first draft of the human genome in 2001 (Lander et al., 2001; Venter et al., 2001).

The availability of full genome sequences led to the development of key techniques aiming at tackling questions on the genome-wide scale. PCR allowed the amplification of any region of a genome and facilitated the generation of microarrays. These microarrays, displaying all the ORFs of a genome, were used notably to assess the expression profile of the entire set of genes in a genome (transcriptome, Schena et al., 1995). Furthermore, microarrays were combined with chromatin immunoprecipitation (ChIP-chip) (Gilmour and Lis, 1984), a technique that quantifies the deposition of a protein of interest along the chromosome(s) (Blat and Kleckner, 1999; Iyer et al., 2001; Ren et al., 2000). Together, these techniques paved the way to new structural and temporal insights on chromosomal behaviour during the cell cycle (e.g. “C” technology, see section 1.2.2).

At the turn of the century, the development of high-throughput DNA sequencing, referred to as second-generation sequencing, further boosted the field of genomics. Massive sequencing and analysis of genomic sequences provided information on a full spectrum of genomic alterations, such as single nucleotide polymorphism (SNPs), insertions and deletions, inversions and translocations, chromosomal rearrangements, and copy number alterations (CNVs). New computational (Langmead and Salzberg, 2012; Li et al., 2009; McGinnis and Madden, 2004; Robinson et al., 2011) and experimental approaches were developed, whose practicality, increasing power and reduced costs almost made the use of microarrays obsolete. For instance RNA-seq is routinely used to investigate whole-genome expression (Nagalakshmi et al., 2010), and ChIP-seq conveniently provides genome-wide maps of protein occupancy (Furey, 2012; Mardis, 2007). The gene expression omnibus (GEO) database stores high-throughput functional genomic data, including those that examine SNPs, CNVs, genome-protein binding surveys, methylation status and transcription factor binding (Edgar et al., 2002). Altogether these techniques and tools have become fundamental methods in many fields of biology and medicine. For instance, cancer cells accumulate mutations over generations and eventually escape the elaborate set of controls that normally prevent cells to divide unchecked. The analysis of cancer genomes and structures, using high-throughput sequencing, has elucidated mechanisms of cancer pathogenesis, leading to the improvement of tumour diagnosis and treatment.

1.1.3 Yeasts as convenient model organisms

Retrospectively, studies on different species have shed light on the evolutionary conserved nature of the molecular machineries and control systems that are involved in the DNA replication and segregation mechanisms. However, a large part of our current understanding about the cell cycle has emerged from pioneering work on single-celled organisms, such as yeasts. In this regard, the two yeast species *Schizosaccharomyces pombe* and *Saccharomyces cerevisiae* have proved to be convenient model organisms. Both *S. pombe* and *S. cerevisiae* possess compact genomes (~12 Mb) and have been completely sequenced and fully annotated. They contain approximately 5,000 and 6,000 genes distributed along 3 and 16 chromosomes, respectively (Goffeau et al., 1996; Wood et al., 2002). These microorganisms contain the major subcellular organelles found in higher eukaryotes. They are easy to cultivate clonally, fast growing and well-suited for genetic studies thanks to their haplo-diplobiontic cell cycle (haploid and diploid states of almost equal duration).

An important difference between the two species lies in their physiology and the symmetry of cellular division (Figure 3A). The fission yeast, *S. pombe* is a rod-shaped cell, approximately 3 μm in diameter, which grows by elongation at the two extremities and divides by the formation of a septum that cleaves the cell in two. A complete cell division by fission is achieved in 2 to 4 hours. Fission yeast normally proliferates in a haploid form of two mating types, either "P" or "M", whose fusion results in a diploid cell (Hayles and Nurse, 1989). On the other hand, the budding yeast, *S. cerevisiae* is an ovoid cell of approximately 5 μm in diameter. During late G1/early replication, a protrusion designated to become the daughter cell appears at the apex of the cell. This "bud" grows continuously during S and M phases until it reaches a size slightly smaller than the mother. A complete cell division by budding is achieved in ~90 min. Budding yeast haploid cells consist of two mating types, either "a" or "alpha"; the diploid is the fusion of the two different types.

1.1.4 Yeast genetics

Yeasts have been used as model organisms by geneticists for decades. Their relatively small genomes combined with an efficient homologous recombination system, especially in the case of *S. cerevisiae*, have facilitated genetic manipulations. For example, one can easily disrupt specific genes by replacing them with defined mutant forms or by integrating them at various locations in the genome (Rothstein, 1983). Therefore, before the recent advent of CRISPR technology (Mojica et al., 2005), yeast

genetics was fundamental in the investigations of DNA metabolism during the cell cycle, including processes such as DNA replication, transcription and segregation.

Yeasts have also been extensively used for random mutagenesis screenings. Mutations were induced randomly into the genomes through the exposure to chemicals or by irradiation. The resulting effect on cell viability was paramount for the discovery of conditional mutations of essential genes.

Genetic screens were also used to show that the cell cycle consists in a carefully controlled succession of interdependent events in both *S. cerevisiae* and *S. pombe* (Hartwell et al., 1973; Nurse et al., 1976).

1.1.4.1 Identification of cell-division cycle (*cdc*) genes

These screens were performed on haploid strains, so that any deleterious mutation would have a dominant effect, with a phenotype readily visible in the progeny of the mutagenized population. Essential genes were therefore studied using conditional mutants, such as temperature sensitive (*ts*) mutants. These *ts* mutants grow normally in permissive growing conditions (e.g. 23°C), while they arrest cell cycle progression in non-permissive growing conditions (e.g. 37°C) (Figure 3B).

The first temperature-sensitive screens were performed on *S. cerevisiae* by L. H. Hartwell and colleagues in the late 1960s and early 1970s. In budding yeast, the progression through the cell cycle can be monitored by the size of the bud easily visualized by light microscopy. In this study, the researchers used a mutagenized yeast population to identify mutant cells that stopped growing when the temperature was shifted to 37°C. Under these conditions, cells carrying cell-division cycle (*cdc*) *ts* mutations were able to grow normally until they reached the step where the function of the particular *cdc* gene proved essential, and thus stopped their progression in the cell cycle. This observation provided clear evidence of the temporal relationship between individual phases. A large collection of 148 *cdc* genes were characterized (through genetic complementation) and exploited to block the cell cycle at specific stages. This allowed the authors to address questions about the interdependence of yeast cell cycle events. The different *cdc* genes were isolated, physiologically characterized, cloned by complementation, and the cloned genes used as starting points for subsequent biochemical analysis. Many of these genes turned out to be directly or indirectly involved in cell growth, cell division and cell cycle progression. The functional roles of these genes in cell cycle progression have been characterized over the years and only a subset of them have been shown to be directly involved in the “quality control” system of the cell cycle (Hartwell and Weinert, 1989).

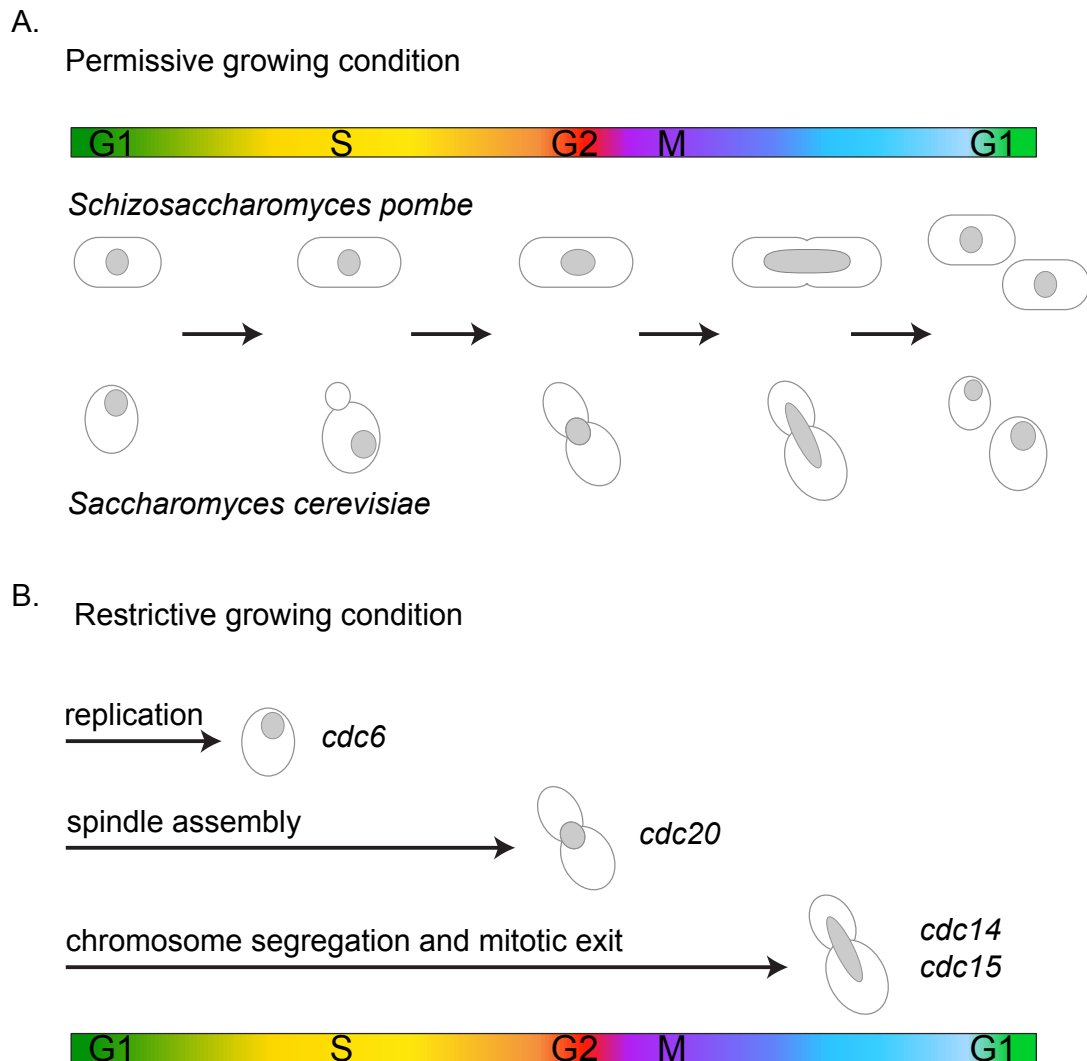


Figure 3 Cell cycle progression in unicellular yeast microorganisms. (A) In favourable or permissive growing conditions both *Schizosaccharomyces pombe* and *Saccharomyces cerevisiae* progress throughout the cell cycle and divide by fission and budding, respectively. (B) In restrictive growing conditions (e.g. variation of growing temperature) conditional cell-division cycle (*cdc*) mutant cells arrest at the stage where the function of the mutated gene product is required. Cdc6 protein is essential to initiate replication therefore *cdc6* mutant arrests in G1; Cdc20 is required for anaphase spindle assembly therefore this mutant arrests in metaphase; Cdc14 and Cdc15 are required for chromosome segregation and exit mitotic phase, therefore these mutants arrest cell cycle at the respective stages during M phase.

1.1.4.2 Cell-cycle control system

Replication and segregation of the genetic material are processes under the strict control of a complex regulatory network: the cell-cycle control system. This control system functions as an essential biochemical timer and is programmed to licence the succession of cell-cycle events at the correct time and in the correct order. This order is reinforced by the dependency of one event on another, for instance the entry into M phase is dependent on the completion of DNA synthesis, ensuring the segregation of only fully replicated genetic information (Hartwell et al., 1974).

In 1982, while searching for proteins that fluctuate during the cell cycle of marine invertebrates, Tim Hunt and co-workers discovered the cyclins (Evans et al., 1983). The observed fluctuation pattern suggested that cyclins were important for controlling cell division and in turn led to the identification of cyclin-dependent kinases (CDKs), regulated by the cyclins. Cdks were shown to act as universal, conserved cell cycle regulators in eukaryotes, with a human CDC2 gene able to complement a *cdc2* mutation in fission yeast (Lee and Nurse, 1987). In budding yeast, there is only one Cdk (Cdk1 – or also Cdc28) (Hartwell et al., 1973) and nine different cyclins (Cln1-3, Clb1-6) (Morgan, 1995). While the concentration of the different cyclins oscillate during the cell cycle progression; the level of Cdk protein remains constant (Figure 4A). The Cdk association with different cyclins at different stages of the cell cycle results in the formation of distinct cyclin-Cdk complexes. Each complex phosphorylates a specific subset of target proteins and determines the “cycling” of the cells from phase to phase (Ubersax et al., 2003).

1.1.4.3 Checkpoints

The yeast cell cycle has three critical checkpoints, each regulated by one of three major cyclin-Cdk complexes (Hartwell and Weinert, 1989; Mendenhall and Hodge, 1998). These complexes are called G1-, G1/S-, S- and M-Cdks (Figure 4B). In G1, the cell prepares for DNA replication and has to synthesize the machineries required to replicate the genome. This growing process is regulated according to nutrient availability and ensures that the cell is in an environment favourable for cell division. During late G1 the concentration of G1/S-Cdk complex rises and triggers progression through the Start checkpoint and entrance into S phase (see section 1.3.2). The rise of G1/S cyclins is accompanied by the appearance of the S cyclins, which directly stimulate DNA replication. This means that once the cell passes the Start checkpoint it becomes committed to division. The M-Cdk rises when the cell approaches mitosis and is responsible for the correct attachment of the mitotic spindle to the sister chromatids in

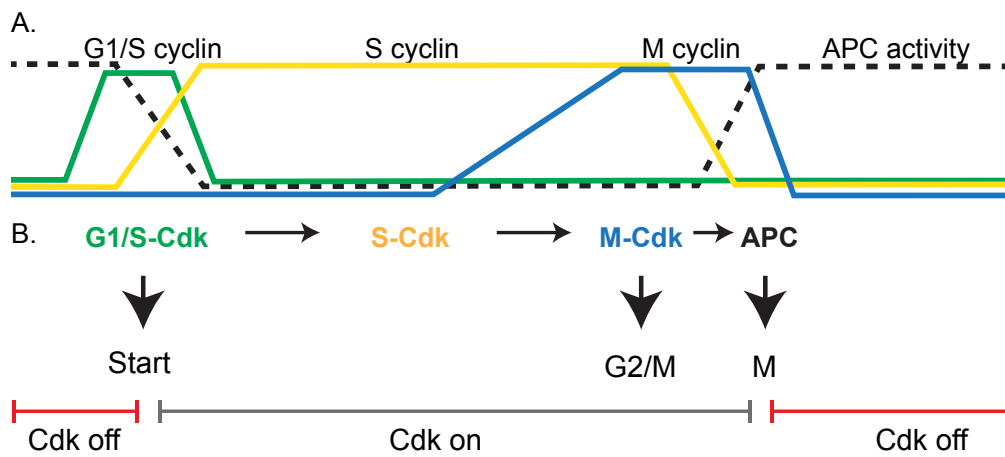


Figure 4 View on the cell-cycle control system. (A) Levels of the three major cyclin types oscillate during the cell cycle progression, providing the specific type of active cyclin-Cdk complex during each phase. (B) Formation of active cyclin-Cdk complexes drive the progression through the cell-cycle checkpoints. G1/S-Cdk complex commits the cell to a new cell division at the Start checkpoint in late G1; S-Cdk initiates DNA replication at the beginning of S phase; M-Cdk activation occurs at the end of S phase and drives the cells through G2/M checkpoint and assembly of the mitotic spindle. APC activation triggers chromosomes separation at the metaphase to anaphase transitions and causes the destruction of cyclins, thus, Cdk inactivation.

metaphase (G2/M checkpoint). Finally, the activation of anaphase-promoting complex (APC) triggers the sister chromatid separation at metaphase to anaphase transition (M checkpoint). In addition, the APC complex induces the destruction of the S and M cyclins and promotes completion of mitosis and cytokinesis (see section 1.3.3.3) (Alberts et al., 2002; Morgan, 1995).

1.1.5 Cell cycle synchronization methods in *S. cerevisiae*

The study of cell cycle phase-specific metabolic changes necessitates the isolation of cells at each corresponding stage. Besides single cell sorting - an increasingly popular technique - synchronizing populations has proved convenient to study the cell cycle. Upon synchronization, cells can eventually be restarted and progress synchronously throughout the cell cycle. The great advantage offered by synchronization methods is that they often provide large amounts of uniformly arrested cells, presumably displaying similar biological processes. This reveals metabolic transitions during the cell cycle progression that would otherwise be undetected in asynchronous populations. In synchronisation experiments, it is important to monitor cell cycle position/progression, this can be achieved using several methods, such as microscopy and flow cytometry. In yeast *S. cerevisiae*, microscopy is used to evaluate the size of the bud, which indicates cell cycle progression. Flow cytometry measures cell synchrony through determining DNA content for every cell in the population (Figure 5).

This section focuses on different approaches used to synchronize budding yeast. Although a variety of similar synchronization methods have been described for other eukaryotes, including mammals (Jackman and O'Connor, 2001). Based on the synchronization strategy, the different methods have been classified as genetic (*cdc* mutations), chemical (drug treatments) or mechanical (centrifugal elutriation) (Futcher, 1999).

1.1.5.1 Genetic synchronization

Genetic synchronization relies on *cdc* mutations (see section 1.1.4; Hartwell et al., 1973). When grown in restrictive conditions, each *cdc* mutant progresses normally through the cycle until it reaches the point where the function of the specific Cdc protein is required and stops growing. For instance, the *cdc6* ts mutant arrests at the G1/S checkpoint, since it cannot initiate DNA replication. Similar mutants exist to arrest at metaphase (*cdc20*) and anaphase (*cdc15*) (Figure 3B).

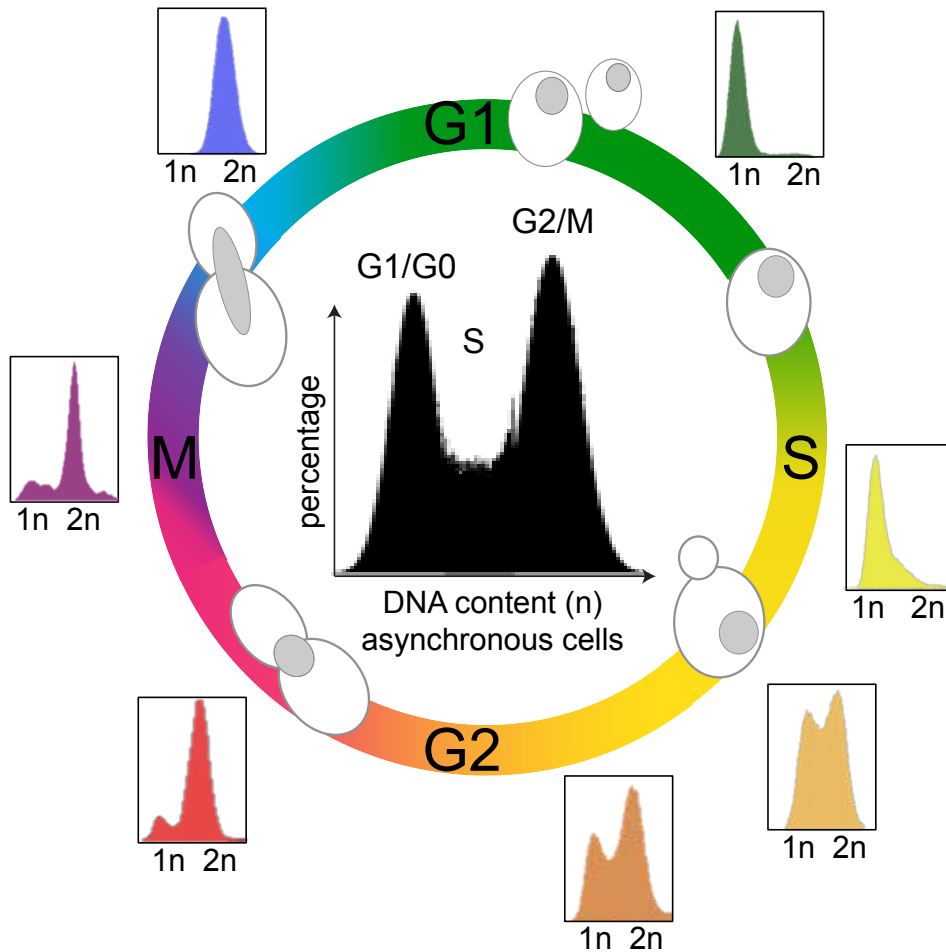


Figure 5 Cell cycle analysis of *S. cerevisiae* by DNA content measurement using flow cytometry. Cells are permeabilised and treated with a fluorescent dye that stains DNA quantitatively, such as propidium iodide (PI). The fluorescence intensity of the stained cells correlates with the DNA content (n). Thereby, the intensity of fluorescence of cells in G0 and G1 (1n), in S phase (1n→2n), and in G2 and M phase (2n) identifies the cell cycle phase position (G0/G1, S, G2/M). The cellular DNA content of individual cells is often plotted as their frequency histogram to provide information about the relative percentage of cells in the major phases of the cell cycle.

1.1.5.2 Chemical synchronization

Yeast cells can also be blocked using a pheromone or drug treatment. Alpha factor (α -factor) is a peptide produced and released in the growing medium by mating type alpha ($\text{MAT}\alpha$) cells. This mating pheromone binds to its corresponding receptor in mating type a (MATa) cells and, by inhibiting the activity of Cln-Cdk1, induces cell cycle arrest at G1/S. Cells arrested in G1 phase have an enlarged “schmoo” morphology (Herskowitz, 1988). α -factor is particularly useful as cells recover rapidly and progress relatively synchronously during one or two cell cycles. However, investigations of the nuclear organization in cells treated with α -factor have observed deformed nuclear shapes (Wang et al., 2016).

Chemical inhibitors of DNA synthesis, such as hydroxyurea and thymidine, and spindle assembly, such as nocodazole and benomyl, have also been used to synchronize cells. Nocodazole is perhaps the most broadly employed drug. It affects the microtubule system and causes the arrest of the cells at the G2/M checkpoint, resulting in cells with a typical dumbbell shape (Jacobs et al., 1988a). As, nocodazole and other chemically-induced arrests are likely to disturb the cell metabolism, it is recommended to combine several methods to alleviate the experimental caveats that may result from these effects.

1.1.5.3 Mechanical synchronization

Mechanical synchronization is less invasive method to purify cells within the same stage of the cell cycle from an asynchronous population. Centrifugal elutriation allows this by separating cells on the basis of their coefficient of sedimentation, a characteristic of their size and shape. This procedure uses a spinning centrifuge to oppose a counterflow and creates two opposing forces on the cells. Large budded cells and irregularly shaped cells travel slower than small newborn G1 cells. Therefore, by adjusting these forces it is possible to elute and collect considerable amounts of small, newborn G1 cells (Marbouty et al., 2014).

Altogether these synchronisation methods have been used in studies that have defined a “canonical” eukaryotic cell cycle. This articulates around the replication and segregation of the genomic material, events that impose important structural reorganization of the DNA molecule.

1.2 Investigate genome organization in eukaryotes

At the end of 1940s, biologists knew that the DNA molecule was responsible for heredity in genes and chromosomes (Avery et al., 1944). However, many doubts were raised concerning its apparent simple chemistry. How four bases together could ensure all the complex functions of the genetic material? It is now well established that there is a strong functional link between the genetic information encoded in the DNA sequence (1D) and the spatial structure (3D) of this molecule. Part of this mystery was solved in the early 1950s, when the DNA was investigated through x-ray diffraction analysis, leading to the resolution of the 3D atomic structure of the molecules. Since the discovery of the two strands wound into a double helix (Watson and Crick, 1953), the folding of the DNA molecule(s) inside the nucleus or the cell has remained an important question. This section provides a brief historical overview of the major techniques currently employed to decipher chromosomes organization and its function in eukaryotes.

1.2.1 Imaging approaches

Over the centuries much has been learnt about the chromosome structure shared between all living organisms and also revealed in the fossils (Bomfleur et al., 2014). At the end of the 19th century, several investigations of human karyotypes estimated a number of chromosomes between 16 and 38 chromosomes (Arnold, 1879). These counts were performed on dispersed chromosomes imaged using light microscopy. A correct count was only achieved in 1956 by using cell cultures treated with colchicine to accumulate mitoses (Tjio and Levan, 1956). This has permitted to discover the first human chromosome aberration, in 1958 by Marthe Gautier and colleagues. They found an extra small chromosome in fibroblast cells from patients with Down syndrome (Lejeune et al., 1959). The simple optical microscopy, used in the 1960s, was sufficient to detect gross structural aberrations but was unable to provide any information on chromosome identity. This problem was resolved with the implementation of chromosome banding, technique based on differential staining along chromosome's length (Caspersson et al., 1970). Successively, DNA hybridization-based variants of this technique have been developed and overall indicated with the name of "chromosome painting". Above all, the fluorescence *in situ* hybridization (FISH) has become the standard method for karyotype analysis (Pinkel et al., 1986) and chromosome structure investigation. For instance, the territorial organization of chromosomes, first suggested by Carl Rabl and Theodor Boveri at the end of 19th century, was experimentally confirmed in the 1980s using FISH (Figure 6A) with chromosome-specific DNA probes

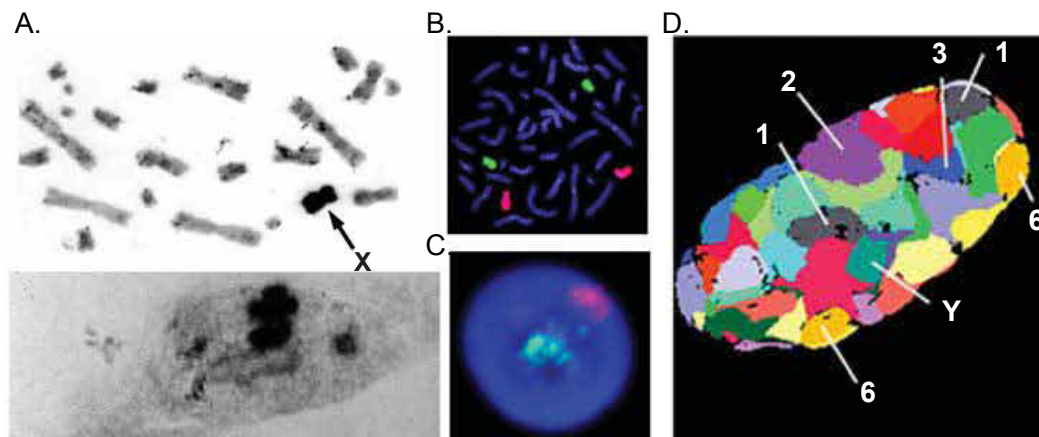


Figure 6 Chromosome territories (CTs) by *in situ* hybridization. (A) *In situ* hybridization with biotinylated human genomic DNA of a Chinese hamster × human hybrid cell line carrying a single human X chromosome reveals human X chromosome (arrow) in metaphase (top; Giemsa stained) and its respective human X territory in interphase nuclei (bottom) (Schardin et al., 1985). (B) Visualization of individual chromosomes in a human (HSA) metaphase plate (chr18 in red, chr19 in green) after fluorescence in situ hybridization (FISH) using labelled chromosome painting probes. (C) A single light optical section through the nucleus of a human lymphoblastoid cell after 3D FISH with the same painting probes shows a HSA 19 CT (green) in the nuclear centre and a HSA 18 CT (red) at the periphery (Tanabe et al., 2002). (D) Simultaneous delineation of all chromosomes in a human fibroblast nucleus by multi-color FISH. Light optical sections with false colour representation of all CTs are shown. Examples of individual CTs are denoted with their respective karyotypic number (Bolzer et al., 2005). Adapted from Cremer and Cremer, 2010.

(Schardin et al., 1985). To study the spatial arrangement of chromosome territories (CTs), three-dimensional FISH protocols in combination with serial sectioning of nuclei by laser confocal microscopy and 3D image reconstruction were recently developed (Figure 6C, D) (Cremer and Cremer, 2010). One of the limitations of the FISH protocol is the necessity of using fixed cells. The use of the fluorescent repressor operator systems (FROS) technique was shown to overcome this limitation and one could visualize chromatin in living cells. It relies on the expression of the bacterial repressor (LacI) fused to a fluorescent protein (e.g. GFP). The fusion protein binds to the respective operator DNA sequences (LacO), which are integrated as multicopy tandem arrays at specific chromosomal locations. Accumulation of the fluorescent proteins at the tagged DNA region is then visible using conventional fluorescent microscopy (Belmont and Straight, 1998; Robinett et al., 1996). Applications of this method have facilitated the investigation of chromatin dynamics at specific loci in yeast cells (Lassadi and Bystricky, 2011). One of the biggest limitation of the conventional fluorescence microscopy is the relatively low resolution imposed by the diffraction of light. In recent years, a number of “super-resolution” fluorescence microscopy techniques have been implemented to overcome this barrier. Eventually, these methods have reached the nanometre resolution at which the localization of individual fluorescent molecules is possible (Betzig et al., 2006).

Although, the distinction between low-density euchromatin and high-density heterochromatin was present since 1928 (Heitz, E. 1928), a high resolution analysis at the fibre level of these structures was possible only with the advent of the electron microscopy. In 1974, the chromatin appeared similar to “beads on a string”, observation that led to suggest the model of the nucleosomal organization of the 10 nm chromatin fibre (Kornberg, 1974). Today, it is known that in all eukaryotes DNA molecules are wrapped around octamers of histone proteins (H2A, H2B, H3, and H4) forming nucleosomes, which are in turn folded into elaborated higher-order chromatin fibres (Figure 7) (Hayes and Hansen, 2001; Luger et al., 2012). Exactly how this process is accomplished is still unclear. Recent electron microscopy studies and modelling approaches have reported a broad variety of heteromorphic secondary structure of the chromatin, characterized by alternative interactions between the nucleosomes (from 5 nm to 24 nm fibres). The resulting heterogeneous chromatin fibres are then packed into complex tertiary structures with different protein density, whose end point give rise to metaphase chromosomes (Grigoryev et al., 2009; Nishino et al., 2012; Ou et al., 2017).

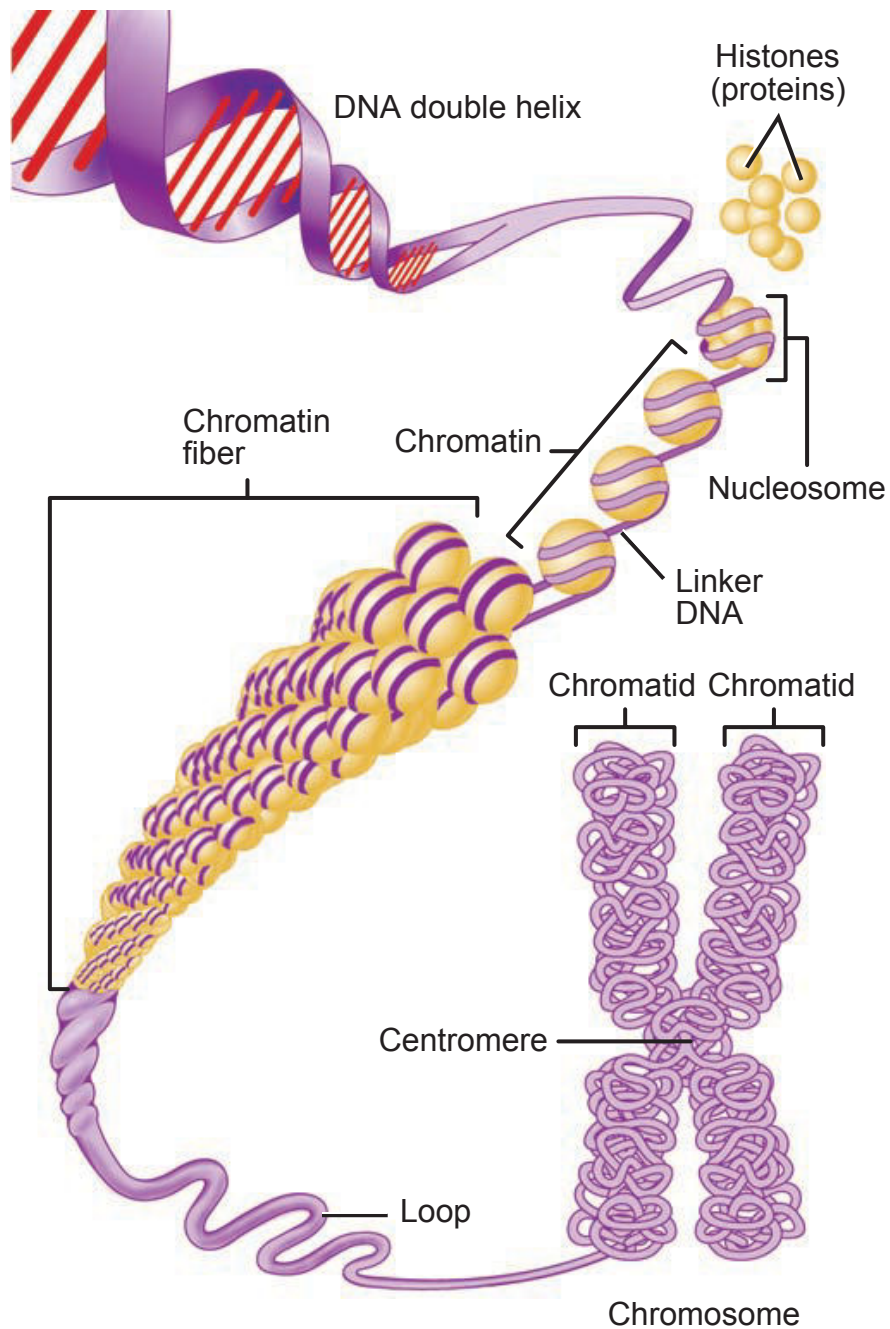


Figure 7 Folding of the DNA fibre into a chromosome. DNA molecule wrapped around octamers of histone proteins (yellow) to form nucleosomes, which are basic units of the 10 nm “beads on a string” chromatin fibre. The string between the beads is linker DNA that holds adjacent nucleosomes and regulate the folding of the chromatin fibre into more elaborate and compact structures, such as loops. Before cell division the loops are packed into chromatids, which are held together by a centromere (Tortora-PAP 12).

1.2.2 Multiscale genome-wide approaches

With the completed genome sequence in a variety of species, genome-wide studies have become powerful strategies to investigate the interplay between chromatin structure and genome function. Chromatin immune-precipitation in combination with genome sequencing (ChIP-seq) has been thoroughly used to map the DNA binding sites of many proteins. This technique allowed to generate nucleosomal maps (Lee et al., 2007; Schones et al., 2008) and to identify transcription factor binding sites (Farnham, 2009). Nucleosome interactions, both between themselves and with non-histone DNA binding proteins, are influenced by histone modifications. As a general rule histone acetylation is associated with highly transcribed genes located in the decondensed euchromatic regions. Whereas, methylation is a marker of transcriptional repression, associated with highly compact heterochromatic regions. These histone-modifications have been characterized and mapped genome-wide (Venkatesh and Workman, 2015; Zhou et al., 2011).

In addition, large-scale studies have been performed to understand the collective regulation of thousands of genes that lead to the development and functionality of complex organisms. For instance, the ENCODE, Roadmap Epigenome, the International Human Epigenome Project and FANTOM projects have led to the annotated tens of thousands of genes and millions of candidate regulatory elements (e.g. enhancers, insulators and promoters) and described features of chromatin accessibility and histone modification in the human and mouse genomes. Overall these studies have found strong regulatory correlations of the genomic landscapes (both sequence and epigenetic related) with both replication and transcription programs (ENCODE Project Consortium et al., 2007).

However, the understanding of where and how these elements contribute to gene regulation across genomic distances, ranging from kilobases to megabases, is still incomplete. The development of the chromosome conformation capture (3C) technique (Dekker et al., 2002) and of the high-throughput genomic variants (e.g. Hi-C, Lieberman-Aiden et al., 2009) (Figure 8) have proved to be powerful approaches to analyse the hierarchical higher-order organization of genomes in a myriad of organisms (Crane et al., 2015; Duan et al., 2010; Le et al., 2013; Marbouty et al., 2015; Mizuguchi et al., 2014; Sexton et al., 2012). These methods are based on capturing contacts/interactions between genome fragments at both short and long distances, using crosslinking agents (e.g. formaldehyde). Contacts between fragments are then revealed using DNA amplification-based techniques (e.g. quantitative PCR, deep-sequencing) and the results

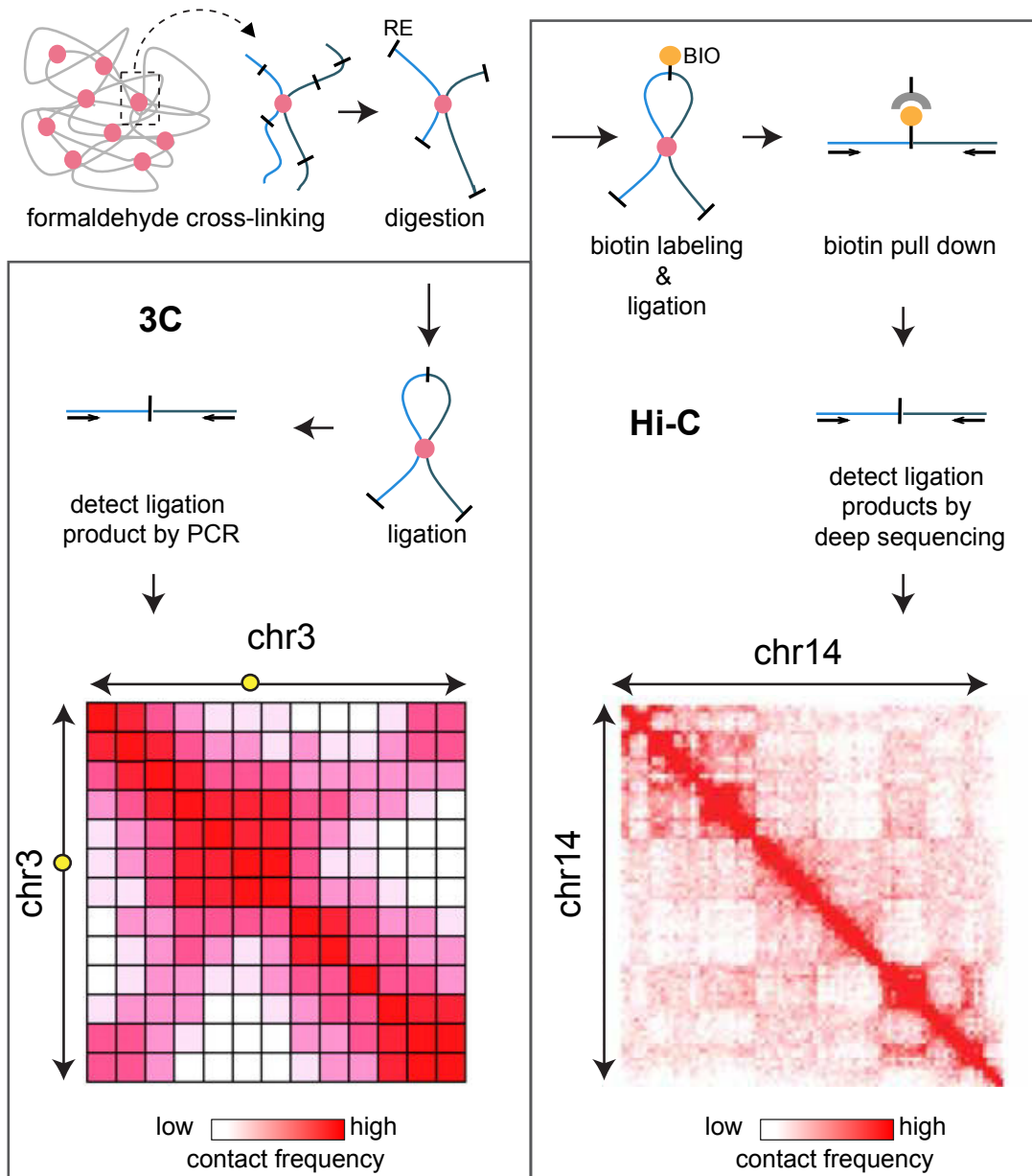


Figure 8 Schematic representation of the Chromosome Conformation Capture (“C”) methodology. Left panel shows the first developed 3C assay consisting of: genomic DNA cross-linking with formaldehyde, digestion with a restriction enzyme (RE) and ligation, followed by quantitative PCR to detect ligation products. Bottom left: schematic representation of the first complete contact map of *S. cerevisiae* chromosome 3 (25 kb resolution), showing chromosome bending at the level of the centromere (yellow) with the two arms contacting each other (adapted from Dekker et al., 2002). Right panel shows the genome-wide variant of this technique, Hi-C, in which the digested and ligated DNA ends are labelled with biotin (BIO). A biotin purification is performed to enrich these fragments for genome-wide analysis using deep-sequencing. Bottom right: genome-wide contact map of mammalian chromosome 14 (1 Mb resolution), showing a compartmental organization of the chromatin (adapted from Lieberman-Aiden et al., 2009). Colour scale indicates the frequency of contacts.

are displayed using heat maps that reflect contact frequencies between loci in the genome. Finally, genomic contact maps can also be displayed as 3D structures (Lesne et al., 2014). The first chromosome map, described by Dekker and colleagues, showed the organization of chr3 in *S. cerevisiae*, that appeared to form a ring-like structure bending near the centromere and the telomeres in close proximity with each other (Figure 8, left contact map). This was confirmed by fluorescent microscopy that have tagged the two telomere extremities (Bystricky et al., 2005).

The different variants of the “C” technique (Dekker et al., 2013) can detect a broad range of chromatin contacts and structural features, including (i) compartments of active/inactive chromatin, (ii) long-range loops bridging together distant DNA regions, and (iii) large domains corresponding to sub-megabase chromosomal regions that interact within themselves more frequently than with other genomic loci (topologically associated domains or TADs in metazoan, macrodomains or MD, and chromosome interacting domains or CIDs in prokaryotes) (Figure 8, right contact map) (Dixon et al., 2012, 2016). Noteworthy, not all organisms have genomes organized in topological domains. A well-studied example is provided by the genome of *S. cerevisiae*, in which 3C studies have revealed the major features of the Rabl-like chromosomal organization, while they have failed to detect any large scale TAD (see section 1.3) (Duan et al., 2010; Guidi et al., 2015).

TADs are primarily characterized and maintained by their boundaries, e.g. sequences associated with DNA binding proteins and/or insulating proteins (Parelho et al., 2008). Particularly, the highly conserved CTCF protein is often found at TADs boundaries, and has been shown to colocalize with chromatin structural proteins, called cohesin (see section 1.3.2.3), and to enhance domain boundaries (Sofueva et al., 2013) and chromatin loop formation (Sanborn et al., 2015). These topological structures of the chromatin fibre have been shown in recent years to play important regulatory roles in transcription regulation (Nora et al., 2012), DNA replication (Pope et al., 2014), genome stability (Aymard et al., 2017) and genomic/developmental diseases (Franke et al., 2016; Lupiáñez et al., 2016). Recent Hi-C studies, have also unveiled genome-wide chromosomal maps of the cell cycle stages in bacteria (Marbouty et al., 2015), yeast (Lazar - Stefanita et al., 2017) and mammals (Nagano et al., 2017; Naumova et al., 2013). In all these species, the most prominent changes of the chromatin structure have been observed to occur during DNA replication and the subsequent segregation of the duplicated chromosomes. However, the molecular mechanisms involved in the establishment and regulation of these 3D changes remain still difficult to address. This is due to the current intrinsic limitations of Hi-C experiments, such as cell-to-cell

variability and the inability to distinguish between sister chromatids. The cell-to-cell variability due to the use of cell populations has been recently tackled by Nagano and colleagues using single-cell Hi-C. Analysis on hundreds of single-cell Hi-C maps have unveiled a dynamic reorganization of mammalian chromosomes during cell cycle, showing the disappearance of TADs during replication. This study has also confirmed the absence of TADs in mitotic chromosomes, that was observed on synchronized mammalian cells by Hi-C (Naumova et al., 2013). Altogether these recent studies seem to point at a highly dynamic reorganization of the nuclear architecture that may not be fully understood, yet, because of many technical and experimental limitations.

Nevertheless, the joint effort between microscopy and genome-wide approaches have achieved a remarkable knowledge on genome organization in a broad variety of species. Next sections of this manuscript provide an overview of the organization of chromosomes in *S. cerevisiae* in light of the cell cycle events.

1.3 Integrating genome organization and cell cycle in *S. cerevisiae*

Budding yeast chromosomes display a Rab1-like organisation (historical reference section 1.1.1) throughout the entire cell cycle (Figure 9A) (Duan et al., 2010; Jin et al., 1998; Bystricky et al., 2005; Taddei and Gasser, 2012). The peculiarity of the budding yeast Rab1 organization consists of the distinct orientation of the chromosomes. Yeast's centromeres consist in discrete, short ~125 bp sequences held together at the nuclear envelope by a short array of microtubules departing from the spindle pole body (SPB, microtubule organizing centre in yeast) (Jin et al., 2000). The structure of the pericentromeric chromatin and the attachment to microtubules is rather complex and it is discussed later in sections 1.3.3.1-2. Chromosomes' arms are then free to explore the inner space of the nucleus while the telomeres are tethered at the nuclear envelope where they associate in dynamic clusters (Gotta et al., 1996). Yeast telomeres consist of 250 – 300 bp of irregular tandem repeats (called TG₁₋₃) (Shampay et al., 1984). The binding of Rap1 protein to this repeat recruits the silent information regulator (SIR: Sir2, Sir3 and Sir4) complex (Gotta et al., 1996; Marcand et al., 1996; Moretti et al., 1994; Renauld et al., 1993). The binding and spreading of SIR proteins organize the heterochromatin at the subtelomeres (Hecht et al., 1996) and mediate transcriptional silencing (Dubarry et al., 2011; Laura N. Rusche et al., 2003).

Besides the Rab1 organisation, another obvious feature of yeast nucleus consists in the nucleolus, a compartment that occupies almost one third of the nuclear volume opposite the SPB (Yang et al., 1989). This compartment is the site of rDNA transcription into rRNA. The rDNA sequence is formed of 100 to 200 units of 9.1 kb repeated in tandem in

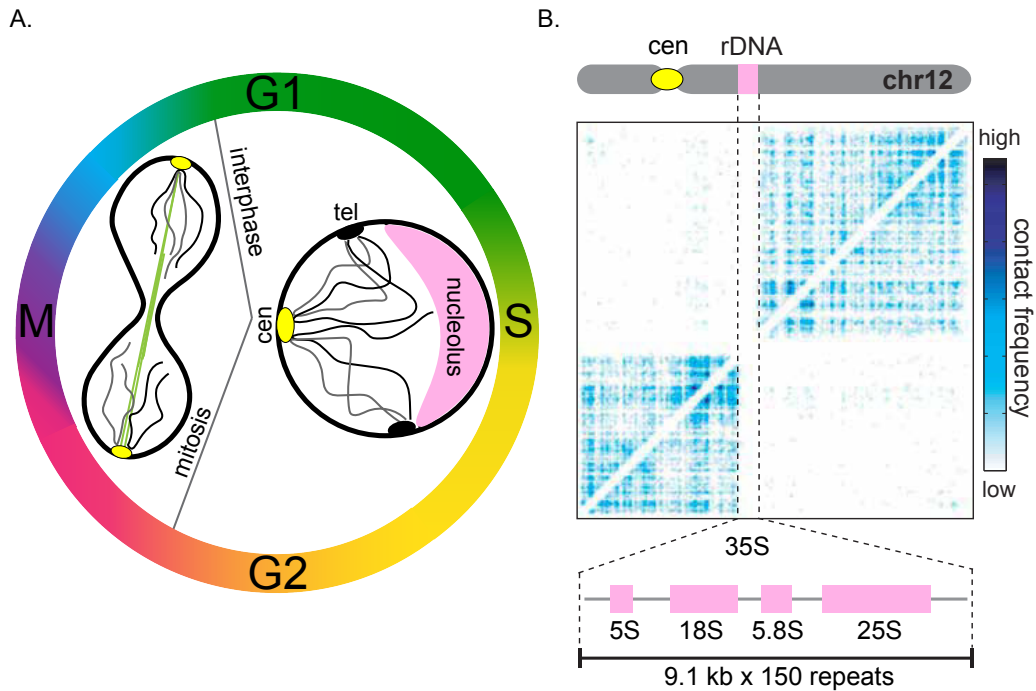


Figure 9 Rabl-like organization of *S. cerevisiae*'s chromosomes. (A) Chromosomes are anchored at the nuclear periphery (spindle pole body, SPB not shown) through their centromeres (cen in yellow), located opposite to the nucleolus (rDNA locus in pink). Centromere attachment is preserved throughout the entire cell cycle. Chromosomes' arms are free to explore the nuclear inner space while telomeres form several distinct clusters at the nuclear periphery in interphase (tel in black). Telomere localization at the nuclear periphery is lost in mitosis (B). Contact map of chromosome 12. Note that the two ends of chr12 (schema atop the map) exhibit extensive local interactions, but very little interaction with each other. Separating the ends of chr12 are 100–200 rDNA repeats (schema at the bottom). Colour scale indicates the frequency of contacts (adapted from Duan et al., 2010).

the middle of the right arm of chromosomes 12 (chr12) (Johnston et al., 1997). Given its repeated nature, this locus is “unmappable” by deep-sequencing and thus unsuitable for “C”-based investigations. The contact map of chr12 therefore displays an abrupt termination of the intra-chromosomal contacts at both ends of the nucleolus (Figure 9B) (Duan et al., 2010). The extended array of rDNA repeats is an ideal template for homologous recombination which is therefore actively repressed both by SIR-mediated silencing and by nuclear envelope tethering (Kaeberlein et al., 1999; Mekhail et al., 2008). rDNA genes are either transcribed or non-transcribed and they can adopt different conformations based on their activation status. Inactive genes are condensed/heterochromatic while the active are decondensed/euchromatic (Conconi et al., 1989; Huang and Moazed, 2003). It has been suggested that the different forms of rDNA chromatin have evolved to be responsive to the needs of the cell: RNA levels can be modulated either by controlling the rate of transcription or by regulating the number of genes available for transcription (Lin et al., 2000). Notably, the balance between hetero-/silence and euchromatic/active form of chromatin have been shown to vary drastically between the different stages of the cell cycle (see section 1.3.3.4)(Clemente-Blanco et al., 2009; Guacci et al., 1994).

The general compaction of yeast chromatin fibre has been analysed with both microscopy (Bystricky et al., 2004; Hajjoul et al., 2013) and 3C (Dekker, 2008), suggesting a loose structure, with 1.2 – 3.6 nucleosomes per 11 nm (Wang et al., 2015). These results are in agreement with the low detected levels of Hho1, H1 histone variant in yeast (Freidkin and Katcoff, 2001). This study has shown that Hho1 is about 37 fold fewer than the number of total estimated nucleosomes. Moreover, the authors have observed an increase of this protein at the nucleolus, locus that have been shown to condense in mitosis (Guacci et al., 1994).

The motility of the chromatin fibre has been analysed at DNA loci and could be considered as a non-directed motion partially dependent on the ATP levels (Marshall et al., 1997; Heun et al., 2001a). These studies have shown that telomeres and centromeres exhibit a slower diffusion rate than internal loci. This greater confinement was not surprising given the fact that both these loci are anchored at the nuclear envelope. In addition to this diffusive motion, occasional jumps in motility ATP-dependent have been detected. Although, the mechanisms for potential active motions have not been yet fully understand, they seem partially dependent on forces that originate outside the nucleus and driven by the cytoskeleton (Koszul et al., 2008; Spichal et al., 2016).

The physical properties of the chromatin fibre as well as its mobility have been suggested to change according to the metabolic state of the cells. First, changes in

mobility has been observed during the cell cycle progression. For instance, less movement has been observed in S phase than in G1 phase nuclei, a drop that correlates inversely with the number of active replication forks (Heun et al., 2001a). Similar results have been also obtained in mammalian cells by measuring distances explored by chromosome territories (Walter et al., 2003). These results suggested that biological processes may influence the mobility of chromosomal loci. Indeed, it has been shown that transcriptionally silenced telomere-proximal genes are tethered at the nuclear periphery (Gotta et al., 1996) and that chromatin movements lead to gene re-localization upon transcription activation (Taddei et al., 2006). Moreover, an increase of local and global mobility after DNA damage has been reported to enhance the efficiency of repair due to an active search for repair partners (Miné-Hattab and Rothstein, 2012). Taken together these observations suggest that genome organization in budding yeast is a highly dynamic structure, that is shaped in response to the metabolic state of the cell. Next sections describe cell cycle in yeast in light of the DNA-related metabolic processes that may impact chromosomal structure.

1.3.1 Quiescent (G0) state

In natural ecosystems, starvation is one of the most common stress encountered by almost all microbial species. Cells are able to respond to the hostile environment by forming inert structures commonly called spores. These differentiated cells are capable of surviving during extended periods of nutrients deprivation.

Budding yeast cope-up with starvation by ceasing growth and entering into a non-proliferative state referred to as stationary phase. If the cells are kept for extended periods without nutrients they enter quiescent state, that allows maintenance of viability but retains the ability to resume growth when nutrients become available (Werner-Washburne et al., 1993). The “cell quiescence cycle” is the process by which nutrient limitation causes exit from the active proliferation (cell division cycle) and triggers entry into the nonproliferating state. Notably, the quiescence cycle and the cell division cycle intersect at the G1 phase, when cells have not been yet committed to enter S phase. Therefore, based on the amount of nutrients at G1/S checkpoint cells will enter one cycle or the other (Gray et al., 2004). This is a highly regulated and programmed phenomenon. Quiescent cells share a number of salient characteristics such as unreplicated genomes; condensed chromosomes, referred to as G0 chromosomes (Schäfer et al., 2008; Yang et al., 2006); reduced rates of transcription and translation (Galdieri et al., 2010); fail to accumulate mass and volume (Jorgensen et al., 2007); develop a thicker and more resistant cell wall (Gray et al., 2004). Several studies have

also shown changes of the nuclear geometry in the long-living cells, in association with modifications of the nucleolar size (Wang et al., 2016). Microscopy and 3C analysis revealed a telomere hypercluster, which was repositioned in the middle of the nuclear space (Guidi et al., 2015; Laporte et al., 2016). This peculiar feature was found to be dependent on the activity of the SIR-silencing complex at these loci. These latter features are furthermore detailed in chapter 2.2 in light of our results. Whereas, other studies on quiescent cells have reported a global reorganization of the nuclear interior dependent on the microtubule cytoskeleton (Laporte and Sagot, 2014; Laporte et al., 2013). The authors have observed the assembly a long and stable array of nuclear microtubules on which the centromeres also localize and the displacement of the nucleolus.

In favourable growing conditions G1 cells pass the G1/S checkpoint and become irreversibly committed to S phase.

1.3.2 Chromosome replication during S phase

The replication of the DNA molecule in eukaryotes occurs during S phase. Chromosomes need to be accurately (one error in 10^9 nucleotides) and rapidly (5-100 nucleotides per second) copied to ensure the transmission of the genome. This process involves the coordinated activity of many enzymes and accessory proteins, such as: DNA polymerases, that copy the template strand; helicases, that unwind the helix; and structural proteins that pack the nascent molecules. Altogether these proteins form the replication machineries that assemble at genomic loci, named origins of replication, giving rise to replisomes (Morgan, 2007).

Budding yeast's replication origins are well defined genetic elements called autonomously replicating sequences (ARS) (Figure 10A). The first direct evidence that ARS was acting as a replication element was brought by two-dimensional (2D) gel analysis of plasmid DNA replication (Brewer and Fangman, 1987). Each ARS contains a specific DNA consensus sequence of 11 bp that, in late mitosis and early G1, recruits the pre-replication complex (pre-RC) (Figure 10B). The origin recognition complex (ORC) is the central player in the assembly of the pre-RC on the replication origins (Bell and Stillman, 1992). Indeed, it has been shown that mutations in ORC genes cause defects in initiation (Piatti et al., 1995). Moreover, despite the origin diversity between yeast and metazoans, ORC-related proteins exist in all eukaryotes (Li and Stillman, 2012). The binding of the ORC complex recruits two additional proteins Cdc6 and Cdt1, that are responsible for the recruitment of the six-subunit Mcm complex (Mcm2-7) (Wyrick et al., 2001). Once the Mcm2-7 is loaded the formation of the pre-RC is completed and the

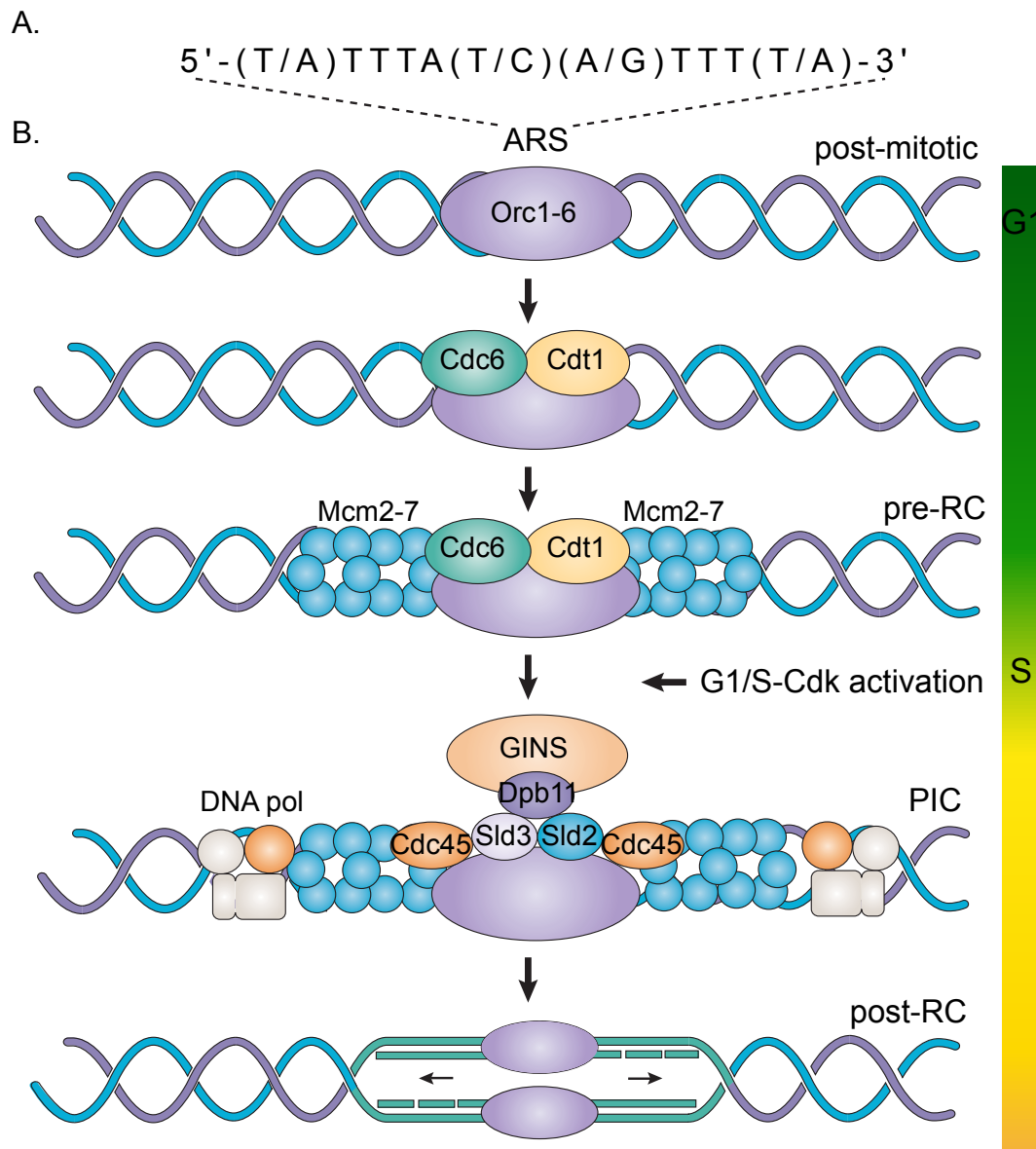


Figure 10 Assembly of pre-replication and pre-initiation complexes. (A) Autonomously replicating sequence (ARS), 11 bp consensus sequence of *S. cerevisiae*. (B) A six-subunit complex called the origin recognition complex (ORC) serves as a platform for the assembly of pre-replication (pre-RC) complex. ORC binds ARS sequence throughout the cell cycle. During the mitosis - G1 transition, chromatin-bound ORC recruits Cdc6 and Cdt1, which facilitate the loading of a helicase complex consisting of MCM (minichromosome maintenance) proteins 2-7 (licensing). The resulting complex is termed the pre-replication complex (pre-RC). In late G1, G1/S-Cdk complex induces the expression and activation of the S-Cdk complex, that triggers origin firing by promoting the formation of the preinitiation complex (PIC). PIC complex is formed by additional factors including Cdc45, Sld2-3, Dpb11, the GINS complex and DNA polymerases. The successive disassembly of the pre-RC coupled with the destruction of S-cyclins prevents the re-activation of this complex later during the cell cycle, commonly known as post-RC (adapted from Aladjem, 2007).

“licensed” origin is ready to “fire” replication. The start signal comes in late G1 from the cell-cycle control system, when the G1- and G1/S-Cdk complexes are activated. The G1/S-Cdk induces the expression and activation of the S-Cdk complex (Morgan, 1995; Ubersax et al., 2003). Activation of S-Cdk triggers origin firing by promoting the formation of the preinitiation complex (PIC). Formation of PIC requires the displacement of pre-RC factors (Cdc6 and Cdt1), and the recruitment of other factors including the DNA polymerases (Aparicio et al., 1999). PIC activates the Mcm2-7 helicase that unwinds the DNA helix, making Y-shaped DNA structures called replication forks. Recently, real time dynamics of replisome activation have been observed directly at single-molecule level (Duzdevich et al., 2015). DNA synthesis proceeds in a 5' to 3' direction and is semi-continuous (Aladjem, 2007). The template leading strand is the one in which 5'→3' synthesis proceeds in the same direction as replication fork movement and is continuously synthesized. The lagging strand is discontinuously synthesized in short pieces (Okazaki fragments) in a direction opposite to the direction of fork movement. When the polymerase dissociates from the synthesized DNA fragment, the DNA ligase can join the adjacent Okazaki fragments together to form a continuous strand (Okazaki et al., 1967).

The successive disassembly of the pre-RC coupled with the destruction of S- and M-cyclins prevents the re-activation of this complex later during the cell cycle, commonly known as post-RC (Diffley, 1996). This ensures that the firing of the licensed origins occurs “once-and-only-once” per cell cycle (Nguyen et al., 2001). Finally, the replication initiation program is a carefully coordinated process both spatially and temporally.

1.3.2.1 Spatial-temporal organization of the replication program

Not all regions are replicate at the same time. Large regional differences between early-replicated centromeres and late-replicated telomeres were shown using Meselson & Stahl-like experiments in 1988 (McCarroll and Fangman, 1988). Successively, a few number of ARSs were mapped and their activation timing characterized using two-dimensional (2D) gel electrophoresis (Brewer and Fangman, 1991). This first investigation has led to classify ARSs into early and late firing. This temporal difference is the result of differences in origin efficiency, defined as the percentage of cell cycles that a specific ARS initiates replication (Figure 11A). As a consequence, efficient origins are fired in most of the cells in the population while the inefficient ones are fired stochastically at the population level (Ferguson and Fangman, 1992).

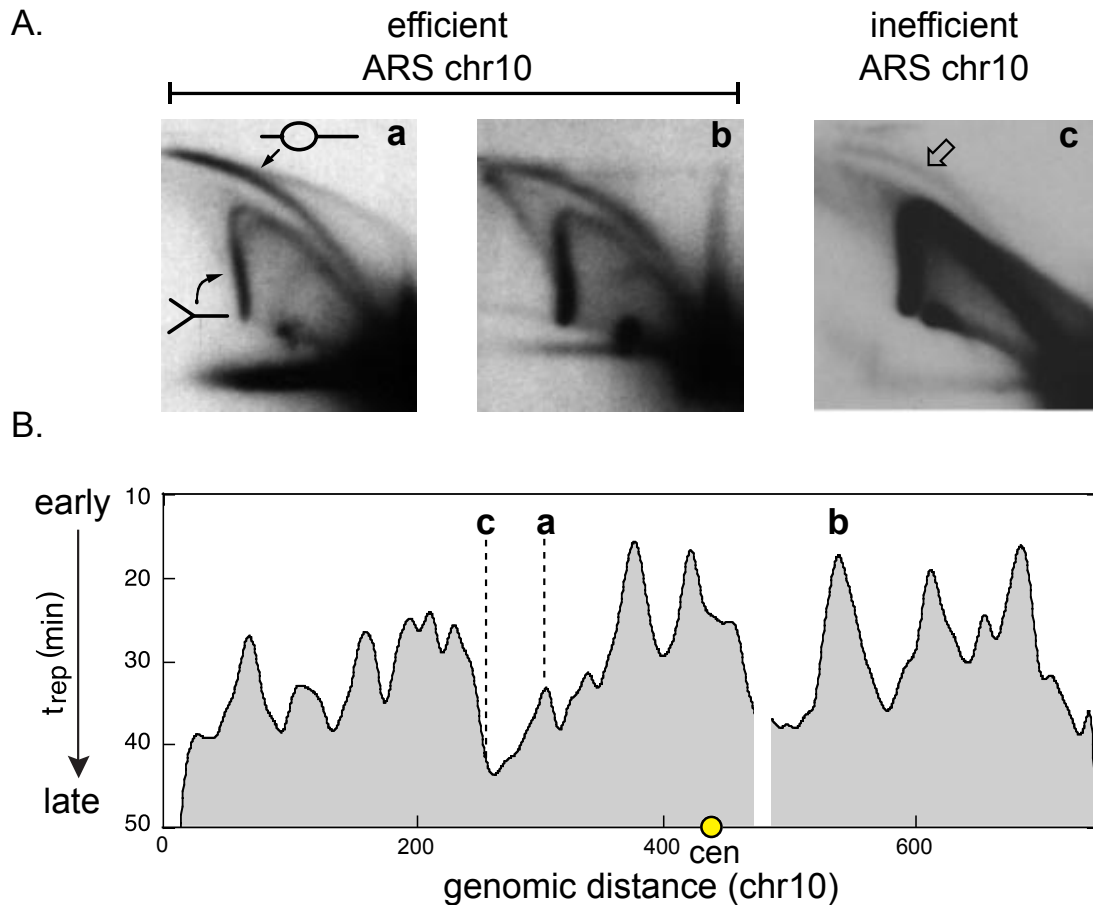


Figure 11 Origin firing and replication profile. (A) Three locations (a, b and c) on chromosome 10 were tested for origin activity by 2D gel electrophoresis. Bubble structures were detected at all locations, indicating the presence of active origins. The amount of these structures indicate that a and b are efficient origins (fired in most of the cells) while c is inefficient (Y structures indicate passive replication of this region). (B) Replication profile deduced from the microarray data for chromosome 10 (x-axis) is shown. Positions marked a, b, and c on the profile correspond to the origins analysed in (A). They show that efficient origins are early replicated while inefficient are late. Centromere-proximal region is relatively early replicated while telomeres are late (adapted from Raghuraman et al., 2001).

In 2001 a comprehensive genome-wide study conducted by Raghuraman and colleagues have identified and characterized approximately 300 ARSs on yeast genome (e.g. chromosome 10 replication profile shown in Figure 11B). The authors observed that ARSs are distributed throughout all chromosomes with an average genomic interval of 30 kb and they are mostly located in the intergenic regions. This latter observation pointed at a negative correlation between transcription activity and replication initiation in budding yeast, also observed in mammals (Kalejta et al., 1998). Moreover, only a fraction of the ARSs were efficiently fired and they were mostly concentrated in the centromeric regions of the chromosomes. Later studies have confirmed these results and provided a detailed topography of the replication profile at hundreds of sites across the genome of budding yeast (McCune et al., 2008; Raghuraman et al., 2001; Yabuki et al., 2002). They all have observed a continuous activation of origins throughout the entire S phase and confirmed the existence of a global pattern of the replication timing: starting at the early replicating centromeres and finishing at the late telomeric regions. Nevertheless, recent single molecule studies have also shown a stochastic component of the replication initiation (Tuduri et al., 2010). The stochastic firing was suggested to be required especially under perturbed conditions to rescue replication of arrest forks (Barberis et al., 2010).

How individual origins are selected to fire is still a matter of debate. In this regard, a pioneer study on origin relocalization have suggested that temporal activation might be determined by differences in chromatin landmarks (Ferguson and Fangman, 1992). It is now known that the epigenetic status of the chromatin plays a partial role in the regulation of the activation time (Aparicio et al., 2004; Heun et al., 2001b; Vogelauer et al., 2002). Consistent with this observation the heterochromatic regions, such as the late replicated telomeres, exhibit histone deacetylation marks (Pappas et al., 2004; Pasero et al., 2002).

Replication foci. Microscopy studies have observed a spatial association of origins of replication into foci of replication throughout S phase, both in mammals (Jackson and Pombo, 1998; O'Keefe et al., 1992) and in yeasts (Kitamura et al., 2006; Meister et al., 2007; Pasero et al., 1997). It has been suggested that the replication foci are created by topological reorganizations of the chromosome to facilitate/accelerate chromatin-template processes in nuclear space. In this regard, studies in mammalian cells have revealed that the down-regulation of the chromosome structural proteins (e.g. cohesins) increases the average inter-fork distance by reducing the assembly of origins in replication foci (Guillou et al., 2010). In budding yeast forkhead transcription factors

(Fkh1 and Fkh2) have been observed to regulate the timing of origin activation (Knott et al., 2012). As a general rule, the binding of Fkh1 factor positively regulates early firing origins while represses late origins. Moreover, 4C analysis have shown an Fkh-dependent enrichment in contacts between early centromeric origins. This study provided plausible candidates required for the replication factory formation in budding yeast. Other Hi-C studies have confirmed the model of the replication factory with the description of “stable topological domains” of replication timing (Eser et al., 2017; Pope et al., 2014). Notably, Ester and colleagues have analysed the clustering of centromere-proximal regions and they observed that only a fraction of these origins colocalize dependently of Fkh. Given that centromeres are associated into a stable cluster, part of these contacts between early regions may be a consequence of the Rabl organization, *per se*.

Although attractive, the model of the replication factory/domain has been recently questioned both in mammals and in yeast. First, super-resolution microscopy studies have shown that replication foci are consequences of single replisome progression (Saner et al., 2013; Chagin et al., 2016). Second, single-cell Hi-C in mammal has shown that TADs are not permanent replication domains, on the contrary they dissolve during replication (Nagano et al., 2017).

These observations will be further discussed later in this manuscript and in light of our results (see chapter 2.3).

1.3.2.2 DNA damage response at replication forks

DNA replication is a startling complex step during the cell cycle, that needs to be constantly monitored to preserve replication forks (RFs) integrity. RF progression can be slowdown and/or arrest at different replication fork blocks (RFBs) (Branzei and Foiani, 2010a). In budding yeast as well as in other eukaryotes, natural impediments of replication forks have been identified (Mirkin and Mirkin, 2007). These include centromeres, tRNA genes, *Ty* long terminal repeats (LTRs), the repeated rDNA locus, the heterochromatic/silenced loci (e.g. HML and HMR mating cassettes), late replication zones (e.g. telomeres) and at-risk motifs (ATMs) (Lambert and Carr, 2013). These “naturally difficult to replicate” loci employ different mechanisms to obstacle DNA synthesis. For instance ATM sequences can give rise to secondary structures, such as: long tri-nucleotide repeats, palindromic sequences (Lobachev et al., 2007) or GC rich motifs forming G-quadruplexes (Lopes et al., 2011), which are known to stall the DNA polymerase. Non-histone protein/DNA binding sites, such as: Fob1/*RFB* in the rDNA locus of budding yeast (Brewer and Fangman, 1988; Kobayashi and Horiuchi, 1996),

Rtf1/*RTS1* upstream mating type locus in fission yeast (Dalgaard and Klar, 1999) and Tus/*Ter* replication termination system in *E. coli* (Hill et al., 1987), are all well characterized programmed replication blocks. Finally, products of DNA metabolic processes (e.g. DNA/RNA hybrids associated with highly transcribed regions) can give rise to replication–transcription clashes that have also been shown to interfere with replication progression (Lin and Pasero, 2012). At RFB the replisome, replication machinery in complex with the stalled fork, is typically stabilized (Lopes et al., 2001a). This mechanism protects the nascent DNA ends and allows either to “resume” replication once the block is removed or the fork to be “rescued” by an incoming fork from a neighboring replication origin (Cobb et al., 2003a; De Piccoli et al., 2012). However, not all arrested forks are efficiently stabilized and some eventually collapse, freeing single-stranded DNA (ssDNA) and/or double-stranded DNA (dsDNA) ends (Sogo et al., 2002). These structures carry potential recombinogenic consequences and can lead to chromosomal rearrangements (Carr et al., 2011; Magdalou et al., 2014). For instance, ectopic insertions of programmed protein/DNA RFBs have been found to increase recombination rate and give rise to deletions (Tus/*Ter* in *E. coli*, Bierne et al., 1997) and gross chromosomal rearrangements (Rtf1/*RTS1* in *S. pombe* (Lambert et al., 2005).

Experimental and empirical evidences point at several prominent mechanisms to account for rearrangement formation following replication fork stalling and collapse (Figure 12). The pathway of choice during replication is the homologous recombination (HR) repair (Ira et al., 2004; Pâques and Haber, 1999; Truong et al., 2014). The HR uses the information provided by the genetically identical, or almost identical, DNA molecules (usually provided by the sister chromatid) to repair damaged DNA. HR is initiated by a ssDNA 5' → 3' resection followed by the assembly of the Rad51 protein on the presynaptic filament, which can give rise to three fork stabilization and restart mechanisms (Shinohara et al., 1992). In the first mechanism, a stalled fork structure might undergo fork regression - re-annealing of the excessive ssDNA by pairing the newly synthesized strands - to form a Holliday junction structure called “chicken foot” (Long and Kreuzer, 2008; Lopes et al., 2001b). In the second mechanism, the Holliday junction facilitates fork restart by strand invasion, forming a displacement loop (D-loop) (Seigneur et al., 1998). In a D-loop, one strand of a dsDNA molecule is displaced by a third strand of homologous sequence, which is the newly synthesized strand. In the third mechanism, the Holliday junction is processed into a DSB and fork restart is achieved through D-loop formation and resolution of homologous sequences (Michel et al., 2004; Neelsen and Lopes, 2015).

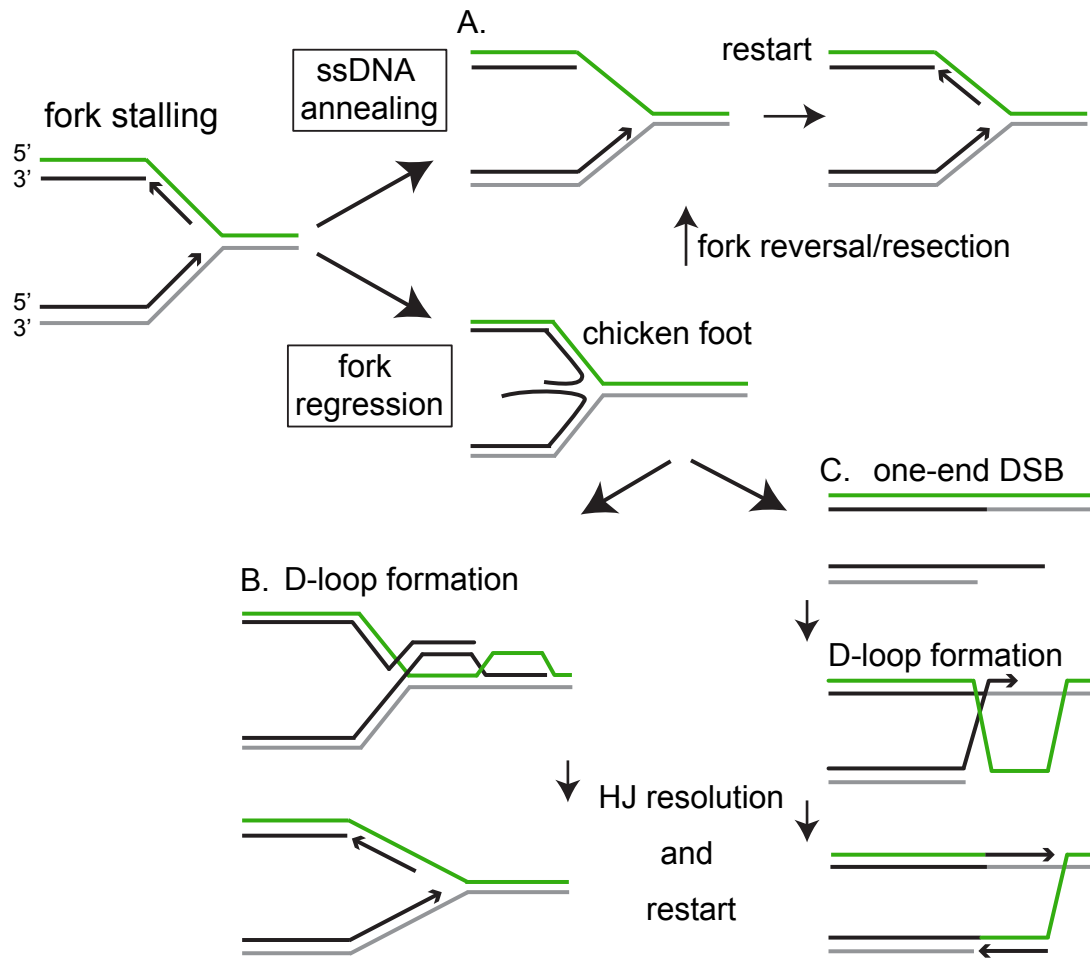


Figure 12 Mechanisms of replication fork restart. (A) A stalled replication fork may be stabilized by the re-annealing of single-strand DNA (ssDNA) generated by excessive unwinding of the template, or may undergo regression and pairing of the newly synthesized strands to form a Holliday junction (HJ) in a structure termed a "chicken foot". Restart after HJ formation may be difficult, as it requires the removal and subsequent re-loading of the replisome. (B) HJ-mediated fork restart. The dsDNA end of the HJ is recombined with the template through strand invasion, forming a displacement loop (D-loop). This D-loop may facilitate the re-loading of the replisome. The invading strand results in the generation of a HJ. Replication restart occurs when the HJ is removed, by either HJ resolution or dissolution. (C) Double-strand break (DSB)-mediated restart. The HJ is processed into a one-ended DSB and fork restart is achieved through homologous recombination repair of the DSB in a mechanism involving D-loop formation and restart after HJ resolution. Leading and lagging strands are shown in grey and green, respectively.

Other mechanisms to restart replication, independently form the HR, but still relying on short sequence homology is the micro-homology/microsatellites induced replication events (MMIR, MMBIR)(Hastings et al., 2009a; Ira and Haber, 2002; Payen et al., 2008). These mechanisms envisage the annealing of the free ssDNA end (at the collapsed fork) on an exposed ssDNA region of micro-homology (a few nucleotides in length), that might be located on an adjacent replication fork. Improper strand invasion events can result in large structural changes leading to copy number variants, a major structural feature of mammalian genomes (Hastings et al., 2009b; Iraqui et al., 2012; Koszul et al., 2004; Lambert et al., 2010; Payen et al., 2014).

During replication, cells need to coordinate DNA synthesis with other cellular processes, such as chromatin reassembly, epigenetic modifications and establishment of cohesion between sister chromatids (Gunjan and Verreault, 2003; Mejlvang et al., 2013; Tittel-Elmer et al., 2012). It has also been observed that structural proteins, such as cohesin and condensin, maintain chromosomes integrity following replication stress (Jeppsson et al., 2014). The recruitment of these proteins to DNA breaks and stalled forks might stabilize fragile structures and aid the repair (Unal et al., 2007).

1.3.2.3 Sister chromatid cohesion during replication

Cohesin is a complex of four subunits – Smc1, Smc3, Scc1 and Scc3 – that are essential for sister chromatid cohesion (Michaelis et al., 1997; Uhlmann et al., 1999). Two of the cohesin subunits, Smc1 and Smc3, are members of the structural maintenance of chromosomes (SMC) family of proteins (two other members of this family, Smc2 and Smc4 involved in chromosome condensation, are discussed in section 1.3.3.4) (Figure 13A). All SMC proteins contain a long coiled-coil region flanked by a globular ATPase domain on one end, and a dimerization domain on the other. The dimerization domain allows two SMC proteins to form a ring-shaped dimer. The “kleisin” subunit, Scc1, bridges the Smc1-Smc2 heterodimer while Scc3 stabilizes this complex by binding to Scc1 (Gligoris et al., 2014; Haering et al., 2002). The ATP hydrolysis triggers conformational changes that might drive opening and closing of the ring (Figure 13B, C). SMC proteins contribute to numerous aspects of chromosome structure and dynamics along the entire cell cycle progression (Uhlmann, 2016).

To provide sister chromatid cohesion, cohesins must first be loaded onto chromosomes before S phase (Lengronne et al., 2004, 2006). Cohesin is initially loaded onto chromosomes in G1 and genome-wide studies have mapped these locations (Glynn et al., 2004). Cohesin is present all along chromosomes; however, it is not uniformly associated with all regions of the genome. Cohesin-associated regions (CARs, of 1–4 kb)

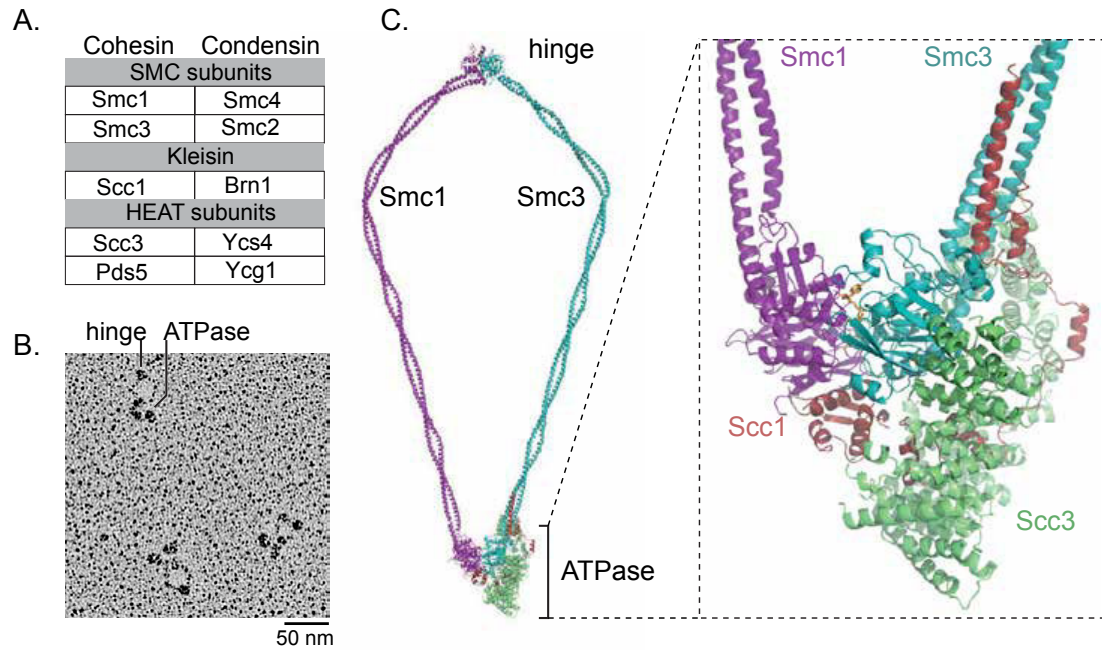


Figure 13 Architecture of cohesin and condensin complexes. (A) Overview of eukaryotic cohesin and condensin complexes and their subunits. The names are those used in budding yeast. Smc1-2-3-4, structural maintenance of chromosomes protein 1, 2, 3 and 4; Scc1-3, sister chromatid cohesion protein 1 and 3; Brn1, barren homologue 1; Ycg1, yeast cap G 1; Ycs4, yeast condensin subunit 4. (B) Electron micrograph of recombinant human cohesin tetramer complexes. (C) Composite model of a nucleotide-bound cohesin tetramer, incorporating available crystal structures. Cohesin and condensin ring circumference is made up of long stretches of coiled-coil of the two SMC subunits. The coiled-coil segments are connected at one end by a stable dimerization interface known as the “hinge”. At the other end the ATPase domains dimerize in the presence of ATP. An enlargement of the HEAD complex is shown. The exact location of Scc3 is speculative (adapted from Uhlmann, 2016).

are spaced at intervals of 10–15 kb along chromosomal arms, and tend to correlate with intergenic regions (Blat and Kleckner, 1999; Glynn et al., 2004; Laloraya et al., 2000). The most notable cohesin binding site is the large pericentromeric region (~25 kb), surrounding the small (125 bp) yeast centromere. The role of pericentromeric cohesin enrichment is to facilitate the proper biorientation of sister chromatids on the metaphase spindle during sister chromatid segregation (see section 1.3.3.1) (Ng et al., 2009). Experimental evidence have shown that cohesin complexes bind DNA dynamically in G1 (residence time of several minutes), whereas their stability increases after DNA replication (residence time of many hours) (Gerlich et al., 2006). This process is associated with the establishment of sister chromatid cohesion (Uhlmann et al., 1999). The structural mechanism by which cohesin hold chromosomes together is still under debate. The ring-like structure of the cohesin complex has led to propose the so called “embrace” model. This model suggests that the sister chromatids are embraced together within the cohesin ring. Whereas, other models, such as “snap” and “bracelet”, postulate that cohesin binds to the DNA of one sister chromatid and then oligomerizes with one or more cohesin molecules bound to the other sister chromatid (Huang et al., 2005). Altogether these studies have indicated that cohesins determine the topology of chromosomes both in *trans* by holding together sister chromatids, and in *cis* by forming long-range interactions in-between chromatid’s binding sites (Aragon et al., 2013; Mizuguchi et al., 2014; Sofueva et al., 2013).

These observations emphasize a structural reorganization of chromosomes in interphase, that culminates with the establishment of sister chromatid cohesion until their segregation in mitosis.

1.3.3 Chromosome segregation during M phase

The eukaryotic cell undergoes a dramatic reorganization during M phase. The structure of almost every subcellular compartment/organelle and macromolecule is altered so to prepare sister chromatids for segregation. These processes are under the control of the mitotic cyclin-Cdk complexes (M-Cdks) (see section 1.1.4.3; Figure 4). M-Cdks are responsible for the assembly of the mitotic spindle and its correct attachment to the replicated chromosomes (Alberts et al., 2002).

Mitosis is the central event of the M phase and consists in the equal separation of the duplicated chromosomes. In most eukaryotes, DNA damage in S phase or in G2 blocks the entry in mitosis. This mechanism avoids that the cell makes a potentially dangerous attempt to segregate damaged chromosomes. Conversely, in budding yeast mitotic entry is not a discrete regulatory transition. In the presence of DNA damage cells enter mitosis but arrest in metaphase. The molecular mechanism of this arrest most likely involves the system that activates sister chromatid separation at metaphase-anaphase transition (Morgan, 2007). This system involves the degradation of cohesins that hold together sister chromatids, after their duplication until they establish bipolar attachments to the mitotic spindle in metaphase (Yeh et al., 2008). Condensins, on the other hand, attempt to resolve sister chromatids by counteracting the cohesins (Guacci et al., 1997; Hirano, 2012; Renshaw et al., 2010). The products of the balancing acts of cohesins and condensins are metaphase chromosomes, in which the two chromatids are connected primarily at the centromere. In anaphase, this connection is released by the action of separase that proteolytically cleaves the remaining cohesins (Amon, 2001; Yu, 2002). The maintenance of this tightly-held chromatid state is a prerequisite for the accurate distribution of the genetic information into two daughter cells. Chromosomes need to be separated without tangling to avoid breakage during segregation (Baxter and Aragón, 2012).

These mitotic events and the mechanisms that govern the structural reorganization of the chromatin during segregation are discussed in the next paragraphs of this manuscript.

1.3.3.1 Mitotic entry: spindle assembly and pericentromeric chromatin

The molecular machine that provides the force to separate the two sets of chromosomes is the mitotic spindle. In contrast to higher eukaryotes, *S. cerevisiae* undergoes a closed mitosis, in which the nuclear envelope remains intact throughout mitosis. Yeast's spindle is a relatively simple structure that departs from protein complexes embedded

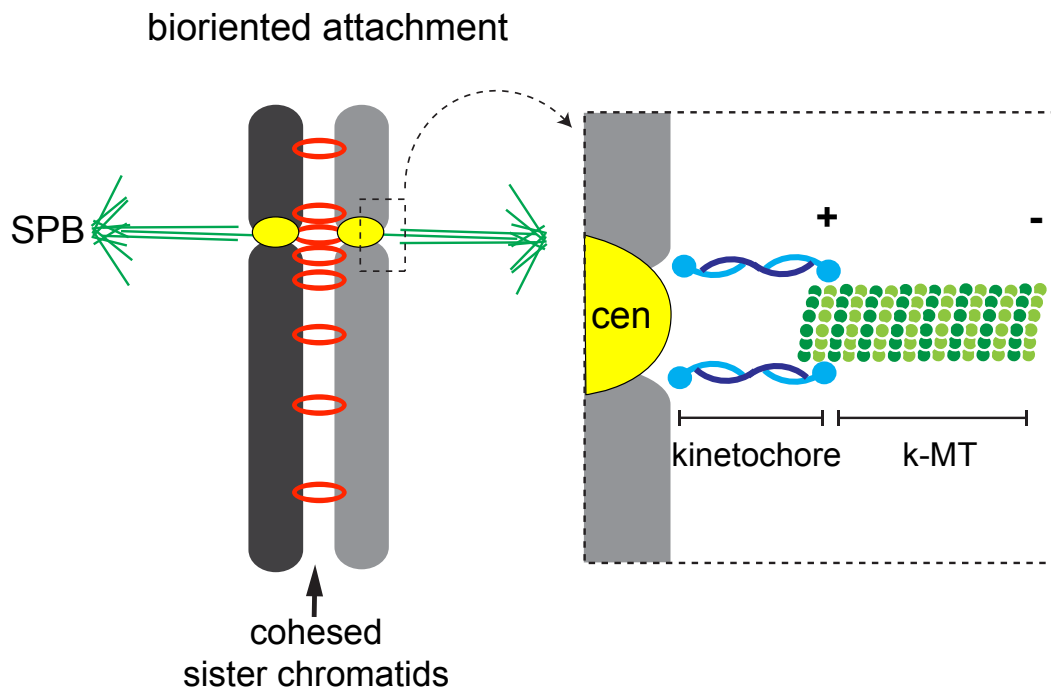


Figure 14 Bioriented attachment of mitotic chromosomes. Cohesed sister chromatids (cohesin, red circle) are attached at the level of the centromeres (yellow) by microtubules (green), originating from opposite spindle pole bodies (SPBs). Inset shows a magnification of the kinetochore-microtubule (k-MT) attachment. Tubulin dimers (α and β monomers; different shades of green) assemble to form oriented microtubule fibres with structurally different ends, “+” and “-”. The “-” end associates with the SPB while the “+” attaches the kinetochore (protein complex assembled on the centromere; different shades of blue).

in the nuclear envelope, called spindle pole bodies (SPBs, microtubule-organizing centre in yeast) (Jaspersen and Winey, 2004; Yoder et al., 2003). The spindle apparatus contains three types of microtubules. Short kinetochore microtubules (k-MT) are responsible for tethering centromeres anchored at the SPBs throughout the cell cycle (Kitamura et al., 2007). Long interpolar microtubules link the two SPBs and intersect in the spindle midzone. Whereas the astral microtubules extend away from the SPBs inside the cytoplasm and are involved in spindle anchoring and positioning inside the cell (Peterson and Ris, 1976; Winey and Bloom, 2012).

During entry into mitosis a bipolar array of interpolar microtubules nucleates and extends from the duplicated SPBs, causing the migration of the two SPBs towards the opposite site of the nucleus. Simultaneously, each chromatid has to be correctly attached to an individual k-MT via the kinetochore, a large protein complex that assembles on the centromeric DNA. The attachment of all sister chromatids has to occur in a bipolar manner or “biorientated”, with the two chromatids bound to k-MTs originating from opposite poles (Figure 14). As microtubule attachment to kinetochores proceeds through a random “search and capture” mechanism, it does not guarantee the proper sister chromatid orientation (Winey and Bloom, 2012; Winey et al., 1995). Dedicated surveillance mechanisms monitor the correct orientation of this process to ensure the faithful segregation of the chromatids (Gillett et al., 2004).

Cells determine if sister chromatids are properly attached and oriented on the spindle by monitoring the status of tension at sister-kinetochores. Tension is generated at kinetochores when cohesin complexes, linking together sister chromatids, resist the pulling force exerted by the microtubules (Stern and Murray, 2001).

The 16 kinetochore microtubules (~0.35 μm long) and the 4 interpolar microtubules (~1 μm long) yield ~20 μm of microtubule polymer in the spindle with an approximate mass of 3.25×10^6 kDa. The mass of the DNA in a cell is ~ 10×10^6 kDa, thus the spindle represents approximately 1/3 the mass of the DNA and only 1/6 the mass of the chromatin. This has raised questions about how the spindle alone can generate a force sufficient to promote chromatid segregation. Recently, it has been suggested that the pericentromeric chromatin (~25 kb around the kinetochore) constitutes the elastic component of the spindle (Figure 15). Interestingly, cohesin and condensin are three fold enriched in the pericentromeric chromatin where they may contribute to the elastic properties of this region (D'Ambrosio et al., 2008a; Glynn et al., 2004; Yeh et al., 2008). Moreover, they show distinct distribution patterns: cohesins are radially displaced from the spindle microtubules while condensins localize proximal on the spindle axis (Bachelier-Bassi et al., 2008; Yeh et al., 2008). It was suggested that this chromosomal

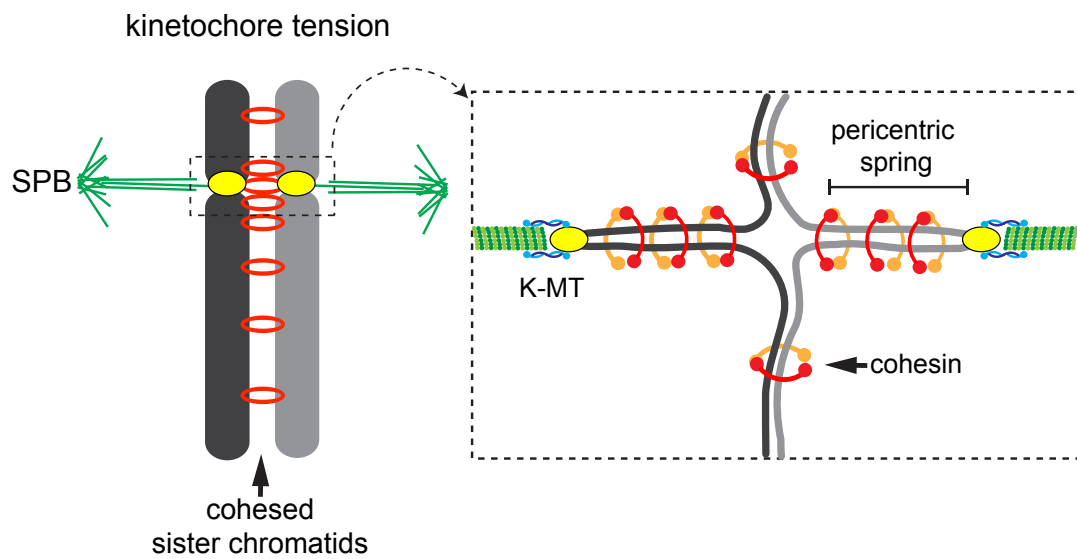


Figure 15 A spring of pericentromeric chromatin in metaphase. Bioriented attachment of cohesed sister chromatids (see Figure 14) generates kinetochore tension. Inset shows a magnification of the pericentromeric chromatin: cohesin rings are radially enriched around the centromere where they oppose the pulling force of the k-MT and contribute to the elastic properties of this region.

region is organized in “pericentric chromatin loops”, forming a molecular spring (Yeh et al., 2008). The spring is bound to the spindle at the kinetochore/microtubule interface and provides an inward force to counterbalance the outward-pulling force generated by the kinetochore and spindle (Winey and Bloom, 2012).

1.3.3.2 Metaphase to anaphase transition

Kinetochore-microtubule attachments that fail to generate tension activate the spindle assembly checkpoint (SAC) (Gillett et al., 2004; London and Biggins, 2014). SAC activation delays the metaphase-anaphase transition until all sister chromatids are properly bioriented on the spindle. For instance, the treatment with the microtubule disrupting agent nocodazole leads to SAC activation and causes cells to permanently arrest in a pre-anaphase (G2/M) state. Upon removal of nocodazole, cells rapidly reassemble the spindle and the chromosome biorientation (Jacobs et al., 1988a; Li and Murray, 1991). Only when tension is detected across all sister chromatids, SAC is deactivated and metaphase proceed into anaphase (Figure 16) (Ng et al., 2009; Stern and Murray, 2001). Cohesin cleavage marks the transition from metaphase to anaphase and requires the activity of anaphase promoting complex (APC) (Uhlmann et al., 1999; Visintin et al., 1997). This molecular machinery attaches ubiquitin to lysine residues and targets the associated proteins for proteasome degradation (Peters, 2002). APC activity is regulated by its association with the so-called “coactivators”, that are thought to present specific substrates to APC for ubiquitylation. In budding yeast, there are two possible coactivators, Cdc20 and Cdh1 (Visintin et al., 1997). Cdc20 is targeted by the SAC and becomes active at metaphase-anaphase transition, when the checkpoint is deactivated (Yu, 2002). APC-Cdc20 complex is responsible for triggering the degradation of the anaphase inhibitor known as securin (Pds1) that, consequently, releases separase (Esp1) (Ciosk et al., 1998). Esp1 is then free to cleave Scc1 subunit of the cohesin and trigger sister chromatid separation (Ciosk et al., 1998; Uhlmann et al., 1999). Thus, Cdc20 is essential for anaphase onset. Cdh1 is not required for chromosome segregation, but is activated later in the cell cycle where it promotes mitotic exit by targeting cyclins for degradation (Visintin et al., 1997).

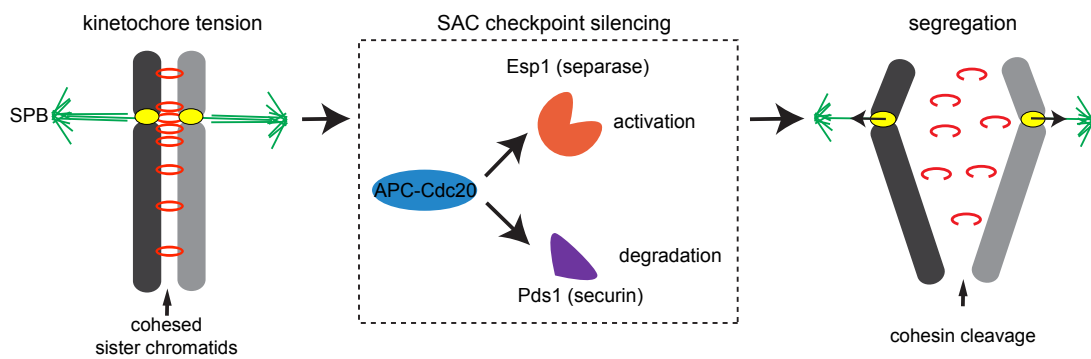


Figure 16 Chromosome segregation occurs at metaphase to anaphase transition. Kinetochore tension (see Figure 15) inactivates the spindle assembly checkpoint (SAC), that allows the anaphase promoting complex (APC) to bind to its coactivator, Cdc20. APC-Cdc20 leads to the degradation of securin (Pds1) and the release of the separase (Esp1). The activated Esp1 cleaves the cohesin rings and triggers the segregation of the sister chromatids.

1.3.3.3 Mitotic exit: early to late anaphase

The degradation of the mitotic cyclins by the APC-Cdc20/Cdh1 leads to a reduction of Cdk activity (Figure 17A) (Yeong et al., 2000). Whereas, the complete inactivation of Cdk is achieved with the activation of Cdc14 phosphatase, that triggers the crucial steps during mitotic exit (Visintin et al., 1998).

Many mitotic processes, such as chromatids segregation, nuclear positioning, mitotic spindle disassembly and cytokinesis are irreversible. Therefore, the activity of Cdc14 needs to be tightly coordinated with the rest of the mitotic events. One mechanism relies on changes in the subcellular localization of the phosphatase (Figure 17B). Until metaphase, Cdc14 is kept inactive in the nucleolus in complex with its inhibitor Net1 (Visintin et al., 1999). At the onset of anaphase, the fourteen early anaphase release (FEAR) network promotes a transient nuclear release of Cdc14 from its nucleolar inhibitor (see section 1.3.3.4). The active Cdc14 spreads in the nucleus and in the cytoplasm, where it dephosphorylates its substrates (D'Amours and Amon, 2004; Stegmeier et al., 2002; Yoshida et al., 2002). During later stages in anaphase, a sustained release of the phosphatase drives the conclusive mitotic exit, allowing cells to enter cytokinesis. After the exit from mitosis is completed, Cdc14 is re-sequestered in the nucleolus (Amon, 2008; Sullivan and Uhlmann, 2003).

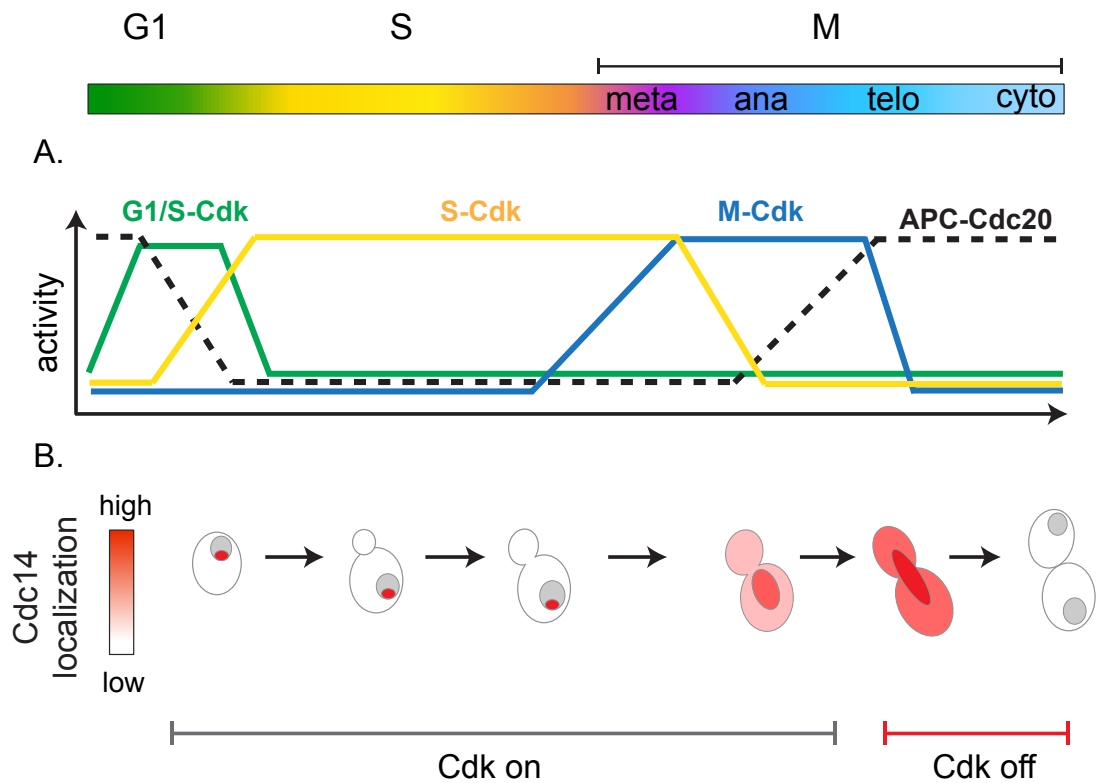


Figure 17 Temporal and spatial regulation of Cdc14 activation during the cell cycle progression. (A) Graph shows how the levels of the three major cyclin-Cdk complexes oscillate during the cell cycle progression (see Figure 4). (B) Cdc14 cellular localization. Inactive Cdc14 is sequestered inside the nucleolus (in complex with Net1, red plain circle) till anaphase, when a first release induces its enrichment in the nucleus and cytoplasm. A successive prominent release in late anaphase drives the mitotic exit. The main function of Cdc14 released, together with APC-Cdc20, is to inactivate M-Cdk (Cdk off) and exit mitosis.

1.3.3.4 Mitotic exit: rDNA condensation and segregation in anaphase

Here we focus on the role described for FEAR network in chromosome segregation, specifically in the segregation of heterochromatic/repetitive regions of the genome.

In 1917 Guilliermondii observed that the nucleolus of the yeast *Schizosaccharomyces octosporus* separates much later than the rest of the nucleus in meiosis. This observation has been confirmed in *Saccharomyces cerevisiae*, in which the repetitive heterochromatic sequences (e.g. telomeres and rDNA) show the same trend (Straight et al., 1997). Eukaryotic genomes contain many rDNA gene copies, ranging from hundreds to thousands in some plants, organized in tandem arrays and distributed among different chromosomes (Santoro, 2005). In humans, rDNA genes are located between the short arm and the satellite body of acrocentric chromosomes 13, 14, 15, 21, and 26. In budding yeast, rDNA genes are located chromosome 12 (chr12R) in a tandem array of 100–200 copies and represent almost 10% of the yeast genome (Figure 9; 18A) (Johnston et al., 1997; Yang et al., 1989). As Chr12 is the longest chromosome in yeast, a key issue with the segregation of the rDNA-bearing arm is the reduction of its size. During anaphase, this chromosomal arm is shortened to a length at least half the length of the anaphase spindle (Machín et al., 2005). An extensive characterization of the role of FEAR in chromosome segregation revealed that Cdc14 is activated during early anaphase and is necessary to promote the efficient segregation of the rDNA and telomeres, but not for the segregation of other regions of the genome (Figure 18B) (D'Amours et al., 2004; Sullivan et al., 2004). Several observations pointed out the possibility that Cdc14 mediates rDNA segregation by promoting the enrichment of condensins at this locus (Bhalla et al., 2002). As cohesins, condensins are members of the structural maintenance of chromosome (SMC) proteins (see section 1.3.2.3; Figure 13). Briefly, the backbone of these ring-like complexes is formed by members of the SMC family (Smc2 and Smc4) and is closed by kleisin proteins (Brn1) (Aragon et al., 2013; Haering et al., 2002). Unlike cohesins, which form inter-sister chromatids linkages, condensins are thought to build intra-sister linkages and stabilize chromatin loops (Cuylen et al., 2011). Condensins are highly enriched at centromeres, telomeres, tRNA genes and rDNA locus (D'Ambrosio et al., 2008b; Wang et al., 2005). Cells carrying mutation in subunits of the condensin complex exhibit nucleolar segregation defects similar to that of a Cdc14 loss of function mutant (Figure 18B; 19A, *smc2-8* and *ycg1-10*) (D'Amours et al., 2004; Strunnikov et al., 1995; Sullivan et al., 2004). CDC14 overexpression induces ectopic enrichment of condensin at the rDNA locus and ectopic rDNA segregation (D'Amours et al., 2004). Whereas, the inactivation of condensin in

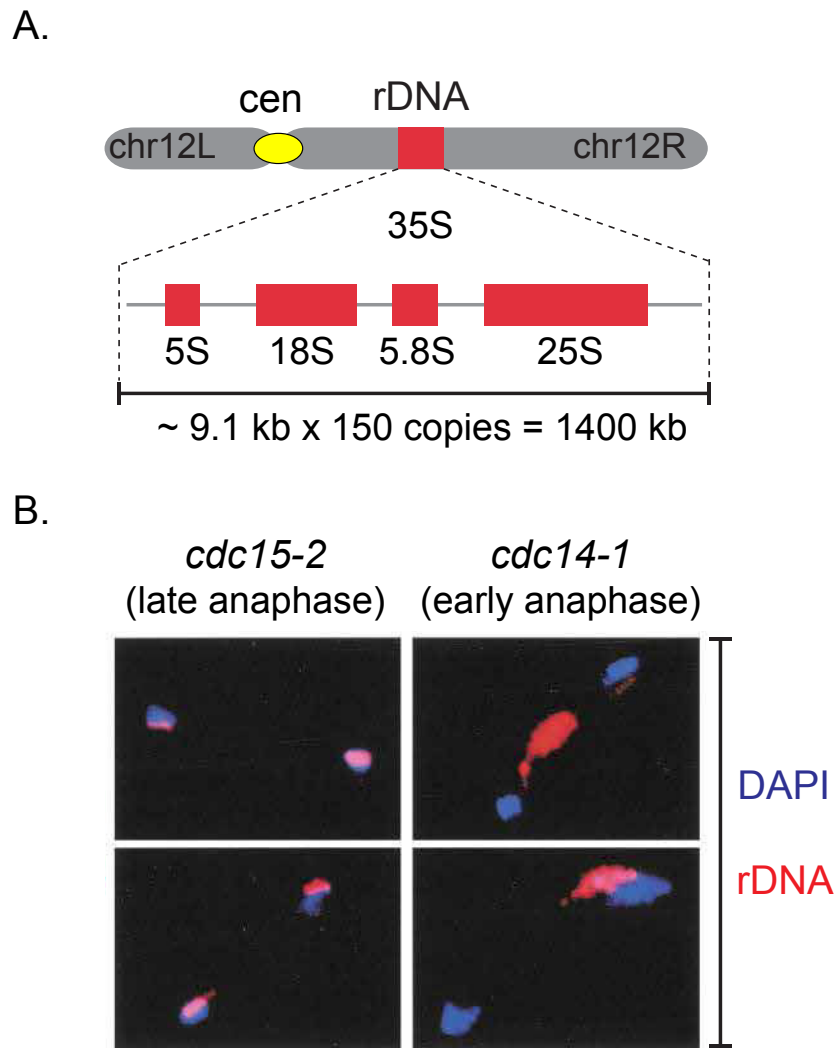
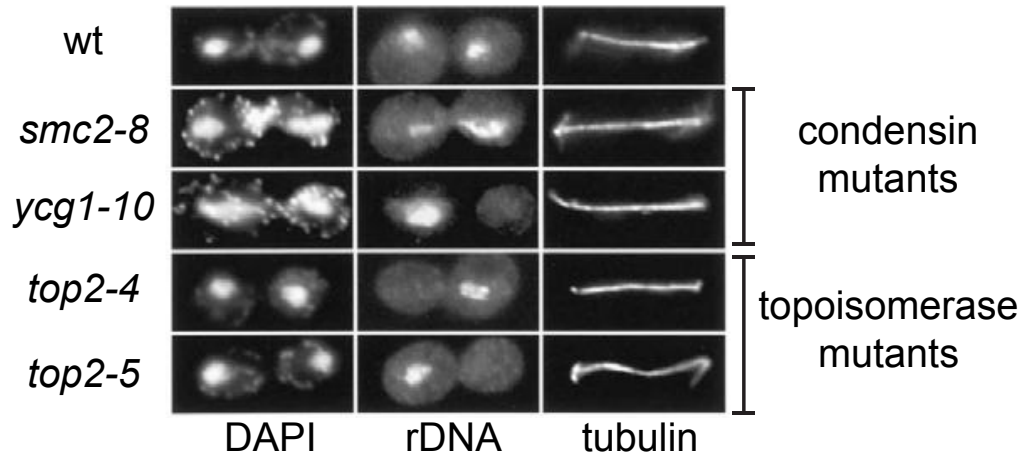


Figure 18 Cdc14 is required for rDNA segregation in late anaphase. (A) Schema shows the location of rDNA locus (red) on the right arm of chromosomes 12. This locus consists of approximately 150 copies of ribosomal RNA genes (5S, 18S, 5.8S, 25S), repeated in tandem and accounting for 1-2 Mb. (B) Representative FISH images of budding yeast cells show defects of rDNA (red) segregation in *cdc14* mutant, whereas the rest of the genome is not affected (blue). This segregation defect is absent in cells arrested in a later stage of anaphase (*cdc15*) (adapted from Sullivan et al., 2004).

CDC14 overexpressing cells prevents rDNA segregation (D'Amours et al., 2004). Furthermore, recently it has been shown that Cdc14 promotes the removal of RNA Pol I subunit from the nucleolus, thereby inhibiting the transcription of the rDNA in anaphase (Clemente-Blanco et al., 2009; Machín et al., 2006). The transcriptional silencing of rDNA genes (Cdc14-dependent) during anaphase is thought to be necessary for the condensins (e.g. Smc2 and Ycg1) to access and achieve condensation at the rDNA locus, from a "puff" to a "line" structure (Figure 19B).

Condensin binding to chromosome arms during anaphase enables supercoiling (Baxter et al., 2011) of stretched chromosomes and promotes the complete removal of residual cohesin (Renshaw et al., 2010). During this process of segregation, the action of condensin is assisted by other enzymes, such as topoisomerase 2 (Top2) that solves DNA topological problems, such as catenates (Nitiss, 2009). These can arise from difficulties to replicate regions (e.g. rDNA) or an excessive condensin-mediated supercoiling (Baxter and Aragón, 2012; Sullivan et al., 2004). It has been observed that Top2 mutations impede rDNA segregation but not its condensation (Figure 19A, B *top2-4* and *top2-5*) (Sullivan et al., 2004). This has led to the proposal that the condensin-dependent rDNA supercoiling may facilitate decatenation by Top2 (Baxter and Aragón, 2012; D'Ambrosio et al., 2008b).

A.



B.

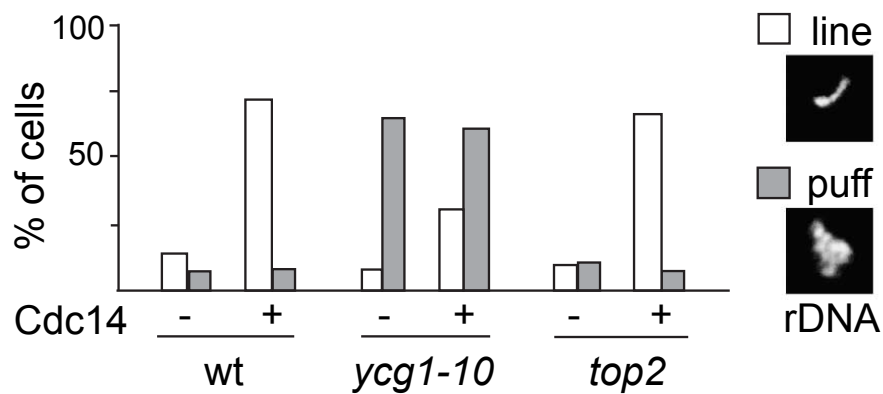




Figure 19 Condensin and Cdc14 are required for rDNA condensation and segregation. (A) Condensin (*smc2-8* and *ycg1-10*) and topoisomerase 2 (*top2-2* and *top2-5*) are required during anaphase for the resolution and segregation of the rDNA. (B) rDNA condensation (short line-like structures) in anaphase is dependent on Cdc14 and condensin but not on Top2 (adapted from Sullivan et al., 2004).

2. Results

Part 1 :

2.1 Chromosome dynamics during the cell cycle

Cohesins and condensins orchestrate the 4D dynamics of yeast chromosomes during the cell cycle

Luciana Lazar-Stefanita^{1,2,3,4}, Vittore F Scolari^{1,2,3}, Guillaume Mercy^{1,2,3,4}, Héloïse Muller^{1,2,3}, Thomas M Guérin⁵, Agnès Thierry^{1,2,3}, Julien Mozziconacci^{6,7,*}  & Romain Koszul^{1,2,3,**} 

Abstract

Duplication and segregation of chromosomes involves dynamic reorganization of their internal structure by conserved architectural proteins, including the structural maintenance of chromosomes (SMC) complexes cohesin and condensin. Despite active investigation of the roles of these factors, a genome-wide view of dynamic chromosome architecture at both small and large scale during cell division is still missing. Here, we report the first comprehensive 4D analysis of the higher-order organization of the *Saccharomyces cerevisiae* genome throughout the cell cycle and investigate the roles of SMC complexes in controlling structural transitions. During replication, cohesion establishment promotes numerous long-range intra-chromosomal contacts and correlates with the individualization of chromosomes, which culminates at metaphase. In anaphase, mitotic chromosomes are abruptly reorganized depending on mechanical forces exerted by the mitotic spindle. Formation of a condensin-dependent loop bridging the centromere cluster with the rDNA loci suggests that condensin-mediated forces may also directly facilitate segregation. This work therefore comprehensively recapitulates cell cycle-dependent chromosome dynamics in a unicellular eukaryote, but also unveils new features of chromosome structural reorganization during highly conserved stages of cell division.

Keywords chromosome segregation; Hi-C; loop extrusion; replication profile; SMC

Subject Categories Cell Cycle; Chromatin, Epigenetics, Genomics & Functional Genomics; DNA Replication, Repair & Recombination

DOI 10.15252/embj.201797342 | Received 21 May 2017 | Revised 29 June 2017 | Accepted 4 July 2017

Introduction

The chromosomes of prokaryotes and eukaryotes display multiple levels of hierarchical organization, whose dynamic changes influence or regulate metabolic processes including gene expression and DNA replication and repair (Taddei & Gasser, 2012; Wang *et al*, 2013; Dekker & Mirny, 2016). The improper coordination of chromosome condensation and segregation during the cell cycle can lead to important structural abnormalities and result in cell death or diseases such as cancer (Valton & Dekker, 2016). In recent years, major advances in imaging and chromosome conformation capture approaches (Dekker *et al*, 2002; Lieberman-Aiden *et al*, 2009; 3C, Hi-C) have complemented earlier work by describing at an unprecedented resolution the multiple hierarchical layers of genome organization. A variety of remarkable 3D chromosomal structures have been described in a number of species, including in unicellular organisms such as bacteria and yeasts.

The genome of budding yeast *Saccharomyces cerevisiae* presents a Rabl organization driven by (i) centromeres clustering at the spindle pole body (SPB, *S. cerevisiae* microtubule organizing center), (ii) telomeres tethering to the nuclear envelope, (iii) the nucleolus where the rDNA is sequestered opposite to the SPB, and (iv) chromosome arm length (Burgess & Kleckner, 1999; Taddei & Gasser, 2012). Hi-C experiments have confirmed this Rabl organization, but the existence of sub-megabase structures within yeast chromosomes similar to mammalian topological associated domains or their bacterial equivalent is still controversial (Duan *et al*, 2010; Hsieh *et al*, 2015; Eser *et al*, 2017). Importantly, genomic analysis of chromosome 3D architectures has usually been done using asynchronous populations, in which cells are found in various stages of the cell cycle. However, the initiation and progression of replication, followed by the segregation of the sister chromatids (SCs) into daughter cells, is expected to modify the genome higher-order

1 Institut Pasteur, Department Genomes and Genetics, Unité Régulation Spatiale des Génomes, Paris, France

2 CNRS, UMR 3525, Paris, France

3 Institut Pasteur, CNRS, Center of Bioinformatics, Biostatistics and Integrative Biology (C3BI), USR 3756, Paris, France

4 Sorbonne Universités, UPMC Université Paris 6, Complexité du Vivant, Paris, France

5 Laboratoire Télomères et Réparation du Chromosome, CEA, INSERM, UMR 967, IRCM, Université Paris-Saclay, Fontenay-aux-Roses, France

6 Sorbonne Universités, Theoretical Physics for Condensed Matter Lab, UPMC Université Paris 06, Paris, France

7 CNRS, UMR 7600, Paris, France

*Corresponding author. Tel: +33 1 44 27 45 40; E-mail: mozziconacci@lptmc.jussieu.fr

**Corresponding author. Tel: +33 1 40 61 33 25; E-mail: romain.koszul@pasteur.fr

organization. Recent studies have unveiled cell-cycle stage-specific genome-wide topological variations in bacteria, yeast, fly, and mammals (Naumova *et al*, 2013; Guidi *et al*, 2015; Marbouty *et al*, 2015; Hug *et al*, 2017). As expected, in all species the largest reorganization transition is associated with SC condensation, a fundamental process occurring concomitantly to their individualization, and facilitating their proper segregation.

Pioneer studies on yeasts proved essential to study these processes. Mutations in cell-division cycle (*cdc*; Hartwell *et al*, 1973) genes can block the cell cycle progression, enabling the study of global and/or local chromosome reorganization at specific cycle phases (Hartwell *et al*, 1973; Guacci *et al*, 1994; Sullivan *et al*, 2004; Renshaw *et al*, 2010; Rock & Amon, 2011). The evolutionary conserved structural maintenance of chromosomes (SMC) proteins bind to chromosomes and modify their structure in spatially and temporarily regulated manner during the cell cycle (Aragon *et al*, 2013; Uhlmann, 2016). Cohesins, such as *Scc1*, promote SC cohesion during DNA replication (Blat & Kleckner, 1999; Glynn *et al*, 2004) and get cleaved at the metaphase-to-anaphase transition (Uhlmann *et al*, 1999). At the same time, condensins such as *Smc2* are loaded onto SCs to facilitate their segregation (Renshaw *et al*, 2010; Stephens *et al*, 2011; Hirano, 2012). In fission yeast, the binding of SMCs modifies the level of chromosome compaction defined as the ratio between long (> 10 kb)- and short-range (< 10 kb) contacts at specific loci (Mizuguchi *et al*, 2014; Kim *et al*, 2016).

While Hi-C studies on mammalian and *drosophila* cells have confirmed this compaction change and provided important insights on the organization of mitotic chromosomes' internal structure (Naumova *et al*, 2013; Hug *et al*, 2017), no comprehensive analysis of the 4D dynamics of the chromosomes during an entire eukaryotic cell cycle has been achieved. To explore new chromosomal structural features over the cell cycle progression, we analyzed the internal folding and overall organization of *S. cerevisiae* genome over 15 synchronized time points and the role of cohesin and condensin using Hi-C (Dekker *et al*, 2002; Lieberman-Aiden *et al*, 2009). This analysis provides a broad overview and in-depth insight on SMC-dependent structural transitions resulting in chromosome individualization and segregation, including a potential role for a condensin-dependent loop in contributing to the segregation of the rDNA cluster.

Results

Comparison of chromosome contact maps of synchronized cells

Hi-C libraries were generated from cell cultures synchronized in G1 with elutriation (Marbouty *et al*, 2014) and/or arrested at different stages of the cell cycle through thermosensitive (*ts*) *cdc* mutations (Fig 1A; Hartwell *et al*, 1973). After sequencing, the corresponding normalized genome-wide contact maps were computed (bin: 5 kb; Fig 1C and D, left panels; Fig EV1; Materials and Methods; Cournac *et al*, 2012).

These 2D maps were translated into 3D representations to visualize the main folding features (Lesne *et al*, 2014; e.g., centromeres and telomeres clustering in G1; Figs 1B and EV1). These 3D structures are average representations of the contact frequencies quantified over a population of cells and therefore do not represent the

exact structure found in individual cells. For instance, on these 3D representations all the telomeres loosely cluster together. In a single nucleus, telomeres rather form small groups scattered all around the nuclear membrane (Taddei & Gasser, 2012). Since in different cells the composition of these clusters differs, all telomeres end up being regrouped together in the average 3D structure that reflects the population average of contacts. In addition, they are not polymer models and cannot be interpreted as such. Nevertheless, these representations conveniently highlight important structural features not readily apparent in the 2D maps (Mercy *et al*, 2017).

The differences between two conditions were determined by computing the log-ratio between the maps (bin: 5 kb; Fig 1C; Materials and Methods). The color scale reflects the variations in contact frequency for each bin between two different contact maps. The ratio of contact maps generated from two independent G1 cell populations (experimental replicates) displays a relatively homogenous white (i.e., null) signal, corresponding to little differences between them (Fig 1C, right panel). These minor variations between the maps result in occasional faint colored areas and reflect experimental noise (Appendix and Materials and Methods). On the other hand, the ratio between exponentially growing G1 and quiescent G0 cells contact maps (Fig 1D, right panel) shows a strong difference in inter-telomere contact frequencies, reflecting the formation of the telomeres hyper-cluster characteristic of the G0 metabolic state (Guidi *et al*, 2015; Fig 1D, black arrowheads).

Multiple maps can also be compared altogether by computing their pairwise distance matrix, showing that the genome organization of cells in anaphase (*cdc15*) differs the most compared to other time points (Fig 1E; Materials and Methods). The overall similarities/differences between datasets can then be summarized using principal component analysis (PCA; Fig 1F). This 2D representation shows that the experimental duplicates (such as G1, or anaphase *cdc15*) clustered together, while the distance increases progressively between G1 (obtained with either elutriation or *cdc6* *ts* mutant), metaphase (*cdc20*), and the distant anaphase (*cdc15*) datasets.

Altogether, these comparisons highlight major changes in chromosome higher-order architecture taking place in cells progressing throughout the cell cycle into metaphase and anaphase.

Cohesin-mediated compaction during S phase

To decipher the chromosome structural changes that take place during replication, synchronized G1 cells were released into S phase and Hi-C maps generated for six time points sampled from two independent kinetics (Figs 2A and EV2; Materials and Methods). The PCA reveals a progressive structural evolution from G1 to late S/G2 phase (Fig 2B). The dependency of the contact probability *P* on genomic distance reflects the chromosome compaction state (Lieberman-Aiden *et al*, 2009; Naumova *et al*, 2013; Mizuguchi *et al*, 2014). The *P*(*s*) shows a gradual and consistent enrichment in long-range intra-chromosomal contacts (> 20 kb) with respect to short-range (< 10 kb) during replication (Fig 2C). This compaction change is absent when replication is impaired, for instance, in the absence of the replication-checkpoint regulator *cdc6* (Piatti *et al*, 1995), even though cells enter mitosis and engage into segregation of non-replicated chromosomes (Fig 2D, left panel). The progressive increase in long-range contacts stops with the completion of S

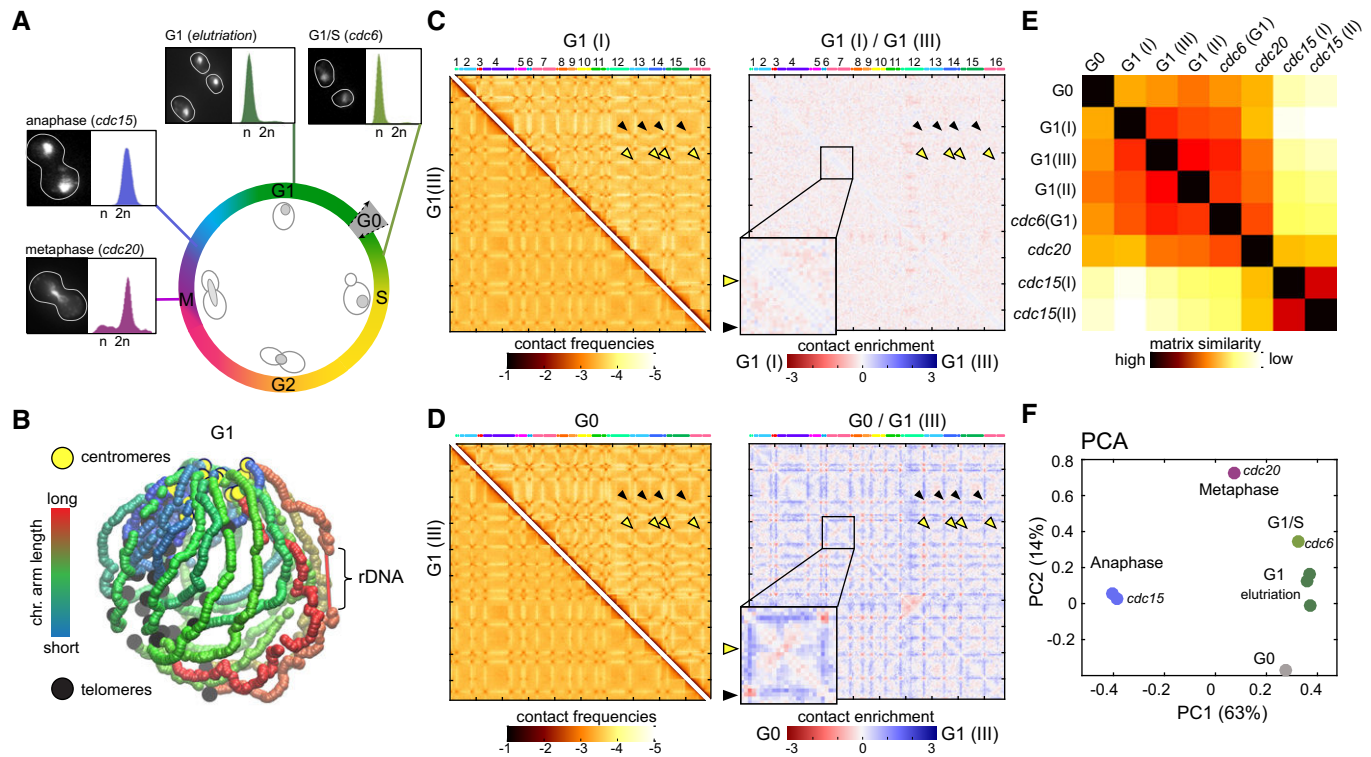


Figure 1. Comparison of genome structures recovered from five synchronized stages over the cell cycle.

- A Overview of the different synchronization time points with corresponding FACS profiles and representative images of DAPI-stained cells.
- B 3D average representation of the Hi-C contact map of a yeast G1 population. The color code reflects chromosomal arm lengths, and centromeres, telomeres, and rDNA are highlighted.
- C, D Comparison of contact maps. The 16 yeast chromosomes are displayed atop the maps. Black arrowheads: inter-telomere contacts. Yellow arrowheads: inter-centromeric contacts. Left panels: Hi-C maps obtained from two G1 cell populations synchronized independently (C) and from G1 and G0 populations (D). Brown to yellow color scales reflect high to low contact frequencies, respectively (\log_{10}). Right panels: log-ratio between each pair of maps. Insets display magnifications of chr4. Blue to red color scales reflect the enrichment in contacts in one population with respect to the other (\log_2).
- E Pairwise Euclidian distances between contact maps of populations of G0, G1 either synchronized with elutriation or blocked using a *cdc6* mutant, metaphase (*cdc20* mutant), and anaphase (*cdc15* mutant) cells. Color code: contact map similarity.
- F Principal component analysis (PCA) of the distance matrix in (E).

phase, when it reaches the level observed in cells arrested at the G2/metaphase transition (G/M) with the microtubule-depolymerizing drug nocodazole (Jacobs *et al*, 1988; Fig 2D, middle panel). The crossing of the $P(s)$ slopes from the early to late replication time points occurs around 10–20 kb (Fig 2C, highlighted in gray), a window within the range of the spacing reported between cohesin binding sites (~11 kb on average; Glynn *et al*, 2004), suggesting that this change in compaction could be due to cohesin activity. In agreement with the key role of cohesin in sister-chromatid folding during replication, Scc1 depletion using an auxin-inducible degron *scc1-aid* strain prevents the enrichment in long-range contacts in S/G2 (Fig 2D, right panel). This result supports the hypothesis that distant regions enriched in cohesin are tethered together, resulting in chromatin loops (Guillou *et al*, 2010).

Chromosome compaction is concomitant with chromosome individualization

The Scc1-dependent compaction occurs concomitantly with a gradual individualization of the SC pairs throughout replication, as shown by the overall increase in the ratio between intra- and

inter-chromosomal contacts from $63 \pm 10\%$ in G1 (six time points) to $73 \pm 4\%$ in S/G2 (four time points) and illustrated by the ratio between G1 and G2 maps (Fig 2E, top right ratio). In sharp contrast to this overall decrease in inter-chromosomal contacts, the centromeres of different chromosome tend to strongly cluster in G2. In the absence of the cohesin Scc1, intra-chromosomal contacts in G2 cells decrease to levels similar to or even below G1 (Fig 2E, bottom left ratio), while the major binding sites for cohesin (i.e., centromeres; Glynn *et al*, 2004) also exhibit a reduced level of contacts (Fig 2F; Appendix Fig S1). These results suggest that cohesins affect the genome organization through the gradual compaction of SC, the clustering of centromeres, and chromosome individualization. Although yeast chromosomes are shorter than mammalian chromosomes, they similarly change their internal conformation and individualize themselves prior to entering metaphase.

Spatial resolution of the replication timing program

In budding yeast, replication initiates at discrete autonomously replicating sequences (ARSs; Brewer & Fangman, 1987). ARSs display

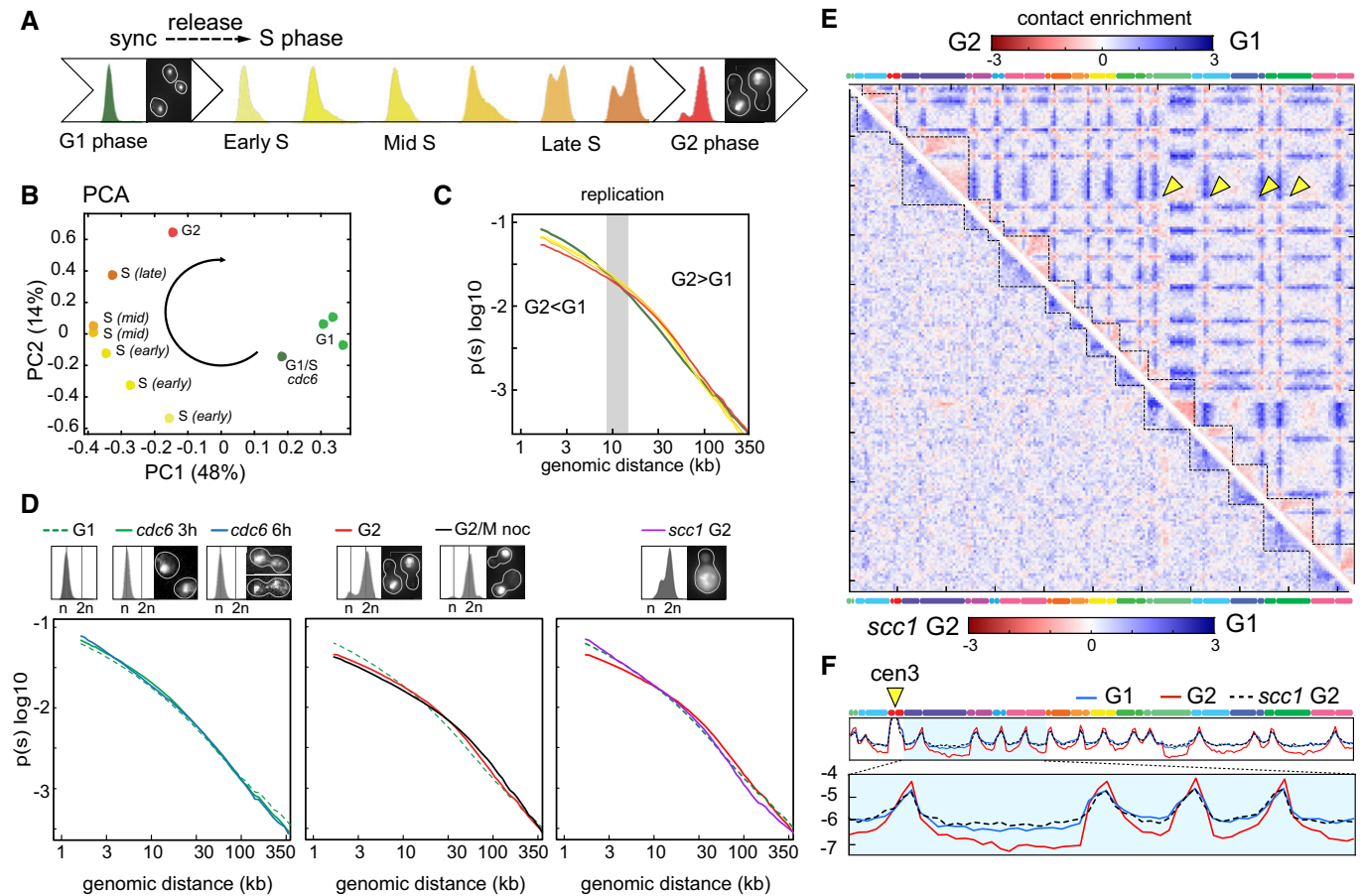


Figure 2. Dynamic reorganization of chromosomes during replication.

- A FACS profiles and representative DAPI-stained cells of G1 synchronized cells released in S phase.
- B PCA of the distance matrix between the contact maps of the population displayed in (A).
- C $P(s)$, that is, average intra-chromosomal contact frequency P between two loci with respect to their genomic distance s along the chromosome (log–log scale) during replication (color code identical to FACS profiles and PCA).
- D Left panel: $P(s)$ of replication-defective cells (*cdc6* thermosensitive mutant). G1 elutriated cells were released for 3 h and 6 h in non-permissive conditions. The corresponding FACS profiles show no S-phase progression. Middle panel: $P(s)$ of cells that completed replication. G1 elutriated cells were released in S phase in the absence or presence of nocodazole (G2/M noc). Right panel: $P(s)$ of cohesin-depleted (*scc1* G2) and nocodazole-arrested cells.
- E Log-ratio of contact maps between G2 and G1 cells (top right) and *scc1* G2 and G1 cells (bottom left). Blue to red color scales reflect the enrichment in contacts in one population with respect to the other (log2). Yellow arrowheads: inter-centromere contacts.
- F Normalized contact frequencies between chr3 centromere (*cen3*; yellow arrowhead) and the rest of the genome for G1, G2, and *scc1* G2.

partially stochastic activation, with only a subset of origins activated early during S phase. The distribution of early origins is uneven, with an enrichment in pericentromeric regions, and a depletion in subtelomeric regions. The genome-wide pattern of ARS activation timing defines a population-average replication timing program (Raghuraman *et al*, 2001). To investigate the link between genome organization and replication timing, the read coverage of the Hi-C libraries was used to compute the replication timing profile of the cell population for each of the time point, and follow their progression through S phase. The average profile correlates well with previously published pattern (Raghuraman *et al*, 2001; McCune *et al*, 2008; Fig 3A; Materials and Methods). To visualize the progression of replication on the higher-order architecture of the genome, we colored the 3D structures recovered from three early replication time points according to their replication progression status. The

superimposition of the three structures recapitulates intuitive properties of yeast replication program, with a “replication wave” propagating from the centromeric regions enriched in early origins, through chromosomal arms, and toward the late replicating subtelomeric regions (Fig 3B and C; red and blue signal, respectively).

We also asked whether our data support the proposed co-localization of adjacent early replication origins (Kitamura *et al*, 2006; Knott *et al*, 2012; Saner *et al*, 2013). We found a statistically significant enrichment in contacts between these positions and their surrounding regions, but whether it results from an active co-localization or from their positioning in the pericentromeric regions co-localized due to the Rab1 organization remains unclear (not shown). More analyses are required to solve this question and integrate the different observations.

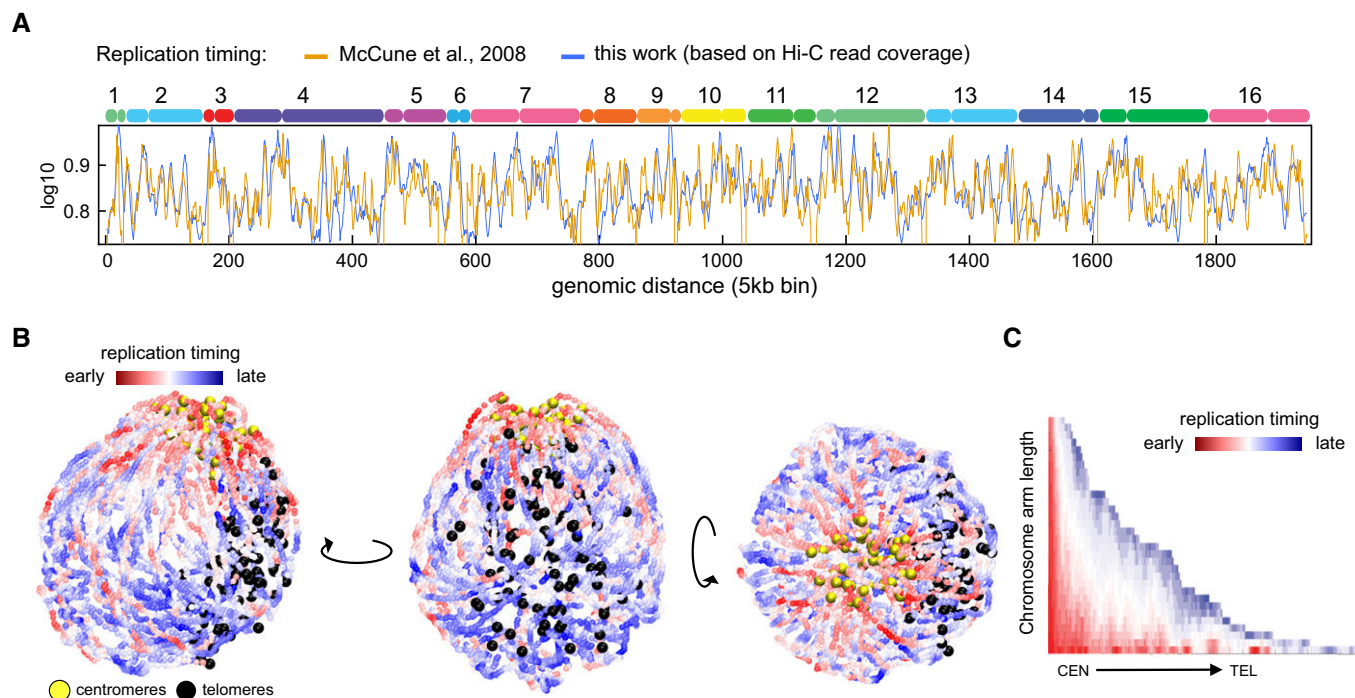


Figure 3. 3D replication profile.

- A Comparison of replication profiles of the synchronized populations used for the analysis displayed in Fig 2G. The read coverage of raw Hi-C libraries reflects the replication progression throughout S phase, plotted along the 16 chromosomes of the yeast genome (top axis; blue curve). The replication timing obtained in this study is highly similar to the one from McCune *et al* (2008) (yellow curve).
- B Superposition of three 3D representations of chromosomes in early replication (I, II, III). The color scale indicates the replication timing. Centromeres and telomeres are highlighted. Different views of the structure are presented.
- C Pattern of the replication profile for each of the chromosomal arms. The color code reflects the timing of replication.

Global structural changes during mitotic transitions

After replication, cells progress into mitosis (M phase). During metaphase, microtubules originating from opposite SPBs attach to the kinetochores of the two SCs (London & Biggins, 2014). The anaphase-promoting complex (APC) co-activator Cdc20 is essential for the proper activation of separase, resulting in the cleavage of cohesin and SC segregation in anaphase (Uhlmann *et al*, 1999; Visintin *et al*, 1997; 20). In the absence of Cdc20, cohesins are not cleaved and cells remain blocked in metaphase. Another key player in mitosis progression is the Cdc15 kinase which promotes mitotic exit at the end of anaphase by activating cytokinesis (Rock & Amon, 2011). In the absence of Cdc15, cells are therefore blocked into late anaphase. The higher-order changes in the organization of chromosomes that take place during metaphase and anaphase were investigated using populations of cells synchronized with conditional mutants of *cdc20* and *cdc15*, respectively. Contact maps of *cdc20*-, *cdc15*-, and *cdc15*-arrested cells released into permissive conditions were generated to characterize chromosome reorganization throughout M phase (Figs 4A and EV3; Materials and Methods). PCA shows that the major structural change occurs during mitotic exit and that cells released from the *cdc15* arrest display after 60 min a G1-like genome structure, reflecting the fact that the entire cell cycle is now covered by our analysis (Fig 4B). The $P(s)$ reveals a strong increase in short-range contacts (< 10–20 kb) from G2 to anaphase,

exceeding G1 levels which are only restored after anaphase completion (Fig 4C, left panel). This increase in short-range contacts and the accompanying drop in long-range contacts suggest the formation of an elongated, stretched structure. Upon spindle destabilization using the microtubule-depolymerizing drug nocodazole in *cdc15*-arrested cells (*cdc15 noc*), the two segregated chromosomal masses get closer as shown by imaging of DAPI-stained cells (Fig 4C, inset; Fig EV4; Materials and Methods), in agreement with former reports (Jacobs *et al*, 1988). In these cells, the stretched chromosomal structure disappears as shown by a $P(s)$ that now overlaps the G2 curve (Fig 4C, right panel). Besides the change in $P(s)$, the global contact pattern of *cdc15*-arrested cells remains unaltered following nocodazole treatment (Fig 4D, upper right ratio). Altogether, these results show that microtubule-dependent segregation forces contribute to the stretching the chromosomes in anaphase, possibly in combination with additional constraints resisting this force such as the cohesion of SC arm extremities (see Discussion).

Nocodazole affects chromosome 12 conformation

Nocodazole is commonly used to synchronize cells at the G2/M transition. We took advantage of having contact maps of *cdc20*-arrested cells in metaphase to compare them with those obtained from nocodazole-arrested cells (Fig EV4; Materials and Methods). The ratio map appeared globally similar, although we noticed in the

presence of nocodazole a small drop in inter-chromosomal contacts (Fig 4D, bottom left ratio). Chromosome 12 (chr12) also presents a peculiar signal at the level of the rDNA cluster (Fig 4E, left panel), with an enrichment in contacts between the two flanking regions of the rDNA cluster in G2/M nocodazole-treated cells compared to

cdc20-arrested cells (Fig 4E, right panel). These results indicate that the G2/M nocodazole arrest is associated with a destabilization of the chr12 structure at the level of the rDNA locus. The intra-chromosomal contact increase within chr12 is also accompanied by a global decrease in inter-chromosomal contacts in the presence of

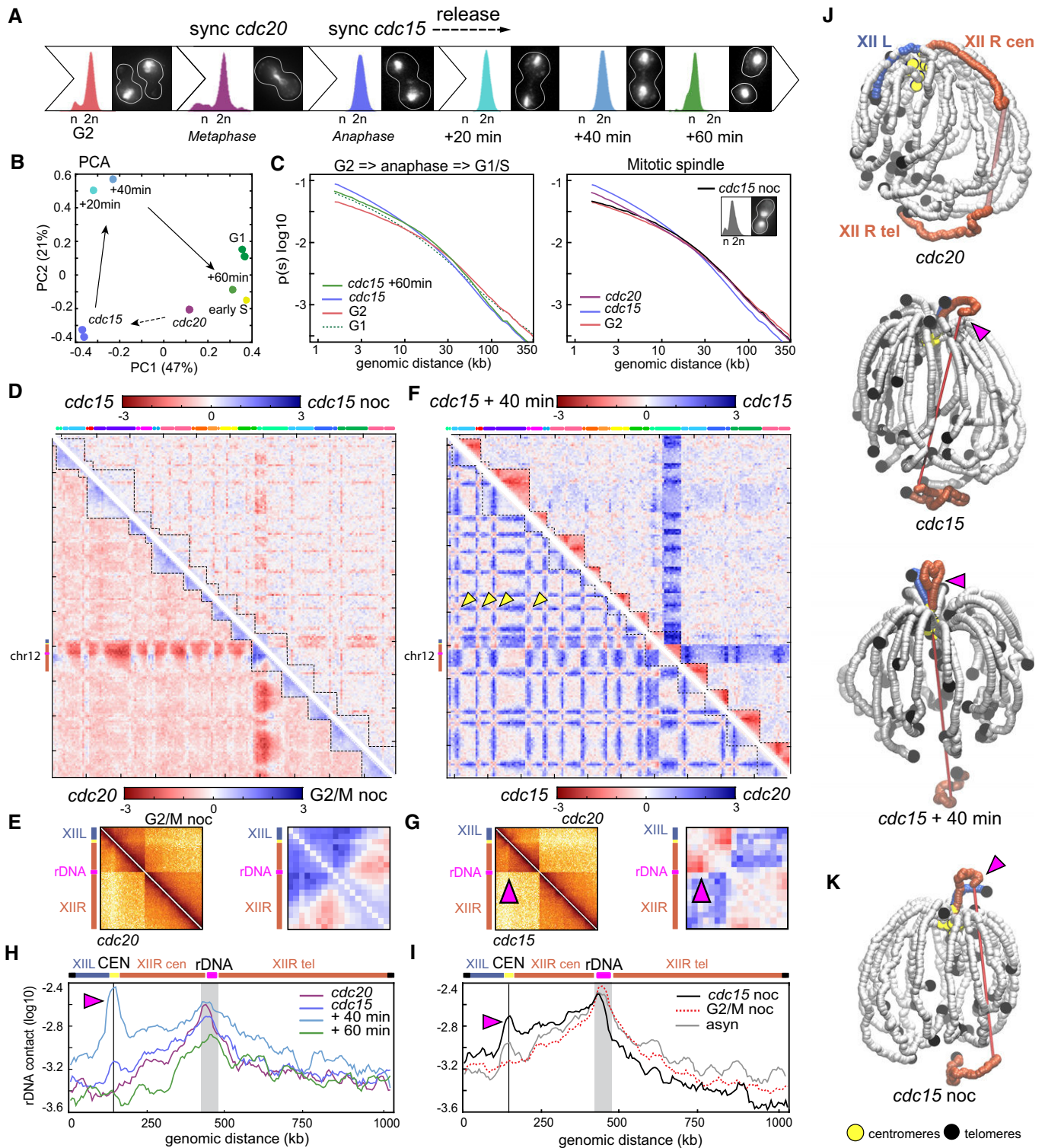


Figure 4.

nocodazole (Fig 4D, bottom left ratio). Remarkably, chr12 organization was not affected when *cdc15*-arrested cells were treated with nocodazole (Fig 4D, top right ratio). Altogether, these observations point to a role for the microtubule array in maintaining the organization of the nucleolus inside the nucleus, before its segregation in anaphase. In summary, while chromosome structures are overall similar in cell synchronized in G2 by nocodazole or in a *cdc20* ts mutant, nocodazole-arrested cells present a slightly different nucleolus structure (and, by extension, chr12). One interpretation could be that the condensation of the rDNA is not yet completed in G2/M nocodazole arrest and that as a result, rDNA flanking regions are freer to contact each other's.

Chromosome 12 looping during anaphase

The comparison of *cdc15* and *cdc20* maps shows an increase in centromere clustering in anaphase, leading to the formation of a prominent polymer brush structure (Daoud & Cotton, 1982; Fig 4F, bottom left ratio, yellow arrowheads). Such increase is in agreement with the role of condensin in forming a “spring” of chromatin at pericentromeric regions at the metaphase-to-anaphase transition (Stephens *et al*, 2011). Surprisingly, a peculiar loop pattern appears on chr12 in *cdc15*-arrested cells, bridging the centromere and the centromere-proximal left flanking region of the rDNA cluster (see pink arrowheads in Fig 4F, G and H). Upon release from the *cdc15* arrest, the telomere-proximal right flanking region of the rDNA cluster becomes strongly isolated from the rest of the genome (Fig 4F, upper right ratio; *cdc15*+40 min), while the contacts of the centromere-rDNA loop intensify (Fig 4H; *cdc15*+40 min). After completion of mitosis and re-entry in interphase (*cdc15*+60 min), the loop disappears (Fig 4H). Interestingly, this loop can be seen in asynchronous populations while it is only present in anaphase (Fig 4I). 3D representations illustrate the dramatic reorganization of chr12 and the formation of the loop bridging centromeric region and the rDNA (Fig 4J, pink arrowheads). Microtubules are not required to maintain this loop in anaphase, since it remains present in *cdc15*-arrested cells treated with nocodazole (Fig 4D, upper right ratio; Fig 4I and K), suggesting that the left flanking region of the rDNA is physically bound through an unknown mechanism to the

centromeric regions. These results complement imaging studies showing that the rDNA exhibits a dense, line-like shape that extends throughout the nucleus at anaphase (2.1 SD, 0.2 μ m; Sullivan *et al*, 2004).

Condensin promotes dramatic reorganization of chromosomes during anaphase

The proper condensation and segregation of the rDNA cluster requires the nucleolar release of the Cdc14 phosphatase. Cdc14 mediates a shutdown of rDNA transcription, facilitating the loading of the Smc2 condensin and hence the condensation of the cluster (Yoshida *et al*, 2002; D'Amours *et al*, 2004; Sullivan *et al*, 2004, 14; Machín *et al*, 2006; Clemente-Blanco *et al*, 2009). In addition, topoisomerase II (Top2), which decatenates the intertwining structures that appear between SCs during replication, is also required for rDNA segregation to proceed (Sullivan *et al*, 2004; D'Ambrosio *et al*, 2008; Baxter *et al*, 2011; Leonard *et al*, 2015). We investigated the influence of those factors on the 3D structure of the rDNA locus during anaphase (Figs 5A and EV5; Materials and Methods).

First, Smc2 depletion in *smc2-aid cdc15*-arrested strain affects anaphase genome organization by (i) reducing centromere clustering and (ii) suppressing the formation of the rDNA loop, with a resulting contact map highly similar to the *cdc20* map (Fig 5B, bottom left ratio). Therefore, condensins are responsible for the observed increase in inter-centromere contacts at anaphase compared to metaphase (Fig 4F, bottom left ratio), while they are also required for the formation of the loop bridging the centromere of chromosome 12 with the rDNA cluster (two loci enriched in condensin deposition). The *smc2 cdc15* and *cdc14* maps are strikingly similar (Fig 5C, bottom left ratio). The 3D representations of *smc2 cdc15* and *cdc14* cells (Fig 5E) and the rDNA contact plots with the rest of chr12 (Fig 5F) illustrate the loss of the rDNA loop in the absence of Smc2 and/or Cdc14. In addition to this effect, both mutants also display the same decrease in centromere clustering compared to *cdc15* cells (Fig 5C, upper right ratio; Fig 5G), pointing at their functional relationship on the same pathway.

The organization of the genome was also compared in *cdc15*-arrested cells in the presence or absence of Top2, *top2-aid*

Figure 4. Dynamic reorganization of chromosomes during mitosis.

- A FACS profiles and representative DAPI-stained cells of synchronized and/or released populations, from G2 until re-entry in G1/S.
- B PCA of the distance matrix between the contact maps of the populations described in (A).
- C Left panel: $P(s)$ of cells in G1, G2, and anaphase (*cdc15*) and released from a *cdc15* arrest (*cdc15*+60 min). Right panel: $P(s)$ of G2, *cdc20*-, and *cdc15*-arrested cells in the absence or presence of nocodazole (*cdc15* noc).
- D Log-ratio of contact maps. Bottom left: ratio between cells arrested in metaphase (*cdc20*) or at the G2/M transition with nocodazole (G2/M noc). Top right: ratio of cells blocked in anaphase and treated or not with nocodazole (*cdc15* noc and *cdc15*, respectively). Blue to red color scales reflect the enrichment in contacts in one population with respect to the other (\log_2).
- E Left: chr12-normalized contact maps of cells arrested at the G2/M transition and *cdc20*-arrested cells. Right: magnification of the log-ratio map from (D, bottom left).
- F Log-ratio of contact maps. Bottom left: log-ratio between *cdc20*- and *cdc15*-arrested cells. Top right: log-ratio of *cdc15*-arrested and *cdc15*-released (40 min) cells. Blue to red color scales reflect the enrichment in contacts in one population with respect to the other (\log_2). Yellow arrowheads: inter-centromere contacts.
- G Left: chr12-normalized contact maps in *cdc20*- and *cdc15*-arrested cells. Right: magnification of the log-ratio map from (F, bottom left). Pink arrowheads point at the right arm anaphase loop.
- H, I Distributions of intra-chromosomal contacts made by a 20-kb cen-proximal rDNA flanking region (highlighted in gray) with the rest of chr12 in *cdc20*-, *cdc15*-, *cdc15*-released (+40 min, +60 min), nocodazole-treated (G2/M noc, *cdc15* noc), and asynchronous (asyn) cells. Schematic representations of chr12 are displayed atop the graphs. Gray lines indicate centromere position. Pink arrowheads point at the right arm anaphase loop.
- J 3D representations of the contact maps from *cdc20*- and *cdc15*-arrested and *cdc20*- and *cdc15*-released (+40 min) cells. The right (XII R) and left (XII L) arms of chr12 are highlighted in red and blue, respectively. Pink arrowheads point at the right arm anaphase loop. Centromeres and telomeres are highlighted.
- K 3D representation of the contact map from *cdc15* noc cells. Pink arrowhead points at the right arm anaphase loop.

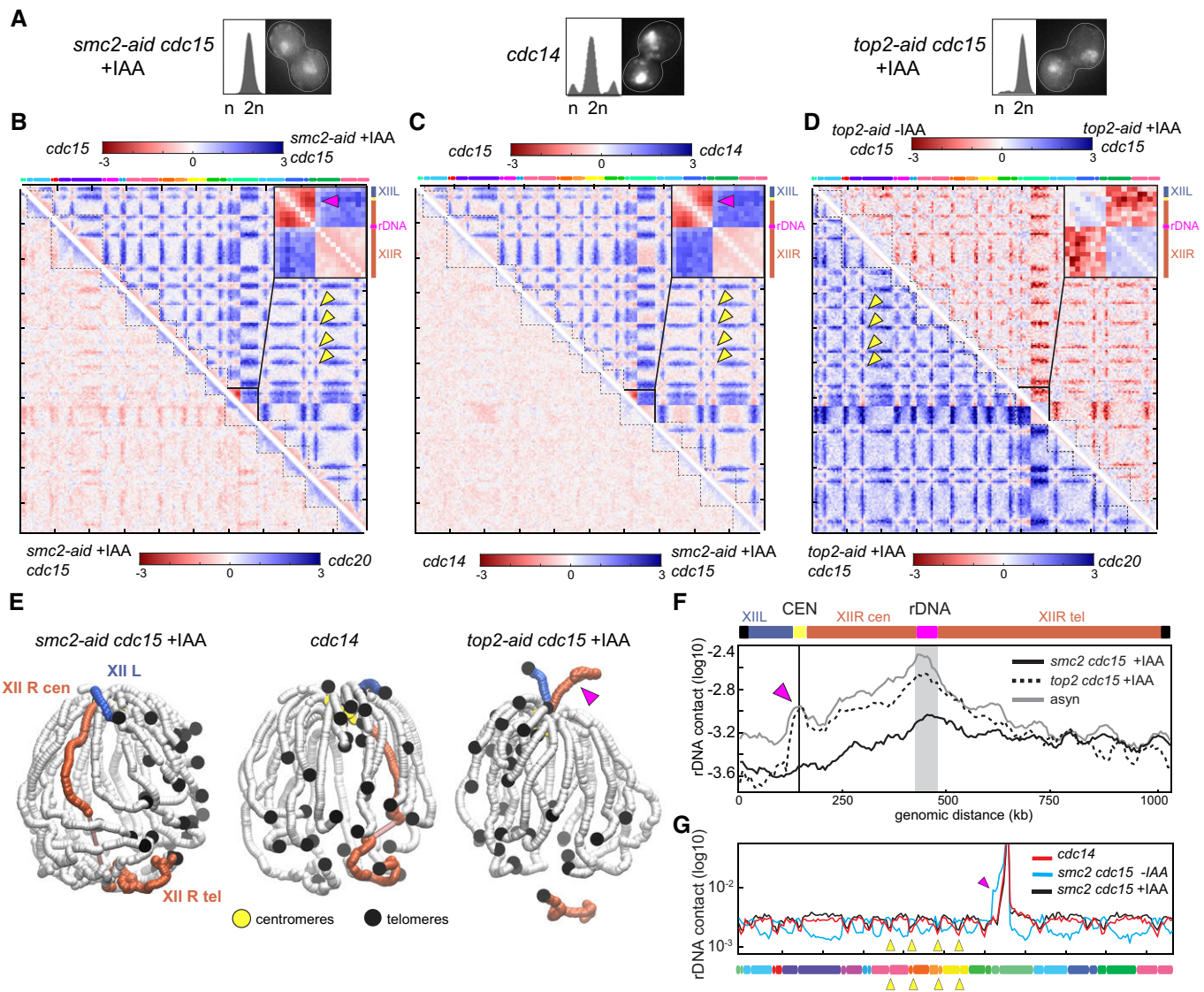


Figure 5. The anaphase rDNA loop is condensin-dependent.

- A** FACS profiles and representative DAPI-stained cells of cells blocked in anaphase, in the absence of condensin (*smc2-aid cdc15 +IAA* and *cdc14*) or topoisomerase 2 (*top2-aid cdc15 +IAA*).
- B–D** Log-ratio of contact maps. Yellow arrowheads: inter-centromere contacts. The pink arrowheads point at the right arm anaphase loop on chr12. Insets display magnification of the chr12 ratio map. (B) Ratio map between (bottom left) *cdc20* and *smc2-aid cdc15 +IAA* cells and between (top right) cells blocked in anaphase with or without condensin depletion (*cdc15* and *smc2-aid cdc15 +IAA*). (C) Ratio map between (bottom left) *cdc14* and *smc2-aid cdc15 +IAA* cells and between (top right) *cdc14* and *cdc15* cells. (D) Ratio map between (bottom left) *top2-aid cdc15 +IAA* and *cdc20* cells and (top right) *top2-aid cdc15 -IAA* and *top2-aid cdc15 +IAA* cells.
- E** 3D representations of the contact maps from *smc2-aid cdc15 +IAA*-, *cdc14*-, and *top2-aid cdc15 +IAA*-arrested cells. The right (XIIIR) and left (XIIIL) arms of chr12 are highlighted in red and blue, respectively. Pink arrowhead points at the right arm anaphase loop.
- F** Distribution of intra-chromosomal contacts of a cen-proximal rDNA flanking region (highlighted in gray) with the rest of chr12 in *smc2 cdc15*, *top2 cdc15*, and asynchronous (*asyn*) cells. Pink arrowhead points at the right arm anaphase loop.
- G** Normalized contact frequencies between the left rDNA flanking region (50 kb) and the rest of the genome in *cdc15 smc2-aid (-IAA)* and *cdc15 smc2-aid (+IAA)* cells. Yellow arrowheads point at a subset of centromeric positions. Pink arrowhead points at the right arm anaphase loop.

cdc15-arrested (Fig 5D, upper right ratio; Fig 5E and F; Materials and Methods). Top2-depleted cells display a strong decrease in contacts between the telomere–proximal region of chr12R and the rest of the genome (including chr12L). The signal is consistent with the essential role played by Top2 in rDNA segregation, showing that

the non-segregated regions are isolated from the segregated chromosomal sets. The comparison between *top2 cdc15* and *cdc20* cells reveals an enrichment in contacts at centromeres and the persistence of the centromere–rDNA loop in the Top2 mutant (Fig 5D, bottom left ratio). These results indicate that the formation of these

condensin-dependent structures in anaphase is independent from the decatenation and/or the segregation of the rDNA cluster.

Discussion

This study consists of an experimental and analysis framework to systematically investigate and compare chromosome folding and organization at different stages of the cell cycle. We applied Hi-C to populations of cells synchronized at different points of the cycle, generating genome-wide, 5-kb-resolution contact maps which unveil their average 3D genome organization. The global influence of cohesin, condensin, and topoisomerase 2 has been investigated in the corresponding mutants, as well as the effects of the microtubule-depolymerizing drug nocodazole. Comparative approaches between contact maps provided a global view of the structural transitions between the different stages of the cycle, some expected, such as

chromosome compaction during replication, and others that had not been described before, such as topological structures involving the rDNA cluster.

An overview of chromosome structural changes during the cell cycle can be summarized from centromere contacts, intra-/inter-chromosomal contact ratio, and short-/long-range contact ratio computed for each of the time points (Fig 6A).

Centromere clustering gradually increases during the cell cycle, through the establishment of sister-chromatid cohesion during replication, and through condensin-dependent clustering during anaphase (Fig 6A, upper panel). A potential consequence of this increased clustering in anaphase could be the generation of a stronger polymer brush, that is, the mechanical phenomenon that leads to the self-organization of a polymer tethered to a surface into stretched, non-intermingling structure (de Gennes, 1987). Interestingly, the strengthening of the polymer brush organization could consequently contribute to chromosome individualization during

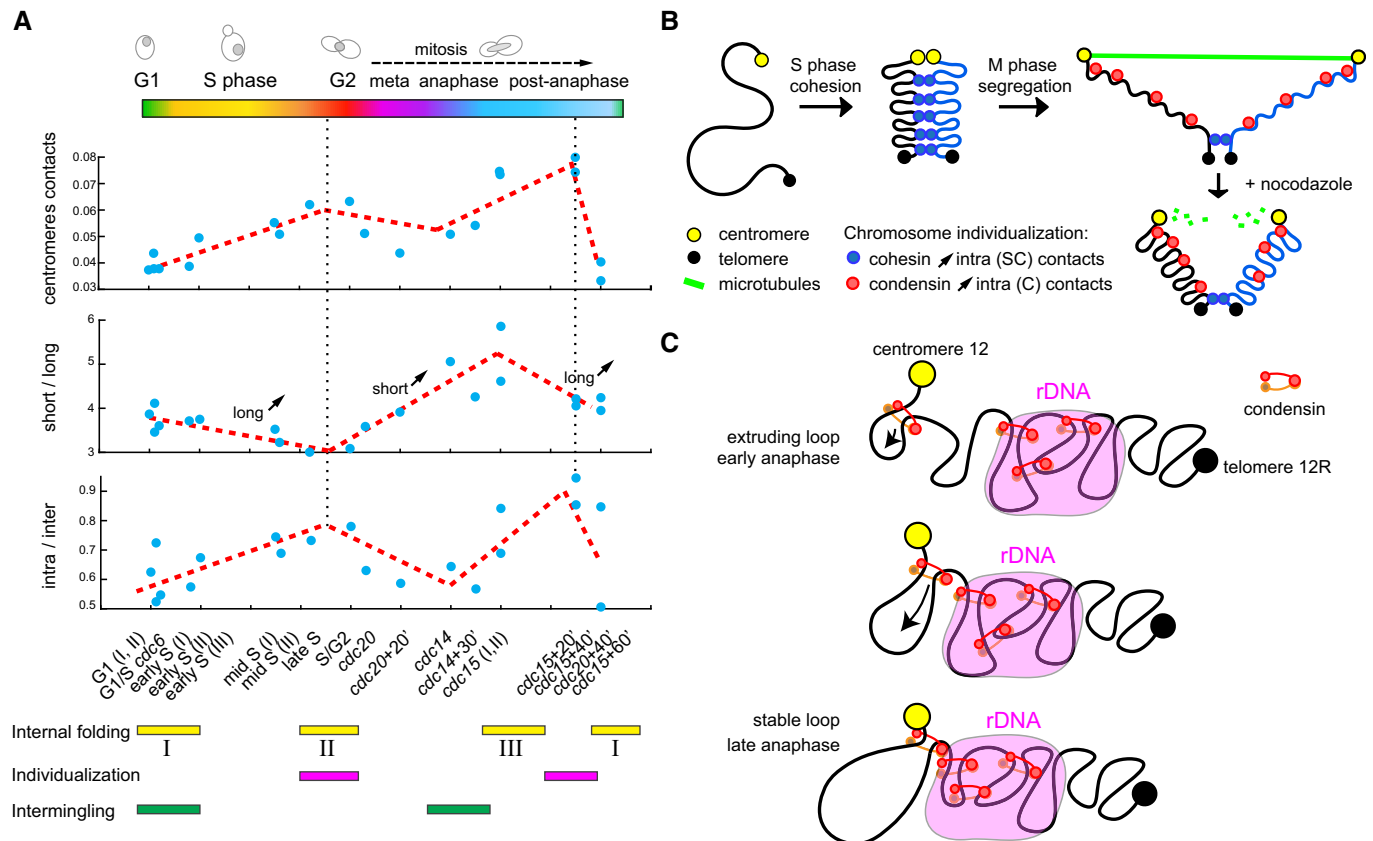


Figure 6. 4D reorganization of the yeast genome.

A Dynamics of centromere contacts (top panel), Short-/long-range contact ratio (middle panel) and intra-/inter-chromosomal contact ratio (bottom panel) for each of the 20 time points (blue dots; see bottom x-axis) during the cell cycle. The three folding states (I, II, and III; Fig EV4) identified in the analysis are indicated under the panels, as well as interpretation with respect to individualization status.

B Illustration of the three chromatin folding states characteristic of each of the cell cycle phases. Establishment of sister-chromatid (SC) cohesion during S phase increases intra-SC long-range contacts and leads to the individualization of the replicated chromosomes. Then during M phase, the two sisters are segregated and each chromatid (C) individualized thanks to the action combination of cohesin cleavage, condensin loading and spindle elongation. The chromosomes display a stretched internal structure, which relaxed upon destabilization of the spindle with nocodazole.

C Model of loop extrusion generating the condensin-dependent loop formation between the centromere and the rDNA cluster, two regions enriched in condensin deposition. A loop formed in between the centromere and the rDNA cluster may extend until it reaches these two discrete positions, and stall because of mechanic impediment blocking further extrusion.

anaphase. The intra-/inter-chromosomal contact variations reflect the successive phases of chromosome individualization and intermingling, with individualization taking place during replication (cohesin-dependent) and during anaphase (spindle-dependent; Fig 6A, bottom panel). The intra-/inter-chromosomal contact ratio correlates strongly with centromere clustering ($c = 0.72$, $p = 10^{-4}$), with both ratios peaking during anaphase exit.

Short-/long-range contact ratio recapitulates the three different internal folding (I, II, and III) states of chromosomes (G1, G2, and anaphase; Fig 6B, middle panel). These three states can be determined based on a quantitative analysis of the significance of changes between $P(s)$ curves obtained using several replicates in different phases of the cycle (Fig 7). During replication, cohesins mediate the compaction of chromosomes from state I to II. The chromosomes are then stretched by the mitotic apparatus during anaphase (state III) before returning to state I in G1. The mechanical constraint imposed by the anaphase spindle appears responsible for the state III stretching, as a nocodazole treatment results in relaxation of chromosomes, which switch back to state II. Imaging of the two sets of segregated chromosome during nocodazole treatment supports this spring relaxation effect, with the two masses being brought back together upon the depolymerization of microtubules. The nature of the mechanical constraints remains unknown, but it is tempting, in light of our observation of chr12 behavior (below), to propose a role for condensins in actively promoting this movement. In this scenario, condensins could favor the segregation of sister chromatids by pulling the chromosomes toward the centromere cluster. As a result, the loss of microtubule and tethering to the SPB may lead cohesin to actively pull back the segregated region together. We anticipate that whether condensins play an active role

in the segregation of chromosomes in addition to the pulling force imposed by the microtubule spindle will be thoroughly investigated in the years to come.

In addition, we also show that the two main regions of condensin deposition, *that is*, the centromeres and the rDNA locus, are bridged during anaphase through a condensin-dependent mechanism resulting in a loop-like structure on the right arm of chromosome 12. Whether this structure is systematically found in all cells, or only in a subset of the population, remains to be determined through single-cell imaging approaches such as FISH analysis. Although the precise mechanisms of formation remain unknown as well as its functional importance, we show that the setting up of the loop depends on condensin. Several mechanisms can be envisioned for the generation of this loop. One possibility is that starting from regions with a high condensin density, an active mechanism such as DNA extrusion through the action of condensins would pull the centromere and the rDNA cluster together (Fig 6C). Condensin depletion (leading to disruption of the loop) is associated with segregation defects. Overall, this structure therefore appears to *de facto* play a role in the segregation of the rDNA cluster, potentially through the application of a force that would drag the rDNA region to the centromere cluster before the completion of anaphase. A consequence of this model, would be that a similar loop extrusion mechanism could facilitate the segregation of other chromosomes as well. In this case, one or more loops could actively facilitate the segregation of large regions of chromosomes toward the tethered centromeres, down the telomeric regions. Chromosome 12, in this scenario, would appear as an exception with the large rDNA cluster generating a physical barrier in the middle of the right arm that is not present in other chromosomes. More experiments are nevertheless needed to investigate this proposed role. Yeast chromosome 12 could therefore prove a convenient model to study the action of loop extrusion mechanism (Alipour & Marko, 2012).

The importance of the rDNA loop remains to be further characterized as well as its similarity with loops found in other eukaryotic species. Overall, our exhaustive dataset opens new avenues for the comprehensive analysis of the 3D chromosome choreography during replication and segregation and brings to light new perspectives regarding these fundamental processes.

Materials and Methods

Media and culture conditions

All strains were grown in rich medium (YPD: 1% bacto peptone (Difco), 1% bacto yeast extract (Difco), and 2% glucose), except for YKL051 (*MET3-HA-CDC20*) that was grown in synthetic complete medium deprived of methionine (SC: 0.67% yeast nitrogen base without amino acids (Difco), supplemented with a mix of amino acids, uracil and adenine, and 2% glucose). Cells were grown at either 30°C or 23–25°C (the later temperature corresponding to the permissive temperature of the conditional thermosensitive mutations *cdc6-1*, *cdc14-3*, and *cdc15-2*; see below for details). Dataset corresponding to the quiescent state (G0) comes from already published data by Guidi *et al* (2015) and was obtained by carbon source exhaustion. All strains are described in Table EV1.

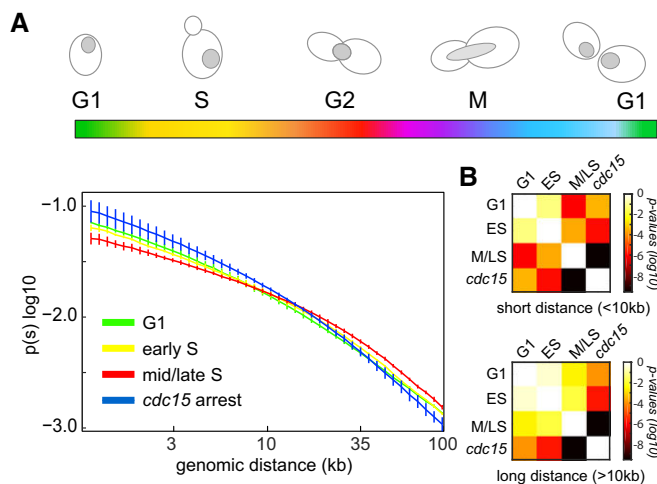


Figure 7. Variation in $P(s)$ for different phase of the cell cycle.

- A $P(s)$ for four different time points along the cycle. Each curve represents the average between three replicates with error bars corresponding to the standard deviation.
- B To assess the statistical significance of the differences between short (resp. long)-range contacts between these three time points, we computed a P -value for each pairwise comparison between two time points using Wilcoxon signed-rank test. The two distributions to compared were built by aggregating all the data points below (resp. above) 10 kb for the three replicates for each time point.

Elutriation (recovery of G1 cells)

To recover G1 daughter cells, the exponentially growing cultures were elutriated—a physical method of synchronization, used to separate cells according to their density and sedimentation velocity (see Appendix Supplementary Methods; Marbouty *et al*, 2014). The G1 daughter cells recovered through elutriation were suspended in fresh YPD at 30°C for 30 min, so they could recover from the elutriation procedure (i.e., stay in PBS). To minimize the potential variability introduced by the age heterogeneity of the bulk population, G1 daughter cells were used as starting point for all cell cycle synchrony and in combination with genetic and chemical synchronization methods (see below).

Release into S phase

G1 elutriated cells were released into S phase to analyze genome conformation during this stage. 2×10^9 G1 cells—originating from the same elutriated fraction to minimize heterogeneity in replication initiation—were inoculated into 150 ml YPD at 25°C (to slow down replication fork progression). Upon release, the synchronized cultures were sampled every 5 min and the cells analyzed through FACS, revealing an approximate lag of 130 min before replication restart. Therefore, aliquots were cross-linked and processed into Hi-C libraries at 135, 140, 145, 150, 155, 160, and 165 min. The progression of each fraction throughout the S phase (from G1 to G2) was monitored with flow cytometry.

Synchronization through thermosensitive mutations

Synchronizations using thermosensitive (ts) *cdc* strains (Hartwell *et al*, 1973) were all performed starting from elutriated G1 daughter cells growing in non-permissive temperature conditions designed to arrest the progression of the cycle at specific phases. See Appendix Supplementary Methods for details of synchronization procedures of strains YKL052 (*cdc14-3*), YKL053 (*cdc15-2*), and YKL054 (*cdc6-1*).

Synchronization through chemical compounds

Chemical synchronization was also performed on elutriated G1 daughter cells.

Synchronization at the G2/M transition was achieved by restarting G1 cells (strain YKL050) in YPD at 30°C for 1 h, followed by the addition of nocodazole (Calbiochem; 15 µg/ml) and incubation for another 2 h at 30°C. Cells arrested in G2/M with nocodazole were either processed into Hi-C libraries, or washed and inoculated in fresh YPD medium at 30°C. The washing of nocodazole allowed G2/M synchronized cells to proceed into M phase (cells sampled after 20, 45, 60 and 90 min were processed into Hi-C libraries).

To investigate the constraints imposed by the spindle during anaphase, elutriated YKL053 cells were elutriated and the recovered G1 daughter cells processed and blocked into anaphase using the *cdc15-2* thermosensitive mutation. A sample of the population was then incubated with nocodazole (15 µg/ml) for 20 min. A sample was released at permissive temperature in the presence of nocodazole for 20 min. Finally, a sample was released at the permissive

temperature for 20 min before being incubated with nocodazole for 20 min.

For synchronization in metaphase, a system allowing induced depletion of *cdc20* was used (MET3-HA-CDC20; strain YKL051). Elutriated G1 daughter cells were restarted in YPD complemented with 50 µg/ml methionine for 5 h at 30°C. Cells arrested in metaphase were split into different aliquots. One sample was immediately processed into a Hi-C library, while two others were washed, suspended in SC medium without methionine, and processed into Hi-C after 20 and 40 min.

To investigate the influence of SMC on chromosome organization, strains carrying auxin-inducible degron (*aid*) versions of Scc1 (strain YKL055) and Smc2 (YKL056) proteins were processed into Hi-C libraries. The degradation of these proteins is induced when auxin (IAA) is added to the medium at a final concentration of 2 mM. Both asynchronous populations of strains YKL055 and YKL056 were elutriated in the absence of IAA. G1 daughter cells were incubated in YPD supplemented with IAA at 30°C. A sample of the YKL055 population (*scc1-aid*) was processed into a Hi-C library in late S/G2 (see Release into S phase). For the YKL056 population (*smc2-aid*), the cells were arrested in late anaphase using the *cdc15-2* mutation also present in the genome of this strain, before being processed into a Hi-C library.

To study the influence of topoisomerase II-mediated decatenation on chromosome organization, we used a strain (YKL057) in which *TOP2* gene is tagged by *aid* (*top2-aid*) and that also carries the *cdc15-2* mutation. An asynchronous exponentially growing culture of YKL057 cells was split into two fractions incubated for 3 h at the non-permissive temperature of 37°C in either the presence or absence of IAA (20 mM). The synchrony of each time point was monitored with flow cytometry and microscopy, and the cells were processed by Hi-C.

Flow cytometry

About 5×10^6 cells were fixed in ethanol 70% and stored at 4°C overnight. Cells were then pelleted, washed, and incubated in sodium citrate 50 mM (pH 7.4) complemented with RNase A (10 mg/ml; Roche) for 2 h at 37°C. Next, Sytox green (2 µM in sodium citrate 50 mM; ThermoFisher) was added and cells incubated for 1 h at 4°C. Flow cytometry was performed on a MACS-Quant Analyzer (Miltenyi Biotec), and data were analyzed using FlowJo X 10.0.7 software (Tree Star).

Microscopy

Fractions of cells fixed in ethanol 70% and stored at 4°C overnight were pelleted and washed three times for 5 min in $1 \times$ PBS. Cells were permeabilized by immersion in 0.2% Triton X-100 (Biosolve) for 5 min. To remove the Triton, cells were pelleted and washed three times in $1 \times$ PBS. The liquid was aspirated and cells were suspended in DAPI labeling solution (2 µg/ml in $1 \times$ PBS) for 10 min at room temperature. Before imaging acquisition, the labeling solution was aspirated and the cells were washed three times for 5 min in $1 \times$ PBS. Cells were imaged at 350 nm excitation wavelength with Nikon fluorescence microscope (Camera Andor Neo sCMOS, software Andor IQ2 2.7.1, LED Lumencor Spectra X).

Hi-C libraries

Hi-C libraries were generated using the four-cutter enzyme DpnII through a protocol adapted from Belton *et al* (2012). The protocol is detailed in Appendix Supplementary Methods. The resulting libraries were used as template for the Illumina amplification by PE-PCR primers and paired-end-sequenced on the NextSeq 500 or HiSeq 2000 Illumina platform (2 × 75 or 2 × 150 bp kits; see Table EV2 for details).

Generation and normalization of contact maps

Raw Hi-C data were processed as follows. PCR duplicates were removed using the 6 Ns present on each of the custom-made adapter and the 2 trimmed Ns. Paired-end reads were mapped independently using Bowtie 2.1.0 (mode: `-very-sensitive -rdg 500,3 -rfg 500,3`) against the *S. cerevisiae* reference genome (S288C). An iterative alignment, with an increasing truncation length of 20 bp, was used to maximize the yield of valid Hi-C reads (mapping quality > 30). Only uniquely mapped reads were retained. On the basis of their DpnII restriction fragment assignment and orientation, reads were classified as either valid Hi-C products or unwanted events to be filtered out (i.e., loops and non-digested fragments; for details, see Cournac *et al*, 2012, 2016). To generate contact matrices for all time points along the cycle, filtered Hi-C reads were binned into units of single restriction fragments, and then, successive fragments were assigned to fixed size bins of either 5 or 50 kb. Bins that exhibited a high contact frequency variance (< 1.5 Standard Deviation or 1.5–2 SD. from the mean) were filtered out for all maps to allow pairwise comparison of the data. On average, around 15 million of valid reads were used to build each contact map. To remove potential biases resulting from the uneven distribution of restriction sites and variation in GC content and mappability, the contact maps were normalized using the sequential component normalization (SCN) procedure (Cournac *et al*, 2012).

Similarity between contact maps

To assess the similarity between normalized matrices, these were binned at 50 kb and quantile-normalized (Hicks & Irizarry, 2015). We then measured their similarity by computing the Euclidean distance between them. In order to visualize similarities between sets of matrices, we did a principal component analysis (PCA) of the pairwise distance matrix between samples.

Contact probability within increasing genomic distance

Polymers display a decrease in contact probability, $P(s)$, as a function of the genomic distance, s . The degree of decay of $P(s)$ was often interpreted as informative of the polymer state. To compute the intra-chromosomal $P(s)$ plots, pair of reads aligned in intra-chromosomal positions were partitioned by chromosome arms. Reads oriented toward different directions or separated by < 1.5 kb were discarded to filter for self-circularizing events. For each chromosome, read pairs were log-binned in function of their genomic distance s (in kb), according to the following formula:

$$\text{bin} = \lceil \log_{1.1}(s) \rceil$$

The $P(s)$ plot is the histogram computed on the sum of read pairs for each bin. This sum is weighted by the bin size $1.1^{(1+\text{bin})}$ (because of the log-binning), as well as the difference between the length of the chromosome and the genomic distance s . The difference acts as a proxy for the number of possible events.

4C-like interaction plots

To obtain the 4C-like intra- and inter-chromosomal contact profiles for rDNA and centromeres, adjacent bins were indexed on the respective chromosomes. The resulting indexed and filtered matrices at either 5- or 50-kb bin were normalized using SCN (see Generation and normalization of contact maps). The profiles for the selected bins were plotted and compared using Matlab (no smoothing was applied).

Computation of the replication profile from Hi-C data

The replication profile was computed from the raw 5-kb-binned contact maps. Firstly, G1 replicates were averaged and the sum of contact over each 5-kb bin was computed. The same computation was repeated for datasets obtained from cells released into S phase. To obtain the replication timing, we computed the ratio of these two signals and smoothed this ratio using a running-average window of six bins.

3D representation of contact maps

The 3D representations of the contact maps were generated using ShRec3D (Lesne *et al*, 2014) on the normalized contact maps, filtered for low-signal bins. First, the algorithm computes the distance matrix from the contact map, by assuming that distances are inversely proportional to the normalized contact counts. A shortest path algorithm is then used to insure that the distance matrix satisfies the triangular inequality. Finally, we used Sammon mapping to recover the optimal 3D coordinates from the distance matrix (Morlot *et al*, 2016). All the 3D structures presented here were rendered using VMD (Humphrey *et al*, 1996). Besides the cautiousness regarding the interpretation of 3D structure we mention in the main text, we also underline that the 3D structures are not used to compare datasets: All computational analyses are performed using the contact map data.

Comparison of centromeres, intra-/inter-, and short-/long-range contacts between datasets

To compare contacts between centromeric regions, the sum of normalized inter-chromosomal contacts between 100-kb regions centered on centromeres was computed and divided by the total number of normalized inter-chromosomal contacts between all chromosomes. To compare short- versus long-range contacts, a ratio of intra contacts was computed as follows. The number of intra contacts involving fragments positioned < 30 kb apart was divided by the number of intra contacts involving fragments positioned more than 30 kb apart, for all chromosomes. For intra-versus inter-chromosomal contacts, the total number of normalized

intra-chromosomal contacts was divided by the sum of normalized inter-chromosomal contacts.

Quantification of variability between replicates

To assess for the contribution of experimental variability to the variations in contacts between different conditions, we proceeded as follows. Density histograms displaying the distribution of the log₂ contact ratio of all elements of Hi-C matrices (50-kb bins) between pairs of biological and experimental replicates (3×G1, 2×G2, 3×M) were computed and compared to similar histograms computed from pairs of Hi-C matrix obtained in different experimental conditions (see Appendix Fig S2).

An estimation of the replicate variability at the centromeres was obtained by plotting the boxplots representing the distribution of the log₂ contact ratios between pairs of biological and experimental replicates only of the bins encompassing the centromeres (50-kb bins; see mask; Appendix Figs S3 and S4). The same computation was performed on pairs of matrices obtained in different conditions to estimate the statistical significance of the variations. All replicates were taken into account. *P*-values were obtained by the Wilcoxon signed-rank test.

Expanded View for this article is available online.

Acknowledgements

We thank Martial Marbouty and Axel Cournac for contributions to the early stage of this project. Sample description and raw contact maps are accessible on the GEO database through the following accession number: GSE90902. Raw sequences are accessible on SRA database through the following accession number: SRP094582. We are also grateful to Armelle Lengronne, Stephane Marcand, Philippe Paseri, Etienne Schwob, Emmanuelle Fabre, Nancy Kleckner, and Angela Taddei for sharing strains and for discussions. Vittore Scolari and Heloise Muller were partly supported by Pasteur-Roux-Cantarini postdoctoral fellowships. This research was supported by funding to R.K. from the European Research Council under the 7th Framework Program (FP7/2007-2013, ERC grant agreement 260822), from Agence Nationale pour la Recherche (MeioRec ANR-13-BSV6-0012-02), and from ERASynBio and Agence Nationale pour la Recherche (IESY ANR-14-SYNB-0001-03).

Author contributions

LL-S and RK designed research. LL-S performed the experiments, with contributions from GM, AT, and HM. TMG generated the smc2-aid mutant. VFS and JM analyzed the data, with contributions from LL-S, LL-S, JM, and RK interpreted the data and wrote the manuscript.

Conflict of interest

The authors declare that they have no conflict of interest.

References

- Alipour E, Marko JF (2012) Self-organization of domain structures by DNA-loop-extruding enzymes. *Nucleic Acids Res* 40: 11202–11212
- Aragon L, Martinez-Perez E, Merckenschlager M (2013) Condensin, cohesin and the control of chromatin states. *Curr Opin Genet Dev* 23: 204–211
- Baxter J, Sen N, Martínez VL, Carandini MEMD, Schwartzman JB, Diffley JFX, Aragón L (2011) Positive supercoiling of mitotic DNA drives decatenation by topoisomerase II in eukaryotes. *Science* 331: 1328–1332
- Belton J-M, McCord RP, Gibcus JH, Naumova N, Zhan Y, Dekker J (2012) Hi-C: a comprehensive technique to capture the conformation of genomes. *Methods* 58: 268–276
- Blat Y, Kleckner N (1999) Cohesins bind to preferential sites along yeast chromosome III, with differential regulation along arms versus the centric region. *Cell* 98: 249–259
- Brewer BJ, Fangman WL (1987) The localization of replication origins on ARS plasmids in *Saccharomyces cerevisiae*. *Cell* 51: 463–471
- Burgess SM, Kleckner N (1999) Collisions between yeast chromosomal loci *in vivo* are governed by three layers of organization. *Genes Dev* 13: 1871–1883
- Clemente-Blanco A, Mayán-Santos M, Schneider DA, Machín F, Jarmuz A, Tschochner H, Aragón L (2009) Cdc14 inhibits transcription by RNA polymerase I during anaphase. *Nature* 458: 219–222
- Cournac A, Marie-Nelly H, Marbouty M, Koszul R, Mozziconacci J (2012) Normalization of a chromosomal contact map. *BMC Genom* 13: 436
- Cournac A, Marbouty M, Mozziconacci J, Koszul R (2016) Generation and analysis of chromosomal contact maps of yeast species. In *Yeast functional genomics*, Devaux F (ed) pp 227–245. New York: Springer Available at: https://doi.org/10.1007/978-1-4939-3079-1_13 [Accessed April 25, 2017]
- D'Ambrosio C, Kelly G, Shirahige K, Uhlmann F (2008) Condensin-dependent rDNA decatenation introduces a temporal pattern to chromosome segregation. *Curr Biol* 18: 1084–1089
- D'Amours D, Stegmeier F, Amon A (2004) Cdc14 and condensin control the dissolution of cohesin-independent chromosome linkages at repeated DNA. *Cell* 117: 455–469
- Daoud M, Cotton JP (1982) Star shaped polymers: a model for the conformation and its concentration dependence. *J Phys* 43: 531–538
- Dekker J, Rippe K, Dekker M, Kleckner N (2002) Capturing chromosome conformation. *Science* 295: 1306–1311
- Dekker J, Mirny L (2016) The 3D genome as moderator of chromosomal communication. *Cell* 164: 1110–1121
- Duan Z, Andronescu M, Schutz K, Mcllwain S, Kim YJ, Lee C, Shendure J, Fields S, Blau CA, Noble WS (2010) A three-dimensional model of the yeast genome. *Nature* 465: 363–367
- Eser U, Chandler-Brown D, Ay F, Straight AF, Duan Z, Noble WS, Skotheim JM (2017) Form and function of topologically associating genomic domains in budding yeast. *Proc Natl Acad Sci USA* 114: E3061–E3070
- de Gennes PG (1987) Polymers at an interface; a simplified view. *Adv Colloid Interface Sci* 27: 189–209
- Glynn EF, Megee PC, Yu H-G, Mistrot C, Unal E, Koshland DE, DeRisi JL, Gerton JL (2004) Genome-wide mapping of the cohesin complex in the yeast *Saccharomyces cerevisiae*. *PLoS Biol* 2: e259
- Guacci V, Hogan E, Koshland D (1994) Chromosome condensation and sister chromatid pairing in budding yeast. *J Cell Biol* 125: 517–530
- Guidi M, Ruault M, Marbouty M, Loiodice I, Cournac A, Billaudeau C, Hocher A, Mozziconacci J, Koszul R, Taddei A (2015) Spatial reorganization of telomeres in long-lived quiescent cells. *Genome Biol* 16: 206
- Guillou E, Ibarra A, Coulon V, Casado-Vela J, Rico D, Casal I, Schwob E, Losada A, Méndez J (2010) Cohesin organizes chromatin loops at DNA replication factories. *Genes Dev* 24: 2812–2822
- Hartwell LH, Mortimer RK, Culotti J, Culotti M (1973) Genetic control of the cell division cycle in yeast: V. Genetic analysis of cdc mutants. *Genetics* 74: 267–286

- Hicks SC, Irizarry RA (2015) Quantro: a data-driven approach to guide the choice of an appropriate normalization method. *Genome Biol* 16: 117
- Hirano T (2012) Condensins: universal organizers of chromosomes with diverse functions. *Genes Dev* 26: 1659–1678
- Hsieh T-HS, Weiner A, Lajoie B, Dekker J, Friedman N, Rando OJ (2015) Mapping nucleosome resolution chromosome folding in yeast by micro-C. *Cell* 162: 108–119
- Hug CB, Grimaldi AG, Kruse K, Vaquerizas JM (2017) Chromatin architecture emerges during zygotic genome activation independent of transcription. *Cell* 169: 216–228.e19
- Humphrey W, Dalke A, Schulten K (1996) VMD: visual molecular dynamics. *J Mol Graph* 14: 33–38, 27–28
- Jacobs CW, Adams AE, Szanislo PJ, Pringle JR (1988) Functions of microtubules in the *Saccharomyces cerevisiae* cell cycle. *J Cell Biol* 107: 1409–1426
- Kim K-D, Tanizawa H, Iwasaki O, Noma K (2016) Transcription factors mediate condensin recruitment and global chromosomal organization in fission yeast. *Nat Genet* 48: 1242–1252
- Kitamura E, Blow JJ, Tanaka TU (2006) Live-cell imaging reveals replication of individual replicons in eukaryotic replication factories. *Cell* 125: 1297–1308
- Knott SRV, Peace JM, Ostrow AZ, Gan Y, Rex AE, Viggiani CJ, Tavaré S, Aparicio OM (2012) Forkhead transcription factors establish origin timing and long-range clustering in *Saccharomyces cerevisiae*. *Cell* 148: 99–111
- Leonard J, Sen N, Torres R, Sutani T, Jarmuz A, Shirahige K, Aragón L (2015) Condensin relocation from centromeres to chromosome arms promotes Top2 recruitment during anaphase. *Cell Rep* 13: 2336–2344
- Lesne A, Riposo J, Roger P, Cournac A, Mozziconacci J (2014) 3D genome reconstruction from chromosomal contacts. *Nat Methods* 11: 1141–1143
- Lieberman-Aiden E, van Berkum NL, Williams L, Imakaev M, Ragoczy T, Telling A, Amit I, Lajoie BR, Sabo PJ, Dorschner MO, Sandstrom R, Bernstein B, Bender MA, Groudine M, Gnirke A, Stamatoyannopoulos J, Mirny LA, Lander ES, Dekker J (2009) Comprehensive mapping of long-range interactions reveals folding principles of the human genome. *Science* 326: 289–293
- London N, Biggins S (2014) Signalling dynamics in the spindle checkpoint response. *Nat Rev Mol Cell Biol* 15: 736–748
- Machín F, Torres-Rosell J, Piccoli GD, Carballo JA, Cha RS, Jarmuz A, Aragón L (2006) Transcription of ribosomal genes can cause nondisjunction. *J Cell Biol* 173: 893–903
- Marbouty M, Ermont C, Dujon B, Richard G-F, Koszul R (2014) Purification of G1 daughter cells from different *Saccharomycetes* species through an optimized centrifugal elutriation procedure. *Yeast Chichester Engl* 31: 159–166
- Marbouty M, Le Gall A, Cattoni DI, Cournac A, Koh A, Fiche J-B, Mozziconacci J, Murray H, Koszul R, Nollmann M (2015) Condensin- and replication-mediated bacterial chromosome folding and origin condensation revealed by Hi-C and super-resolution imaging. *Mol Cell* 59: 588–602
- McCune HJ, Danielson LS, Alvino GM, Collingwood D, Delrow JJ, Fangman WL, Brewer BJ, Raghuraman MK (2008) The temporal program of chromosome replication: genomewide replication in *clb5{Delta}* *Saccharomyces cerevisiae*. *Genetics* 180: 1833–1847
- Mercy G, Mozziconacci J, Scolari VF, Yang K, Zhao G, Thierry A, Luo Y, Mitchell LA, Shen M, Shen Y, Walker R, Zhang W, Wu Y, Xie ZX, Luo Z, Cai Y, Dai J, Yang H, Yuan YJ, Boeke JD et al (2017) 3D organization of synthetic and scrambled chromosomes. *Science* 355: eaaf4597
- Mizuguchi T, Fudenberg G, Mehta S, Belton J-M, Taneja N, Folco HD, FitzGerald P, Dekker J, Mirny L, Barrowman J, Grewal SIS (2014) Cohesin-dependent globules and heterochromatin shape 3D genome architecture in *S. pombe*. *Nature* 516: 432–435
- Morlot J-B, Mozziconacci J, Lesne A (2016) Network concepts for analyzing 3D genome structure from chromosomal contact maps. *EPJ Nonlinear Biomed Phys* 4: 2
- Naumova N, Imakaev M, Fudenberg G, Zhan Y, Lajoie BR, Mirny LA, Dekker J (2013) Organization of the mitotic chromosome. *Science* 342: 948–953
- Piatti S, Lengauer C, Nasmyth K (1995) Cdc6 is an unstable protein whose *de novo* synthesis in G1 is important for the onset of S phase and for preventing a “reductional” anaphase in the budding yeast *Saccharomyces cerevisiae*. *EMBO J* 14: 3788–3799
- Raghuraman MK, Winzeler EA, Collingwood D, Hunt S, Wodicka L, Conway A, Lockhart DJ, Davis RW, Brewer BJ, Fangman WL (2001) Replication dynamics of the yeast genome. *Science* 294: 115–121
- Renshaw MJ, Ward JJ, Kanemaki M, Natsume K, Nédélec FJ, Tanaka TU (2010) Condensins promote chromosome recoiling during early anaphase to complete sister chromatid separation. *Dev Cell* 19: 232–244
- Rock JM, Amon A (2011) Cdc15 integrates Tem1 GTPase-mediated spatial signals with Polo kinase-mediated temporal cues to activate mitotic exit. *Genes Dev* 25: 1943–1954
- Saner N, Karschau J, Natsume T, Gierliński M, Retkute R, Hawkins M, Nieduszynski CA, Blow JJ, de Moura APS, Tanaka TU (2013) Stochastic association of neighboring replicons creates replication factories in budding yeast. *J Cell Biol* 202: 1001–1012
- Stephens AD, Haase J, Vicci L, Taylor RM, Bloom K (2011) Cohesin, condensin, and the intramolecular centromere loop together generate the mitotic chromatin spring. *J Cell Biol* 193: 1167–1180
- Sullivan M, Higuchi T, Katis VL, Uhlmann F (2004) Cdc14 phosphatase induces rDNA condensation and resolves cohesin-independent cohesion during budding yeast anaphase. *Cell* 117: 471–482
- Taddei A, Gasser SM (2012) Structure and function in the budding yeast nucleus. *Genetics* 192: 107–129
- Uhlmann F, Lottspeich F, Nasmyth K (1999) Sister-chromatid separation at anaphase onset is promoted by cleavage of the cohesin subunit Scc1. *Nature* 400: 37–42
- Uhlmann F (2016) SMC complexes: from DNA to chromosomes. *Nat Rev Mol Cell Biol* 17: 399–412
- Valton A-L, Dekker J (2016) TAD disruption as oncogenic driver. *Curr Opin Genet Dev* 36: 34–40
- Visintin R, Prinz S, Amon A (1997) CDC20 and CDH1: a family of substrate-specific activators of APC-dependent proteolysis. *Science* 278: 460–463
- Wang X, Montero Llopis P, Rudner DZ (2013) Organization and segregation of bacterial chromosomes. *Nat Rev Genet* 14: 191–203
- Yoshida S, Asakawa K, Toh-e A (2002) Mitotic exit network controls the localization of Cdc14 to the spindle pole body in *Saccharomyces cerevisiae*. *Curr Biol* 12: 944–950



License: This is an open access article under the terms of the Creative Commons Attribution 4.0 License, which permits use, distribution and reproduction in any medium, provided the original work is properly cited.

Expanded View Figures

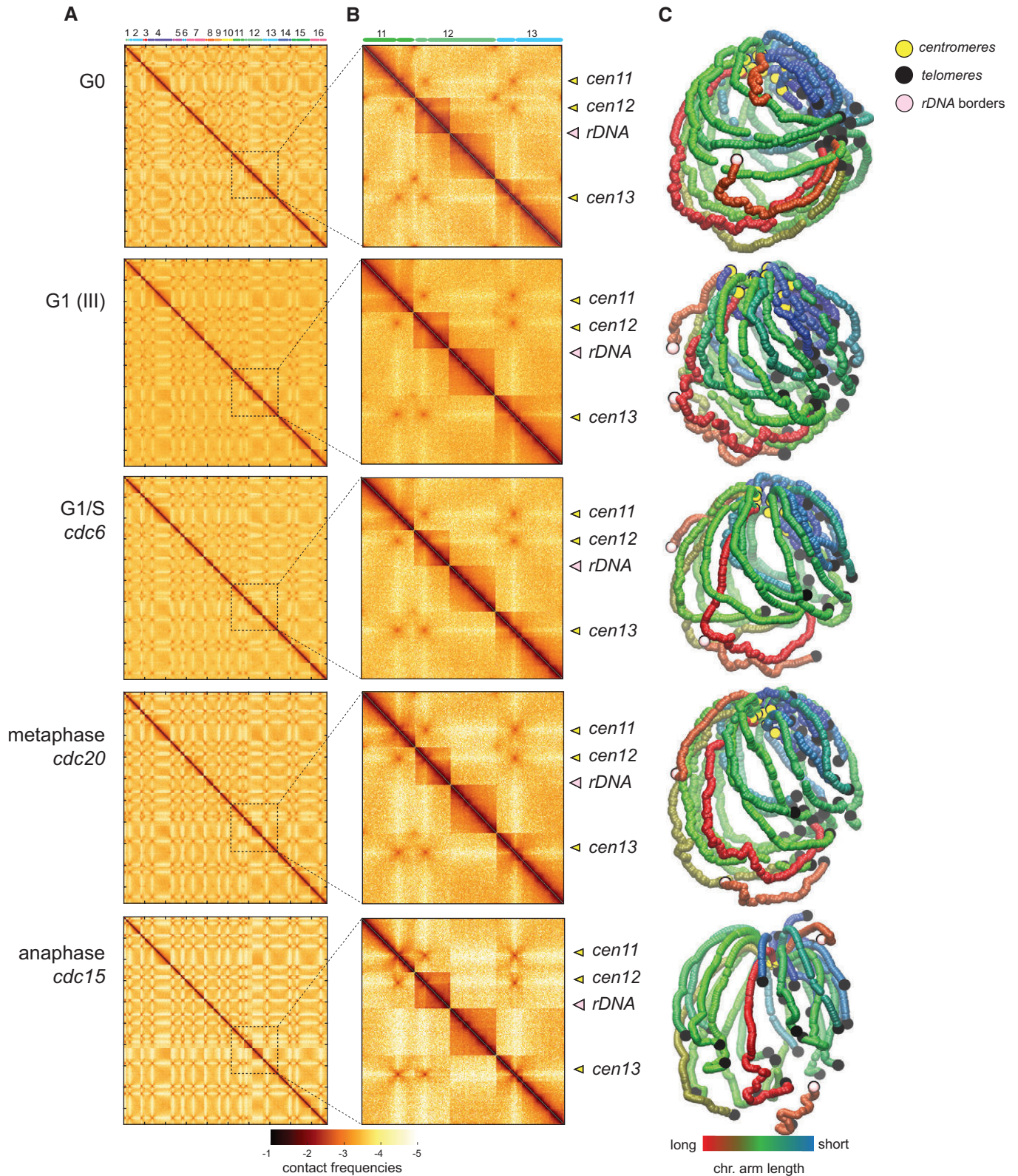


Figure EV1.

**Figure EV1. Contact maps and 3D genome representations of the five cell cycle synchronization states.**

- A, B Contact maps generated from synchronized cell populations described in this study, with each vector (or bin) corresponding to 5 kb. x- and y-axis represent the 16 chromosomes of the yeast genome, displayed atop the maps. Brown to yellow color scales reflect high to low contact frequencies, respectively (log10). Magnification panels in (B) show variations of the contact frequencies between synchronized populations. Yellow and pink arrowheads point at centromeres and rDNA positions, respectively.
- C 3D average representations of the Hi-C contact maps of synchronized cell populations of panel (A). The color code represents the chromosomal arm length, and centromeres, telomeres, and rDNA flanking regions are highlighted.

Figure EV2. Contact maps and 3D genome representations during replication.

- A, B Contact maps recovered from cell populations undergoing replication after G1 release. For each contact map, the FACS profile is displayed. x- and y-axis represent the 16 chromosomes of the yeast genome. The same color code as in Fig. EV1. Magnification panels in (B) highlight changes of the contact frequencies during S-phase progression. Yellow and pink arrowheads point at centromeres and rDNA positions, respectively.
- C 3D average representations of the Hi-C contact maps of synchronized cell populations of panel (A). The color code represents the chromosomal arm length, and centromeres, telomeres, and rDNA flanking regions are highlighted.



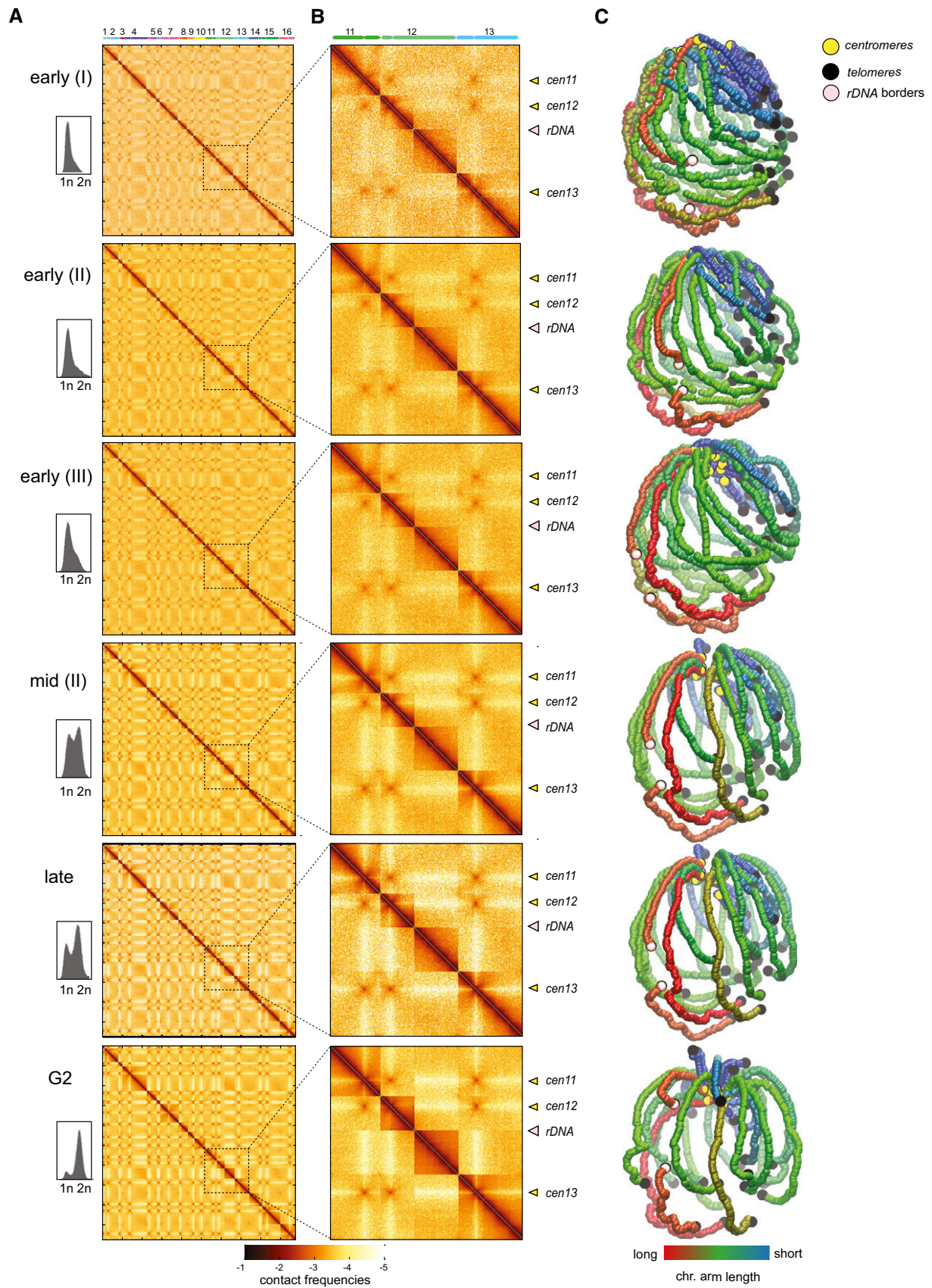


Figure EV2.

Figure EV3. Contact maps and 3D genome representations during M phase.

- A, B Contact maps of cell populations synchronized in metaphase (*cdc20*) and anaphase (*cdc15*) and released into mitosis from *cdc15* block (+20 min, +40 min, and +60 min). The corresponding FACS profiles and representative DAPI-stained cells are displayed on the left on the maps. x- and y-axis represent the 16 chromosomes of the yeast genome. The same color code as in Fig EV1. Magnification panels in (B) display variations of the contact frequencies during mitotic progression. Yellow and pink arrowheads point at centromeres and rDNA positions, respectively.
- C 3D average representations of the Hi-C contact maps of panel (A). The color code represents the chromosomal arm length, and centromeres, telomeres, and rDNA flanking regions are highlighted.

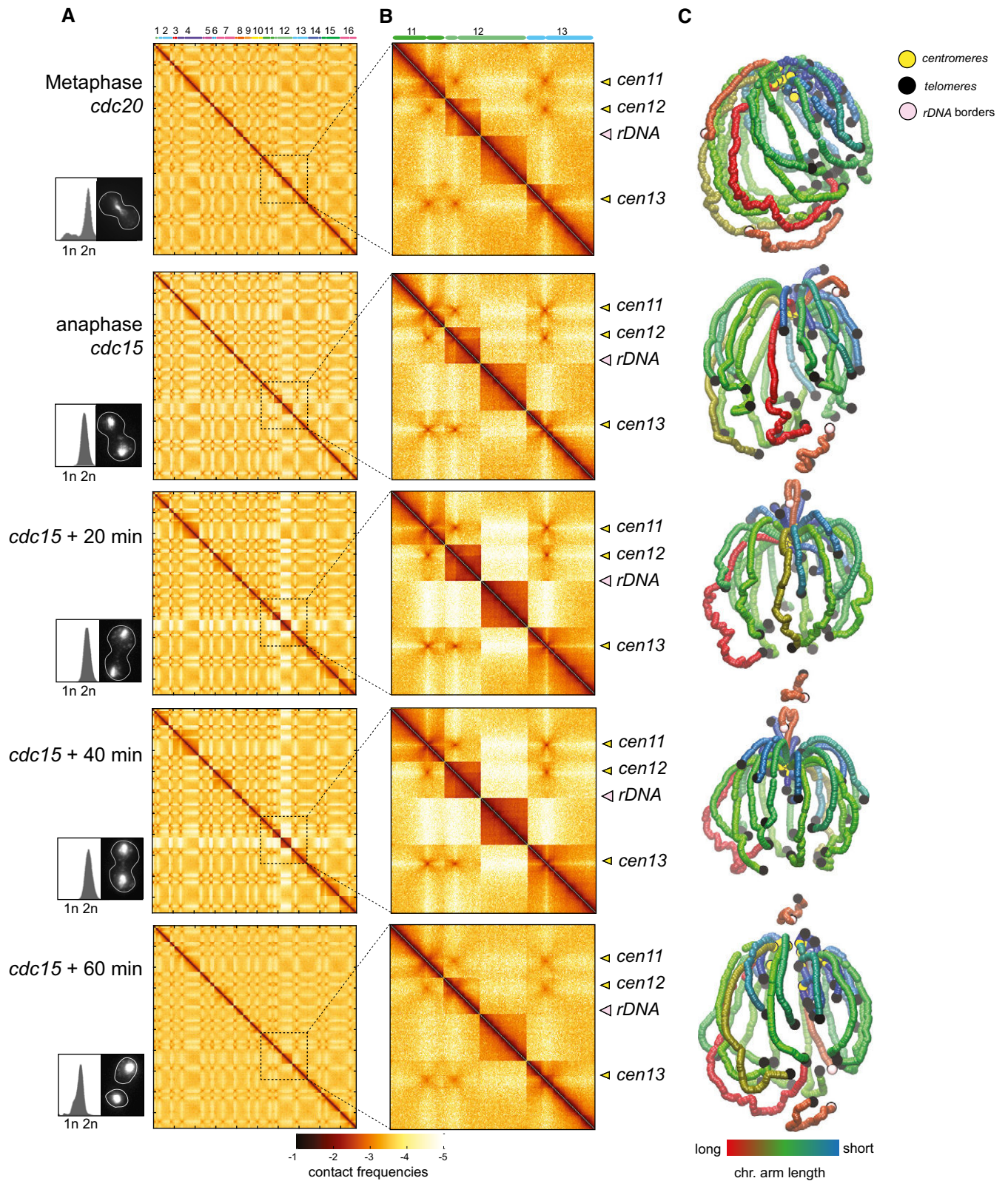


Figure EV3.

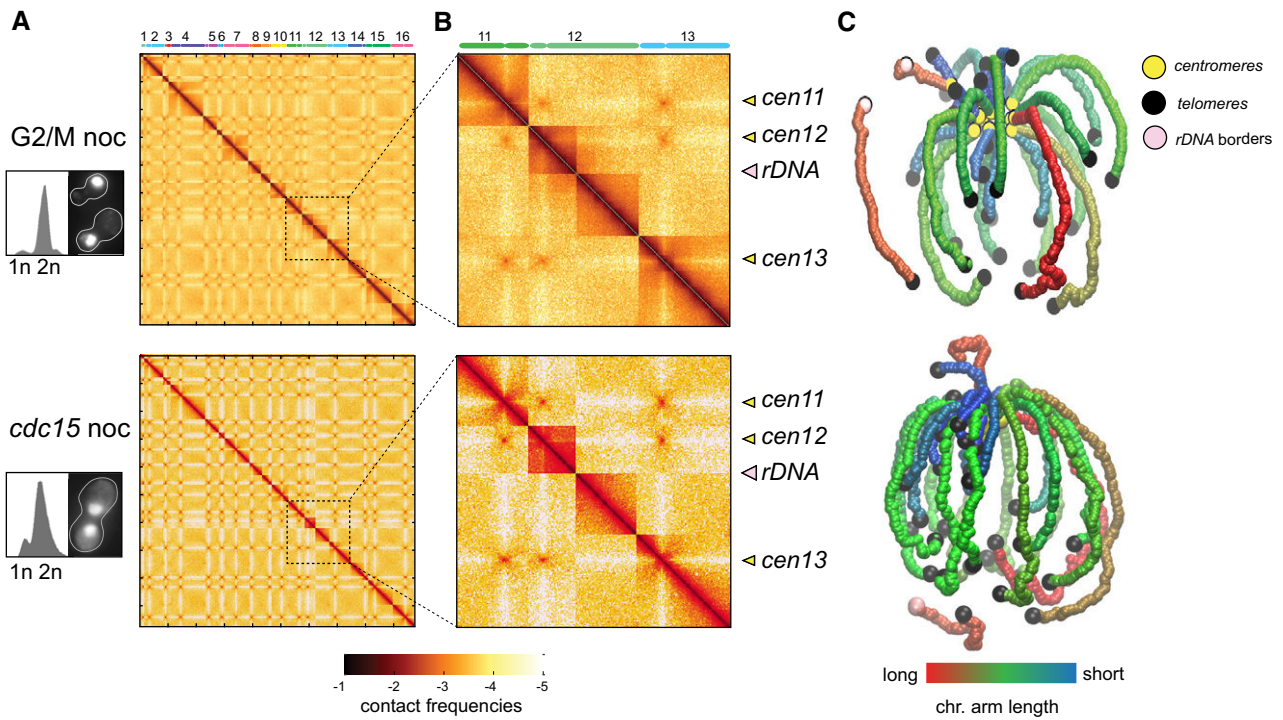


Figure EV4. Nocodazole affects chromosome 12 conformation.

- A, B Contact maps of G1 synchronized cell populations released either in the presence of nocodazole (G2/M noc) or at *cdc15* non-permissive temperature followed by a nocodazole treatment (*cdc15* noc). The corresponding FACS profiles and representative DAPI-stained cells are displayed on the left on the maps. x- and y-axis represent the 16 chromosomes of the yeast genome. The same color code as in Fig EV1. Magnification panels in (B) display variations of the contact frequencies. Yellow and pink arrowheads point at centromeres and rDNA positions, respectively.
- C 3D average representations of the Hi-C contact maps of panel (A). The color code represents the chromosomal arm length, and centromeres, telomeres, and rDNA flanking regions are highlighted.

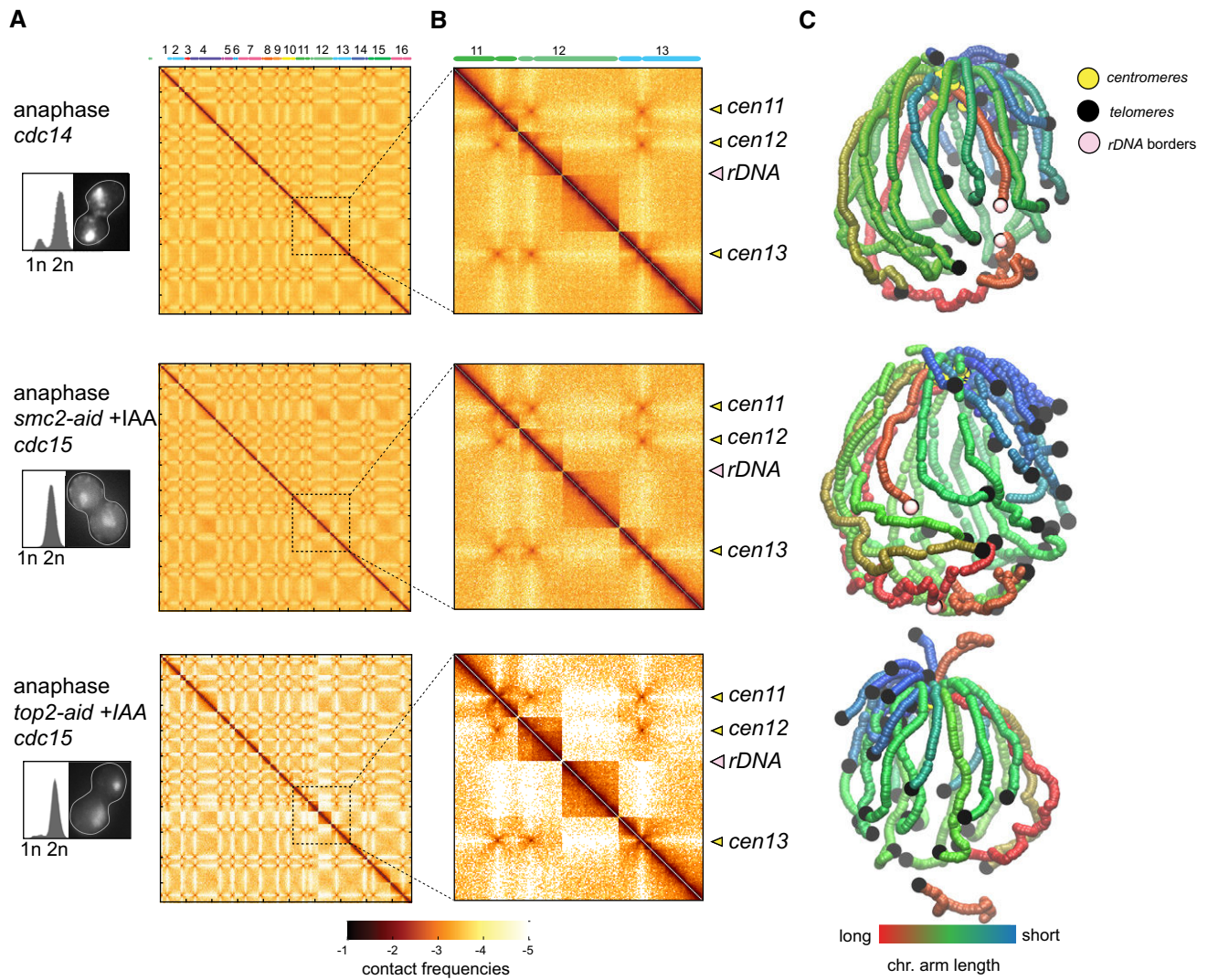


Figure EV5. Condensin and decatenation influence on chromatin structure during mitosis.

- A, B Contact maps of cell populations arrested in anaphase, either defective with condensation (*cdc14* or *smc2-aid cdc15 +IAA*) or depleted of topoisomerase 2 (*top2-aid cdc15 +IAA*). The corresponding FACS profiles and representative DAPI-stained cells are displayed on the left on the maps. x- and y-axis represent the 16 chromosomes of the yeast genome. The same color code as in Fig EV1. Magnification panels in (B) display variations of the contact frequencies. Yellow and pink arrowheads point at centromeres and rDNA positions, respectively.
- C 3D average representations of the Hi-C contact maps of panel (A). The color code represents the chromosomal arm length, and centromeres, telomeres, and rDNA flanking regions are highlighted.

Table EV1. List of strains used in this study.

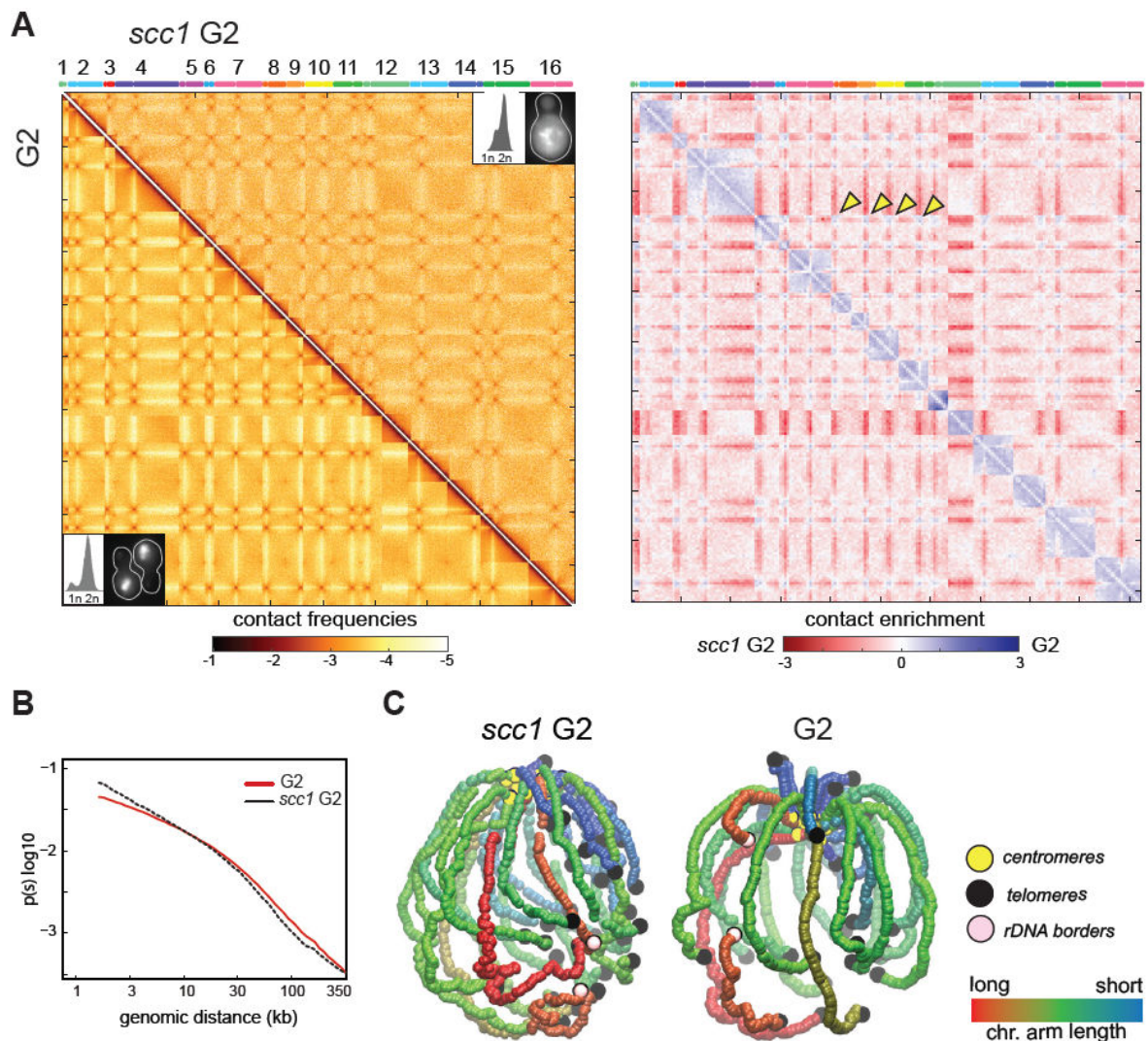
*: strain YKL050 carries a ~130 kb region where some restriction sites have been reordered to generate fixed size restriction fragments to investigate the resolution of the Hi-C assay, a work that will be described elsewhere.

Strain	Genetic background	Genotype	Used to study:	Reference
BY4741	S288C	<i>MATα his3Δ1 leu2Δ0 met15Δ0 ura3Δ0</i>	asynchronous, G0 and G1	Mortimer and Johnston, 1986
YKL050*	BY4742	<i>MATα his3Δ1 lys2Δ0 ura3Δ0 IV(715448-845757)::synIV(715448-845757 LEU2)</i>	asynchronous, G1, S and G2 phase and nocodazole treatment	
YKL051	W303	<i>MATα his3Δ leu2Δ ura3Δ0 can1Δ ade2Δ cdc20::MET-HA3-CDC20::TRP1</i>	M phase (metaphase)	Uhlmann et al., 2000
YKL052	W303	<i>MATα his3Δ leu2Δ ura3Δ0 trp1Δ can1Δ ade2Δ cdc14-3(ts)</i>	M phase (early anaphase)	Visinti et al., 1998
YKL053	W303	<i>MATα his3Δ leu2Δ ura3Δ trp1Δ can1Δ ade2Δ cdc15-2(ts)</i>	M phase (late anaphase) and mitosis exit	Surana et al., 1993
YKL054	W303	<i>MATα his3Δ ura3Δ0 trp1Δ can1Δ ade2Δ DBF4-Myc18::LEU2 cdc6-1(ts)</i>	G1/S and M phase	Piatti et al., 1995
YKL055	W303	<i>MATα (rad5?) pADH1-OsTIR1-myc9::TRP1 GPD-TK(x7)::URA3 scc1-AID::KANr</i>	G2 phase	Courtesy of Philippe Pasero (strain PP1792)
YKL056	W303	<i>MATα cdc15-2(ts) smc2-AID-9myc::NAT OsTIR1-9myc::URA3 SPO20^{S1-91}-TTYeGFP::TRP1 HTA1-mCherry::HPH KANr-pGAL1-CEN6-pGAL1-skHIS3 leu2-2</i>	M phase (late anaphase)	Courtesy of Stephane Marcand
YKL057	W303	<i>MATα cdc15-2(ts) top2-AID::HPH TIR1::URA3 KANr-pGAL1-CEN6-pGAL1-skHIS3</i>	M phase (late anaphase)	Courtesy of Stephane Marcand

Appendix

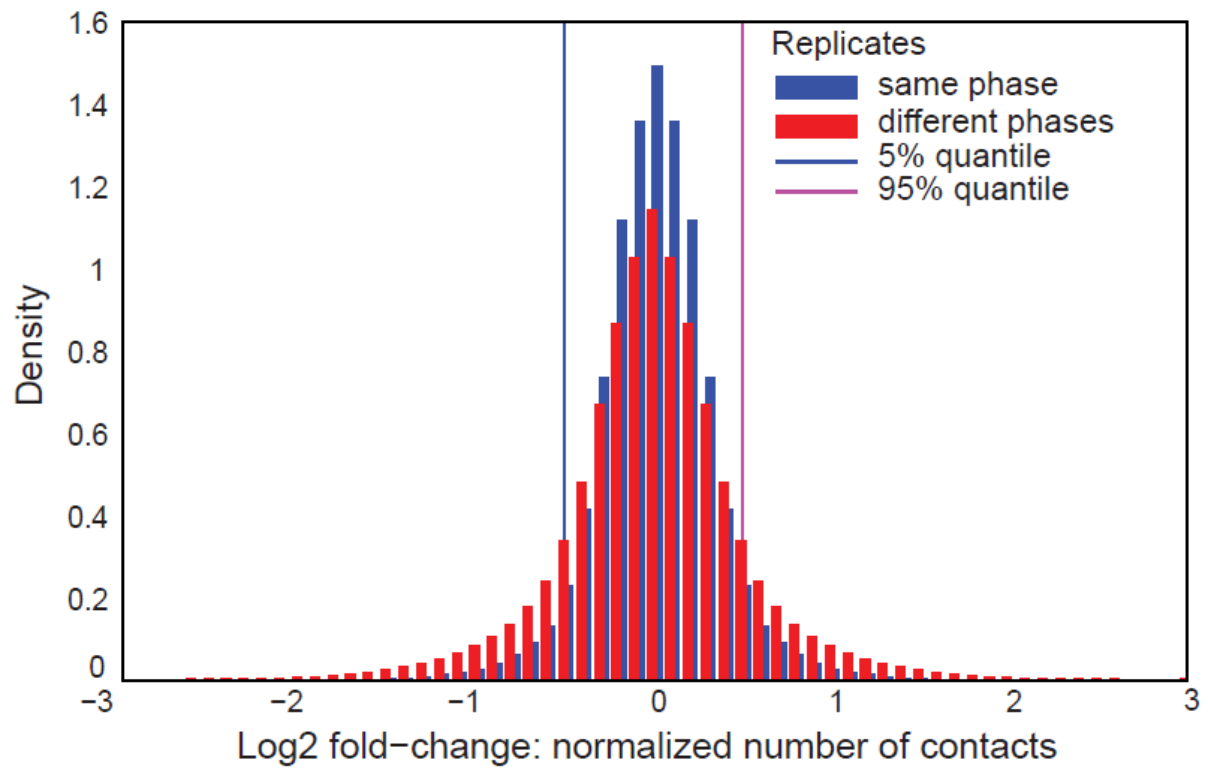
Table of content

Appendix Figure S1	Page 2
Appendix Figure S2	Page 3
Appendix Figure S3	Page 4
Appendix Figure S4	Page 5
Appendix Supplementary Methods	Page 6



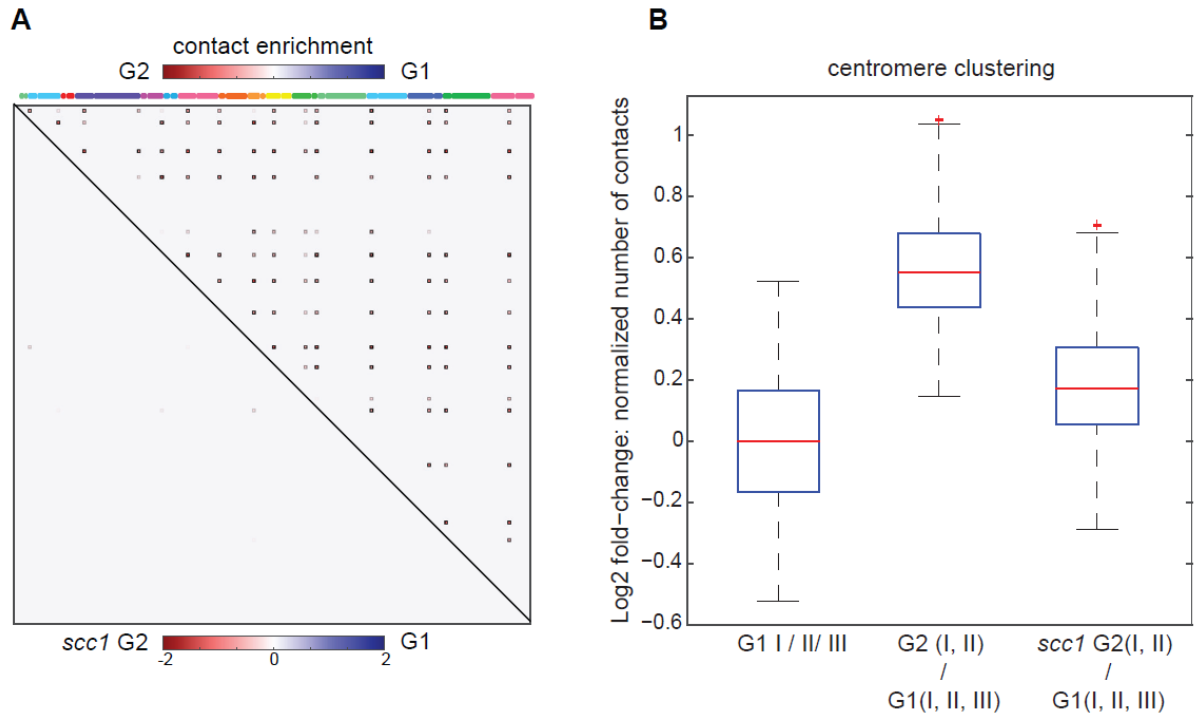
Appendix Figure S1. Cohesin required for genome-wide chromatin organization during replication.

(A) Left panel: Hi-C contact maps of cell populations G1 released and processed in G2 wild-type (G2, bottom left) and in cohesin depleted (*scc1* G2, upper right) cells. The corresponding FACS profiles as well as representative DAPI-stained cells are displayed in boxes on the bottom left and upper right corners, respectively. X and y axis represent the 16 chromosomes of the yeast genome. Same color code as in Figure EV1. Right panel: log-ratio of G2 and *scc1* G2 contact maps. Yellow arrowheads: inter-centromere contacts. The color code reflects the enrichment in contacts in one population with respect to the other. (B) Contact probability $p(s)$ decay in G2 and *scc1* G2. (C) 3D average representations of the Hi-C contact maps of panel (A). Color code represents chromosomal arm length and centromeres, telomeres and rDNA flanking regions are highlighted.



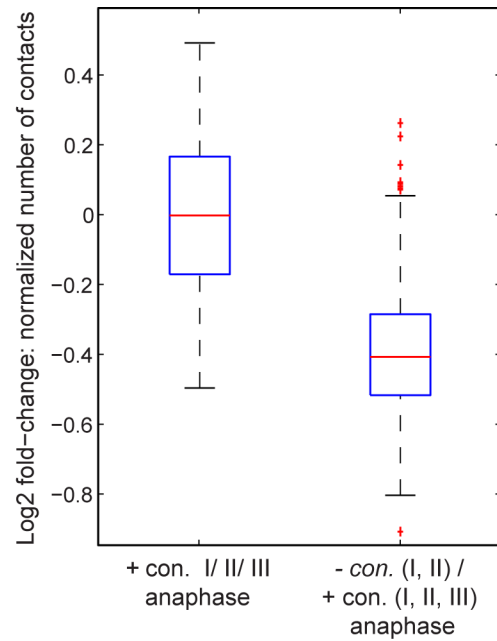
Appendix Figure S2. Analysis of the variability of Hi-C data.

Distribution of the fold-change in contacts made by bins in over different conditions. Blue: fold change in contacts in replicates. Red: fold change in contacts between all non-replicated conditions. This results backs the co-localization in the PC space of replicates in the PCA.



Appendix Figure S3. Centromere clustering is cohesin-dependent.

A) Positions within the contact map of bins whose specific variations in contacts in trans will be investigated between two conditions (here, the 16 bins corresponding to centromeres, between G1 and G2 [top right] and between *scc1* and G1 [bottom left]). **B)** Boxplots representing the variation in number of normalized contacts for a subset of bins between different contact maps (corresponding to different conditions). Left: variations between three G1 replicates. Middle: variations between G2 and G1 cells replicates. The relative Wilcoxon test provides a p-value $< 10^{-10}$, supporting an increase in contacts in G2 compared to G1. Right: variations between *scc1* arrested cells and G1 replicates.



Appendix Figure S4. Condensins increase centromere clustering in anaphase.

Left boxplot shows the centromere contact variability between anaphase replicates (*cdc15* I, II, III) in presence of condensins (+con.). Right boxplot shows the variation of contacts between centromeres between *cdc15* replicates and condensin defective strains arrested in anaphase (*cdc14* and *smc2 cdc15*; -con. I, II). The boxplots show that the centromere cluster in anaphase is condensin-dependent ($P < 0.05$).

Appendix Supplementary Methods

Generation of Hi-C libraries. Aliquots of $1-3 \times 10^9$ cells in 150 ml YPD/synthetic medium were fixed in 3% formaldehyde (Sigma) for 20 min at room temperature and quenched with 25 ml glycine 2.5 M for 20 min at 4°C. Cross-linked cells were recovered through centrifugation, washed with YPD and a 150 mg pellet was stored at -80°C. The pellet was thawed on ice and incubated for 30 min in 10 ml of sorbitol 1M, DTT 5mM and Zymolyase 100T (C_{Final}=1 mg/ml; Armsbio). Spheroplasts were washed once with 5 ml sorbitol 1M, once with 5 ml 1X RE buffer (DpnII NEB buffer) and finally suspended in 3.5 ml of 1X RE buffer. The spheroplasts were treated with 3% SDS for 20 min at 65°C and the lysate was digested overnight with DpnII (C_{Final}=450 U/pellet; NEB) at 37°C. The digestion was centrifuged for 20 min at 18000 g, the supernatant discarded and the pellet suspended in 400 µL of water. The 5' overhangs from DpnII digestion were filled in using dNTP 30 µM (biotin-14-dCTP, dATP, dGTP and dTTP; Invitrogen), at 37°C for 45 min. The biotinylated DNA fragments were ligated by T4 DNA ligase (C_{Final}=250 Weiss U/pellet; Thermo Scientific) for 4 h at 16°C. DNA purification was achieved through an overnight incubation at 65°C in presence of proteinase K 250 µg/ml and EDTA 6.2 mM, followed by a phenol/chloroform extraction on the precipitated DNA and an RNase A DNase-free 500 µg/ml treatment. The biotinylated but not ligated DNA fragments were removed by T4 DNA polymerase (C_{Final}=5 U/pellet; NEB) treatment. Hi-C DNA libraries were 500 bp sheared, using CovarisS220 apparatus, and the biotin-labeled fragments were selectively captured by Dynabeads Myone Streptavidin C1 (Invitrogen). The resulting libraries were used as template for the Illumina amplification by PE-PCR primers and paired-end sequenced on the NextSeq500 or HiSeq 2000 Illumina platforms (2x75 or 2x150 bp kits; see [Table EV2](#)).

Elutriation (recovery of G1 cells). 800 ml overnight culture was centrifuged, washed in 1X PBS and pelleted cells were suspended in 1000 ml of fresh YPD for 2 h at 30°C. This additional growing step allowed cells in stationary phase to reenter exponential phase before being elutriated. For each elutriation experiment, $1.2-1.8 \times 10^{11}$ cells were washed and suspended in 30 ml of 1X PBS and injected in the 40 ml elutriation chamber at an average flow rate ranging from 20 ml/min to 25 ml/min (MasterFlex L/S pump from Cole-Parmer), at 2,500 r.p.m. and 23°C. Cells were then left to equilibrate in 1X PBS for 45 min at a constant

flow and rotational speed. To start collecting the first fractions containing the small G1 cells, a periodic 2 ml/min increment of the flux was applied between each fraction. The resulting 600 ml fractions were centrifuged and approximately 2.5×10^9 G1 cells/fraction were recovered. Before fixating the G1 state, cells were suspended in fresh YPD at 30°C for 30 min, so they could recover from their stay in PBS during the elutriation. To minimize the potential variability introduced by the age heterogeneity of the bulk population, G1 daughter cells were used as starting point for all cell cycle synchrony and in combination with genetic and chemical synchronization methods (see below).

Synchronization through thermosensitive mutations. Synchronizations using thermosensitive (ts) *cdc* strains (Hartwell *et al*, 1973) were all performed starting from elutriated G1 daughter cells growing in non-permissive temperature conditions designed to arrest the progression of the cycle at specific phases.

The G1/S checkpoint (*cdc6-1* mutation; YKL054 strain) was activated by growing cells overnight at 25°C, restarted in fresh YPD media and elutriated while in exponentially growing stage, still at 25°C. The elutriated G1 cells were incubated in fresh YPD at the non-permissive temperature of 37°C for 3 h. To study non-replicated mitotic chromosomes, the *cdc6-1* arrested cells were maintained in non-permissive growing conditions for an extended period of 6 h. During this time period, G1 cells bypass the G1/S checkpoint and proceed into M phase without having replicated their chromosomes.

A similar protocol was applied to *cdc14-3* (YKL052) and *cdc15-2* (YKL053) G1 cells exposed to non-permissive temperature of 30°C and 37°C after elutriation, respectively. *Cdc15* and *cdc14* arrested cells blocked into anaphase were shifted at the permissive temperatures of 25°C and 23°C, with different time-points were sampled after release (YKL052: 30 min; YKL053: 20 min, 40 min and 60 min). The synchrony of each time point (in G1/S, anaphase and release) was monitored with flow cytometry and microscopy.

Part 2 :

2.2 Organization and maintenance of silenced chromatin

Summary

DNA in eukaryotic species is wrapped around octamers of histone proteins to form nucleosomes, which in turn can be folded into secondary/higher-order chromatin structures (Hayes and Hansen, 2001). Different patterns of chromatin packaging influence the transcriptional activity of these regions. An open chromatin state (euchromatin) promotes transcription whereas a highly condensed state (heterochromatin) is often associated with transcription repression or silencing (Venkatesh and Workman, 2015). The establishment of different levels of chromatin condensation as well as the rapid reorganization of the fibre are processes that depend on chromatin-remodelling enzymes, such as histone modifying enzymes or silencing proteins (Laura N. Rusche et al., 2003; Luger et al., 2012; Zhou et al., 2011). With the development of chromosome conformation capture techniques (e.g. Hi-C), the relationship between the 3D organization of chromosomes at multiple levels and the underlying chromatin proteins can be investigated genome-wide (Dekker, 2008; Guidi et al., 2015; Lazar - Stefanita et al., 2017; Lieberman-Aiden et al., 2009; Van Bortle and Corces, 2012). In the continuity of the work done in collaboration with the group of Angela Taddei at Institut Curie on chromosome reorganization during quiescence, we pursued the investigation of the folding properties of silenced heterochromatin using Hi-C. I focused mostly on characterizing the interplay between genome organization and the spreading of telomeric heterochromatin on the subtelomeric regions in different metabolic conditions.

Introduction

Imaging and genome-wide studies such as ChIP-seq and Hi-C have revealed key features of nuclear organization, such as the existence of sub-compartments in which specific DNA sequences and proteins associate. These create microenvironments that can favour or impede particular enzymatic activities (Taddei et al., 2010). Well-characterized examples of these microenvironments are clusters of certain genes and/or repetitive DNA sequences, such as telomeres and rDNA genes. In budding yeast, both these regions form discrete nuclear compartments, enriched in silent information regulators (SIR factors: Sir2, Sir3 and Sir4) (Taddei et al., 2004). The binding of the SIR complex on the

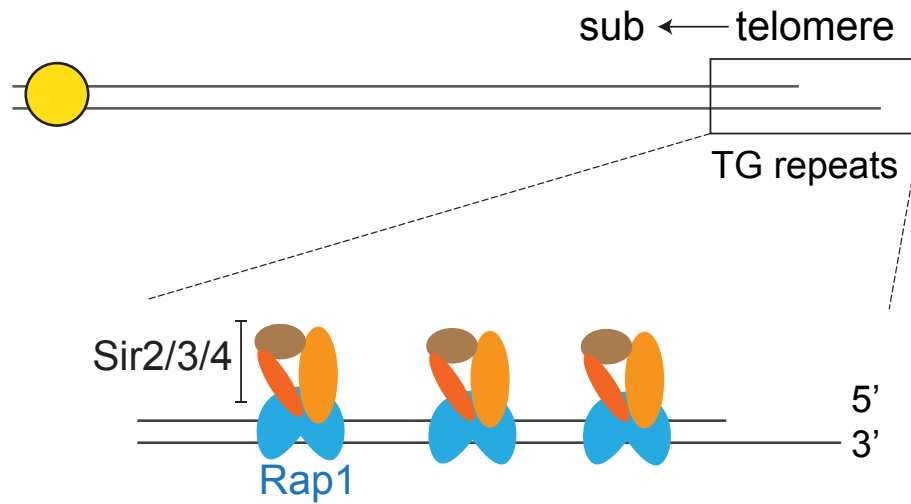


Figure 1. Structure of yeast telomeres. Schematic representation of a yeast telomere, showing the terminal TG repeat overhangs. Rap1 binds at the telomeric repeats and recruits SIR complex (Sir2-Sir3-Sir4). This complex then spreads on the adjacent subtelomeric region.

chromatin induces gene silencing and maintain of genomic stability of these regions (Dubarry et al., 2011; Gotta et al., 1996; Kaeberlein et al., 1999). SIR-dependent silencing has been well characterized at the telomeric regions in yeast. Each telomere consists of 250–300 bp of irregular tandem repeats of the consensus sequence TG₁₋₃ (Shampay et al., 1984). Repressor activator protein 1 (Rap1) binds to the telomeric repeat, and recruits Sir3 and Sir4 (Moretti et al., 1994). Sir3 and Sir4 form a stoichiometric complex with the histone deacetylase Sir2, that deacetylates neighbouring histones, promoting more binding sites for Sir3 and Sir4 (Figure 1). This leads to the spreading of the Sir2–3–4 complex from TG repeats into the subtelomeric domain for approximately 2 to 3 kb (Hecht et al., 1996; Laura N. Rusche et al., 2003). The spreading of the silent chromatin from the telomeric nucleation point is limited by the cellular amounts of the Sir proteins, in particular by Sir3 (Renauld et al., 1993). In agreement with this concept of distance-dependent silencing of SIR proteins, the overexpression of Sir3 and Sir4 was able to induce the repression of reporter genes distant from the silenced chromatin (Marcand et al., 1996).

Besides being silenced, the 32 telomeres of the 16 (haploid) yeast chromosomes tend to cluster at the nuclear periphery into several foci (Gotta et al., 1996; Kupiec, 2014). Imaging of telomeres, bound by Rap1 tagged with GFP, showed that Sir3 is necessary for telomere clustering (Figure 2A, top panels) and that Sir3 overexpression (*GAL1p-SIR3*) leads to an increase in telomere clustering (resulting in a “hypercluster” of telomeres; Ruault et al., 2011). The large Rap1-GFP hypercluster positions itself away from the nuclear periphery, in the inner-space of the nucleus (Figure 2A, bottom left panel). Interestingly, the overexpression of the spreading deficient *sir3-A2Q* mutant, which contains a N-terminal substitution that blocks its acetylation and thus silencing, also resulted in the formation of the telomere hypercluster (Wang et al., 2004). (Figure 2A, bottom right panel). Recent collaborative work between our lab and Angéla Taddei’s lab showed that Sir3 is also responsible for the formation of a telomere hypercluster in wild-type quiescent cells (G0). These hyperclusters are required to preserve cell viability over a long period of time (Figure 2B, black arrowheads) (Guidi et al., 2015). Their formation was associated to mitochondrial-related metabolic changes and was not related to an increase in the amount of Sir3 protein. Altogether, these observations suggested a model in which arrays of Sir3 binding sites are sufficient to promote telomere trans-interactions, and that these interactions occur independently of spreading-mediated silencing or anchoring at the nuclear periphery.

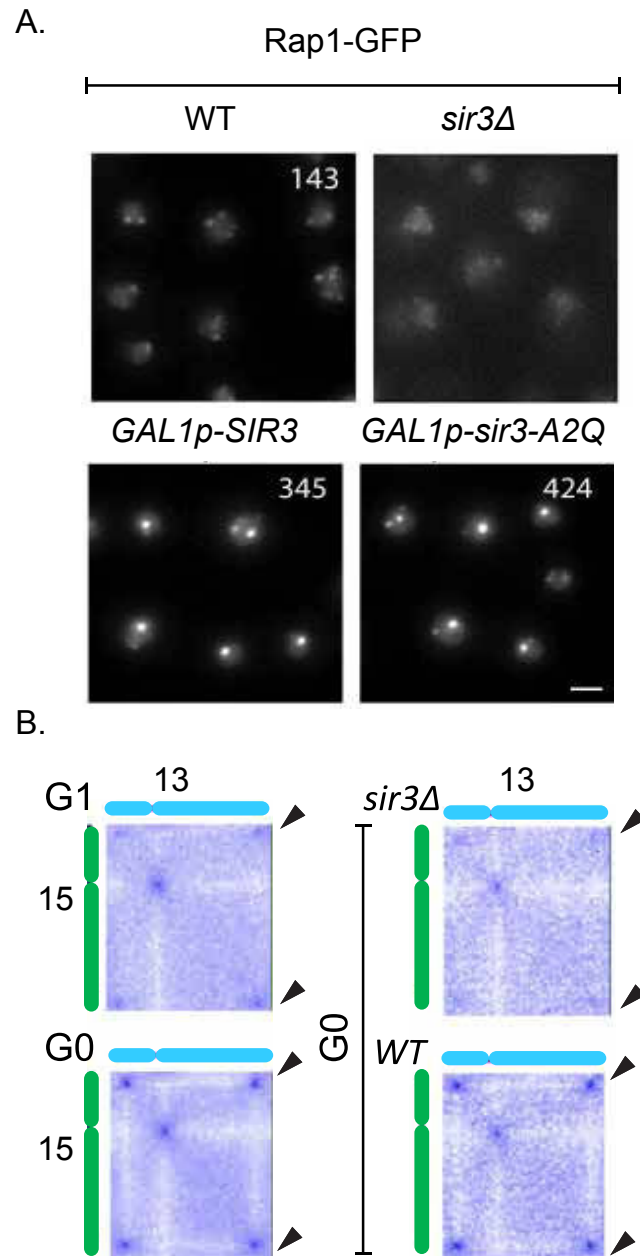


Figure 2 Telomeres: from no cluster to hypercluster. (A) Representative fluorescent images of the telomere-associated protein Rap1 tagged with GFP, show: few clusters in WT, no clusters in *sir3Δ* background and hyperclusters when Sir3 is overexpressed (*GAL1p-SIR3* and *GAL1p-sir3-A2Q*) (adapted from Ruault et al., 2011). (B) 3C contact maps corresponding to the inter-chromosomal contacts between chromosome 13 and chromosome 15 in G1 and G0 stages (WT and *sir3Δ*). Black arrowheads point at inter-telomeric contacts (adapted from Guidi et al., 2015).

Nutrient deprivation induces metabolic shutdown of transcription (Galdieri et al., 2010), which is linked to gene silencing and heterochromatin spreading (Laura N. Rusche et al., 2003). Here we used Hi-C to investigate the reorganization of Sir3-bound chromatin in response to metabolic changes and at different stages of the cell cycle. We observed that nutrient depletion after overnight growth seems to induce interactions between the rDNA and the telomeres in G1 cells. Although, these contacts were Sir3-independent and they were not preserved in quiescent cells (induced by starvation), they may be required to achieve the proper silencing at these loci. Therefore, to further investigate the structural adjustments of the chromatin in the presence and/or absence of Sir3 spreading activity, we analysed genome organizations in strains overexpressing this protein (Ruault et al., 2011). We showed that the overexpression of Sir3 (*SIR3* and *sir3-A2Q*) increases trans-telomere contacts, in agreement with the telomere grouping into hyperclusters. However, the intensity of telomere contacts was strongly correlated with the spreading activity of the protein, revealing internal structural differences between silenced and non-silenced hyperclusters. In addition to the telomeric regions, other 18 telomere-distal Sir3 binding sites were mapped using ChIP-seq. These were used to define a maximal spreading distance of the silenced chromatin (~45 kb) from the telomeres. Among these internal binding sites, we found that the rDNA and a locus positioned ~84 kb from the right telomere of chromosome 6 were recruited close to the telomeres in G1 cells, following Sir3 overexpression. These contacts were dependent on the spreading activity of Sir3 and were lost in G2/M arrested cells, although the telomere hyperclusters were maintained. These observations support the co-localization of rDNA and telomeres in G1 cells originated from overnight cultures. Possibly, this event may enhance Sir3 silencing activity and the propagation of heterochromatin on these loci.

Results

Telomere-proximal interactions independent of Sir3

In light of the relationship previously observed between cell metabolism and telomere clustering (Guidi et al., 2015), we studied cell populations synchronized in either G0, G1 or G2/M (Material and Methods). G0 quiescent cells were obtained by gradient density fractionation of carbon source starved cultures as described in Guidi et al. (2015). G1 daughter cells were obtained by elutriation of exponential growing cultures (Marbouty et al., 2014). Finally, G2/M cells were obtained from G1 elutriated cells released into rich medium in presence of nocodazole. Fractions of 2×10^9 synchronized cells were processed into Hi-C libraries and analysed as previously described (chapter 2.1, section Material and Methods). Genomic contact maps were generated (5 kb bin resolution) and the different conditions were compared using log-ratio representations (50 kb bin). The colorscale reflects the contact variation in one map compared to the other (Figure 3A). Hi-C experiments confirmed the requirement of Sir3 protein for trans-telomere interactions, both in G0 and G1 cell populations (Figure 3A). The 3D structure illustrates the complete disassembly of the telomere cluster in the absence of Sir3 (Figure 3B, *sir3Δ* G0 and *sir3Δ* G1).

An in-depth investigation of the Hi-C contact map of Sir3-depleted cells (*sir3Δ* G1) revealed also unexpected contacts. Although telomere clusters are disrupted in this condition, telomere-proximal regions of chr1R and chr9R (two chromosome arms of approximate equal size ~78 kb) appear to maintain trans-contacts between two *FLO* genes, *FLO1* and *FLO11* (Figure 4A). The proximity of these genes to the telomeres may have masked these contacts in the wild-type contact map (Figure 4B). Flo1 and Flo11 are members of the cell-surface adhesins family, required for morphological changes of yeast cells when the flocculation and/or adhesion processes are induced by external stimuli (Verstrepen et al., 2004). The unusual large size of the 5' regulatory region of *FLO11* (~3.6 kb) (Rupp et al., 1999) coupled with the fact that both *FLO* genes share similar trans regulatory elements (Fichtner et al., 2007) led us to speculate a possible functional role of their spatial proximity during transcription activation.

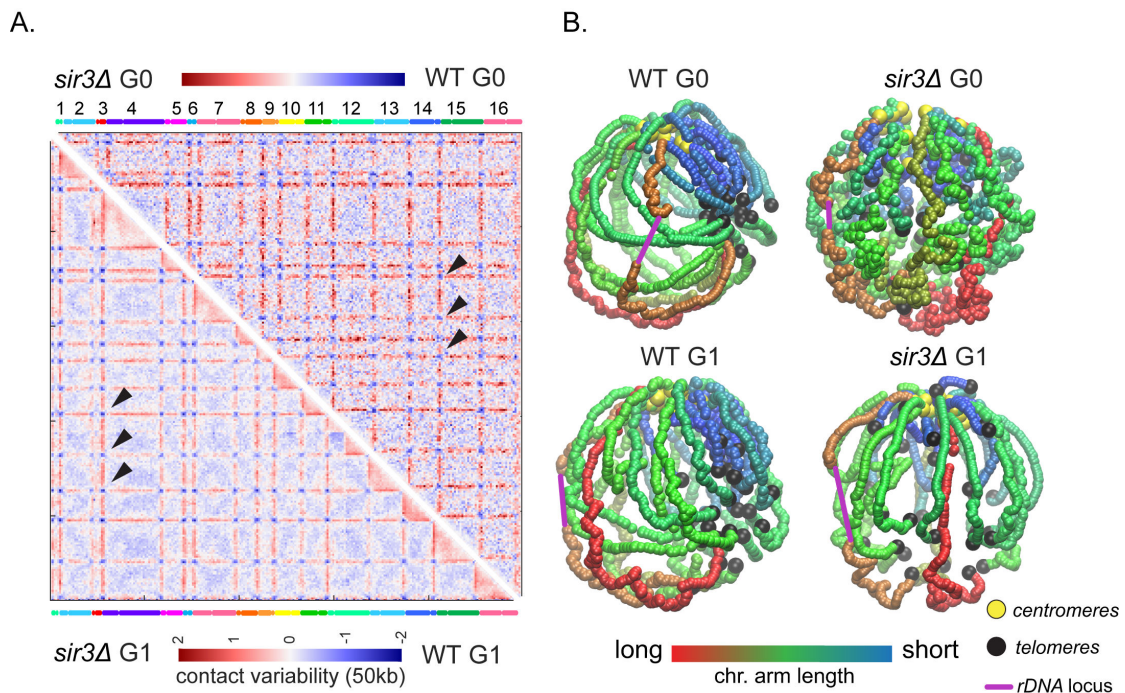


Figure 3 Telomere clusters are Sir3 dependent. (A) Comparison of contact maps (50 kb bin). Top right map: log-ratio between *sir3Δ* G0 and WT G0 cells. Bottom left map: log-ratio between *sir3Δ* G1 and WT G1 cells. The 16 yeast chromosomes are displayed above the maps. Blue to red colour scales reflect the enrichment in contacts in one population with respect to the other. Black arrowheads point at inter-telomere contacts. (B) 3D average representation of the Hi-C contact maps (5 kb bin): WT G0, *sir3Δ* G0, WT G1 and *sir3Δ* G1. The colour code reflects chromosomal arm lengths and, centromeres, telomeres and rDNA are highlighted.

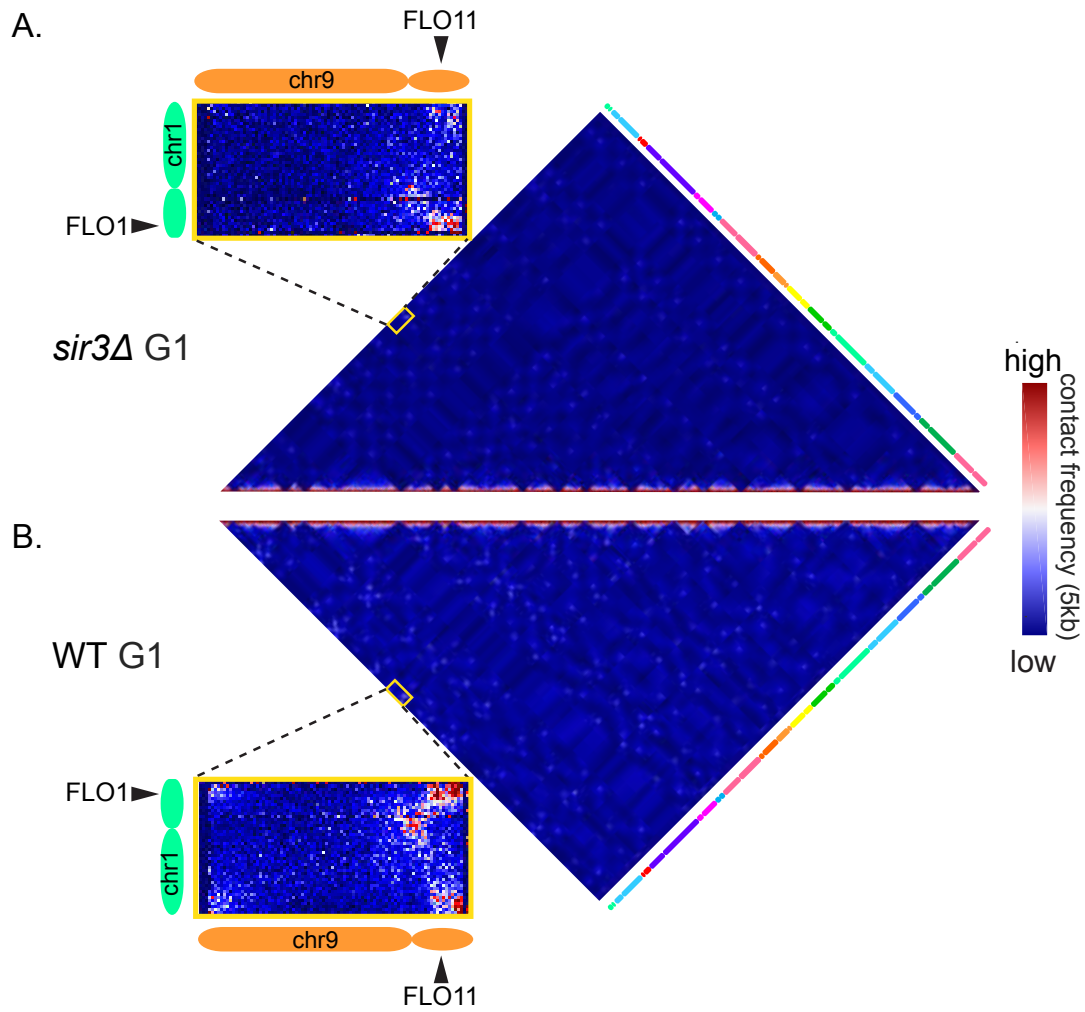


Figure 4 Telomere-proximal *FLO* genes interact independently of Sir3. Hi-C contact maps obtained from *sir3Δ* G1 (A) and WT G1 (B) cell populations (5 kb bin). Insets display magnifications of the inter-chromosomal contacts between chr1R and chr9R and point at the *FLO1* and *FLO11* interaction. Blue to red colour scale reflects low to high contact frequency.

Telomere hyperclusters: a consequence of metabolic adaptation

Yeast cells grown in liquid rich-medium metabolize glucose and release ethanol in the medium. When glucose becomes limiting, cells enter a diauxic shift characterized by a decreased growth rate and a switch of the metabolism from fermentation to aerobic respiration using ethanol. Then, when ethanol is in turn depleted, cells finally enter stationary phase and, eventually, quiescent state (G0). These processes are accompanied/reflect many physiological changes: the overall transcription and translation are drastically reduced whereas chromatin compaction is increased (Gray et al., 2004). This latter observation is supported by the role of Hho1 (histone variant H1) in chromatin compaction, as a consequence of low transcriptional activity during stationary phase (Schäfer et al., 2008). In light of these observations we investigated genome organization both at the final stage of adaptation to nutrient deprivation (G0) and also during the first moments of this stress condition. Where the overnight saturated cultures may represent an example of first adaptation to nutrient limitation. Therefore, G1 cells were isolated from overnight cultures (onG1) and processed by Hi-C. The log-ratio comparison confirmed telomeres forming hyperclusters in quiescent G0 cells (Guidi et al., 2015), while also revealed that telomeres start to increase clustering already during overnight growth (Figure 5A, black arrowheads, boxplots). In addition a reorganization of the chromatin fibre occurs and promotes an increase in intra-chromosomal contacts during G0. This is clearly visible on chromosomes 12 (Figure 5A, box bottom right) that starts to reorganize itself during the overnight growth (onG1), giving rise to peculiar contacts between the rDNA and the telomeres (Figure 5A, purple arrowheads). The rDNA contact profiles were extracted from the log-ratio maps and displayed as 4C-like contact profiles (Material and Methods). These plots show that rDNA-telomere contacts are established in overnight cultures (onG1/expoG1), independently of Sir3 protein (*sir3Δ* onG1/expoG1), and that they are lost in G0 (G0/expoG1) (Figure 5B). These results led to the hypothesis that stress conditions, such as nutrient depletion, may trigger a silencing program that relies on the recruitment of the telomeres at the rDNA locus. The spreading/silencing ability of the telomeric Sir3 may be enhanced by the activity of the nucleolar Sir2 (Gotta et al., 1997). Therefore, it is possible that the G0 hyperclusters are a consequence of Sir3 spreading activity. However, this observation was in contrast with microscopy imaging showing that overexpressed Sir3 induces telomere hyperclusters independently of the spreading activity (absent in *sir3-A2Q* mutant) (Ruault et al., 2011). To shed light on this discrepancy we decided to investigate the nature of these hyperclusters in different growth conditions.

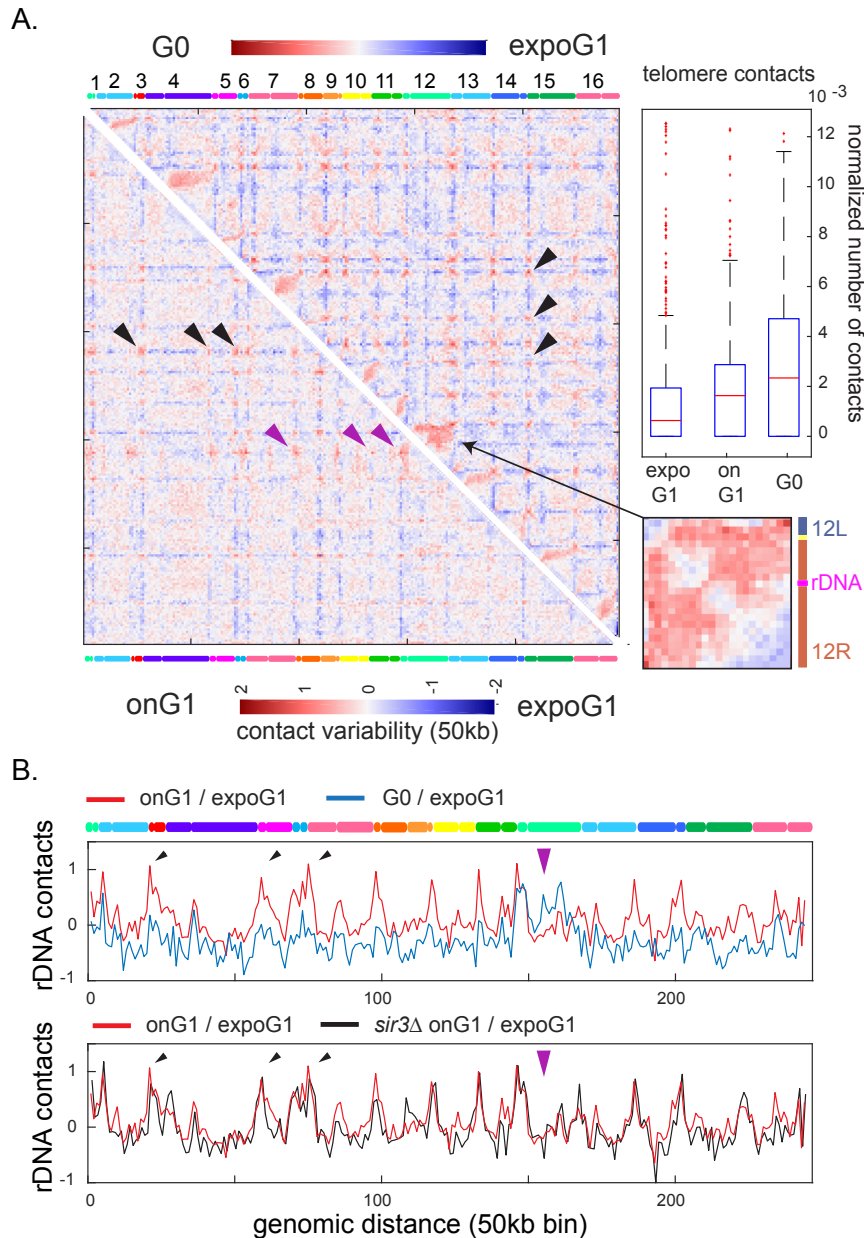


Figure 5 Genomic structural differences in metabolic different cells. (A) Log-ratio contact maps (50 kb bin) of G1 exponentially growing cells (expoG1) with: G0 (top right) and overnight G1 (onG1, bottom left) cell populations. The 16 yeast chromosomes are displayed above the maps. Blue to red colour scales reflect the enrichment in contacts in one population with respect to the other. Black arrowheads point at inter-telomere contacts. Purple arrowheads point at contacts between rDNA and telomeres. Boxplot quantifications of telomere contacts (expoG1, onG1 and G0) show a direct correlation between changes in metabolism and intensity of the contact signal (5 kb bin contact maps). Bottom right inset displays a magnification of the log-ratio map of chromosome 12, that shows an increase of intra-chromosomal contacts in G0. **(B)** Log-ratio distributions of normalized chromosomal contacts made by a 50 kb cen-proximal rDNA flanking region with the rest of the genome in onG1/expoG1, G0/expoG1 and *sir3Δ* onG1/expoG1. Arrowheads indicate telomere (black) and rDNA (purple) positions.

Investigating hyperclusters in exponentially growing cells

Sir3 binding sites in wild-type (WT) and *SIR3* overexpression were mapped using ChIP-seq by Antoine Hocher, in Angela Taddei lab (Figure 6). The results show that the majority of the sites enriched for Sir3 binding are telomere-proximal, although the degree of spreading varies between telomeres. To investigate the organization of the chromatin inside the hyperclusters, we performed Hi-C on G1 cells isolated from exponentially growing cultures and overexpressing the Sir3 protein (wild-type *SIR3* G1 and *sir3-A2Q* G1). We then computed the log-ratio maps between the overexpressed and non-overexpressed conditions (WT G1). Although, both the overexpression of *SIR3* and *sir3-A2Q* result in an increase of trans-telomere contacts, this increase was enhanced when Sir3 protein is able to spread (Figure 7A, black arrowhead, boxplots). The enrichment in contacts in *sir3-A2Q* may therefore result from an excessive binding of Sir3-A2Q mutant only at telomeric repeats, without altering the structure of the chromatin. Whereas, the spreading of the wild-type Sir3 protein increases the amount of the highly packed subtelomeric heterochromatin.

In addition, a strong enrichment in contacts between the rDNA and telomeres is observed in the strain overexpressing *SIR3* (Figure 7A, B, purple arrowheads). The 3D representation of the corresponding contact map clearly illustrates the interaction between the rDNA and telomere hypercluster (Figure 7C). Notably, the overexpression of *sir3-A2Q* is not able to reposition the telomere cluster in proximity to the rDNA locus in G1 exponential cells. These results are in agreement with the previously observed rDNA-telomere contacts in G1 overnight cells. Altogether they support the hypothesis that “naturally-induced” telomere hyperclusters are a consequence of the spreading of Sir3 on the telomeres’ ends. This spreading coupled with silencing is probably more efficient if the Sir3-bound telomeres are relocated proximal to the nucleolus where the majority of Sir2 deacetylase is found (Gotta et al., 1997). It is tempting to speculate that the internal reorganization of chromosomes in G0 (Figure 5A) could be partially the consequence of the assembly of chromosomal ends into dense heterochromatic hyperclusters.

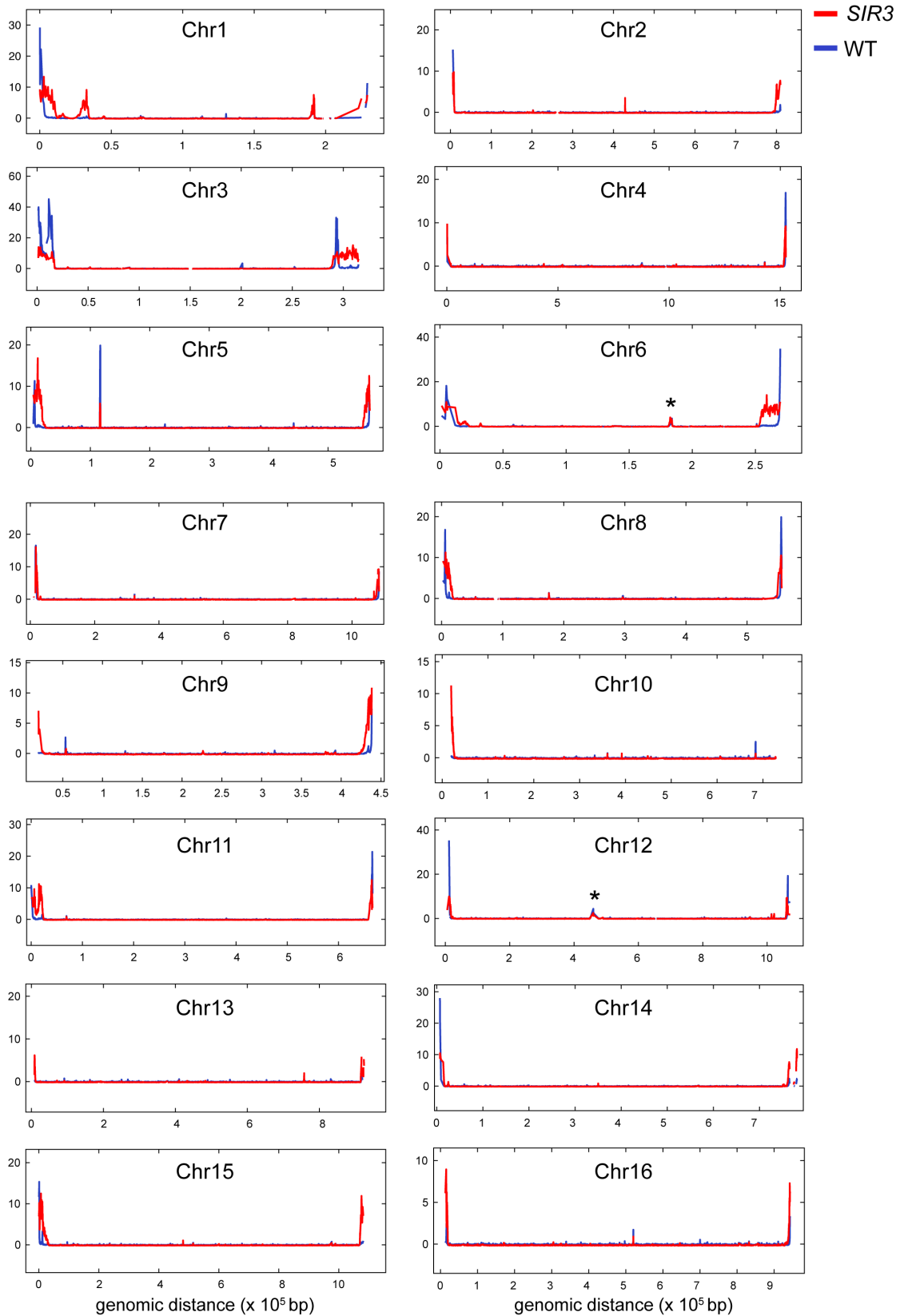


Figure 6 Sir3 binds and spreads in the telomere's proximity. ChIP-seq analysis mapping binding sites of the Sir3 protein in wild-type (WT, blue) and *SIR3* overexpression strains (*SIR3*, red). Stars indicate internal binding sites of Sir3 protein. Performed by Antoine Hocher (Taddei Lab, Institut Curie, Paris).

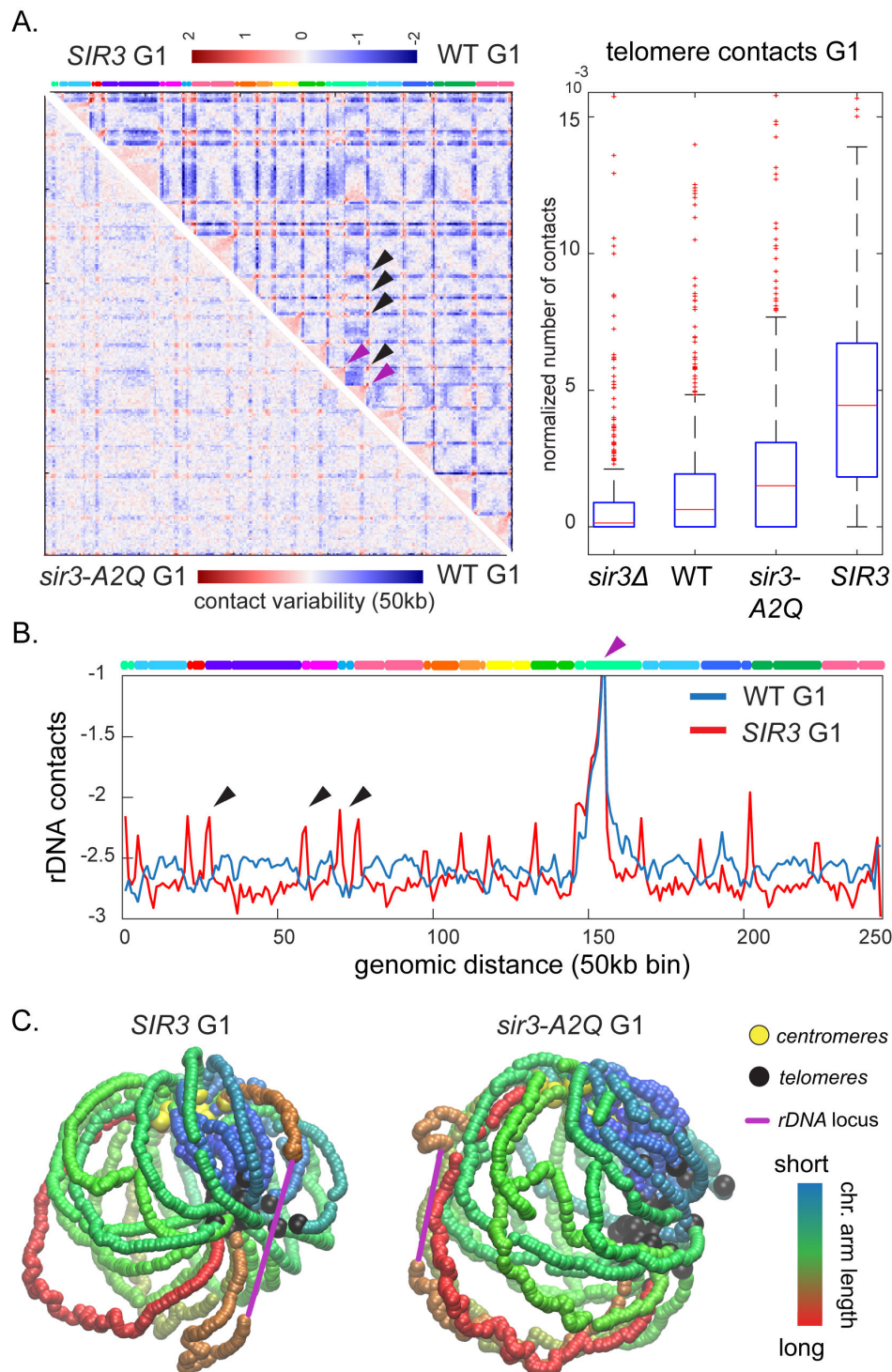


Figure 7 Structural differences between silenced and non-silenced hyperclusters. (A) Comparison of G1 contact maps (50 kb bin). Top right map: log-ratio between *SIR3* and WT cells. Black arrowheads point at inter-telomere contacts. Purple arrowheads point at contacts between the rDNA and the telomeres of chr12. Bottom left map: log-ratio between *sir3-A2Q* and WT cells. The 16 yeast chromosomes are displayed above the maps. Blue to red colour scales reflect the enrichment in contacts in one population with respect to the other. Boxplot quantifications of G1 telomere contacts show a direct correlation between the amount of protein and the intensity of

the contact signal (5 kb bin contact maps). **(B)** Distributions of G1 normalized chromosomal contacts made by a 50 kb cen-proximal rDNA flanking region with the rest of the genome in WT and *SIR3* cells. Arrowheads indicate telomere (black) and rDNA (purple) positions. **(C)** 3D average representation of the G1 Hi-C contact maps (5 kb bin): *SIR3* and *sir3-A2Q*. The colour code reflects chromosomal arm lengths and, centromeres, telomeres and rDNA are highlighted.

The replication of telomeres causes their release from the nuclear envelope (Ebrahimi and Donaldson, 2008), whereas the relocation of the telomere hyperclusters towards the nuclear interior persists in cells at different cell cycle stages. We investigated the dynamics of post-replicative telomeres in the WT, *sir3Δ* and *SIR3* strains. Populations of G1 elutriated cells for each of these strains were released into S phase and arrested with nocodazole at G2/M for Hi-C. The depletion of the Sir3 protein in G2/M arrested cells (*sir3Δ* G2/M) displays only a mild reduction of the telomere contacts compared with the wild-type (WT G2/M) (Figure 8A, boxplot). This is likely a consequence of the expected post-replication telomere detachment from the nuclear periphery. Cells overexpressing *SIR3* maintain strong contacts between telomeres in G2/M (Figure 8A, black arrowheads and boxplot), whereas the contacts between the rDNA and the telomeres are completely lost (Figure 8B). The 3D representation of the corresponding contact map illustrates the separation of the rDNA locus from the telomere hypercluster (Figure 8C). In light of this observation, it is possible that the exclusion of the rDNA locus from the telomere hyperclusters is due to a different nuclear localizations of these loci after replication. That could be the consequence of their different mechanisms of nuclear envelope attachment (Mekhail et al., 2008, 2008). However, we cannot exclude a potential secondary effect due to the treatment of the cells with nocodazole, known to cause centromere detachment from the nuclear envelope (Jacobs et al., 1988b). As previously discussed (chapter 2.1 section "Nocodazole affects chromosome 12 conformation", Lazar - Stefanita et al., 2017), cells treated with nocodazole display a different organization of chromosome 12 when compared with cells in G2 or cells arrested in metaphase using conditional mutants (such as *cdc20*). Therefore, these results remain to be further clarified.

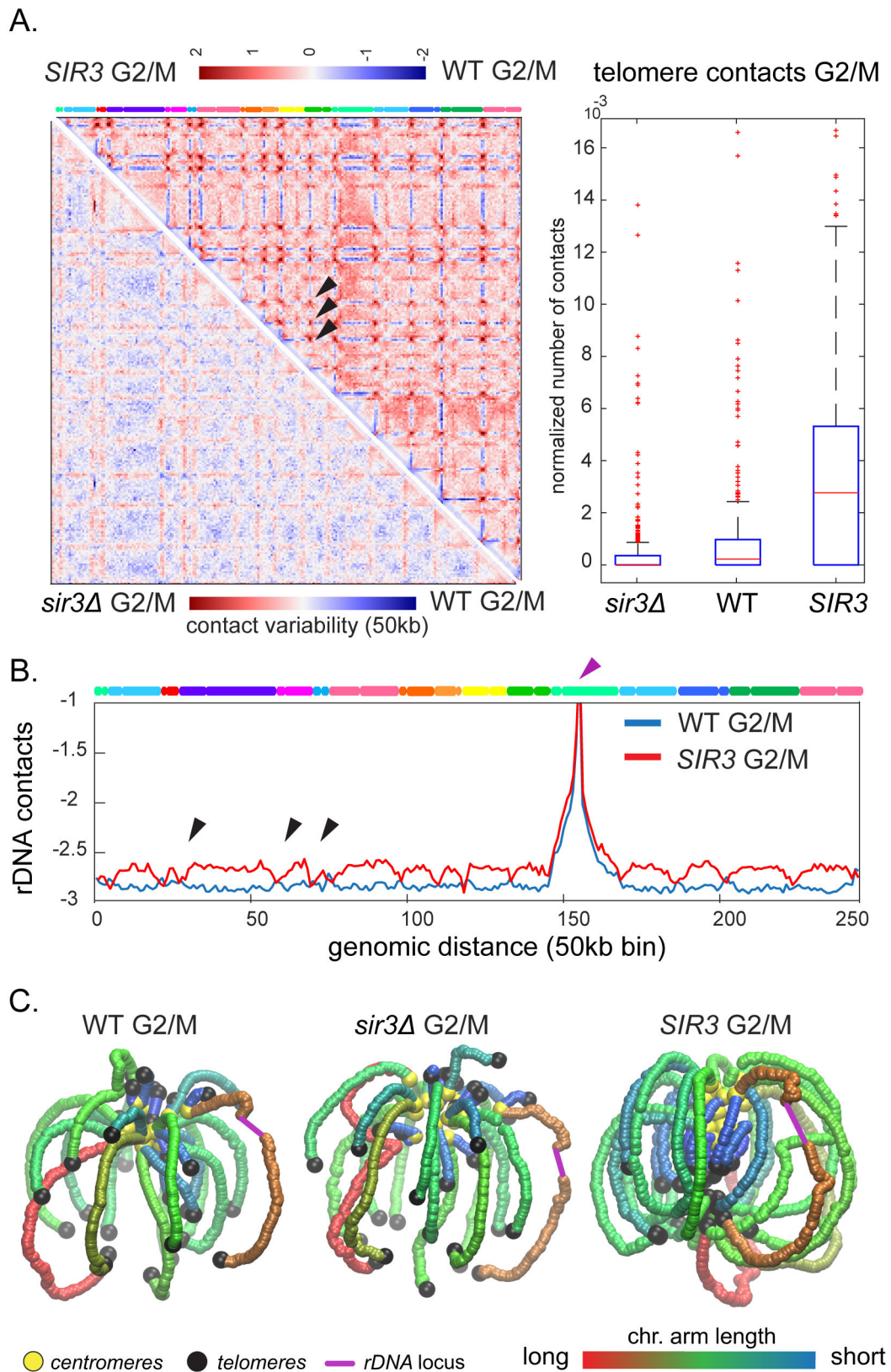


Figure 8 Reorganization of telomere hyperclusters in G2/M arrested cells. (A) Comparison of G2/M contact maps (50 kb bin). Top right map: log-ratio between *SIR3* and WT cells. Black arrowheads point at inter-telomere contacts. Bottom left map: log-ratio between *sir3Δ* and WT cells. The 16 yeast chromosomes are displayed above the maps. Blue to red colour scales reflect

the enrichment in contacts in one population with respect to the other. Boxplot quantifications of G2/M telomere contacts (5 kb bin contact maps). **(B)** Distributions of G2/M normalized chromosomal contacts made by a 50 kb cen-proximal rDNA flanking region with the rest of the genome in WT and *SIR3* G2/M cells. Arrowheads indicate telomere (black) and rDNA (purple) positions. **(C)** 3D average representation of the G2/M Hi-C contact maps (5 kb bin): WT, *sir3Δ* and *SIR3*. The colour code reflects chromosomal arm lengths and, centromeres, telomeres and rDNA are highlighted

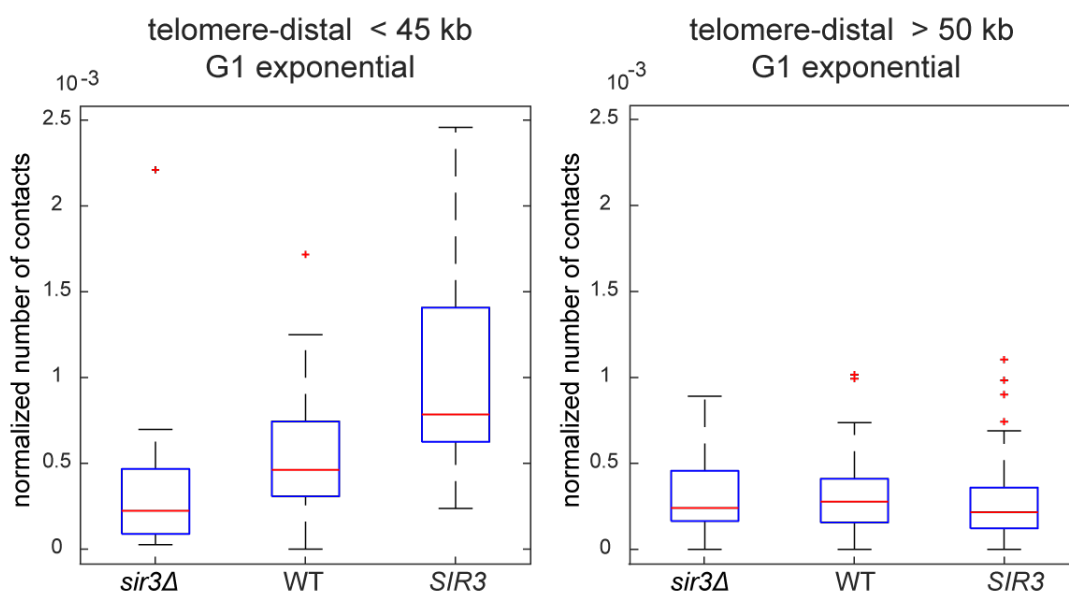
Telomere-distal binding sites of Sir3: how far can you go?

As previously showed (Figure 6), several telomere-distal binding sites of Sir3 (located more than 30 kb from the nearest telomere) were mapped in the wild-type and overexpressed *SIR3* strains by ChIP-seq (Table 1) (Antoine Hocher, Taddei's lab). This analysis has found that the size of the binding sites were quite variable from 1 kb up to almost 10 kb and they were located at different distances from the telomeres.

The overexpression of Sir3 provides an ideal condition to map the maximal spreading distance of the silenced chromatin from the telomeres. We reasoned that at increasing distances from the telomeres the probability of contacts should diminish and, eventually, drop at the chromosomal position where the spreading ends. For this analysis we used the contact maps of G1 exponential cells of: *sir3Δ*, WT and *SIR3* strains. We quantified the contact frequency between the 18 telomere-distal sites and revealed that sites mapped more than 50 kb from the telomeres drastically diminished their interaction (Figure 9A). To further investigate whether these sites preferentially interact between each other or with the telomere hyperclusters, the 4C contact profiles were analysed. Examples of 4C profiles show two binding sites on chromosome 7: one located < 45 kb from the telomere, contacting all the telomeres while the other located > 50 kb does not (Figure 9B). Altogether these analyses suggest that Sir3-bound regions up to 45 kb from the telomeres' ends are probably included and silenced inside the hyperclusters.

Among the 11 telomere-distal sites (> 50 kb) a discrete locus on the right arm of chromosome 6 and positioned ~84 kb away from the telomere stood out during the analysis. This locus is particularly enriched for Sir3 binding in both WT and *SIR3* overexpression conditions (Figure 6, star). In addition, this locus presents strong contacts with both the telomeres and the rDNA in G1 overexpression (Figure 10). Whereas, the other internal sites contact neither the telomeres nor the rDNA (examples in Figure 9B). The contact on chr6 is dependent on Sir3 (absent in *sir3Δ*) and requires the spreading activity of the protein (absent in *sir3-A2Q*) (Figure 10A). It imposes a fold inside the arm of Chr6 and gives rise to a peculiar pattern of contacts that appear as "butterfly-like" shape on the contact map (Figure 10A). As a consequence of the hypercluster formation, this locus establishes contacts with all the telomeres. Similarly to the rDNA, these contacts disappear in G2/M (Figure 10B). So far, we could not find any significant genomic feature in this region that might provide indications on the functional role of this structure.

A.



B.

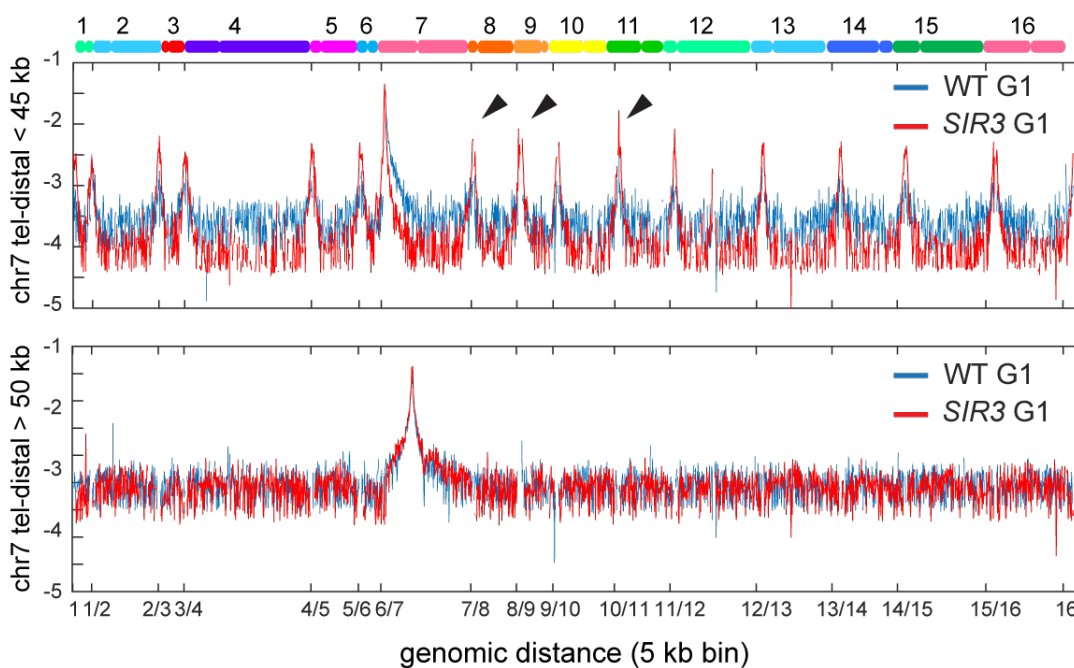


Figure 9 Contacts between telomere-distal Sir3 binding sites indicate a maximum hypercluster size of ~45 kb. (A) Boxplot quantifications of contacts (5 kb bin contact maps) between telomere-distal Sir3 binding sites in *sir3Δ*, WT and *SIR3* strains synchronized in G1. Left boxplot: contacts between sites that are located less than 45 kb from the telomeres. Right boxplot: contacts between sites that are located more than 50 kb from the telomeres. (B) Distributions of normalized chromosomal contacts made by two telomere-distal binding sites located on chromosome 7 (5 kb bin) with the rest of the genome in WT G1 and *SIR3* G1 cells. Top panel: position centered on the 32 kb coordinate chr7L. Bottom panel: position centered on the 370 kb coordinate chr7L. Black arrowheads indicate telomere positions.

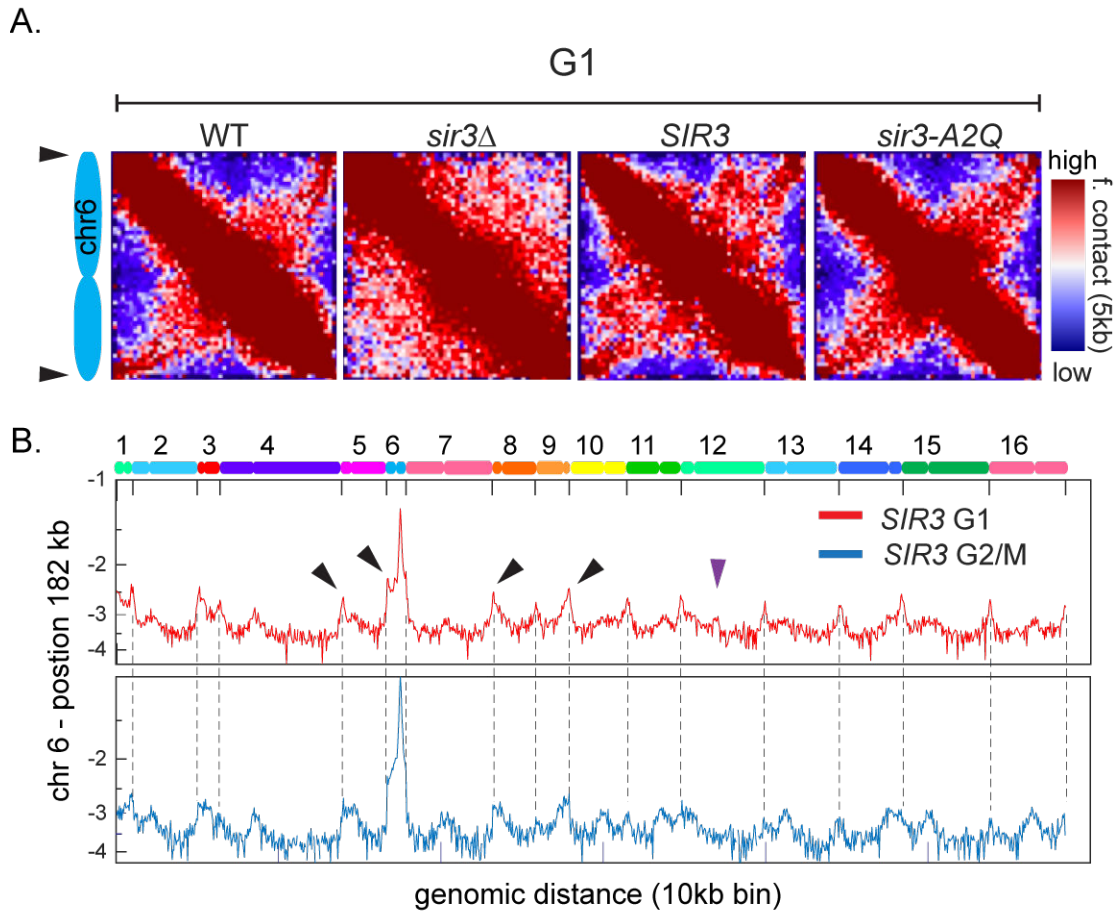


Figure 10 Dynamics of a telomere-distal Sir3 binding site. (A) Hi-C contact maps of chromosome 6 in G1: WT, *sir3Δ*, *SIR3* and *sir3-A2Q* strains (5 kb bin). Chromosome 6 is displayed on the left side, arrowheads point at the two telomeres. Blue to red colour scale reflects low to high contact frequency. (B) Distributions of normalized chromosomal contacts made by a 10 kb region on chr6 (centered on the 182 kb coordinate) with the rest of the genome in *SIR3* G1 and *SIR3* G2/M. Arrowheads indicate telomere (black) and rDNA (purple) positions.

Discussion

In this work we combined Hi-C and ChIP-seq to investigate the organization of the telomeric chromatin in different metabolic conditions in the presence or absence of the silencing protein Sir3.

Our results confirmed the essential role of Sir3 in the formation of telomere clusters (Guidi et al., 2015; Marcand et al., 1996; Moretti et al., 1994) and showed that an increase in protein concentration resulted in telomere and subtelomere hyperclusters (Ruault et al., 2011). The spreading of Sir3 on the subtelomeres gives rise to dense heterochromatic clusters (including up to ~45 kb), well isolated from the rest of the genome. By microscopy, it was observed that the hyperclusters of telomeres tend to relocalize in the middle of the nuclear space (Ruault et al., 2011), a position which could reflect the physical constrain imposed by the small arms. Moreover, natural-induced telomere hyperclusters have been reported to play a role in maintaining the viability of quiescent G0 cells, characterized by significantly reduced metabolic rates (Guidi et al., 2015). Our analysis of G1 cells from overnight saturated cultures revealed that telomeres start to increase clustering relatively early during cell adaptation to nutrient depletion and that this process is Sir3-dependent. Although at this stage, telomeres are not yet assembled into hyperclusters. In addition, during this early reorganization telomeres start to contact the rDNA locus. It was shown that only 20% of the 150 - 200 copies of the ribosomal RNA gene copies of the rDNA cluster (Johnston et al., 1997) are actively transcribed. Whereas, the others are silenced in a SIR-dependent manner (Gotta et al., 1997), a process that increases the genomic stability of this repeated locus (Huang and Moazed, 2003; Kaeberlein et al., 1999; Pasero et al., 2002). Moreover, the prolonged lifespan in nutrient deprivation correlates with the enhanced rDNA silencing that this is partially dependent on Sir2 (Kaeberlein et al., 1999). In addition, it has been shown that the nucleolar Sir2 recruits Sir3 for silencing and, that in the absence of Sir3, the subtelomeric localization of Sir2 is lost (Gotta et al., 1997). Although, the rDNA-telomere contact observed in overnight cells was neither dependent on Sir3 nor preserved in G0 cells, the overexpression of Sir3 in exponential growing cells displayed this contact. Interestingly, the bridge between the rDNA and the telomere hypercluster was impaired in the spreading/silencing defective protein (*sir3-A2Q*). These results suggest that a “first” response to starvation may rely on the re-localization of the Sir3-bound telomeres close to the Sir2-enriched nucleolus to achieve silencing and eventual hyperclusters. The colocalization of the two major prone-to-silencing loci (rDNA and telomeres) would sequester the SIR factors in subnuclear compartments where they are needed, avoiding unwanted ectopic silencing. These rDNA–telomere contacts were lost after replication in

cells arrested in G2/M by nocodazole, although the telomere hyperclusters were maintained. In the previous section 2.1 we showed that nocodazole treatment affects the organization of chromosomes 12. This is probably the result of centromere detachment from the nuclear envelope, microtubule-dependent attachment (Heun et al., 2001a; Jacobs et al., 1988b). Whereas, the microtubule-independent perinuclear anchoring of the rDNA is not altered (Mekhail et al., 2008). Therefore, the exclusion of the rDNA from the G2/M hyperclusters could be an artefact of the drug treatment on the global structure of the nucleus.

An additional observation made during these experiments was the Sir3-dependent contacts detected between *FLO* genes. *FLO1* and *FLO11* genes are among those genes involved in the flocculation, adhesion and filamentous processes (Kobayashi et al., 1999). The commonly used *S. cerevisiae* BY4741 strain (Brachmann et al., 1998) is a completely non-adherent yeast. The telomere-proximal flocculin genes are silent with the exception of *FLO11* gene, which is responsible for cell-substrate adhesion within the haploid as well as the diploid yeast life cycle in different environments (Verstrepen et al., 2004). Noteworthy, *FLO* genes contain multiple intragenic tandem repeats, which are sources of inter-*FLO* recombination and functional variability (Verstrepen et al., 2005). Not only do *FLO1* and *FLO11* share similarities in the repeated regions but they are also known to be co-regulated by the same transcription factor, Flo8 (Fichtner et al., 2007; Kobayashi et al., 1999). Analysis of the intergenic region of *FLO11* has reported the longest 5' non-coding region with a regulatory functions in the yeast genome (~3.6 kb upstream of the ATG) (Rupp et al., 1999). Recently, the transcription of two long ncRNA (*ICR1* and *PWR1*) has been reported to control the epigenetic state of the *FLO11* promoter. The authors observed that in function of the transcribed long ncRNA the status of the chromatin becomes more or less accessible to Flo8, therefore switching from transcribed to repressed *FLO11*, respectively (Bumgarner et al., 2009). Although, Flo8 activates *FLO1*, the promoter of this latter lacks all the regulatory region described for *FLO11* (Fichtner et al., 2007). In the light of these observations, maybe the *FLO1* - *FLO11* contacts could be related to a shared transcription regulation system relying on the non-coding region of *FLO11*? Further investigations are needed to understand the regulatory function of this long non-coding region on the chromatin structure. First, a thorough investigation of the transcription activity in this regulatory region and in different growing conditions, is needed. For this purpose we can exploit genome-wide transcription profiles already available on GEO databank (Barrett et al., 2013). This analysis may give us important hints on the potential status of the chromatin (e.g. high

levels of *ICR1* are associated with an open state of the chromatin dependent of Rpd3 histone deacetylase) (Bumgarner et al., 2009). Second, both colocalizing *FLO* genes are located at nearly identical distances from the respective centromeres therefore their colocalization might be favoured by the rabl-like organization of yeast chromosomes. Noteworthy, *FLO9* located on the other arm of chr1 (also short) does not seem to contact *FLO1* and *FLO11*. To investigate this possibilities we could reposition these genes at ectopic locations on the rabl organization (e.g. short and long chromosomal arms).

The compact genome of *S. cerevisiae* is characterized by relatively short genes with little introns and predominantly short regulatory sequences that have made difficult to detect inter-chromosomal links between functionally related genes. To our knowledge the observations reported here could point at contacts between transcriptionally co-regulated genes in budding yeast.

Material and Methods

Yeast strains

All the strains are derivatives of BY4741 (*MATa his3Δ1 leu2Δ0 met15Δ0 ura3Δ0*). Built by Antoine Hocher (Taddei Lab, Institut Curie, Paris). All the strains contain the Rap1 protein tagged with GFP (*rap1::GFP-RAP1*). Several strains overexpress Sir3 protein or the mutated variant under the control of the GAL1 promoter (*SIR3::pGPD-SIR3*, *SIR3::pGPD-sir3-A2Q*).

For **Hi-C experiments and data analysis** refer to the Chapter: 2.1 “Cohesins and condensins orchestrate the 4D dynamics of yeast chromosomes during the cell cycle” . An average of 13 millions of valid Hi-C reads were used to generate each contact map.

Table 1 Sir3 telomere-distal binding sites. ChIP-seq analysis mapped internal binding sites (> 30 kb from the nearest telomere) of the Sir3 protein in *SIR3* overexpression strains. Performed by Antoine Hocher (Taddei Lab, Institut Curie, Paris). The spreading distance is indicated by the start and end coordinates, respectively. The contact frequencies between these sites (see Figure 9) were computed from the 5 kb maps using the average coordinate chromosomal position.

Chromosome	start binding site (bp)	end binding site (bp)	average coordinate of the binding site (kb)	distance from the telomere (kb) (> or < 50kb)
Chr1	40881	47022	44	< 45
Chr1	69000	75000	72	> 50
Chr1	187987	193994	191	< 45
Chr2	428000	431000	430	> 50
Chr3	28487	32005	30	< 45
Chr3	48838	54340	52	> 50
Chr4	433976	438438	436	> 50
Chr5	224000	227000	226	> 50
Chr5	384000	388000	386	> 50
Chr6	30985	34010	32	< 45
Chr6	180274	184861	183	> 50
Chr7	29617	34888	32	< 45
Chr7	366000	367000	367	> 50
Chr7	1066000	1070000	1068	< 45
Chr10	682000	686000	684	> 50
Chr12	1017315	1024251	1021	> 50
Chr13	755250	760317	758	> 50
Chr14	750000	760000	755	< 45

Part 3 :

2.3 Investigating the influence of genome architecture and dynamics on genomic stability during replication in *S. cerevisiae*

Summary

Different aspects of the higher-order organization of the yeast genome have been discussed earlier in this manuscript (sections 2.1 and 2.2). We notably contributed to show that subchromosomal domains of chromosomes (e.g. centromere and telomere clusters) are positioned non-randomly with regard to each other and to nuclear landmarks. Also, we have investigated the structural influence of several protein complexes (e.g. SMC, Top2, SIR, etc.) on chromatin structure during the cell cycle. The functional role of genome organization is a long standing question, and a number of reports have described an influence of this parameter on a number of carefully regulated chromosomal processes, including DNA repair, replication and transcription (Misteli, 2007; Prioleau and MacAlpine, 2016; Taddei and Gasser, 2012). Indeed, one of the original motivations of this work was to study the influence of chromosome organization on DNA repair. Here, I will discuss some of the work tackled during my PhD that aimed to better understand the consequences of improper DNA replication on genome plasticity in light of chromosome organization.

Introduction

In eukaryotes, DNA replication takes place in S phase. The early stages of replication involve the loading of the origin of replication complex along the chromosome at sites dubbed origins of replication, from which functional replisomes (replication forks associated with the replication machinery) progress bidirectionally. The positions of the origins of replication along chromosomes have been characterized genome-wide in many eukaryotes (Prioleau and MacAlpine, 2016). In budding yeast, contrary to most other eukaryotic species, replication origins consist of approximately 500 small (11 bp consensus sequence) discrete loci, called autonomously replicating sequences (ARS, Brewer and Fangman, 1987; Raghuraman et al., 2001). ARS sequences are distributed along chromosomes at relatively even distances (Raghuraman et al., 2001; Yabuki et al., 2002), but their activation is not systematic, nor simultaneous. Differences in firing efficiency between ARSs has led to their categorization into early, mid and late origins (Brewer and Fangman, 1991). The coordinated activation of replication origins ensures

that the duplication of the genome occurs in a timely manner. In other eukaryotes origin consensus sequences (Cayrou et al., 2011; Valton et al., 2014) have been more loosely defined, than the ARS sequences, nevertheless their sequential activation has also led to the characterization of specific temporal programs in a variety of species, such as mammals (Cadoret et al., 2008), flies (Schübeler et al., 2002) and in fission yeast (Patel et al., 2006). Chromatin remodelers such as chromatin-binding proteins (e.g. SIR complex, Stevenson and Gottschling, 1999) and chromatin-modifying enzymes (e.g. histone deacetylases and methylases) control the timing of eukaryotic origin activation (Aparicio et al., 2004; Casas-Delucchi et al., 2012; Rivera et al., 2014; Vogelauer et al., 2002).

Replication factory: a contentious model

Early imaging studies of metazoan replicating cells have suggested a spatial-temporal coordination of DNA replication. Notably, neighboring replication forks were suggested to cluster together in the nucleus, resulting in the generation of “replication factories”. These compartments gather together DNA polymerase and replication cofactors where the DNA duplication of multiple DNA strands proceeds at the same time (Nakamura et al., 1986; Jackson and Pombo, 1998). An alternative way to investigate the spatial organization of the replication program came with the advent of the chromosome conformation capture (3C) technique (Dekker et al., 2002; Lieberman-Aiden et al., 2009). Using Hi-C, Pope et al., (2014) showed that topological associating domains (TADs, ~900 kb) seem to correspond to stable units of replication timing in mammals and proposed a “replication domain model”, derivative of the replication factory concept (Pope et al., 2014).

In unicellular eukaryotes, such as budding yeast, the uneven distribution of early and late origins along chromosomal arms results in replication-timing domains. For instance, centromere-proximal regions, which are enriched in early origins, replicate at the onset of S phase, while telomere-proximal regions replicate late (McCarroll and Fangman, 1988; Raghuraman et al., 2001). In addition, these loci are known to form distinct subnuclear compartments, such as centromere clusters and telomere foci (Figure 1A) (Zimmer and Fabre, 2011). As in metazoans, foci of DNA polymerases were observed in yeasts, suggesting the assembly of origins into factories (Meister et al., 2007; Pasero et al., 1997). A more recent study showed that replication forks, generated from the same origin, remain associated with each other during replication. This work supported the replication factory model, containing about ten replisomes each (Kitamura et al., 2006). Investigation of chromosome 3D structure with 3C in budding

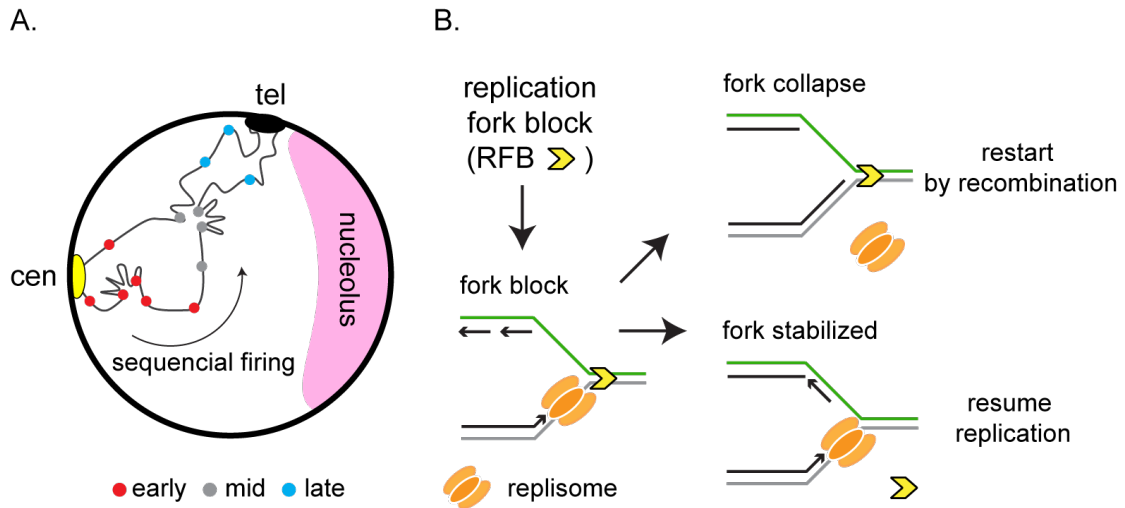


Figure 1 Spatial-temporal organization of DNA replication program. (A) A schematic view of the nuclear organization in yeast, showing regional distributions of replication origins and their hypothesized clustering in distinct replication foci. (B) Replication stress causes the block of the replication fork that can either resume replication (error-free) or collapse and restart replication by recombination (error-prone).

yeast revealed an enrichment in contacts between early replicated regions (Duan et al., 2010), observation that stood proper normalization (Cournac et al., 2012). Other 4C and Hi-C studies confirmed the clustering of early replication origins (Knott et al., 2012) and, more recently, their association into stable TADs (Eser et al., 2017). Noteworthy, these works have detected clusters of early centromeric origins in asynchronous cell populations. However, our recent Hi-C work on cells synchronized in S phase did not reveal any TADs nor discrete, strong contacts between neighboring early replication origins (Lazar - Stefanita et al., 2017). Although, we identified a slight enrichment in contacts between early regions it remains difficult to interpret whether this enrichment results from the uneven distribution of similar replicated regions on the Rab1-like organization.

However, this attractive clustering model remains controversial. Advances in imaging techniques have now weakened the existence of replication factories. Some pieces of evidence came from a super-resolution study in budding yeast, which observed that most of the replication factories consist of one or two pairs of sister replisomes, stochastically associated (Saner et al., 2013). Whereas, super-resolution imaging in metazoans showed that single replisomes are relatively distant from each other, forming discrete foci throughout the nuclei of human and mouse cells (Chagin et al., 2016). Similarly, genome-wide analysis using Hi-C on synchronized cells also alleviate this model: single-cell Hi-C revealed an extensive reorganization of chromosomal compartments and a reduction of the TADs during replication in mammalian cells (Nagano et al., 2017). Altogether these studies point at a stochastic spatial organization of the replication program both in mammals and yeast.

Progression od DNA replication through various roadblocks

During DNA replication the progression of the forks can pause and, eventually, arrest at different replication fork blocks (RFBs) (Figure 1B) (Mirkin and Mirkin, 2007). For instance, sequences prone to generate secondary structures such as long tri-nucleotide repeats (Richard et al., 2000), palindromic sequences (Lobachev et al., 2007) and GC rich motifs forming G-quadruplexes (Lopes et al., 2011), are known to disrupt/slow-down DNA synthesis (Branzei and Foiani, 2010a). Non-histone protein/DNA interactions can programme the pause of a replication fork: Fob1/*RFB* in *S. cerevisiae* rDNA (Brewer and Fangman, 1988; Kobayashi and Horiuchi, 1996); Rtf1/*RTS1* at *S. pombe* mating type locus (Dalgaard and Klar, 1999); Tus/*Ter* replication termination system in *E.coli* (Hill et al., 1987). Finally, DNA metabolic processes such as replication–transcription clashes

have also been shown to interfere with replication progression (Lin and Pasero, 2012; Lu et al., 2014; Takeuchi et al., 2003).

Budding and fission yeast have been used as model organisms to understand the multitude of cellular responses to RFBs. In addition, it has been estimated that the genome of budding yeast contains approximately 1400 natural RFBs caused by protein/DNA interactions (Ivessa et al., 2003). This broad variety of RFBs has allowed us to study how cells i) handle the different types of blocks to avoid the collapse of the forks and the generation of free DNA ends, and ii), in case of collapse, the recruitment of different DNA repair machineries. Most of the RFBs are normally resolved by the Rrm3 helicase that has been suggested to interact with the catalytic subunit of the DNA polymerase and thus progresses with the replication forks (Azvolinsky et al., 2006). In the absence of the “fork clearing” activity of this helicase the RFBs appear as hot spots of recombination (Torres et al., 2004). However, Rrm3-based mechanism is not always sufficient to ensure the progression of the forks through all the RFBs (e.g. the Fob1 programmed RFB) (Kaplan and Bastia, 2009; Mohanty et al., 2006). Therefore, the resulting arrested replication forks can be stabilized via the activity of the intra-S phase checkpoint until the fork block is removed and replication resumed (Lopes et al., 2001a). Alternatively, an unresolved RFB may lead to the disassembly of the replisome that possibly results into a spontaneous or nuclease-mediated collapse, freeing ssDNA or dsDNA ends (Cobb et al., 2003b; De Piccoli et al., 2012). To complete replication the collapsed fork needs to be restarted through DNA repair mechanisms.

Different pathways prevail to repair damaged DNA molecules, depending on the ploidy, the stage of the cell cycle, the type of damage, the nature of the sequence and protein factors involved (Branzei and Foiani, 2010b; Lambert et al., 2007; Sonoda et al., 2006). During replication, repair mechanisms involving homologous or similar sequences appear dominant compared to other pathways (Lambert et al., 2010; Carr and Lambert, 2013; Costes and Lambert, 2012; Truong et al., 2014). Current models involve dissociation/exposure of a ssDNA (Seigneur et al., 1998; Shinohara et al., 1992; Sogo et al., 2002) that will invade a non-allelic template, either through homologous recombination (HR), or through micro-homology/microsatellites induced replication events (MMIR; MMBIR)(Hastings et al., 2009a; Iraqui et al., 2012; Lambert et al., 2010; Mizuno et al., 2013; Payen et al., 2008). However, chromosome rearrangements resulting from the repair of RFBs show that these processes are not error free, and illustrate the recombinogenic potential of these damaged molecules (Hastings et al., 2009b; Koszul and Fischer, 2009; Lambert et al., 2005; Mizuno et al., 2009).

Effect of chromatin mobility on DNA repair

It is logical to assume that the outcome of the repair event is influenced by the chromatin organization and/or dynamics. How do ends of different damaged molecules find each other inside the nuclear volume? Several studies in yeast showed that the presence of a DNA break correlates with an increase in chromatin mobility, not only at the damaged site but also genome-wide (Dion et al., 2012; Heun et al., 2001a; Miné-Hattab and Rothstein, 2012). This increase in mobility has been suggested to enhance the efficiency of repair due to an active search for repair partners (Miné-Hattab and Rothstein, 2013). Moreover, a recent study have reported a global stiffening of the chromatin fibre in response to DNA damage that might be responsible for the increase in chromatin dynamics (Herbert et al., 2017). In addition, chromosome conformation (Hi-C) studies on mammalian cells has also shown genome-wide clustering of double strand brakes, when they are induced in transcriptionally active genes (Aymard et al., 2017). On the other hand, these dynamics would eventually fail to promote the appropriate encounter in specific dispositions of breaks, as for instance the recombination efficiency is correlated with the distance between the breaks (Agmon et al., 2013; Lee et al., 2016). These observations seem to support the so-called “contact-first” model repair mechanism, in which the non-random organization of genomes coupled with global and local modifications of the chromatin fibre would favour spatial-proximal partners for repair choice.

In theory clustered replication forks encountering RFBs at a similar time during S phase should be more likely to generate genomic instability. Indeed, the local concentration of ss/dsDNA at the level of the clustered forks would be higher than in the rest of the genome, favouring the annealing of different DNA regions at very short distances, as predicted by the contact-first model. This model was proposed to explain the prevalence of breakpoints composed of short sequences described by Koszul et al., (2004) and others (Hastings et al., 2009a; Koszul and Fischer, 2009; Koszul et al., 2004; Payen et al., 2008). We reasoned that monitoring the dynamic organization of chromosome segments undergoing replication (using the Hi-C contact maps during S phase) should allow us to determine whether or not specific 3D contacts during replication would lead to preferential chromosomal rearrangements. To investigate at a molecular level such events, we developed a genetic assay that aims to induce multiple replication fork blocks (RFBs) in regions replicated concomitantly or not (according to the replication timing REF). We exploited the replication termination system of *E. coli* chromosome, which relies on the binding of the protein Tus to the sequence *Ter*, to generate RFBs in yeast's

genome (Larsen et al., 2014). The objective of this study was to investigate the potential genomic instability at the RFBs in light of the 3D genome organization and their interplay in the generation of possible chromosomal rearrangements.

Results

Setup for replication fork block

The replication of most bacterial circular chromosomes starts at a unique origin of replication and terminates in the terminus region in a vis-à-vis position. In some bacteria, replication blocks occur at discrete replication terminator sequences, this slowing of the replication fork ensures termination occurs within the terminus region of the chromosome. In *Escherichia coli*, this block occurs at the level of ten *Ter* sites bound by the Tus protein (Figure 2A) (Hill et al., 1987; Duggin and Bell, 2009). The *Ter*-Tus block is unidirectional, meaning that this complex blocks the replication fork coming from one direction. The *Ter* site forms a replication fork “trap” that would allow the fork to enter but not to exit the terminus region. A commonly used assay to monitor the progression and/or the arrest of the replication forks is the neutral-neutral two-dimensional electrophoresis technique (2D gel, Material and Methods). This hybridization-based method allows the detection of the replication intermediates, such as: bubble structures representing firing origins while the Y structures are termination products (Figure 2B, schema left panel). All these branched structures are valid indicators of replication fork integrity (Liberi et al., 2006).

The *Ter*-Tus system has recently been introduced in eukaryotic genomes. The insertion of *Ter* sites in ectopic positions in mammalian chromosomes stimulates homologous recombination between these different regions (Willis et al., 2014). In budding yeast a polarized replication fork pause was observed by 2D gel at the level of *Ter* sites introduced next to the early firing origin ARS305 on chromosome 3 (Figure 2B, arrow on the bottom panel) (Larsen et al., 2014).

We chose to exploit the potential of the *Ter*-Tus complex to induce genomic instability in haploid budding yeast strains at discrete regions selected according to their replication timing profile. First, we reproduced the data from Larsen et al., (2014) by introducing three consecutive *Ter* sites on chromosome 3 at 1.3 kb from ARS305 (Figure 3A, schema). The *TUS* gene encoding the Tus protein was placed under the control of the *GAL1* promoter on a centromeric plasmid (Table 1). Cells were synchronized in G1 using α -factor and released into S phase, concomitantly with the induction of the Tus

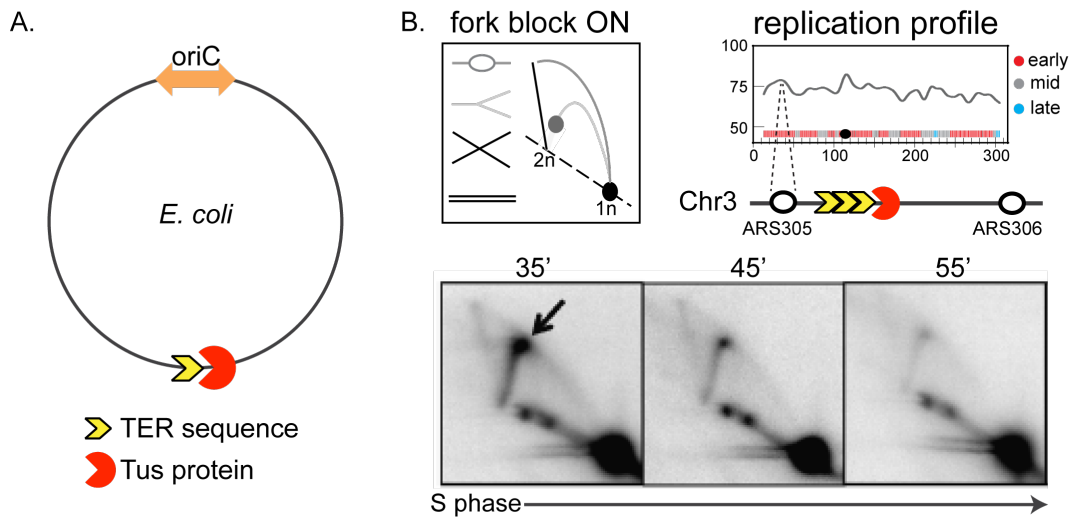


Figure 2 Replication fork block (RFB) by the *Ter*-Tus system. (A) Schematic representation of the *Ter*-Tus replication termination in *E.coli*. (B) Left panel shows the 2D gel pattern expected when fork block is induced. Intermediates of replication (arrow) accumulate on the Y arc as ARS305 fires and disappear as the replication fork from ARS306 approaches. Right panel shows multiple *Ter*-Tus replication blocks placed on chromosome 3 in proximity of the early firing origin ARS305 (replication profile chr3, McCune et al., 2008). Bottom panels: yeast cells synchronized in G1 using α -factor were released in presence of the Tus protein and the pause of the fork was assessed using neutral-neutral two dimensional electrophoresis technique (2D gel) (adapted from Larsen et al., 2014).

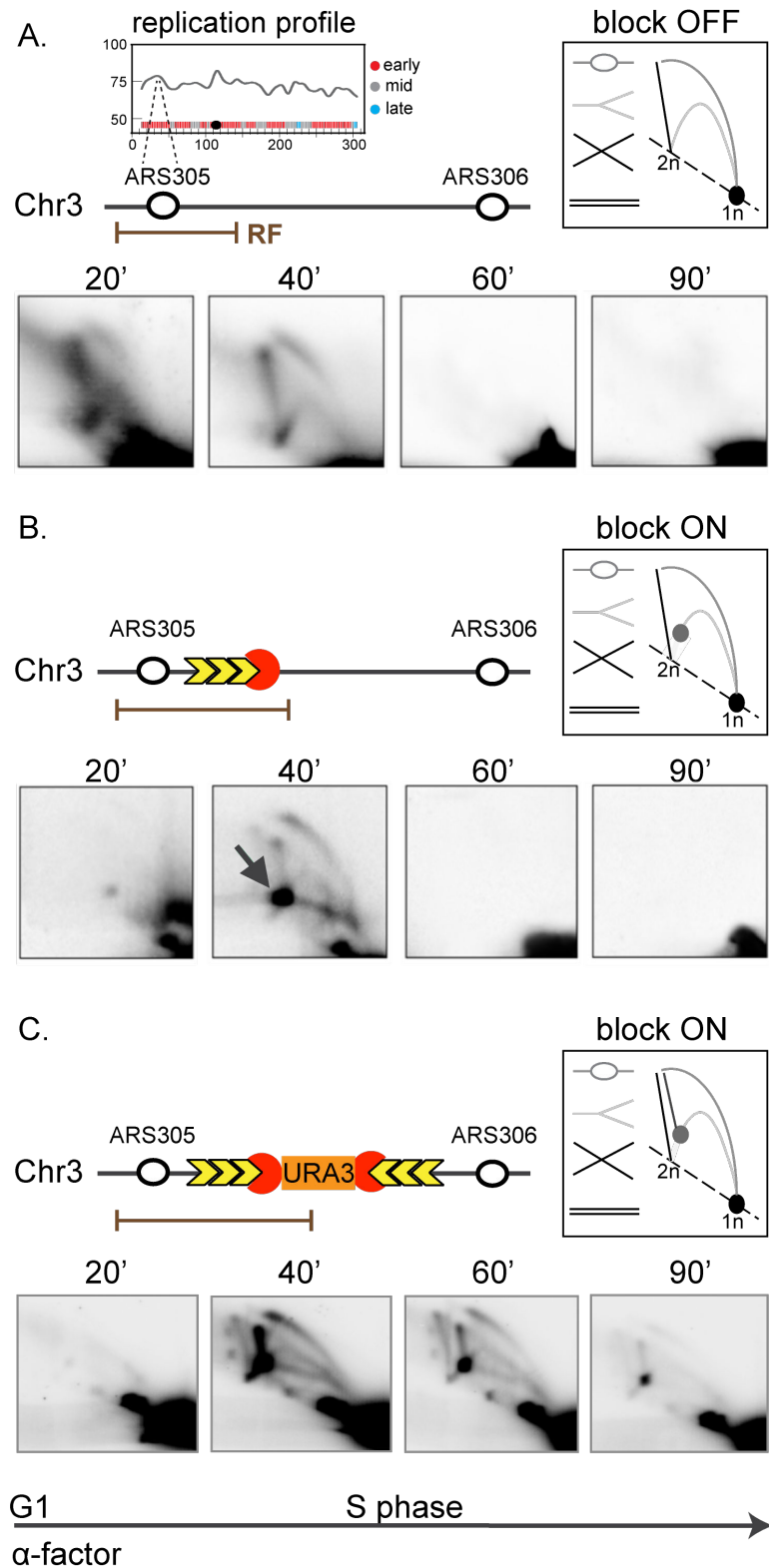


Figure 3 Bidirectional *Ter*-*Tus* replication block is persistent. (A) Wild-type 2D gel firing profile at ARS305 (strain BY4741). RF refers to the restriction fragment probed by 2D. In the right panel, 2D gel pattern expected when fork block is not induced. (B) Three *Ter* sites were placed on chromosome 3 in proximity to the early firing origin, ARS305 (strain YAR016)

(replication profile chr3, McCune et al., 2008). The Tus protein was provided on a centromeric plasmid under the control of *GAL1* promoter (*pRS413-GAL1p-TUS*). Cells were synchronized in G1, released in S phase and the accumulation of the replication intermediates was assessed by 2D gel (arrow). **(C)** A second array of three *Ter* sites, in an opposite orientation to the first, was inserted to increase the persistence and the strength of the replication pause (strain YKL022). The resulting bidirectional block arrests both forks coming from ARS305 and ARS306. On the right panel, 2D gel pattern expected when the bidirectional block is induced.

expression (Material and Methods). The replication pattern of the region carrying the *Ter* sites was investigated by 2D gel (Figure 3B; Table 1, strain YAR016). After 40 minutes from G1 release, a signal corresponding to the stalled fork is detected at the expected position of the *Ter* sites (Figures 3B, arrow). This signal is the result of the accumulation at the *Ter* blocks of Y-branched structures, coming from ARS305 (Figure 3B, schema). The signal rapidly disappears within 20 minutes, suggesting that the branched structures are resolved into linear molecules. The fast recovery of the pause is presumably the result of the directionality of the block, which arrests only the fork coming from ARS305. Therefore, the incoming replication fork, originating from the neighbour ARS306, is most likely to rescue the block and achieve the full replication of this region. To increase the longevity of the block, three additional *Ter* sites were inserted in the opposite direction to the first ones and directed against the fork coming from ARS306 (Figure 3C, schema; Table 1, strain YKL022). As expected, the Y-branched replication intermediates persist for a longer period of time, and are still detectable after more than 90 minutes from G1 release (Figure 3C).

In addition to the prolonged persistence of the Y-shaped structures (Figure 4A grey arrow; 4B,i) the bidirectional block revealed peculiar patterns of replication intermediates partially dependent on the RecQ helicase, Sgs1 (Figure 4A, purple and blue arrows; Table 1, strain YKL045). This helicase preferentially binds to branched DNA substrates and has a 3' → 5' ATP-dependent helicase activity. The nucleolar Sgs1 has been reported to maintain the integrity of the rDNA locus, which is characterized by a similar protein/DNA RFB (Versini et al., 2003). The first pattern we observed on the 2D gel is a conspicuous amount of branched structures located on a spike that extends from the Y-shaped block towards the bubble arc, parallel to the X-spike (Figure 4A, WT 40-60 minutes, purple arrow). Similar structures have been associated with fork regressions or “chicken foot” junctions (Figure 4B, ii), and were observed by 2D gel in the T4 bacteriophage and budding yeast (Long and Kreuzer, 2008; Lopes et al., 2001a; Neelsen and Lopes, 2015). However, no direct evidence of Sgs1 activity has been reported in this process so far. The second pattern detected extends below the Y arc and it is completely absent in *sgs1Δ* (Figure 4A, WT and *sgs1 Δ* 40-60 minutes, blue arrow). In light of the reported role of Sgs1 in the resection of the 5' end of DSBs (Mimitou and Symington, 2008; Zhu et al., 2008), these branched structures may be the result of the resection at regressed forks (Figure 4B, iii). In our working model, the regression into a “chicken foot” (in purple) will expose a DSB end, whose 5' end is unwound by Sgs1. The resulting 5' ssDNA is eventually resected by the reported nuclease (e.g. Dna2) to produce shorter (low molecular weight) Y-branched structures (in blue). Finally, an

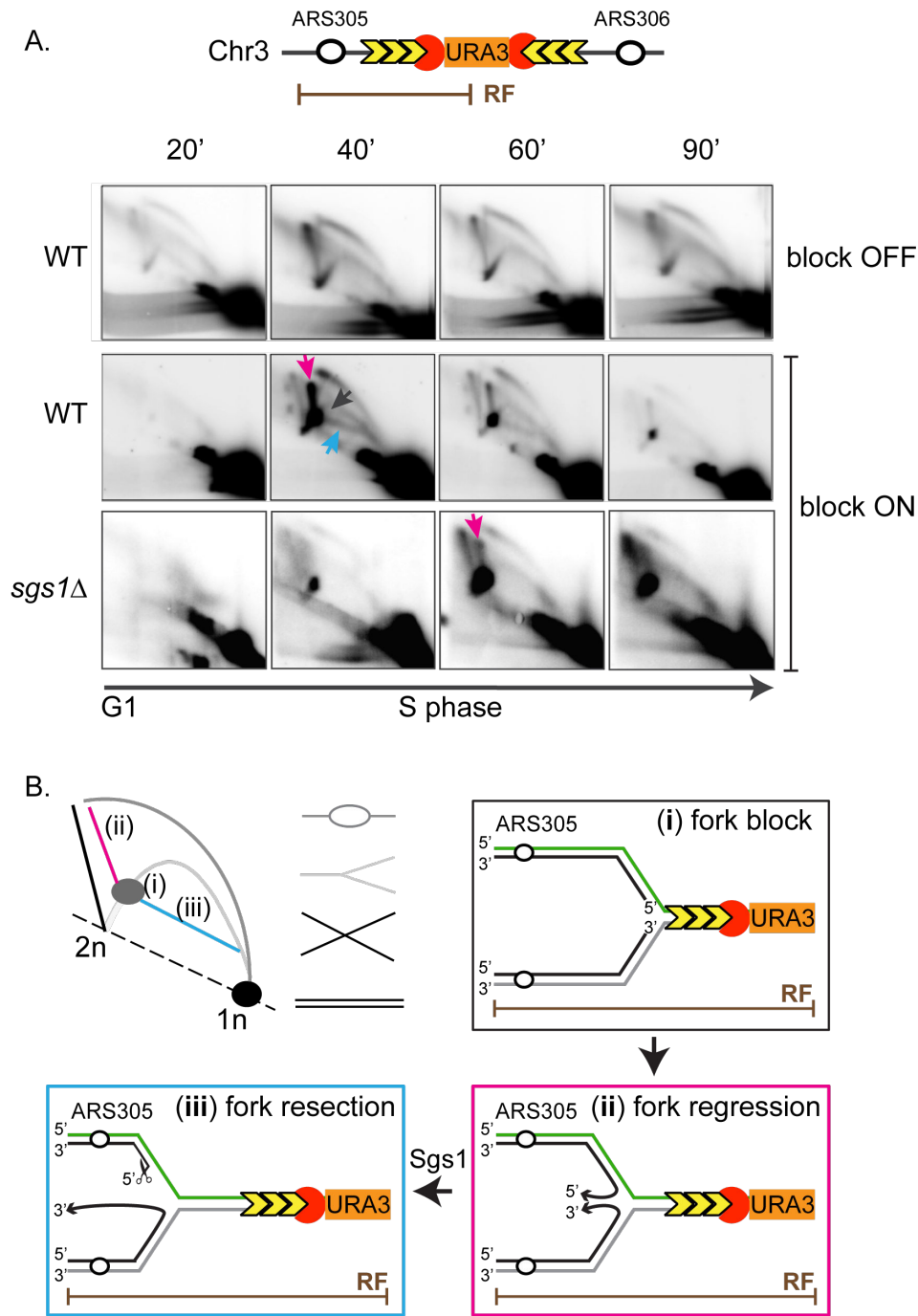


Figure 4 Bidirectional *Ter*-Tus block induces fork regression and resection. (A) 2D gel firing profile at ARS305 (refer Figure 3). RF refers to the restriction fragment probed by 2D. Block ON/OFF refers to the induction of the Tus protein in the wild-type and *sgs1* Δ cells. Grey arrow indicates the Y-shaped block. Purple and blue arrows indicate possible fork regression and resection, respectively. (B) 2D gel pattern expected when the bidirectional block is induced. Y-shaped fork block in grey corresponds to schema in panel (i). “Chickenfoot” fork regression in purple corresponds to schema in panel (ii). Fork resection in blue corresponds to schema in panel (iii).

excessive resection, passing the restriction fragment, will result in a linear structure (1n). In the absence of the helicase, the unprocessed intermediates will eventually accumulate as X-shaped structures (Figure 4A, *sgs1* Δ 90 minutes). However, when Larsen et al., investigated the mechanism employed by the cells to overcome this block they found unprocessed X-shaped structures Rad51-dependent in the absence of Sgs1 (Larsen et al., 2014). This indicated a role for the Sgs1 helicase in resolving recombination intermediates. However, given the short persistence of the investigated unidirectional block these additional replication intermediates were presumably not detectable.

Overall these results show that the resolution of the bidirectional *Ter*-Tus block requires the formation of branched structures, partially dependent on the Sgs1 helicase activity. The processing of these replication intermediates seem to support the hypothesized role of Sgs1 in the regression and resection processes (Cobb et al., 2003b; Mimitou and Symington, 2008; Versini et al., 2003; Zhu et al., 2008). Noteworthy, previous attempts to identify fork regression at similar natural pause site (e.g. Fob1/*RFB*) were unsuccessful, supporting the contention that these structures are pathological rather than physiological replication intermediates (Gruber et al., 2000). As a matter of fact, in *S. pombe* complex chromosomal rearrangements were reported to be the consequence of nascent ssDNA extrusion that can engage in template switching during recombination-mediated restart of an analogous RFB, Rtf1/*RTS1* (Lambert et al., 2010).

Given the persistence of the bidirectional *Ter*-Tus block and the accumulation of replication intermediates, potentially recombinogenic, two other bidirectional RFBs were introduced independently at mid- and late- replicating regions in the genome (Table 1, strains YKL014 and YKL015). These two loci are located on chromosomes 4 at ~171 kb one from the other: one in the vicinity of the mid firing origin ARS419 (~14 kb), and the other one next to the late firing ARS423 (~13 kb) (Figure 5, replication profiles). 2D gels were performed to check the blocking efficiency of the newly introduced bidirectional *Ter* constructs (Figure 5). Y-branched structures consistent with the replication timing were detected at the RFBs: 60 min after G1 release near the mid replicating ARS419 (Figure 5A), and after 90 minutes at late ARS423 (Figure 5B). Therefore, the bidirectional RFB could be conveniently positioned at various genomic locations to efficiently block replication forks for a relatively long period of time. In spite of the longevity of the replication pause, no viability defect was observed by drop test assay in growing conditions that induce the bidirectional block.

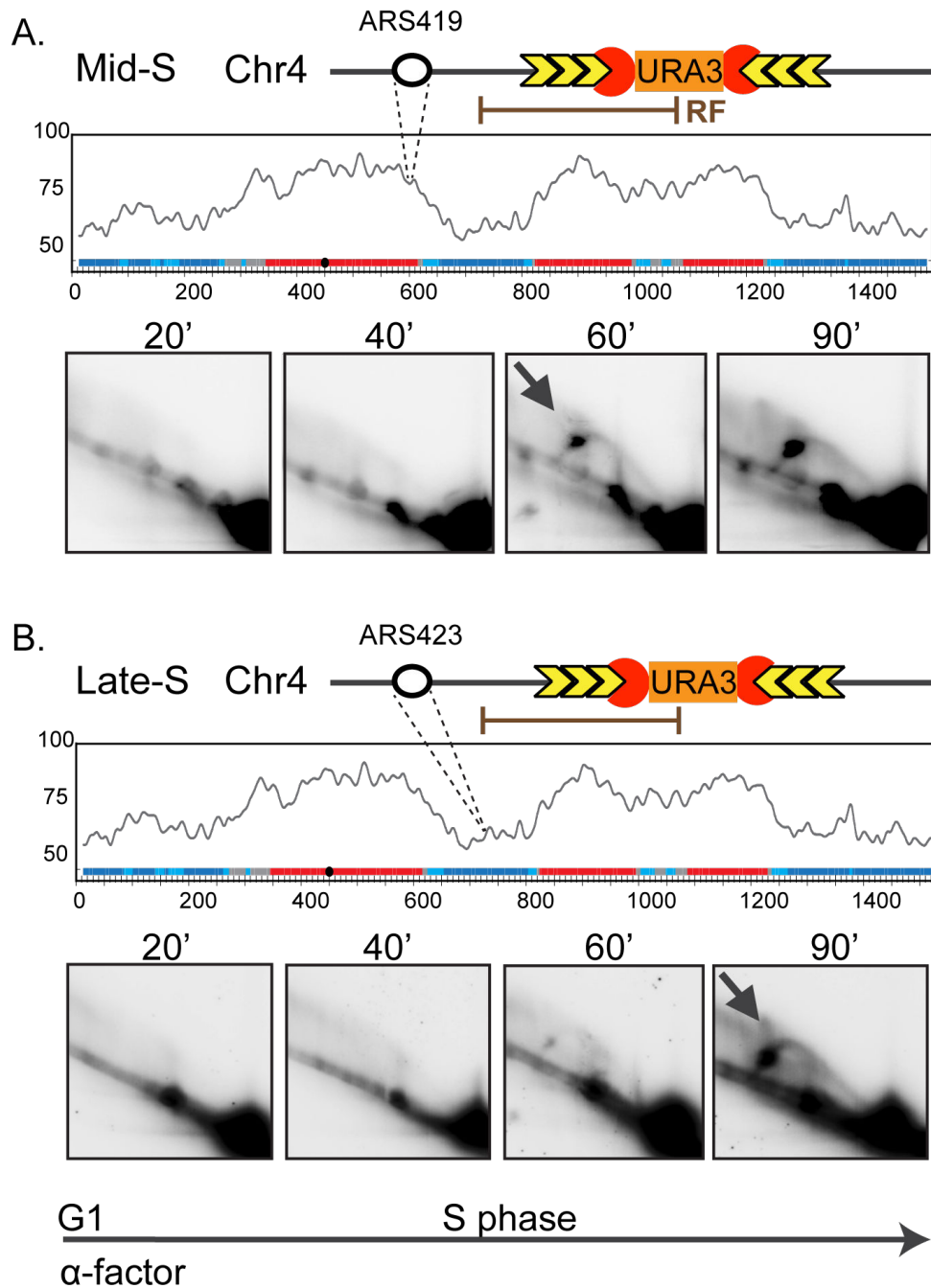


Figure 5 Replication pause arises after the activation of the origin. Bidirectional *Ter*-Tus blocks were placed at mid ARS419 (strain YKL015) (**A**) and late ARS423 (strain YKL014) (**B**) origins, respectively. Top panels show the replication profile of Chr4 (McCune et al., 2008). Bottom panels represent 2D gel profiles (refer Figure 3), with arrows pointing a the onset of the pauses, matching the replication timing of the corresponding region. RF refers to the restriction fragment probed by 2D.

Investigating genome stability at RFB positions

To determine whether loci carrying RFBs are prone to generate chromosomal rearrangements, and if so at which rate, fluctuation assays were performed on strains carrying uni-/bidirectional blocks (Table 1, strain YKL021, YKL022, YKL023). The loss of function of the *URA3* gene located either between the two *Ter* in bidirectional blocks or near the *Ter* of unidirectional block was assessed by growing the cells in presence of 5-fluoroorotic acid (5-FOA) (Luria and Delbrück, 1943). In the presence of 5-FOA, cells expressing the *URA3* gene die since the product of this gene converts the non-toxic 5-FOA into a toxic product. Therefore, 5-FOA selects for *ura3* loss-of-function mutants/survivors either through a point mutation or through chromosomal deletions or other rearrangements (Koszul et al., 2006). Cells were grown overnight for ~10-12 generations with the block induced, and appropriate serial dilutions were plated on 5-FOA containing medium. The colony-forming unit (CFU) counting reported no increase in the degree of mutation rate at the *URA3* locus, suggesting no rearrangements at the ARS305 blocked locus (not shown).

We next investigated whether the concomitant presence of multiple bidirectional replication fork blocks could result in an increase in genomic instability, and whether different chromosomal rearrangements may emerge depending on the 3D positioning and replication timing of the RFB-carrying region. The three strains each carrying a bidirectional block were mated together (Material and Methods) to obtain a strain containing all three replication blocks (3xRFBs; Table 1, strain YKL032) (Figure 6A). The resulting strain was viable when the 3xRFBs were concomitantly induced. Although, it displayed a slight delay of growth rate of ~15 minutes on the total length of cell cycle duration (~90 minutes), as monitored by flow cytometry.

Independent cultures of the 3xRFB strain were propagated in parallel in batch cultures for ~180 generations in the presence (ON) or absence (OFF) of Tus protein induction. Aliquots of the cultures were sampled over 16 timepoints and analysed by pulsed field gel electrophoresis (PFGE), southern blot and deep sequencing. Each timepoint is the result of ~10⁸ cells grown for 11-12 generations. The growth rate delay displayed by the 3xRFBs in presence of Tus was progressively rescued over time and therefore difficult to be associated to a specific timepoint. Clonal isolates sampled for each of the 16 timepoints were investigated using PFGE, a technique often used to identify large chromosomal rearrangements in yeast karyotypes (Koszul et al., 2004; Lambert et al., 2005; Schwartz and Cantor, 1984). Southern blotting was performed on the PFGE and hybridized with probes targeting the RFB-carrying regions, unveiling the expected bands of chromosome 3 and 4 and no large rearrangement in the presence of Tus

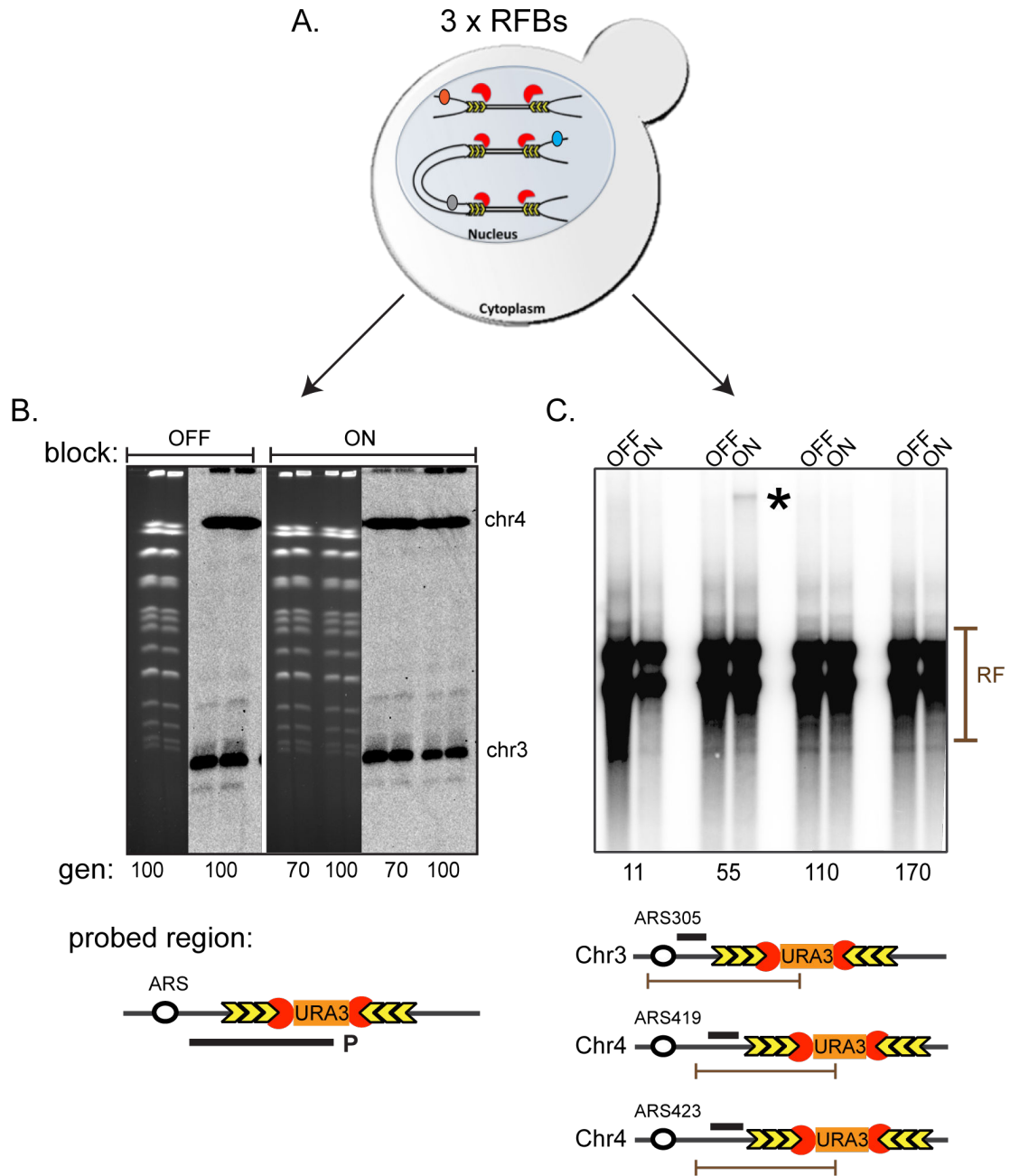


Figure 6 Detecting rearrangements at multiple RFBs. (A) 3xRFB strain (YKL032) carrying multiple bidirectional *Ter*-*Tus* blocks at early, mid and late replication time zones was built. (B-C) Replication blocks were induced for multiple generations (block ON) in batch culture, whereas the strain without the induction (block OFF) was used as a negative control. Genomic DNA was extracted and analyzed by pulsed field gel electrophoresis (PFGE, in B) and southern blotting (C). Probed regions "P" are displayed below the gels. RF refers to the restriction fragment probed.

(Figure 6B). Because PFGE do not offer high resolution and could not, for instance, detect small deletions, Southern blotting was also performed on genomic DNA digested with a combination of restriction enzymes (mix of three unique probes, matching sequences adjacent to the blocks) (Figure 6C, schema). This analysis was performed on several timepoints. Surprisingly, only one signal among 16 analyses was detected corresponding to a chromosomal rearrangement involving the RFB-carrying region and later lost within the population analysis (Figure 6C, star). Therefore, the presence of 3 simultaneous arrested replication forks within the genome did not appear to induce significant instability in the genome. On the contrary, we observed by PCR amplification that the long term block induction was causing the loss of the plasmid encoding the Tus protein.

The absence of rearrangements in the 3xRFB strain appeared as a surprise, given that each of the blocks seemed strong and persistent. However, if the rearrangement frequency was too low, the possibility remained that the rearrangements would escape detection through PFGE and Southern blotting approaches. We therefore used high-throughput Illumina sequencing to search for structural variations in the populations where the blocks were induced for 55 and 110 generations (non-induced timepoints for the same number of generations were used as controls). Paired-end libraries were generated and sequenced (read length 2 x 150 bp). The sequenced reads were aligned against the reference S288C yeast genome (Engel et al., 2014). The libraries were analysed using SVDetect (Zeitouni et al., 2010) and SPAdes (Bankevich et al., 2012) algorithms by our collaborator Varun Khanna at Pasteur (Figure 7, schema). In parallel, I was using the DELLY algorithm (Rausch et al., 2012) to search for structural variants. Overall, both these analyses failed to detect chromosomal rearrangement involving RFB carrying regions (Material and Methods). These results have been also compared with the one obtained from the induction of the 3xRFBs in a strain defective for the homologous recombination pathway (*rad52*Δ; Table 1, strain YKL044). The *rad52*Δ mutant displayed no structural rearrangements between the RFB carrying sites as well. These results show that the yeast genome is able to handle three independent, distant replication fork block without resulting in large genomic instability. That is relatively unexpected given that in both prokaryotes and eukaryotes, the ectopic insertion of DNA/protein RFBs has been often associated with an increase of recombination frequency, such as deletions, duplications and translocations (Bierne et al., 1997; Lambert et al., 2005; Takeuchi et al., 2003; Willis et al., 2014). That have led to the

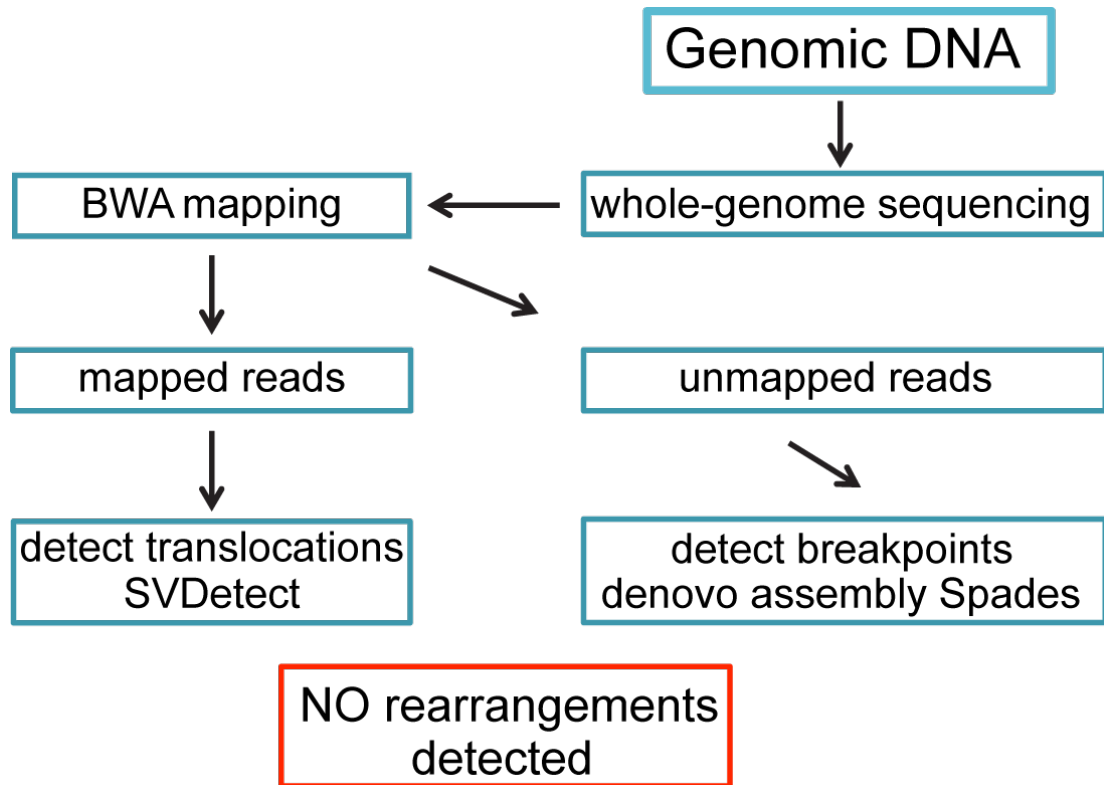


Figure 7 High-throughput method to detect rearrangements at multiple RFBs. Genomic DNA extracts from the induction and non-induction conditions were processed for illumine sequencing. 150 bp long reads were aligned in paired-mode using the maximal exact matches (MEM) option of the BWA alignment. SVDetect software (Zeitouni et al., 2010) was used to detect translocations, while SPAdes *denovo* assembly (Bankevich et al., 2012) was used to search breakpoints.

hypothesis that paused forks stimulate genome rearrangements through the disassembly of the replisome and the collapse of the fork.

Discussion

This section of my PhD focused on understanding new links between genome stability and nuclear organization, in light of the latest S phase chromosomal contacts maps.

The peculiar organization of budding yeast chromosomes was suggested to play a key role in maintaining genome stability. In particular, anchoring of centromere and telomere clusters at the nuclear periphery would avoid the search for improper repair partners when DNA damage occurs (Agmon et al., 2013; Therizols et al., 2006). Moreover, we observed that these subnuclear regions follow a specific spatial-temporal organization: initiating at the early replicating centromeric regions and finishing within the late telomeric regions (see 3D pattern of the replication program, using Hi-C; Lazar - Stefanita et al., 2017). Although in mammals the model of “cluster of replisomes” is controversial (Chagin et al., 2016), in constraints imposed by yeast nuclear architecture on regions that replicate similarly may still influence the choice of repair at RFBs. Therefore, it was tempting to investigate the influence of transient genome reorganizations on repair choice.

Ectopic *Ter*-Tus RFBs were associated with the increase of recombination in bacteria (Bierne et al., 1997) and recently in mammals (Willis et al., 2014). This block was introduced in yeast, in which it was reported to trigger the activation of the homologous recombination pathway (Larsen et al., 2014). Similar DNA-protein replication pauses also exist in eukaryotes. The best characterized example of programmed RFB is mediated by the fork blocking 1 (Fob1) protein (Brewer and Fangman, 1988; Gruber et al., 2000; Kobayashi and Horiuchi, 1996). This polar barrier seems to avoid head-on collisions between replication and transcription at the rDNA locus in *S. cerevisiae*. Head-on collisions are known to stimulate recombination through replication fork pause and successive disassembly of the replisome (Lin and Pasero, 2012; Takeuchi et al., 2003). In addition, Fob1 is required for rDNA silencing that inhibits hyper-recombination and extends the replicative life span of budding yeast (Lucchini and Sogo, 1994; Huang and Moazed, 2003). Another similar system was found to have a crucial role in the recombination reaction that takes place during mating type switching in fission yeast (Dalgaard and Klar, 1999). The transposition of the RTS1 block to other loci was found to stimulate recombination at these sites and induce formation of gross chromosomal rearrangements (Lambert et al., 2005).

In our hands, the insertion of the bidirectional *Ter*-Tus block at three different chromosomal locations, according to the replication timing, has failed to detect any recombination product. Although, we have detected at the blocked loci abundant DNA branched structures, potentially recombinogenic and partially dependent on Sgs1 helicase activity. The dynamics of the replication intermediates suggests possible fork regression followed by Sgs1-dependent resection. Additional experiments using appropriate nuclease mutants (e.g. Dna2) are needed to prove the observed replication intermediates.

In light of these observations, we can also imagine that replication forks arrested at *Ter* sites are extremely stable structures and therefore they are unlikely to collapse. One tempting explanation could be that *S. cerevisiae* is already accustomed to such DNA-protein RFBs (hundreds of Fob1 binding sites are located in the rDNA locus). In addition, the arrested resplisomes at ectopic Fob1 replication fork blocks have been shown to be stable structures (Calzada et al., 2005). Thus, efficient mechanisms to stabilize the replisome and/or remove these pauses may act at these ectopic locations, as well. One example of such mechanisms may rely on the activity of Sgs1. Moreover, the unaffected viability of the 3xRFB strains in different genetic backgrounds (WT, *sgs1* Δ , *rad52* Δ , *clb5* Δ) may also be an indication of unstable fork blocks. In this regard, the strong binding affinity of the Tus protein to the *Ter* sites has been reported, *in vitro* (Moreau and Schaeffer, 2013; Neylon et al., 2000). However, these studies do not take into account neither the presence of the replication machinery and the helicases travelling with it, nor the structure of the chromatin at the terminus location. Therefore, we cannot exclude a relatively unstable *Ter*-Tus binding site, whose purpose is to slow down replication forks, *in vivo*. In this scenario the DNA helicase Rrm3, that has been shown to participate in the removal of a broad variety of RFBs (Ivessa et al., 2003), it is not required to resolve the *Ter*-Tus block (Larsen et al., 2014).

On the other hand, Willis et al., have successfully detected homologous recombination events at the *Ter*-Tus sites in mammalian cells (Willis et al., 2014). This could indicate that our setup might be inefficient. One problem may come from the fact that RFBs contain tandem repeats thus the arrested forks could resume replication inside the same block. A second problematic has been raised by the transcription of the *URA3* gene, located between the inverted blocks, that might interfere with the polarity of the block. Experiments on the *URA3* RNA transcription are needed to investigate this latter option. Finally, our system might be not sensitive enough to detect rearrangements at the population level therefore, to improve sensitivity, a capture-based system could be a

possibility to selectively enrich the deep sequencing libraries with potential recombination intermediates.

In another order of ideas, to further investigate the mechanism lying behind the resolution of this replication blocks and to identify the genetic elements involved, we intend to apply the genetic interaction mapping (GIM) genome-wide screen (Decourty et al., 2008). This genetic screening method, readily available at the Institut Pasteur in the group of Cosmin Saveanu, aims at exploring and quantifying the growth effect of combining systematically the deletion of all the genes in the genome with our genetic feature of interest (in our case, the replication block). The quantification of the effect, ranging from synthetic lethality to growth defect, is then quantified using microarrays (Lelandais and Devaux, 2010). We expect to characterize the genetic background that will allow us to identify a potential 3D effect with respect to chromosomal rearrangements at replication fork blocks events. Moreover, in light of the recent finding that double strand brakes colocalize in mammalian cell nuclei (Aymard et al., 2017), it would be tempting to investigate the nuclear organization at the 3xRFBs using Hi-C. This could give us more indications on the repair dynamics: we speculate that if the RFBs colocalize then they will probably engage in HR between themselves.

Altogether, we expect to identify partners responsible for resolving these strong persistent blocks in the genome, and open the way for future direction of research regarding how the genome cope with such problems.

Material and Methods

Yeast strains

All the strains are derivatives of BY4741 (*MATa his3Δ1 leu2Δ0 met15Δ0 ura3Δ0*). The relevant genotypes of all the yeast strains used in this study are listed in Table 1. The majority of the strains used in this study was generated by dissecting sporulated heterozygous diploid strains, obtained by crossing haploid strains of opposite mating types (see below for procedures).

Yeast transformation

Yeast cells were grown O/N in 50 ml of rich medium (YPD) or of the appropriate medium allowing them to reach the stationary phase. Next morning the cell culture was diluted to OD₆₀₀ of 0.2 and allowed to grow until it had reached an OD₆₀₀ of 0.5. Cells were then harvested at 4000 rpm for 3 min and washed with 50 ml of sterile milli-Q H₂O. The pellet was then washed with 1 ml 1x TE/1x LiAc solution. Approximately 10⁸ cells/transformation were resuspended in 50 μl 1x TE/1x LiAc solution.

Transformation mix: 50 μl of cell suspension, 350 μl of PEG/TE/LiAc solution (40% PEG, 1x TE, 1x LiAc), 5 μl of 10 mg/ml single-stranded salmon sperm denatured DNA, “x” μl (max up to 10 μl) DNA.

The transformation reaction was incubated for 30 min at 30°C. Cells were heat-shocked at 42°C for 20 min and then centrifuged for 3 min at 3000 rpm. The pellet was resuspended in 200 μl milli-Q H₂O and plated on appropriate selective medium.

Solutions:

50% PEG 4000

10x TE: 0.1 M Tris-HCl pH 7.5, 10 mM EDTA

Mating, sporulation and tetrad dissection

MATa and *MATα* strains were mixed and grown on rich medium at 30°C O/N. The next day, the cross mixture of cells were replica plate on the selective medium allowing for the selection of diploid cells, that were successively streaked to single diploid colonies. Single colonies grown under selective conditions were passed on rich media for 1 day (to increase the efficiency of sporulation). The next day diploids were patched on sporulation plates (1% KAcetate, all amino acids at 1/4 of the normal concentration) to induce meiosis and sporulation by starvation. After ~ 10 days diploids were sporulated and tetrads were matured and ready to be dissected. In order to separate individual spores the wall of the ascus or tetrad is removed by enzymatic digestion (0.1 mg/ml

zymolase 100T final concentration). The digestion mixture was then incubated at 30°C for 5 min. Cells were diluted in 1 ml milli-Q H₂O and ~20 µl were dripped in a line on the agar plate. Individual tetrads were dissected using the Nikon dissection microscope. Spores were left to grow at RT for 3-5 days. Colonies were replica plated onto selective media to define their genotype.

G1 synchronization with α -factor

In order to synchronize cells in G1 phase, cell cultures were diluted to OD₆₀₀ = 0.2 – 0.3 and 15 µg/ml α -factor was added. The cultures were incubated for ~2 h at 30°C. The G1 arrest was considered complete when more than 90% of the cells were “shmoo”. For synchronization experiments, after the arrest was complete, cells were released from the G1 block. α -factor was washed out with medium without the pheromone. Cells were next released into the appropriate fresh medium in the absence of the pheromone.

2-D agarose gel electrophoresis

Approximately 2 x 10⁹ synchronized cells/timepoint were used to evaluate different replication intermediates using 2-D gel. Cells were incubated with 0.1 % Sodium azide for 15 min on ice, centrifuged and washed with ice-cold H₂O. The pellet was resuspended in 5ml spheroplast buffer and incubated for 40 min at 30°C. The spheroplasts were collected by centrifugation at 4000 rpm, resuspended in 2.5 ml of solution I (freshly supplemented with 200 µl RNase A 20 mg/ml) and incubated at 50°C for 30 min. 200 µl of Proteinase K 20 mg/ml were added and the mix was incubated O/N at 30°C. Next day the solution was centrifuged, and the pellet and the supernatant were processed separately for genomic DNA extraction.

Supernatant:

- 1) Transfer the supernatant into a 15 ml Falcon tube and add 2.5 ml of Chloroform:Isoamyl alcohol 24:1.
- 2) Mix and separate the two phases by centrifugation at 4000 rpm for 10 min at RT.
- 3) Transfer the clear upper phase into a Corex glass tube and add 10 ml solution II.
- 4) Centrifuge the mix at 8500 rpm for 10 min at RT in a Beckman JS 13.1 swinging bucket rotor, discard the supernatant and re-suspend the pellet in 2.5 ml of solution III.

Pellet:

- 1) Resuspend the pellet in 2 ml of solution III and incubate 1 h at 50°C.
- 2) Transfer the mix into a 15 ml Falcon tube containing 1 ml of Chloroform:Isoamyl alcohol 24:1.
- 3) Mix and separate the two phases by centrifugation at 4000 rpm for 10 min at RT.

- 4) Transfer the clear upper phase into the Corex glass tube containing solution III obtained from the treatment of the supernatant (see Supernatant step 4).
- 5) Precipitate DNA with 5 ml of isopropanol and centrifuge at 8500 rpm for 10 min in a Beckman JS 13.1 swinging bucket rotor at RT.
- 6) Wash the pellet with 2 ml of ethanol 70%.
- 7) Dry the pellet and dissolve in 250 μ l 10 mM Tris-HCl pH 8.

To investigate replication termination structures, 20 μ g of genomic DNA needs to be digested. A combination of restriction enzymes was used (ARS305: EcoRV and NcoI; ARS419, ARS423: AflIII, NEB), so that the band containing the fragment of interest and the band twice that size are separated by 3-5 cm in the first dimension gel.

First dimension gel: 0.35% agarose in 1x TBE (89 mM Tris-HCl pH 7.5, 89 mM Boric Acid, 2 mM EDTA); electrophoresis buffer, 1x TBE. The digested samples and a molecular weight DNA marker (1 kb DNA ladder) were loaded, leaving one empty well between samples, and the gel was run at the constant low voltage at RT (35 V) for around 24 hours. After the migration the gel was stained with 0.3 μ g/ml ethidium bromide for 20 min. The lanes of interest, containing the linear and the replication intermediates, were excised from the first dimension gel.

Second dimension: 0.9% agarose, 0.3 μ g/ml ethidium bromide in 1x TBE. Gel slices were rotated 90° and placed in the tray for the second dimension gel, for 4 – 5 h at the constant high voltage at 4°C (180-250 V) in TBE 1X buffer containing 0.3 μ g /ml ethidium bromide. After electrophoresis the gel was treated for Southern analysis.

Solutions:

Spheroplast buffer: 1 M Sorbitol, 100 mM EDTA pH 8.0, 0.1% β -mercaptoethanol, 1 mg/ml zymolyase final concentration

Solution I: 2% w/v CTAB, 1.4 M NaCl, 100 mM Tris-HCl pH 8, 25 mM EDTA pH 8.0

Solution II: 1% w/v CTAB, 50 mM Tris-HCl pH 8, 10 mM EDTA

Solution III: 1.4 M NaCl, 10 mM Tris-HCl pH 8, 1 mM EDTA

Pulsed-field gel electrophoresis

Approximately 5×10^8 cells were washed and resuspended in 150 μ l of 50 mM EDTA pH 9.0. Next, 75 μ l of solution I, freshly supplemented with 1 mg/ml zymolyase, and 375 μ l of 1% low-melting point (LMP) agarose were added. After the plugs were solidified they were transferred into 5 ml tubes and incubated with 2 ml solution II at 37°C O/N. Next day, solution II was removed and replaced with solution III, freshly supplemented with 1 mg/ml Proteinase K. Plugs were incubated at 65°C O/N. Before were at was added and together and 250 μ l. The mixture was added into several wells. Finally, the plugs were

washed and resuspended in 0.5 M EDTA pH 9 for long conservation at 4°C. Running was performed in a 1% agarose gel in 0.5x TBE (44.5 mM Tris-HCl pH 7.5, 44.5 mM Boric Acid, 1 mM EDTA) with the following conditions: 160 - 80 sec switch time, 110 angle, 130 V, 12°C for 70 h. After electrophoresis the gel was treated for Southern analysis.

Solutions:

SCE: 1 M Sorbitol, 10 mM EDTA pH 9.0, 100 mM Sodium citrate pH 5.8

Solution I: 1 M SCE, 2.5% β -mercaptoethanol

Solution II: 450 mM EDTA pH 9.0, 10 mM Tris-HCl pH 8, 7.5% β -mercaptoethanol

Solution III: 450 mM EDTA pH 9.0, 10 mM Tris-HCl pH 8, 1% N-lauryl sarcosyl

Southern blotting

Prior blotting gel was subjected to depurination 10 min (0.25 N HCl), denaturation 20 min (0.5 M NaOH, 1.5 M NaCl) and neutralization 20 min (1 M AcNH₄, 0.02 M NaOH). Transfer was performed by capillarity on Gene Screen transfer membrane (Perkin Elmer) in 10x SSC O/N. DNA was UV-crosslinked to the membrane using Stratalinker 1800 UV (120000 μ J).

Membrane was prehybridized with ULTRAhy Ultrasensitive Hybridization Buffer for 1 h at 65 °C. Labelled probe was generated using Random Prime Labelling kit. ~40 ng of PCR template in 15 μ l volume were mixed with random hexamer oligonucleotides and boiled at 95°C for 5 min. Following the dNTPs (0.1 mM dCTP, 0.1 mM dGTP, 0.1 mM dTTP), [α -³²P] dATP and Exo(-) Klenow enzyme were added to the DNA and incubated for 1 h at 37°C. Probe was purified using Illustra Microspin G50 column. Purified probe was boiled for 10 min at 95°C and added to the prehybridization buffer. The hybridization was performed at 45°C O/N. Subsequently, the membrane was washed twice with 2x SSC, 1% SDS and twice 0.1x SSC, 1% SDS for 15 min each at 45°C, before exposure.

Table 1 Description of yeast strains used in this work.

Strain	Genetic background	Genotype	Plasmid	Reference
BY4741	S288C	<i>MATa his3Δ1 leu2Δ0 met15Δ0 ura3Δ0</i>		Mortimer and Johnston, 1986
BY4743	S288C	<i>MATa/α his3Δ1/his3Δ1 leu2Δ0/leu2Δ0 LYS2/lys2Δ0 MET15/met15Δ0 ura3Δ0/ura3Δ0</i>		Brachmann et al, 1998
FYBL1-17B		<i>MATa his3Δ200 LEU2 LYS2 MET15 ura3Δ851 trpΔ63</i>		lab collection
YAR016	BY4741	<i>MATa his3Δ1 leu2Δ0 met15Δ0 ura3Δ0 III(40959-41219)::3Ter/III</i>	pRS413-pTUS	this study
YKL014	BY4743	<i>MATa his3Δ1 leu2Δ0 lys2Δ0 met15Δ0 ura3Δ0 IV(766567-766568)::3Ter-rURA3-3Ter/IV</i>	pRS413-pTUS	this study
YKL015	BY4743	<i>MATa his3Δ1 leu2Δ0 lys2Δ0 met15Δ0 ura3Δ0 IV(581846-581849)::3Ter-rURA-3Ter/IV</i>	pRS413-pTUS	this study
YKL021	BY4743	<i>MATa his3Δ1 leu2Δ0 LYS2 met15Δ0 ura3Δ0 III(40959-41219)::3Ter-rURA-3Ter/III</i>	pRS413-pTUS	this study
YKL022	BY4743	<i>MATa his3Δ1 leu2Δ0 LYS2 met15Δ0 ura3Δ0 III(40959-41219)::3Ter-rURA-3Ter/III</i>	pRS413-pTUS	this study
YKL023	BY4743	<i>MATa his3Δ1 leu2Δ0 LYS2 met15Δ0 ura3Δ0 III(40959-41219)::3Ter-rURA/III</i>	pRS413-pTUS	this study
YKL032	(<i>Mata</i> 3Ter-rURA-3Ter) x FYBL-17B sporulation, dissection product	<i>MATa his3Δ/his3Δ200 LEU2 lys2Δ0 trp1Δ63 MET15/met15Δ0 ura3Δ0/ura3-Δ851 III(40959-41219)::3Ter-rURA-3Ter/III IV(581846-581849)::3Ter-rURA-3Ter/IV IV(766567-766568)::3Ter-rURA3-3Ter/IV</i>	pRS413-pTUS	this study
YKL044	(<i>Mata</i> 3Ter-rURA-3Ter) x FYBL-17B sporulation, dissection product	<i>MATa his3Δ/his3Δ200 leu2Δ0 lys2Δ0 trp1Δ63 MET15/met15Δ0 ura3Δ0/ura3-Δ851 rad52::KanMX III(40959-41219)::3Ter-rURA-3Ter/III IV(581846-581849)::3Ter-rURA-3Ter/IV IV(766567-766568)::3Ter-rURA3-3Ter/IV</i>	pRS413-pTUS	this study
YKL045	(<i>Mata</i> 3Ter-rURA-3Ter) x FYBL-17B sporulation, dissection product	<i>MATa his3Δ/his3Δ200 leu2Δ0 lys2Δ0 trp1Δ63 MET15/met15Δ0 ura3Δ0/ura3-Δ851 sgs1::KanMX III(40959-41219)::3Ter-rURA-3Ter/III IV(581846-581849)::3Ter-rURA-3Ter/IV IV(766567-766568)::3Ter-rURA3-3Ter/IV</i>	pRS413-pTUS	this study
YKL046	(<i>Mata</i> 3Ter-rURA-3Ter) x FYBL-17B sporulation, dissection product	<i>MATa his3Δ/his3Δ200 leu2Δ0 lys2Δ0 trp1Δ63 MET15/met15Δ0 ura3Δ0/ura3-Δ851 clb5::LEU2 III(40959-41219)::3Ter-rURA-3Ter/III IV(581846-581849)::3Ter-rURA-3Ter/IV IV(766567-766568)::3Ter-rURA3-3Ter/IV</i>	pRS413-pTUS	this study
YKL049	YKL046	<i>MATa his3Δ/his3Δ200 leu2Δ0 lys2Δ0 trp1Δ63 MET15/met15Δ0 ura3Δ0/ura3-Δ851 clb5::LEU2 rad52::KanMX III(40959-41219)::3Ter-rURA-3Ter/III IV(581846-581849)::3Ter-rURA-3Ter/IV IV(766567-766568)::3Ter-rURA3-3Ter/IV</i>	pRS413-pTUS	this study

3. Conclusion and discussion

This manuscript presents the work I did over the last four years to address the interplay between chromosomal architecture, cell-cycle and genome stability.

Choreography of chromosomes during cell cycle in *S. cerevisiae*

The organization of the chromosomes at different cell-cycle stages was assessed using the chromosome conformations capture (Hi-C) technique (Lieberman-Aiden et al., 2009). We observed that the Rabl-like organization of the chromosomes (centromeric bending of the chromosomes) persists during the entire cell cycle. We also confirmed the absence of topological domains (e.g. TADs) (Duan et al., 2010; Guidi et al., 2015), structural features found in many other species (Dixon et al., 2016) and that have been recently (loosely) observed in yeast (Eser et al., 2017). This discrepancy may be due to different Hi-C protocols coupled to different data processing. Topological domains have been associated with complex regulatory systems such as gene expression and replication. In mammals, genes located in the same TAD share coordinated gene expression profiles (Lupiáñez et al., 2016; Nora et al., 2012; Pope et al., 2014). Given the compact genome of *S. cerevisiae*, characterized by short genes mostly regulated by their own upstream promoters, the absence of TADs could be that this microorganism does not need a global TAD-based genome regulation.

Although the higher-order of yeast chromatin does not form large domains, Hi-C genomic contact maps showed a dynamic reorganization during the entire cell cycle, regulated by chromatin structural proteins. During S phase, we detected a cohesin-dependent increase in long-range intra-chromosomal contacts, accompanied by a global decrease of inter-chromosomal contacts. In agreement with the enrichment of cohesins at centromeres (Glynn et al., 2004), the inter-centromeric contacts were strongly increased pointing to the formation of a tightly-packed cluster of pericentromeric chromatin. We also observed that the centromere cluster was further increased during anaphase in a condensin dependent manner. A current model suggests that cohesin and condensin enrichment in the pericentromeric region (D'Ambrosio et al., 2008a) may behave as a molecular spring during chromosome segregation (chapter 1.3.3.1; Yeh et al., 2008). In light of these observations and in support to the peculiar mechanism of chromosome segregation in yeast (one centromere attached to one single microtubule; Winey and Bloom, 2012), we also speculate that the clustering of pericentromeric

Conclusion and discussion

springs may form a robust and elastic structure that resists the mechanic force of the spindle.

Another interesting aspect of anaphase segregation came from the investigation of the topoisomerase 2 (Top2). The action of this enzymes appeared to oppose the activity of the condensins (Baxter and Aragón, 2012), showing a decrease of both intra-chromosomal and inter-centromere contacts (Figure 1, top right panel), in agreement with the condensin-dependent decatenation activity of Top2 (D'Ambrosio et al., 2008b). Indeed, Top2 may counteract the recoiling activity of condensins (relaxed chromatin fibre, Baxter et al., 2011) that could explain its requirement at the centromeres and rDNA, where the chromatin is more tightly packed and/or entangled (Sullivan et al., 2004).

The most remarkable structural reorganization during the cell cycle progression has been observed for chromosome 12 carrying the rDNA cluster. The repeated nature of the rDNA makes it “invisible” to genomic analyses because of the impossibility to align the reads along the repeats (Langmead and Salzberg, 2012). Nevertheless, we monitored the structural changes of the rDNA flanking regions on chromosome 12 and interpreted the results in light of imaging studies. An abrupt change in the organization of chr12 was detected during late anaphase when the centromere-proximal rDNA-flanking region contacted the centromere. These contacts that bridged the two loci resulted in the formation of a loop-like structure. To confirm that these contacts were mediated by the rDNA, we used a strain in which the rDNA locus was deleted (*rdnΔ*) (Figure 1, bottom left panels). The *rdnΔ* strain arrested in anaphase (*cdc15*) showed no rDNA-centromere contacts. ChIP-seq has found an enrichment of both condensins and Top2 at the rDNA (D'Ambrosio et al., 2008a), while imaging revealed condensation and segregation defects in absence of these proteins (Sullivan et al., 2004). We found that the rDNA-centromere loop is dependent on the condensation process and does not require Top2, in agreement with the condensin-dependent decatenation model. In addition, this structure is independent of the anaphase spindle in support to the rDNA microtubule-independent segregation (Machín et al., 2005). Other studies investigating the motor activity of the condensin complex suggested that its ATPase activity is essential to promote the movement on the DNA molecule (Frosi and Haering, 2015; Terekawa et al., 2017). In light of these observations we speculate that the centromeric condensin may advance along the chromosome arms using a loop extrusion mechanism (Alipour and Marko, 2012; Goloborodko et al., 2016). This model envisages the extrusion of the chromatin through the condensin ring to promote the resolution of the two sister

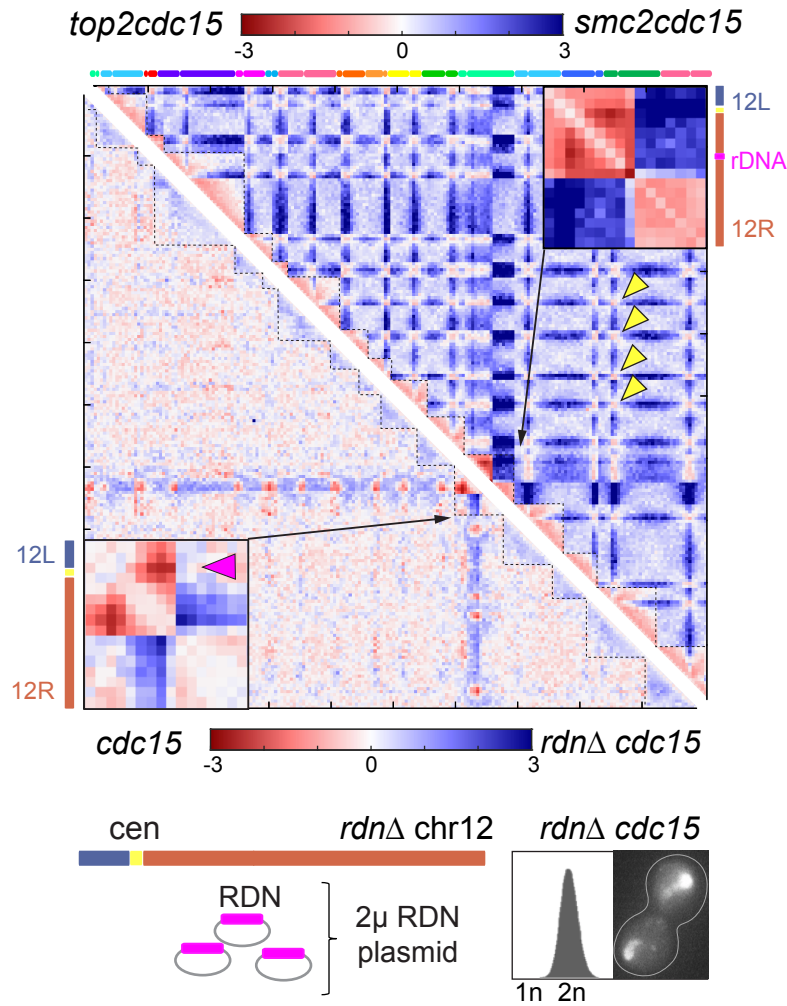


Figure 1 An interplay between condensins and topoisomerase 2 in anaphase. Log-ratio contact maps (50 kb bin) of anaphase arrested cells (*cdc15*). Bottom left panels show the absence of contacts between the rDNA and all centromeres in a strain that lacks the rDNA locus (bottom schema). Top right panels show the persistence of contacts between rDNA and centromere when topoisomerase 2 is depleted. The 16 yeast chromosomes are displayed above the maps. Blue to red colour scales reflect the enrichment in contacts in one population with respect to the other. Purple arrowheads point at contacts between rDNA and centromeres. Insets display magnifications of the log-ratio maps of chromosome 12.

Conclusion and discussion

chromatids. It is a possibility that this movement is blocked once they reach the pool of rDNA condensins, giving rise to a stable/persistent loop that can be visualized at the population level. One can speculate whether this mechanism occurs on all chromosomes, but is particularly visible on chr12 because of the presence of the rDNA locus. This hypothesis is partially supported by the absence of the loop in the *rDNA* strain (above). Increasing the size of the DNA segment between the centromere and the rDNA cluster also resulted in the presence of an anaphase loop, as shown using a strain carrying a fusion between chromosome 4 and 12. This chromosome has only one active centromere (*cen4*) located approximately 1.5 Mb from the rDNA locus (native location on chr12). Cells arrested in anaphase displayed contacts between the rDNA and *cen4*, resulting in the formation of a mega-size loop (Figure 2) However, these results are not a direct proof of the loop extrusion model of chromosome segregation, and more mechanistic investigations are needed to precisely characterize the mechanisms leading to this intriguing structure.

Although our study unveiled new features of chromosomal organization during the cell cycle, they remain to be improved. Notably, our method is limited by the cell-to-cell variability present in the synchronized cell populations we analysed. This emphasises the importance of the development of single cell Hi-C technology (Nagano et al., 2013). This approach is a powerful tool to resolve metabolically-related changes of chromosome organization, and has recently provided interesting insights on chromosome dynamics during replication in mammalian cells (Nagano et al., 2017). Nevertheless, the lack of an “absolute reference” imposes the average of many “relative-to-cell references” to assess significant variations. Therefore, it appears obvious that a proper investigation of the different layers of chromosome organization and their dynamics requires a combination of “C” methods.

Linking structure and function of the chromosomes

Function and structure of the chromatin are strongly correlated. An open/accessible chromatin has been associated with a high level of transcription whereas the close/dense form is usually silenced (Venkatesh and Workman, 2015). In budding yeast, the link between transcription regulation and nuclear organization has been highly investigated at telomeres and rDNA (Kupiec, 2014; Laura N. Rusche et al., 2003; Mekhail and Moazed, 2010; Wellinger and Zakian, 2012). The transcriptional silencing of these loci requires the different enzymatic activity of the SIR-complex proteins (described in section 2.2). In this work we showed that the dense status of the chromatin is strongly correlated with the spreading ability of Sir3 and, consequently, with its silencing

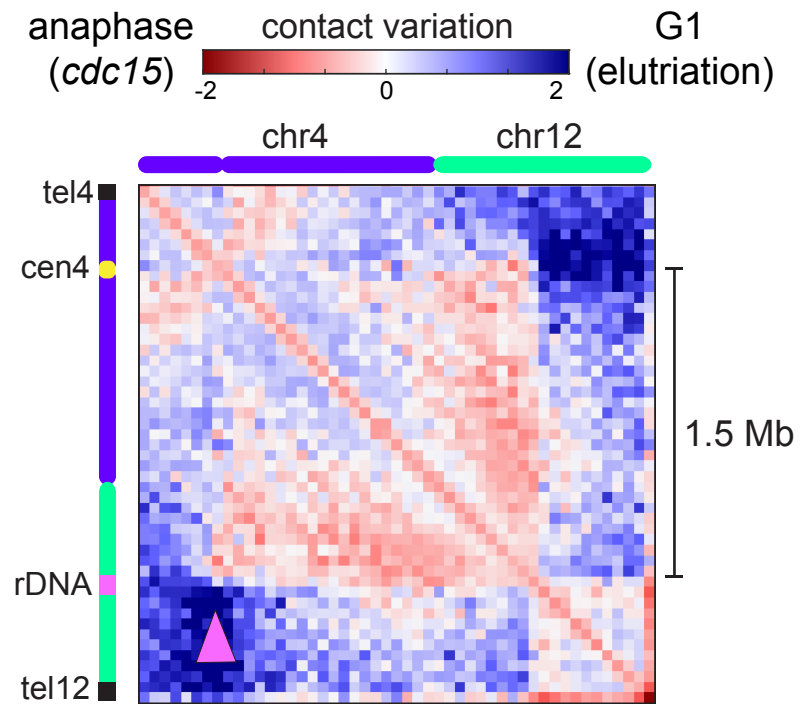


Figure 2 The formation of a mega-sized loop. Log-ratio contact map (50 kb bin) of G1 elutriated cells and anaphase *cdc15*-arrested cells. The fused chromosomes 4 and 12 are displayed on the *x*- and *y*-axis of the map. Purple arrowhead points at contacts between rDNA and centromere of chr4 that are located ~1.5 Mb far from each other. Blue to red colour scale reflects the enrichment in contacts in one population with respect to the other.

Conclusion and discussion

activity. We have shown that similar telomere hyperclusters may enclose different types of chromatin structures, depending on the metabolic state.

Intriguing results have been observed in cells that start to adapt to nutrient starvation during overnight growth. We observed that telomeres start to associate in tighter clusters while establishing contacts with the rDNA. Since the rDNA sequesters the spreading activator, Sir2, we speculate that this colocalization may be an efficient way to control silencing. Notably, while inter-telomere contacts were Sir3-dependent their contacts with the rDNA were Sir3-independent. This is in agreement with a recent study showing that the nuclear localization of telomere clusters was independent of Sir3 (Laporte et al., 2016). The same study reported the role of Esc1 (another protein of the silencing complex) in the telomere repositioning in nutrient limiting conditions. Therefore, it will be interesting to investigate if Esc1 is the factor that mediates rDNA-telomere contacts in our system.

Long periods of nutrient starvation lead cells to enter stationary and eventually quiescent state (G0). Among all features (chapter 1.3.1), G0 cells are characterized by a higher status of chromatin compaction correlated with a low rate of transcription activation (Schäfer et al., 2008). We have indeed observed that in G0 chromosomes tend to increase long-range intra-chromosomal contacts (chapter 2.2; Figure 5A), as was particularly visible on chromosome 12.

An interesting connection between cells in G0 and cells in anaphase is the chromatin compaction associated with a low level of rDNA transcription. The nucleolar Cdc14 phosphatase is part of a complex that is required both for silencing (complex with Sir2) (Huang and Moazed, 2003) and for anaphase exit (rDNA condensation) (Clemente-Blanco et al., 2009), we could imagine that the chromatin reorganization in these stages might share similarities. We showed that anaphase cells need the condensation-related function of Cdc14 to achieve the formation of the rDNA-centromere loop on chromosome 12 (chapter 2.1). However, this loop structure was not detected in G0 cells, indicating that chromatin compaction in G0 is probably condensin-independent.

Although rDNA silencing in G0 and anaphase may be important, lower levels are required to protect cells from hyper-recombination during the other cell-cycle phases (Kaeberlein et al., 1999; Kobayashi and Horiuchi, 1996; Pappas et al., 2004). Indeed, this locus carries a protein/DNA replication fork barrier (Fob1/*RFB*) that has been shown to arrest replication in an orientation-dependent manner to ensure the unidirectionality of replication and transcription. This mechanism has been suggested to prevent

Conclusion and discussion

transcription-replication clashes that could collapse replication forks, giving rise to potentially recombinogenic replication intermediates (Gruber et al., 2000; Lin and Pasero, 2012; Takeuchi et al., 2003). Similar replication blocks have been described in other organisms (e.g. *Rtf1/RTS1* and *Tus/Ter*), where their insertion at ectopic positions in the genome causes chromosomal rearrangements (Lambert and Carr, 2013).

Hi-C chromosomal maps during DNA replication allowed us to build a 3D replication profile (chapter 2.1). The 3D representation illustrated the expected temporal program of replication program, starting at the centromere cluster and finishing at the telomere clusters. To understand new links between the spatial organization of replication and genome stability, we inserted replication fork blocks (*Tus/Ter*) at genomic locations with different replication timing (early, mid and late; Raghuraman et al., 2001). We sought chromosomal rearrangements that may reflect the spatial proximity of the arrested replicating region. Although we detected an abundant amount of replication intermediates at the fork blocks, we have failed to detect replication recombination (if present), so far. Among the many potential reasons that could have impeded the observation of such events (discussed in chapter 2.3), in this section I would focus on those that could be related to the 3D organization. In our hands the analysis of S phase Hi-C maps has revealed only a slight increase in contacts between collinear early replicating origins. This observation could indicate a stochastic association of origins into foci (Saner et al., 2013) but also an effect of the pericentromeric chromatin. The enrichment of cohesins at the pericentromeric chromatin may increase long-range chromosomal contacts in this region, where most of the early origins are. This would suggest that colocalization of early replicated regions is not specific to replication, rather it is an intrinsic property of budding yeast genome organization. This hypothesis could explain the observed colocalization of early pericentromeric regions in both asynchronous and G1 cells (Duan et al., 2010; Eser et al., 2017; Knott et al., 2012).

Another interesting aspect of chromatin dynamics that has been reported to play an important role in DNA repair is the mobility of the chromatin fibre (Dion and Gasser, 2013). A global and local increase in chromatin mobility after DNA damage has been associated with an increase in repair efficiency (Miné-Hattab and Rothstein, 2012). Interestingly, the global mobility in S phase compared to G1 is decreased (Heun et al., 2001a). This mechanism would favour the inter-sister chromatids DNA repair (error-free) and disfavour ectopic recombination (error-prone). In light of these observations, it is a possibility that the replication intermediates, observed at the *Tus/Ter* replication blocks, could be limited during their search for a repair choice.

Conclusion and discussion

Overall, this study remains an ongoing work, which should unveil why the genome remains so stable in presence of multiple blocks, and ideally point at conditions under which this stability will be alleviated.

4. Bibliography

Agmon, N., Liefshitz, B., Zimmer, C., Fabre, E., and Kupiec, M. (2013). Effect of nuclear architecture on the efficiency of double-strand break repair. *Nature Cell Biology* 15, 694–699.

Aladjem, M.I. (2007). Replication in context: dynamic regulation of DNA replication patterns in metazoans. *Nat Rev Genet* 8, 588–600.

Alberts, B., Johnson, A., Lewis, J., Raff, M., Roberts, K., and Walter, P. (2002). *Intracellular Control of Cell-Cycle Events*.

Alipour, E., and Marko, J.F. (2012). Self-organization of domain structures by DNA-loop-extruding enzymes. *Nucleic Acids Res* 40, 11202–11212.

Amon, A. (2001). Together until separin do us part. *Nat Cell Biol* 3, E12–E14.

Amon, A. (2008). A decade of Cdc14 – a personal perspective. *FEBS J* 275, 5774–5784.

Aparicio, J.G., Viggiani, C.J., Gibson, D.G., and Aparicio, O.M. (2004). The Rpd3-Sin3 Histone Deacetylase Regulates Replication Timing and Enables Intra-S Origin Control in *Saccharomyces cerevisiae*. *Mol. Cell. Biol.* 24, 4769–4780.

Aparicio, O.M., Stout, A.M., and Bell, S.P. (1999). Differential assembly of Cdc45p and DNA polymerases at early and late origins of DNA replication. *PNAS* 96, 9130–9135.

Aragon, L., Martinez-Perez, E., and Merckenschlager, M. (2013). Condensin, cohesin and the control of chromatin states. *Current Opinion in Genetics & Development* 23, 204–211.

Arnold, J. (1879). Beobachtungen über Kerntheilungen in den Zellen der Geschwülste. *Archiv f. pathol. Anat.* 78, 279–301.

Avery, O.T., MacLeod, C.M., and McCarty, M. (1944). STUDIES ON THE CHEMICAL NATURE OF THE SUBSTANCE INDUCING TRANSFORMATION OF PNEUMOCOCCAL TYPES. *J Exp Med* 79, 137–158.

Aymard, F., Aguirrebengoa, M., Guillou, E., Javierre, B.M., Bugler, B., Arnould, C., Rocher, V., Iacovoni, J.S., Biernacka, A., Skrzypczak, M., et al. (2017). Genome-wide mapping of long-range contacts unveils clustering of DNA double-strand breaks at damaged active genes. *Nat Struct Mol Biol* 24, 353–361.

Azvolinsky, A., Dunaway, S., Torres, J.Z., Bessler, J.B., and Zakian, V.A. (2006). The *S. cerevisiae* Rrm3p DNA helicase moves with the replication fork and affects replication of all yeast chromosomes. *Genes Dev.* 20, 3104–3116.

Bachelier-Bassi, S., Gadal, O., Bourout, G., and Nehrbass, U. (2008). Cell cycle-dependent kinetochore localization of condensin complex in *Saccharomyces cerevisiae*. *Journal of Structural Biology* 162, 248–259.

Bibliography

Bankevich, A., Nurk, S., Antipov, D., Gurevich, A.A., Dvorkin, M., Kulikov, A.S., Lesin, V.M., Nikolenko, S.I., Pham, S., Prjibelski, A.D., et al. (2012). SPAdes: a new genome assembly algorithm and its applications to single-cell sequencing. *J. Comput. Biol.* *19*, 455–477.

Barberis, M., Spiesser, T.W., and Klipp, E. (2010). Replication Origins and Timing of Temporal Replication in Budding Yeast: How to Solve the Conundrum? *Curr Genomics* *11*, 199–211.

Barrett, T., Wilhite, S.E., Ledoux, P., Evangelista, C., Kim, I.F., Tomashevsky, M., Marshall, K.A., Phillippy, K.H., Sherman, P.M., Holko, M., et al. (2013). NCBI GEO: archive for functional genomics data sets--update. *Nucleic Acids Res.* *41*, D991–995.

Baxter, J., and Aragón, L. (2012). A model for chromosome condensation based on the interplay between condensin and topoisomerase II. *Trends in Genetics* *28*, 110–117.

Baxter, J., Sen, N., Martínez, V.L., Carandini, M.E.M.D., Schwartzman, J.B., Diffley, J.F.X., and Aragón, L. (2011). Positive Supercoiling of Mitotic DNA Drives Decatenation by Topoisomerase II in Eukaryotes. *Science* *331*, 1328–1332.

Bell, S.P., and Stillman, B. (1992). ATP-dependent recognition of eukaryotic origins of DNA replication by a multiprotein complex. *Nature* *357*, 128–134.

Belmont, A.S., and Straight, A.F. (1998). In vivo visualization of chromosomes using lac operator-repressor binding. *Trends Cell Biol.* *8*, 121–124.

Betzig, E., Patterson, G.H., Sougrat, R., Lindwasser, O.W., Olenych, S., Bonifacino, J.S., Davidson, M.W., Lippincott-Schwartz, J., and Hess, H.F. (2006). Imaging intracellular fluorescent proteins at nanometer resolution. *Science* *313*, 1642–1645.

Bhalla, N., Biggins, S., and Murray, A.W. (2002). Mutation of YCS4, a budding yeast condensin subunit, affects mitotic and nonmitotic chromosome behavior. *Mol. Biol. Cell* *13*, 632–645.

Bierne, H., Ehrlich, S.D., and Michel, B. (1997). Deletions at stalled replication forks occur by two different pathways. *EMBO J.* *16*, 3332–3340.

Blat, Y., and Kleckner, N. (1999). Cohesins Bind to Preferential Sites along Yeast Chromosome III, with Differential Regulation along Arms versus the Centric Region. *Cell* *98*, 249–259.

Bomfleur, B., McLoughlin, S., and Vajda, V. (2014). Fossilized Nuclei and Chromosomes Reveal 180 Million Years of Genomic Stasis in Royal Ferns. *Science* *343*, 1376–1377.

Boveri, T. (1902). *Das Problem der Befruchtung* (Jena, G. Fischer).

Boveri, T. (1907). *Zellen-Studien* (Jena, G. Fischer).

Brachmann, C.B., Davies, A., Cost, G.J., Caputo, E., Li, J., Hieter, P., and Boeke, J.D. (1998). Designer deletion strains derived from *Saccharomyces cerevisiae* S288C: a useful set of strains and plasmids for PCR-mediated gene disruption and other applications. *Yeast* *14*, 115–132.

Branzei, D., and Foiani, M. (2010a). Leaping forks at inverted repeats. *Genes Dev* *24*, 5–9.

Bibliography

Branzei, D., and Foiani, M. (2010b). Maintaining genome stability at the replication fork. *Nat. Rev. Mol. Cell Biol.* *11*, 208–219.

Brewer, B.J., and Fangman, W.L. (1987). The localization of replication origins on ARS plasmids in *S. cerevisiae*. *Cell* *51*, 463–471.

Brewer, B.J., and Fangman, W.L. (1988). A replication fork barrier at the 3' end of yeast ribosomal RNA genes. *Cell* *55*, 637–643.

Brewer, B.J., and Fangman, W.L. (1991). Mapping replication origins in yeast chromosomes. *Bioessays* *13*, 317–322.

Bult, C.J., White, O., Olsen, G.J., Zhou, L., Fleischmann, R.D., Sutton, G.G., Blake, J.A., FitzGerald, L.M., Clayton, R.A., Gocayne, J.D., et al. (1996). Complete genome sequence of the methanogenic archaeon, *Methanococcus jannaschii*. *Science* *273*, 1058–1073.

Bumgarner, S.L., Dowell, R.D., Grisafi, P., Gifford, D.K., and Fink, G.R. (2009). Toggle involving cis-interfering noncoding RNAs controls variegated gene expression in yeast. *PNAS* *106*, 18321–18326.

Bystricky, K., Heun, P., Gehlen, L., Langowski, J., and Gasser, S.M. (2004). Long-range compaction and flexibility of interphase chromatin in budding yeast analyzed by high-resolution imaging techniques. *PNAS* *101*, 16495–16500.

Bystricky, K., Laroche, T., van Houwe, G., Blaszczyk, M., and Gasser, S.M. (2005). Chromosome looping in yeast: telomere pairing and coordinated movement reflect anchoring efficiency and territorial organization. *J. Cell Biol.* *168*, 375–387.

Cadoret, J.-C., Meisch, F., Hassan-Zadeh, V., Luyten, I., Guillet, C., Duret, L., Quesneville, H., and Prioleau, M.-N. (2008). Genome-wide studies highlight indirect links between human replication origins and gene regulation. *PNAS* *105*, 15837–15842.

Calzada, A., Hodgson, B., Kanemaki, M., Bueno, A., and Labib, K. (2005). Molecular anatomy and regulation of a stable replisome at a paused eukaryotic DNA replication fork. *Genes Dev.* *19*, 1905–1919.

Carr, A.M., and Lambert, S. (2013). Replication Stress-Induced Genome Instability: The Dark Side of Replication Maintenance by Homologous Recombination. *Journal of Molecular Biology* *425*, 4733–4744.

Carr, A.M., Paek, A.L., and Weinert, T. (2011). DNA replication: Failures and inverted fusions. *Seminars in Cell & Developmental Biology* *22*, 866–874.

Casas-Delucchi, C.S., van Bommel, J.G., Haase, S., Herce, H.D., Nowak, D., Meilinger, D., Stear, J.H., Leonhardt, H., and Cardoso, M.C. (2012). Histone hypoacetylation is required to maintain late replication timing of constitutive heterochromatin. *Nucleic Acids Res.* *40*, 159–169.

Caspersson, T., Zech, L., and Johansson, C. (1970). Differential binding of alkylating fluorochromes in human chromosomes. *Exp. Cell Res.* *60*, 315–319.

Cayrou, C., Coulombe, P., Vigneron, A., Stanojic, S., Ganier, O., Peiffer, I., Rivals, E., Puy, A., Laurent-Chabalier, S., Desprat, R., et al. (2011). Genome-scale analysis of metazoan

Bibliography

replication origins reveals their organization in specific but flexible sites defined by conserved features. *Genome Res.* *21*, 1438–1449.

Chagin, V.O., Casas-Delucchi, C.S., Reinhart, M., Schermelleh, L., Markaki, Y., Maiser, A., Bolius, J.J., Bensimon, A., Fillies, M., Domaing, P., et al. (2016). 4D Visualization of replication foci in mammalian cells corresponding to individual replicons. *Nat Commun* *7*.

Ciosk, R., Zachariae, W., Michaelis, C., Shevchenko, A., Mann, M., and Nasmyth, K. (1998). An ESP1/PDS1 Complex Regulates Loss of Sister Chromatid Cohesion at the Metaphase to Anaphase Transition in Yeast. *Cell* *93*, 1067–1076.

Clemente-Blanco, A., Mayán-Santos, M., Schneider, D.A., Machín, F., Jarmuz, A., Tschochner, H., and Aragón, L. (2009). Cdc14 inhibits transcription by RNA polymerase I during anaphase. *Nature* *458*, 219–222.

Cobb, J.A., Bjergbaek, L., Shimada, K., Frei, C., and Gasser, S.M. (2003a). DNA polymerase stabilization at stalled replication forks requires Mec1 and the RecQ helicase Sgs1. *EMBO J* *22*, 4325–4336.

Cobb, J.A., Bjergbaek, L., Shimada, K., Frei, C., and Gasser, S.M. (2003b). DNA polymerase stabilization at stalled replication forks requires Mec1 and the RecQ helicase Sgs1. *EMBO J.* *22*, 4325–4336.

Conconi, A., Widmer, R.M., Koller, T., and Sogo, J.M. (1989). Two different chromatin structures coexist in ribosomal RNA genes throughout the cell cycle. *Cell* *57*, 753–761.

Costes, A., and Lambert, S.A.E. (2012). Homologous Recombination as a Replication Fork Escort: Fork-Protection and Recovery. *Biomolecules* *3*, 39–71.

Cournac, A., Marie-Nelly, H., Marbouty, M., Koszul, R., and Mozziconacci, J. (2012). Normalization of a chromosomal contact map. *BMC Genomics* *13*, 436.

Crane, E., Bian, Q., McCord, R.P., Lajoie, B.R., Wheeler, B.S., Ralston, E.J., Uzawa, S., Dekker, J., and Meyer, B.J. (2015). Condensin-driven remodelling of X chromosome topology during dosage compensation. *Nature advance online publication*.

Cremer, T., and Cremer, M. (2010). Chromosome Territories. *Cold Spring Harb Perspect Biol* *2*.

Cuylen, S., Metz, J., and Haering, C.H. (2011). Condensin structures chromosomal DNA through topological links. *Nat Struct Mol Biol* *18*, 894–901.

Dalgaard, J.Z., and Klar, A.J.S. (1999). Orientation of DNA replication establishes mating-type switching pattern in *S. pombe*. *Nature* *400*, 181–184.

D'Ambrosio, C., Schmidt, C.K., Katou, Y., Kelly, G., Itoh, T., Shirahige, K., and Uhlmann, F. (2008a). Identification of cis-acting sites for condensin loading onto budding yeast chromosomes. *Genes Dev.* *22*, 2215–2227.

D'Ambrosio, C., Kelly, G., Shirahige, K., and Uhlmann, F. (2008b). Condensin-Dependent rDNA Decatenation Introduces a Temporal Pattern to Chromosome Segregation. *Current Biology* *18*, 1084–1089.

Bibliography

D'Amours, D., and Amon, A. (2004). At the interface between signaling and executing anaphase--Cdc14 and the FEAR network. *Genes Dev.* *18*, 2581–2595.

D'Amours, D., Stegmeier, F., and Amon, A. (2004). Cdc14 and Condensin Control the Dissolution of Cohesin-Independent Chromosome Linkages at Repeated DNA. *Cell* *117*, 455–469.

De Piccoli, G., Katou, Y., Itoh, T., Nakato, R., Shirahige, K., and Labib, K. (2012). Replisome stability at defective DNA replication forks is independent of S phase checkpoint kinases. *Mol. Cell* *45*, 696–704.

Decourty, L., Saveanu, C., Zemam, K., Hantraye, F., Frachon, E., Rousselle, J.-C., Fromont-Racine, M., and Jacquier, A. (2008). Linking functionally related genes by sensitive and quantitative characterization of genetic interaction profiles. *Proc Natl Acad Sci U S A* *105*, 5821–5826.

Dekker, J. (2008). Mapping in Vivo Chromatin Interactions in Yeast Suggests an Extended Chromatin Fiber with Regional Variation in Compaction. *J. Biol. Chem.* *283*, 34532–34540.

Dekker, J., Rippe, K., Dekker, M., and Kleckner, N. (2002). Capturing chromosome conformation. *Science* *295*, 1306–1311.

Dekker, J., Marti-Renom, M.A., and Mirny, L.A. (2013). Exploring the three-dimensional organization of genomes: interpreting chromatin interaction data. *Nat Rev Genet* *14*, 390–403.

Diffley, J.F.X. (1996). Once and only once upon a time: Specifying and regulating origins of DNA replication in eukaryotic cells. *Genes and Development* *10*, 2819–2830.

Dion, V., and Gasser, S.M. (2013). Chromatin movement in the maintenance of genome stability. *Cell* *152*, 1355–1364.

Dion, V., Kalck, V., Horigome, C., Towbin, B.D., and Gasser, S.M. (2012). Increased mobility of double-strand breaks requires Mec1, Rad9 and the homologous recombination machinery. *Nat Cell Biol* *14*, 502–509.

Dixon, J.R., Selvaraj, S., Yue, F., Kim, A., Li, Y., Shen, Y., Hu, M., Liu, J.S., and Ren, B. (2012). Topological Domains in Mammalian Genomes Identified by Analysis of Chromatin Interactions. *Nature* *485*, 376–380.

Dixon, J.R., Gorkin, D.U., and Ren, B. (2016). Chromatin Domains: The Unit of Chromosome Organization. *Mol. Cell* *62*, 668–680.

Duan, Z., Andronescu, M., Schutz, K., McIlwain, S., Kim, Y.J., Lee, C., Shendure, J., Fields, S., Blau, C.A., and Noble, W.S. (2010). A three-dimensional model of the yeast genome. *Nature* *465*, 363–367.

Dubarry, M., Loïodice, I., Chen, C.L., Thermes, C., and Taddei, A. (2011). Tight protein-DNA interactions favor gene silencing. *Genes Dev.* *25*, 1365–1370.

Duggin, I.G., and Bell, S.D. (2009). Termination Structures in the Escherichia coli Chromosome Replication Fork Trap. *Journal of Molecular Biology* *387*, 532–539.

Bibliography

Duzdevich, D., Warner, M.D., Ticau, S., Ivica, N.A., Bell, S.P., and Greene, E.C. (2015). The Dynamics of Eukaryotic Replication Initiation: Origin Specificity, Licensing, and Firing at the Single-Molecule Level. *Molecular Cell* 58, 483–494.

Ebrahimi, H., and Donaldson, A.D. (2008). Release of yeast telomeres from the nuclear periphery is triggered by replication and maintained by suppression of Ku-mediated anchoring. *Genes Dev.* 22, 3363–3374.

Edgar, R., Domrachev, M., and Lash, A.E. (2002). Gene Expression Omnibus: NCBI gene expression and hybridization array data repository. *Nucleic Acids Res.* 30, 207–210.

ENCODE Project Consortium, Birney, E., Stamatoyannopoulos, J.A., Dutta, A., Guigó, R., Gingeras, T.R., Margulies, E.H., Weng, Z., Snyder, M., Dermitzakis, E.T., et al. (2007). Identification and analysis of functional elements in 1% of the human genome by the ENCODE pilot project. *Nature* 447, 799–816.

Engel, S.R., Dietrich, F.S., Fisk, D.G., Binkley, G., Balakrishnan, R., Costanzo, M.C., Dwight, S.S., Hitz, B.C., Karra, K., Nash, R.S., et al. (2014). The reference genome sequence of *Saccharomyces cerevisiae*: then and now. *G3 (Bethesda)* 4, 389–398.

Eser, U., Chandler-Brown, D., Ay, F., Straight, A.F., Duan, Z., Noble, W.S., and Skotheim, J.M. (2017). Form and function of topologically associating genomic domains in budding yeast. *PNAS* 114, E3061–E3070.

Evans, T., Rosenthal, E.T., Youngblom, J., Distel, D., and Hunt, T. (1983). Cyclin: a protein specified by maternal mRNA in sea urchin eggs that is destroyed at each cleavage division. *Cell* 33, 389–396.

Farnham, P.J. (2009). Insights from genomic profiling of transcription factors. *Nat Rev Genet* 10, 605–616.

Ferguson, B.M., and Fangman, W.L. (1992). A position effect on the time of replication origin activation in yeast. *Cell* 68, 333–339.

Fichtner, L., Schulze, F., and Braus, G.H. (2007). Differential Flo8p-dependent regulation of FLO1 and FLO11 for cell–cell and cell–substrate adherence of *S. cerevisiae* S288c. *Mol Microbiol* 66, 1276–1289.

Fiers, W., Contreras, R., Duerinck, F., Haegeman, G., Iserentant, D., Merregaert, J., Min Jou, W., Molemans, F., Raeymaekers, A., Van den Berghe, A., et al. (1976). Complete nucleotide sequence of bacteriophage MS2 RNA: primary and secondary structure of the replicase gene. *Nature* 260, 500–507.

Fleischmann, R.D., Adams, M.D., White, O., Clayton, R.A., Kirkness, E.F., Kerlavage, A.R., Bult, C.J., Tomb, J.F., Dougherty, B.A., and Merrick, J.M. (1995). Whole-genome random sequencing and assembly of *Haemophilus influenzae* Rd. *Science* 269, 496–512.

Flemming, W. (1882). *Zellsubstanz, kern und zelltheilung.* (Leipzig, F. C. W. Vogel).

Franke, M., Ibrahim, D.M., Andrey, G., Schwarzer, W., Heinrich, V., Schöpflin, R., Kraft, K., Kempfer, R., Jerković, I., Chan, W.-L., et al. (2016). Formation of new chromatin domains determines pathogenicity of genomic duplications. *Nature* 538, 265–269.

Bibliography

Frosi, Y., and Haering, C.H. (2015). Control of chromosome interactions by condensin complexes. *Current Opinion in Cell Biology* 34, 94–100.

Furey, T.S. (2012). ChIP-seq and beyond: new and improved methodologies to detect and characterize protein–DNA interactions. *Nat Rev Genet* 13, 840–852.

Futcher, B. (1999). Cell cycle synchronization. *Methods Cell Sci* 21, 79–86.

Galdieri, L., Mehrotra, S., Yu, S., and Vancura, A. (2010). Transcriptional Regulation in Yeast during Diauxic Shift and Stationary Phase. *OMICS* 14, 629–638.

Gerlich, D., Koch, B., Dupeux, F., Peters, J.-M., and Ellenberg, J. (2006). Live-cell imaging reveals a stable cohesin-chromatin interaction after but not before DNA replication. *Curr. Biol.* 16, 1571–1578.

Gillett, E.S., Espelin, C.W., and Sorger, P.K. (2004). Spindle checkpoint proteins and chromosome–microtubule attachment in budding yeast. *J Cell Biol* 164, 535–546.

Gilmour, D.S., and Lis, J.T. (1984). Detecting protein-DNA interactions in vivo: distribution of RNA polymerase on specific bacterial genes. *Proc. Natl. Acad. Sci. U.S.A.* 81, 4275–4279.

Gligoris, T.G., Scheinost, J.C., Bürmann, F., Petela, N., Chan, K.-L., Uluocak, P., Beckouët, F., Gruber, S., Nasmyth, K., and Löwe, J. (2014). Closing the cohesin ring: Structure and function of its Smc3-kleisin interface. *Science* 346, 963–967.

Glynn, E.F., Megee, P.C., Yu, H.-G., Mistrot, C., Unal, E., Koshland, D.E., DeRisi, J.L., and Gerton, J.L. (2004). Genome-Wide Mapping of the Cohesin Complex in the Yeast *Saccharomyces cerevisiae*. *PLoS Biol* 2, e259.

Goffeau, A., Barrell, B.G., Bussey, H., Davis, R.W., Dujon, B., Feldmann, H., Galibert, F., Hoheisel, J.D., Jacq, C., Johnston, M., et al. (1996). Life with 6000 Genes. *Science* 274, 546–567.

Goloborodko, A., Imakaev, M.V., Marko, J.F., and Mirny, L. (2016). Compaction and segregation of sister chromatids via active loop extrusion. *ELife Sciences* 5, e14864.

Gotta, M., Laroche, T., Formenton, A., Maillet, L., Scherthan, H., and Gasser, S.M. (1996). The clustering of telomeres and colocalization with Rap1, Sir3, and Sir4 proteins in wild-type *Saccharomyces cerevisiae*. *J. Cell Biol.* 134, 1349–1363.

Gotta, M., Strahl-Bolsinger, S., Renauld, H., Laroche, T., Kennedy, B.K., Grunstein, M., and Gasser, S.M. (1997). Localization of Sir2p: the nucleolus as a compartment for silent information regulators. *The EMBO Journal* 16, 3243–3255.

Gray, J.V., Petsko, G.A., Johnston, G.C., Ringe, D., Singer, R.A., and Werner-Washburne, M. (2004). “Sleeping Beauty”: Quiescence in *Saccharomyces cerevisiae*. *Microbiol. Mol. Biol. Rev.* 68, 187–206.

Grigoryev, S.A., Arya, G., Correll, S., Woodcock, C.L., and Schlick, T. (2009). Evidence for heteromorphic chromatin fibers from analysis of nucleosome interactions. *Proc. Natl. Acad. Sci. U.S.A.* 106, 13317–13322.

Gruber, M., Wellinger, R.E., and Sogo, J.M. (2000). Architecture of the Replication Fork Stalled at the 3′ End of Yeast Ribosomal Genes. *Mol. Cell. Biol.* 20, 5777–5787.

Bibliography

Guacci, V., Hogan, E., and Koshland, D. (1994). Chromosome condensation and sister chromatid pairing in budding yeast. *J. Cell Biol.* *125*, 517–530.

Guacci, V., Koshland, D., and Strunnikov, A. (1997). A direct link between sister chromatid cohesion and chromosome condensation revealed through the analysis of MCD1 in *S. cerevisiae*. *Cell* *91*, 47–57.

Guidi, M., Ruault, M., Marbouty, M., Loïodice, I., Cournac, A., Billaudeau, C., Hocher, A., Mozziconacci, J., Koszul, R., and Taddei, A. (2015). Spatial reorganization of telomeres in long-lived quiescent cells. *Genome Biology* *16*, 206.

Guillou, E., Ibarra, A., Coulon, V., Casado-Vela, J., Rico, D., Casal, I., Schwob, E., Losada, A., and Méndez, J. (2010). Cohesin organizes chromatin loops at DNA replication factories. *Genes Dev* *24*, 2812–2822.

Gunjan, A., and Verreault, A. (2003). A Rad53 Kinase-Dependent Surveillance Mechanism that Regulates Histone Protein Levels in *S. cerevisiae*. *Cell* *115*, 537–549.

Haering, C.H., Löwe, J., Hochwagen, A., and Nasmyth, K. (2002). Molecular architecture of SMC proteins and the yeast cohesin complex. *Mol. Cell* *9*, 773–788.

Hajjoul, H., Mathon, J., Ranchon, H., Goiffon, I., Mozziconacci, J., Albert, B., Carrivain, P., Victor, J.-M., Gadal, O., Bystricky, K., et al. (2013). High-throughput chromatin motion tracking in living yeast reveals the flexibility of the fiber throughout the genome. *Genome Res.* *23*, 1829–1838.

Hartwell, L.H., and Weinert, T.A. (1989). Checkpoints: controls that ensure the order of cell cycle events. *Science* *246*, 629–634.

Hartwell, L.H., Mortimer, R.K., Culotti, J., and Culotti, M. (1973). GENETIC CONTROL OF THE CELL DIVISION CYCLE IN YEAST: V. GENETIC ANALYSIS OF *cdc* MUTANTS. *Genetics* *74*, 267–286.

Hartwell, L.H., Culotti, J., Pringle, J.R., and Reid, B.J. (1974). Genetic control of the cell division cycle in yeast. *Science* *183*, 46–51.

Hastings, P.J., Ira, G., and Lupski, J.R. (2009a). A Microhomology-Mediated Break-Induced Replication Model for the Origin of Human Copy Number Variation. *PLOS Genetics* *5*, e1000327.

Hastings, P.J., Lupski, J.R., Rosenberg, S.M., and Ira, G. (2009b). Mechanisms of change in gene copy number. *Nat Rev Genet* *10*, 551–564.

Hayes, J.J., and Hansen, J.C. (2001). Nucleosomes and the chromatin fiber. *Current Opinion in Genetics & Development* *11*, 124–129.

Hayles, J., and Nurse, P. (1989). A review of mitosis in the fission yeast *Schizosaccharomyces pombe*. *Exp. Cell Res.* *184*, 273–286.

Hecht, A., Strahl-Bolsinger, S., and Grunstein, M. (1996). Spreading of transcriptional repressor SIR3 from telomeric heterochromatin. *Nature* *383*, 92–96.

Herbert, S., Brion, A., Arbona, J.-M., Lelek, M., Veillet, A., Lelandais, B., Parmar, J., Fernández, F.G., Almayrac, E., Khalil, Y., et al. (2017). Chromatin stiffening underlies

Bibliography

enhanced locus mobility after DNA damage in budding yeast. *The EMBO Journal* **e201695842**.

Herskowitz, I. (1988). Life cycle of the budding yeast *Saccharomyces cerevisiae*. *Microbiol Rev* **52**, 536–553.

Heun, P., Laroche, T., Shimada, K., Furrer, P., and Gasser, S.M. (2001a). Chromosome dynamics in the yeast interphase nucleus. *Science* **294**, 2181–2186.

Heun, P., Laroche, T., Raghuraman, M.K., and Gasser, S.M. (2001b). The positioning and dynamics of origins of replication in the budding yeast nucleus. *Journal of Cell Biology* **152**, 385–400.

Hill, T.M., Henson, J.M., and Kuempel, P.L. (1987). The terminus region of the *Escherichia coli* chromosome contains two separate loci that exhibit polar inhibition of replication. *Proc Natl Acad Sci U S A* **84**, 1754–1758.

Hirano, T. (2012). Condensins: universal organizers of chromosomes with diverse functions. *Genes Dev.* **26**, 1659–1678.

Huang, J., and Moazed, D. (2003). Association of the RENT complex with nontranscribed and coding regions of rDNA and a regional requirement for the replication fork block protein Fob1 in rDNA silencing. *Genes Dev.* **17**, 2162–2176.

Huang, C.E., Milutinovich, M., and Koshland, D. (2005). Rings, bracelet or snaps: fashionable alternatives for Smc complexes. *Philos Trans R Soc Lond B Biol Sci* **360**, 537–542.

Ira, G., and Haber, J.E. (2002). Characterization of RAD51-Independent Break-Induced Replication That Acts Preferentially with Short Homologous Sequences. *Mol. Cell. Biol.* **22**, 6384–6392.

Ira, G., Pelliccioli, A., Balijja, A., Wang, X., Fiorani, S., Carotenuto, W., Liberi, G., Bressan, D., Wan, L., Hollingsworth, N.M., et al. (2004). DNA end resection, homologous recombination and DNA damage checkpoint activation require CDK1. *Nature* **431**, 1011–1017.

Iraqi, I., Chekkal, Y., Jmari, N., Pietrobon, V., Freon, K., Costes, A., and Lambert, S.A.E. (2012). Recovery of Arrested Replication Forks by Homologous Recombination Is Error-Prone. *PLoS Genet* **8**.

Ivessa, A.S., Lenzmeier, B.A., Bessler, J.B., Goudsouzian, L.K., Schnakenberg, S.L., and Zakian, V.A. (2003). The *Saccharomyces cerevisiae* helicase Rrm3p facilitates replication past nonhistone protein-DNA complexes. *Mol. Cell* **12**, 1525–1536.

Iyer, V.R., Horak, C.E., Scafe, C.S., Botstein, D., Snyder, M., and Brown, P.O. (2001). Genomic binding sites of the yeast cell-cycle transcription factors SBF and MBF. *Nature* **409**, 533–538.

Jackman, J., and O'Connor, P.M. (2001). Methods for Synchronizing Cells at Specific Stages of the Cell Cycle. In *Current Protocols in Cell Biology*, (John Wiley & Sons, Inc.), p.

Bibliography

Jackson, D.A., and Pombo, A. (1998). Replicon Clusters Are Stable Units of Chromosome Structure: Evidence That Nuclear Organization Contributes to the Efficient Activation and Propagation of S Phase in Human Cells. *The Journal of Cell Biology* *140*, 1285–1295.

Jacob, F., Perrin, D., Sanchez, C., and Monod, J. (1960). [Operon: a group of genes with the expression coordinated by an operator]. *C. R. Hebd. Seances Acad. Sci.* *250*, 1727–1729.

Jacobs, C.W., Adams, A.E., Szaniszlo, P.J., and Pringle, J.R. (1988a). Functions of microtubules in the *Saccharomyces cerevisiae* cell cycle. *J Cell Biol* *107*, 1409–1426.

Jacobs, C.W., Adams, A.E., Szaniszlo, P.J., and Pringle, J.R. (1988b). Functions of microtubules in the *Saccharomyces cerevisiae* cell cycle. *The Journal of Cell Biology* *107*, 1409–1426.

Jaspersen, S.L., and Winey, M. (2004). THE BUDDING YEAST SPINDLE POLE BODY: Structure, Duplication, and Function. *Annual Review of Cell and Developmental Biology* *20*, 1–28.

Jeppsson, K., Kanno, T., Shirahige, K., and Sjögren, C. (2014). The maintenance of chromosome structure: positioning and functioning of SMC complexes. *Nat Rev Mol Cell Biol* *15*, 601–614.

Jin, Q., Trelles-Sticken, E., Scherthan, H., and Loidl, J. (1998). Yeast Nuclei Display Prominent Centromere Clustering That Is Reduced in Nondividing Cells and in Meiotic Prophase. *J Cell Biol* *141*, 21–29.

Jin, Q.W., Fuchs, J., and Loidl, J. (2000). Centromere clustering is a major determinant of yeast interphase nuclear organization. *J Cell Sci* *113*, 1903–1912.

Johnston, M., Hillier, L., Riles, L., Albermann, K., André, B., Ansorge, W., Benes, V., Brückner, M., Delius, H., Dubois, E., et al. (1997). The nucleotide sequence of *Saccharomyces cerevisiae* chromosome XII. *Nature* *387*, 87–90.

Jorgensen, P., Edgington, N.P., Schneider, B.L., Rupeš, I., Tyers, M., and Futcher, B. (2007). The Size of the Nucleus Increases as Yeast Cells Grow. *Mol. Biol. Cell* *18*, 3523–3532.

Kaeberlein, M., McVey, M., and Guarente, L. (1999). The SIR2/3/4 complex and SIR2 alone promote longevity in *Saccharomyces cerevisiae* by two different mechanisms. *Genes Dev.* *13*, 2570–2580.

Kalejta, R.F., Li, X., Mesner, L.D., Dijkwel, P.A., Lin, H.B., and Hamlin, J.L. (1998). Distal sequences, but not ori-beta/OBR-1, are essential for initiation of DNA replication in the Chinese hamster DHFR origin. *Mol. Cell* *2*, 797–806.

Kaplan, D.L., and Bastia, D. (2009). Mechanisms of polar arrest of a replication fork. *Molecular Microbiology* *72*, 279–285.

Kitamura, E., Blow, J.J., and Tanaka, T.U. (2006). Live-cell imaging reveals replication of individual replicons in eukaryotic replication factories. *Cell* *125*, 1297–1308.

Kitamura, E., Tanaka, K., Kitamura, Y., and Tanaka, T.U. (2007). Kinetochore-microtubule interaction during S phase in *Saccharomyces cerevisiae*. *Genes Dev* *21*, 3319–3330.

Bibliography

Knott, S.R.V., Peace, J.M., Ostrow, A.Z., Gan, Y., Rex, A.E., Viggiani, C.J., Tavaré, S., and Aparicio, O.M. (2012). Forkhead Transcription Factors Establish Origin Timing and Long-Range Clustering in *S. cerevisiae*. *Cell* *148*, 99–111.

Kobayashi, T., and Horiuchi, T. (1996). A yeast gene product, Fob1 protein, required for both replication fork blocking and recombinational hotspot activities. *Genes Cells* *1*, 465–474.

Kobayashi, O., Yoshimoto, H., and Sone, H. (1999). Analysis of the genes activated by the FLO8 gene in *Saccharomyces cerevisiae*. *Curr Genet* *36*, 256–261.

Kornberg, R.D. (1974). Chromatin Structure: A Repeating Unit of Histones and DNA. *Science* *184*, 868–871.

Kozul, R., and Fischer, G. (2009). A prominent role for segmental duplications in modeling eukaryotic genomes. *C. R. Biol.* *332*, 254–266.

Kozul, R., Caburet, S., Dujon, B., and Fischer, G. (2004). Eucaryotic genome evolution through the spontaneous duplication of large chromosomal segments. *The EMBO Journal* *23*, 234–243.

Kozul, R., Dujon, B., and Fischer, G. (2006). Stability of Large Segmental Duplications in the Yeast Genome. *Genetics* *172*, 2211–2222.

Kozul, R., Kim, K.P., Prentiss, M., Kleckner, N., and Kameoka, S. (2008). Meiotic chromosomes move by linkage to dynamic actin cables with transduction of force through the nuclear envelope. *Cell* *133*, 1188–1201.

Kupiec, M. (2014). Biology of telomeres: lessons from budding yeast. *FEMS Microbiology Reviews* *38*, 144–171.

Kuzminov, A. (2013). The chromosome cycle of prokaryotes. *Mol Microbiol* *90*, 214–227.

Laloraya, S., Guacci, V., and Koshland, D. (2000). Chromosomal Addresses of the Cohesin Component Mcd1p. *J Cell Biol* *151*, 1047–1056.

Lambert, S., and Carr, A.M. (2013). Impediments to replication fork movement: stabilisation, reactivation and genome instability. *Chromosoma* *122*, 33–45.

Lambert, S., Watson, A., Sheedy, D.M., Martin, B., and Carr, A.M. (2005). Gross chromosomal rearrangements and elevated recombination at an inducible site-specific replication fork barrier. *Cell* *121*, 689–702.

Lambert, S., Froget, B., and Carr, A.M. (2007). Arrested replication fork processing: Interplay between checkpoints and recombination. *DNA Repair* *6*, 1042–1061.

Lambert, S., Mizuno, K., Blaisonneau, J., Martineau, S., Chanet, R., Fréon, K., Murray, J.M., Carr, A.M., and Baldacci, G. (2010). Homologous Recombination Restarts Blocked Replication Forks at the Expense of Genome Rearrangements by Template Exchange. *Molecular Cell* *39*, 346–359.

Lander, E.S., Linton, L.M., Birren, B., Nusbaum, C., Zody, M.C., Baldwin, J., Devon, K., Dewar, K., Doyle, M., FitzHugh, W., et al. (2001). Initial sequencing and analysis of the human genome. *Nature* *409*, 860–921.

Bibliography

Langmead, B., and Salzberg, S.L. (2012). Fast gapped-read alignment with Bowtie 2. *Nat. Methods* 9, 357–359.

Laporte, D., and Sagot, I. (2014). Microtubules move the nucleus to quiescence. *Nucleus* 5, 113–118.

Laporte, D., Courtout, F., Salin, B., Ceschin, J., and Sagot, I. (2013). An array of nuclear microtubules reorganizes the budding yeast nucleus during quiescence. *J Cell Biol* 203, 585–594.

Laporte, D., Courtout, F., Tollis, S., and Sagot, I. (2016). Quiescent *Saccharomyces cerevisiae* forms telomere hyperclusters at the nuclear membrane vicinity through a multifaceted mechanism involving Esc1, the Sir complex, and chromatin condensation. *Mol. Biol. Cell* 27, 1875–1884.

Larsen, N.B., Sass, E., Suski, C., Mankouri, H.W., and Hickson, I.D. (2014). The *Escherichia coli* Tus–Ter replication fork barrier causes site-specific DNA replication perturbation in yeast. *Nat Commun* 5.

Lassadi, I., and Bystricky, K. (2011). Tracking of single and multiple genomic loci in living yeast cells. *Methods Mol. Biol.* 745, 499–522.

Laura N. Rusche, Ann L. Kirchmaier, and Rine, J. (2003). The Establishment, Inheritance, and Function of Silenced Chromatin in *Saccharomyces cerevisiae*. *Annual Review of Biochemistry* 72, 481–516.

Lazar-Stefanita, L., Scolari, V.F., Mercy, G., Muller, H., Guérin, T.M., Thierry, A., Mozziconacci, J., and Koszul, R. (2017). Cohesins and condensins orchestrate the 4D dynamics of yeast chromosomes during the cell cycle. *The EMBO Journal* e201797342.

Le, T.B.K., Imakaev, M.V., Mirny, L.A., and Laub, M.T. (2013). High-resolution mapping of the spatial organization of a bacterial chromosome. *Science* 342, 731–734.

Leder, P., and Nirenberg, M.W. (1964). RNA CODEWORDS AND PROTEIN SYNTHESIS, III. ON THE NUCLEOTIDE SEQUENCE OF A CYSTEINE AND A LEUCINE RNA CODEWORD. *Proc Natl Acad Sci U S A* 52, 1521–1529.

Lee, M.G., and Nurse, P. (1987). Complementation used to clone a human homologue of the fission yeast cell cycle control gene *cdc2*. *Nature* 327, 31–35.

Lee, C.-S., Wang, R.W., Chang, H.-H., Capurso, D., Segal, M.R., and Haber, J.E. (2016). Chromosome position determines the success of double-strand break repair. *Proc Natl Acad Sci U S A* 113, E146–E154.

Lee, W., Tillo, D., Bray, N., Morse, R.H., Davis, R.W., Hughes, T.R., and Nislow, C. (2007). A high-resolution atlas of nucleosome occupancy in yeast. *Nat. Genet.* 39, 1235–1244.

Lejeune, J., Gautier, M., and Turpin, R. (1959). [Study of somatic chromosomes from 9 mongoloid children]. *C. R. Hebd. Seances Acad. Sci.* 248, 1721–1722.

Lelandais, G., and Devaux, F. (2010). Comparative Functional Genomics of Stress Responses in Yeasts. *OMICS: A Journal of Integrative Biology* 14, 501–515.

Bibliography

Lengronne, A., Katou, Y., Mori, S., Yokobayashi, S., Kelly, G.P., Itoh, T., Watanabe, Y., Shirahige, K., and Uhlmann, F. (2004). Cohesin relocation from sites of chromosomal loading to places of convergent transcription. *Nature* *430*, 573–578.

Lengronne, A., McIntyre, J., Katou, Y., Kanoh, Y., Hopfner, K.-P., Shirahige, K., and Uhlmann, F. (2006). Establishment of Sister Chromatid Cohesion at the *S. cerevisiae* Replication Fork. *Molecular Cell* *23*, 787–799.

Lesne, A., Riposo, J., Roger, P., Cournac, A., and Mozziconacci, J. (2014). 3D genome reconstruction from chromosomal contacts. *Nat Meth* *11*, 1141–1143.

Li, H., and Stillman, B. (2012). The origin recognition complex: a biochemical and structural view. *Subcell Biochem* *62*, 37–58.

Li, R., and Murray, A.W. (1991). Feedback control of mitosis in budding yeast. *Cell* *66*, 519–531.

Li, H., Handsaker, B., Wysoker, A., Fennell, T., Ruan, J., Homer, N., Marth, G., Abecasis, G., Durbin, R., and 1000 Genome Project Data Processing Subgroup (2009). The Sequence Alignment/Map format and SAMtools. *Bioinformatics* *25*, 2078–2079.

Liberi, G., Cotta-Ramusino, C., Lopes, M., Sogo, J., Conti, C., Bensimon, A., and Foiani, M. (2006). Methods to Study Replication Fork Collapse in Budding Yeast. In *Methods in Enzymology*, and P.M. Judith L. Campbell, ed. (Academic Press), pp. 442–462.

Lieberman-Aiden, E., van Berkum, N.L., Williams, L., Imakaev, M., Ragozcy, T., Telling, A., Amit, I., Lajoie, B.R., Sabo, P.J., Dorschner, M.O., et al. (2009). Comprehensive mapping of long-range interactions reveals folding principles of the human genome. *Science* *326*, 289–293.

Lin, Y.-L., and Pasero, P. (2012). Interference Between DNA Replication and Transcription as a Cause of Genomic Instability. *Curr Genomics* *13*, 65–73.

Lin, S.J., Defossez, P.A., and Guarente, L. (2000). Requirement of NAD and SIR2 for life-span extension by calorie restriction in *Saccharomyces cerevisiae*. *Science* *289*, 2126–2128.

Lobachev, K.S., Rattray, A., and Narayanan, V. (2007). Hairpin- and cruciform-mediated chromosome breakage: causes and consequences in eukaryotic cells. *Front. Biosci.* *12*, 4208–4220.

London, N., and Biggins, S. (2014). Signalling dynamics in the spindle checkpoint response. *Nat Rev Mol Cell Biol* *15*, 736–748.

Long, D.T., and Kreuzer, K.N. (2008). Regression supports two mechanisms of fork processing in phage T4. *Proc. Natl. Acad. Sci. U.S.A.* *105*, 6852–6857.

Lopes, J., Piazza, A., Bermejo, R., Kriegsman, B., Colosio, A., Teulade-Fichou, M.-P., Foiani, M., and Nicolas, A. (2011). G-quadruplex-induced instability during leading-strand replication. *EMBO J.* *30*, 4033–4046.

Lopes, M., Cotta-Ramusino, C., Pellicoli, A., Liberi, G., Plevani, P., Muzi-Falconi, M., Newlon, C.S., and Foiani, M. (2001a). The DNA replication checkpoint response stabilizes stalled replication forks. *Nature* *412*, 557–561.

Bibliography

Lopes, M., Cotta-Ramusino, C., Pelliccioli, A., Liberi, G., Plevani, P., Muzi-Falconi, M., Newlon, C.S., and Foiani, M. (2001b). The DNA replication checkpoint response stabilizes stalled replication forks. *Nature* *412*, 557–561.

Lu, S., Lee, K.K., Harris, B., Xiong, B., Bose, T., Saraf, A., Hattem, G., Florens, L., Seidel, C., and Gerton, J.L. (2014). The cohesin acetyltransferase Eco1 coordinates rDNA replication and transcription. *EMBO Rep* *15*, 609–617.

Lucchini, R., and Sogo, J.M. (1994). Chromatin structure and transcriptional activity around the replication forks arrested at the 3' end of the yeast rRNA genes. *Mol Cell Biol* *14*, 318–326.

Luger, K., Dechassa, M.L., and Tremethick, D.J. (2012). New insights into nucleosome and chromatin structure: an ordered state or a disordered affair? *Nat Rev Mol Cell Biol* *13*, 436–447.

Lupiáñez, D.G., Spielmann, M., and Mundlos, S. (2016). Breaking TADs: How Alterations of Chromatin Domains Result in Disease. *Trends Genet.* *32*, 225–237.

Luria, S.E., and Delbrück, M. (1943). Mutations of Bacteria from Virus Sensitivity to Virus Resistance. *Genetics* *28*, 491–511.

Machín, F., Torres-Rosell, J., Jarmuz, A., and Aragón, L. (2005). Spindle-independent condensation-mediated segregation of yeast ribosomal DNA in late anaphase. *J Cell Biol* *168*, 209–219.

Machín, F., Torres-Rosell, J., Piccoli, G.D., Carballo, J.A., Cha, R.S., Jarmuz, A., and Aragón, L. (2006). Transcription of ribosomal genes can cause nondisjunction. *J Cell Biol* *173*, 893–903.

Magdalou, I., Lopez, B.S., Pasero, P., and Lambert, S.A.E. (2014). The causes of replication stress and their consequences on genome stability and cell fate. *Seminars in Cell & Developmental Biology* *30*, 154–164.

Marbouty, M., Ermont, C., Dujon, B., Richard, G.-F., and Koszul, R. (2014). Purification of G1 daughter cells from different *Saccharomyces* species through an optimized centrifugal elutriation procedure. *Yeast* *31*, 159–166.

Marbouty, M., Le Gall, A., Cattoni, D.I., Cournac, A., Koh, A., Fiche, J.-B., Mozziconacci, J., Murray, H., Koszul, R., and Nollmann, M. (2015). Condensin- and Replication-Mediated Bacterial Chromosome Folding and Origin Condensation Revealed by Hi-C and Super-resolution Imaging. *Mol. Cell* *59*, 588–602.

Marcand, S., Buck, S.W., Moretti, P., Gilson, E., and Shore, D. (1996). Silencing of genes at nontelomeric sites in yeast is controlled by sequestration of silencing factors at telomeres by Rap 1 protein. *Genes Dev.* *10*, 1297–1309.

Mardis, E.R. (2007). ChIP-seq: welcome to the new frontier. *Nat Meth* *4*, 613–614.

Marshall, W.F., Straight, A., Marko, J.F., Swedlow, J., Dernburg, A., Belmont, A., Murray, A.W., Agard, D.A., and Sedat, J.W. (1997). Interphase chromosomes undergo constrained diffusional motion in living cells. *Current Biology* *7*, 930–939.

Bibliography

Maxam, A.M., and Gilbert, W. (1977). A new method for sequencing DNA. *Proc Natl Acad Sci U S A* *74*, 560–564.

McCarroll, R.M., and Fangman, W.L. (1988). Time of replication of yeast centromeres and telomeres. *Cell* *54*, 505–513.

McCune, H.J., Danielson, L.S., Alvino, G.M., Collingwood, D., Delrow, J.J., Fangman, W.L., Brewer, B.J., and Raghuraman, M.K. (2008). The Temporal Program of Chromosome Replication: Genomewide Replication in *clb5Δ* *Saccharomyces cerevisiae*. *Genetics* *180*, 1833–1847.

McGinnis, S., and Madden, T.L. (2004). BLAST: at the core of a powerful and diverse set of sequence analysis tools. *Nucleic Acids Res.* *32*, W20-25.

Meister, P., Taddei, A., Ponti, A., Baldacci, G., and Gasser, S.M. (2007). Replication foci dynamics: replication patterns are modulated by S-phase checkpoint kinases in fission yeast. *EMBO J* *26*, 1315–1326.

Mejlvang, J., Feng, Y., Alabert, C., Neelsen, K.J., Jasencakova, Z., Zhao, X., Lees, M., Sandelin, A., Pasero, P., Lopes, M., et al. (2013). New histone supply regulates replication fork speed and PCNA unloading. *J Cell Biol* jcb.201305017.

Mekhail, K., and Moazed, D. (2010). The nuclear envelope in genome organization, expression and stability. *Nat Rev Mol Cell Biol* *11*, 317–328.

Mekhail, K., Seebacher, J., Gygi, S.P., and Moazed, D. (2008). Role for perinuclear chromosome tethering in maintenance of genome stability. *Nature* *456*, 667–670.

Mendenhall, M.D., and Hodge, A.E. (1998). Regulation of Cdc28 cyclin-dependent protein kinase activity during the cell cycle of the yeast *Saccharomyces cerevisiae*. *Microbiol. Mol. Biol. Rev.* *62*, 1191–1243.

Meselson, M., and Stahl, F.W. (1958). THE REPLICATION OF DNA IN *ESCHERICHIA COLI**. *Proc Natl Acad Sci U S A* *44*, 671–682.

Michaelis, C., Ciosk, R., and Nasmyth, K. (1997). Cohesins: Chromosomal Proteins that Prevent Premature Separation of Sister Chromatids. *Cell* *91*, 35–45.

Michel, B., Grompone, G., Florès, M.-J., and Bidnenko, V. (2004). Multiple pathways process stalled replication forks. *PNAS* *101*, 12783–12788.

Mimitou, E.P., and Symington, L.S. (2008). Sae2, Exo1 and Sgs1 collaborate in DNA double-strand break processing. *Nature* *455*, 770–774.

Miné-Hattab, J., and Rothstein, R. (2012). Increased chromosome mobility facilitates homology search during recombination. *Nat. Cell Biol.* *14*, 510–517.

Miné-Hattab, J., and Rothstein, R. (2013). DNA in motion during double-strand break repair. *Trends Cell Biol.* *23*, 529–536.

Mirkin, E.V., and Mirkin, S.M. (2007). Replication Fork Stalling at Natural Impediments. *Microbiol. Mol. Biol. Rev.* *71*, 13–35.

Misteli, T. (2007). Beyond the Sequence: Cellular Organization of Genome Function. *Cell* *128*, 787–800.

Bibliography

Mizuguchi, T., Fudenberg, G., Mehta, S., Belton, J.-M., Taneja, N., Folco, H.D., FitzGerald, P., Dekker, J., Mirny, L., Barrowman, J., et al. (2014). Cohesin-dependent globules and heterochromatin shape 3D genome architecture in *S. pombe*. *Nature* 516, 432–435.

Mizuno, K., Lambert, S., Baldacci, G., Murray, J.M., and Carr, A.M. (2009). Nearby inverted repeats fuse to generate acentric and dicentric palindromic chromosomes by a replication template exchange mechanism. *Genes Dev.* 23, 2876–2886.

Mizuno, K., Miyabe, I., Schalbetter, S.A., Carr, A.M., and Murray, J.M. (2013). Recombination-restarted replication makes inverted chromosome fusions at inverted repeats. *Nature* 493, 246–249.

Mohanty, B.K., Bairwa, N.K., and Bastia, D. (2006). The Tof1p-Csm3p protein complex counteracts the Rrm3p helicase to control replication termination of *Saccharomyces cerevisiae*. *Proc. Natl. Acad. Sci. U.S.A.* 103, 897–902.

Mojica, F.J.M., Díez-Villaseñor, C., García-Martínez, J., and Soria, E. (2005). Intervening sequences of regularly spaced prokaryotic repeats derive from foreign genetic elements. *J. Mol. Evol.* 60, 174–182.

Moreau, M.J.J., and Schaeffer, P.M. (2013). Dissecting the salt dependence of the Tus–Ter protein–DNA complexes by high-throughput differential scanning fluorimetry of a GFP-tagged Tus. *Molecular BioSystems* 9, 3146.

Moretti, P., Freeman, K., Coodly, L., and Shore, D. (1994). Evidence that a complex of SIR proteins interacts with the silencer and telomere-binding protein RAP1. *Genes Dev.* 8, 2257–2269.

Morgan, D.O. (1995). Principles of CDK regulation. *Nature* 374, 131–134.

Morgan, T.H. (1915). Localization of the Hereditary Material in the Germ Cells. *Proc Natl Acad Sci U S A* 1, 420–429.

Nagalakshmi, U., Waern, K., and Snyder, M. (2010). RNA-Seq: a method for comprehensive transcriptome analysis. *Curr Protoc Mol Biol Chapter 4*, Unit 4.11.1-13.

Nagano, T., Lubling, Y., Stevens, T.J., Schoenfelder, S., Yaffe, E., Dean, W., Laue, E.D., Tanay, A., and Fraser, P. (2013). Single cell Hi-C reveals cell-to-cell variability in chromosome structure. *Nature* 502.

Nagano, T., Lubling, Y., Várnai, C., Dudley, C., Leung, W., Baran, Y., Mendelson Cohen, N., Wingett, S., Fraser, P., and Tanay, A. (2017). Cell-cycle dynamics of chromosomal organization at single-cell resolution. *Nature* 547, 61–67.

Nakamura, H., Morita, T., and Sato, C. (1986). Structural organizations of replicon domains during DNA synthetic phase in the mammalian nucleus. *Exp. Cell Res.* 165, 291–297.

Naumova, N., Imakaev, M., Fudenberg, G., Zhan, Y., Lajoie, B.R., Mirny, L.A., and Dekker, J. (2013). Organization of the Mitotic Chromosome. *Science* 342, 948–953.

Neelsen, K.J., and Lopes, M. (2015). Replication fork reversal in eukaryotes: from dead end to dynamic response. *Nat Rev Mol Cell Biol* 16, 207–220.

Bibliography

Neylon, C., Brown, S.E., Kralicek, A.V., Miles, C.S., Love, C.A., and Dixon, N.E. (2000). Interaction of the Escherichia coli Replication Terminator Protein (Tus) with DNA: A Model Derived from DNA-Binding Studies of Mutant Proteins by Surface Plasmon Resonance†. *Biochemistry* *39*, 11989–11999.

Ng, T.M., Waples, W.G., Lavoie, B.D., and Biggins, S. (2009). Pericentromeric Sister Chromatid Cohesion Promotes Kinetochore Biorientation. *Mol Biol Cell* *20*, 3818–3827.

Nguyen, V.Q., Co, C., and Li, J.J. (2001). Cyclin-dependent kinases prevent DNA re-replication through multiple mechanisms. *Nature* *411*, 1068–1073.

Nishino, Y., Eltsov, M., Joti, Y., Ito, K., Takata, H., Takahashi, Y., Hihara, S., Frangakis, A.S., Imamoto, N., Ishikawa, T., et al. (2012). Human mitotic chromosomes consist predominantly of irregularly folded nucleosome fibres without a 30-nm chromatin structure. *EMBO J.* *31*, 1644–1653.

Nitiss, J.L. (2009). DNA topoisomerase II and its growing repertoire of biological functions. *Nat Rev Cancer* *9*, 327–337.

Nora, E.P., Lajoie, B.R., Schulz, E.G., Giorgetti, L., Okamoto, I., Servant, N., Piolot, T., van Berkum, N.L., Meisig, J., Sedat, J., et al. (2012). Spatial partitioning of the regulatory landscape of the X-inactivation centre. *Nature* *485*, 381–385.

Nurse, P. (2000). A Long Twentieth Century of the Cell Cycle and Beyond. *Cell* *100*, 71–78.

Nurse, P., Thuriaux, P., and Nasmyth, K. (1976). Genetic control of the cell division cycle in the fission yeast *Schizosaccharomyces pombe*. *Mol. Gen. Genet.* *146*, 167–178.

Okazaki, R., Okazaki, T., Sakabe, K., and Sugimoto, K. (1967). Mechanism of DNA replication possible discontinuity of DNA chain growth. *Jpn. J. Med. Sci. Biol.* *20*, 255–260.

O’Keefe, R.T., Henderson, S.C., and Spector, D.L. (1992). Dynamic organization of DNA replication in mammalian cell nuclei: spatially and temporally defined replication of chromosome-specific alpha-satellite DNA sequences. *The Journal of Cell Biology* *116*, 1095–1110.

Ou, H.D., Phan, S., Deerinck, T.J., Thor, A., Ellisman, M.H., and O’Shea, C.C. (2017). ChromEMT: Visualizing 3D chromatin structure and compaction in interphase and mitotic cells. *Science* *357*, eaag0025.

Pappas, D.L., Frisch, R., and Weinreich, M. (2004). The NAD(+)-dependent Sir2p histone deacetylase is a negative regulator of chromosomal DNA replication. *Genes Dev.* *18*, 769–781.

Pâques, F., and Haber, J.E. (1999). Multiple Pathways of Recombination Induced by Double-Strand Breaks in *Saccharomyces cerevisiae*. *Microbiol. Mol. Biol. Rev.* *63*, 349–404.

Parelho, V., Hadjur, S., Spivakov, M., Leleu, M., Sauer, S., Gregson, H.C., Jarmuz, A., Canzonetta, C., Webster, Z., Nesterova, T., et al. (2008). Cohesins functionally associate with CTCF on mammalian chromosome arms. *Cell* *132*, 422–433.

Bibliography

Pasero, P., Braguglia, D., and Gasser, S.M. (1997). ORC-dependent and origin-specific initiation of DNA replication at defined foci in isolated yeast nuclei. *Genes Dev.* *11*, 1504–1518.

Pasero, P., Bensimon, A., and Schwob, E. (2002). Single-molecule analysis reveals clustering and epigenetic regulation of replication origins at the yeast rDNA locus. *Genes Dev* *16*, 2479–2484.

Patel, P.K., Arcangioli, B., Baker, S.P., Bensimon, A., and Rhind, N. (2006). DNA replication origins fire stochastically in fission yeast. *Mol. Biol. Cell* *17*, 308–316.

Payen, C., Koszul, R., Dujon, B., and Fischer, G. (2008). Segmental Duplications Arise from Pol32-Dependent Repair of Broken Forks through Two Alternative Replication-Based Mechanisms. *PLoS Genet* *4*.

Payen, C., Di Rienzi, S.C., Ong, G.T., Pogachar, J.L., Sanchez, J.C., Sunshine, A.B., Raghuraman, M.K., Brewer, B.J., and Dunham, M.J. (2014). The Dynamics of Diverse Segmental Amplifications in Populations of *Saccharomyces cerevisiae* Adapting to Strong Selection. *G3 (Bethesda)* *4*, 399–409.

Peters, J.-M. (2002). The Anaphase-Promoting Complex: Proteolysis in Mitosis and Beyond. *Molecular Cell* *9*, 931–943.

Peterson, J.B., and Ris, H. (1976). Electron-microscopic study of the spindle and chromosome movement in the yeast *Saccharomyces cerevisiae*. *J Cell Sci* *22*, 219–242.

Piatti, S., Lengauer, C., and Nasmyth, K. (1995). Cdc6 is an unstable protein whose de novo synthesis in G1 is important for the onset of S phase and for preventing a “reductional” anaphase in the budding yeast *Saccharomyces cerevisiae*. *EMBO J* *14*, 3788–3799.

Pinkel, D., Straume, T., and Gray, J.W. (1986). Cytogenetic analysis using quantitative, high-sensitivity, fluorescence hybridization. *Proc. Natl. Acad. Sci. U.S.A.* *83*, 2934–2938.

Pope, B.D., Ryba, T., Dileep, V., Yue, F., Wu, W., Denas, O., Vera, D.L., Wang, Y., Hansen, R.S., Canfield, T.K., et al. (2014). Topologically associating domains are stable units of replication-timing regulation. *Nature* *515*, 402–405.

Prestige, M. (1972). *THE BIOLOGY OF THE CELL CYCLE*. By J. M. Mitchison. Cambridge University Press, 1971. Pp. 313. £4.60. Also issued as a paperback. *Exp Physiol* *57*, 346–347.

Prioleau, M.-N., and MacAlpine, D.M. (2016). DNA replication origins—where do we begin? *Genes Dev.* *30*, 1683–1697.

RABL, C. (1885). *Über Zellteilung*. *Morphologisches Jahrbuch* *10*, 214–330.

Raghuraman, M.K., Winzeler, E.A., Collingwood, D., Hunt, S., Wodicka, L., Conway, A., Lockhart, D.J., Davis, R.W., Brewer, B.J., and Fangman, W.L. (2001). Replication Dynamics of the Yeast Genome. *Science* *294*, 115–121.

Rausch, T., Zichner, T., Schlattl, A., Stütz, A.M., Benes, V., and Korbel, J.O. (2012). DELLY: structural variant discovery by integrated paired-end and split-read analysis. *Bioinformatics* *28*, i333–i339.

Bibliography

Ren, B., Robert, F., Wyrick, J.J., Aparicio, O., Jennings, E.G., Simon, I., Zeitlinger, J., Schreiber, J., Hannett, N., Kanin, E., et al. (2000). Genome-wide location and function of DNA binding proteins. *Science* *290*, 2306–2309.

Renauld, H., Aparicio, O.M., Zierath, P.D., Billington, B.L., Chhablani, S.K., and Gottschling, D.E. (1993). Silent domains are assembled continuously from the telomere and are defined by promoter distance and strength, and by SIR3 dosage. *Genes Dev.* *7*, 1133–1145.

Renshaw, M.J., Ward, J.J., Kanemaki, M., Natsume, K., Nédélec, F.J., and Tanaka, T.U. (2010). Condensins Promote Chromosome Recoiling during Early Anaphase to Complete Sister Chromatid Separation. *Developmental Cell* *19*, 232–244.

Richard, G.-F., Goellner, G.M., McMurray, C.T., and Haber, J.E. (2000). Recombination-induced CAG trinucleotide repeat expansions in yeast involve the MRE11–RAD50–XRS2 complex. *EMBO J* *19*, 2381–2390.

Rivera, C., Gurard-Levin, Z.A., Almouzni, G., and Loyola, A. (2014). Histone lysine methylation and chromatin replication. *Biochimica et Biophysica Acta (BBA) - Gene Regulatory Mechanisms* *1839*, 1433–1439.

Robinett, C.C., Straight, A., Li, G., Willhelm, C., Sudlow, G., Murray, A., and Belmont, A.S. (1996). In vivo localization of DNA sequences and visualization of large-scale chromatin organization using lac operator/repressor recognition. *J. Cell Biol.* *135*, 1685–1700.

Robinson, J.T., Thorvaldsdóttir, H., Winckler, W., Guttman, M., Lander, E.S., Getz, G., and Mesirov, J.P. (2011). Integrative Genomics Viewer. *Nat Biotechnol* *29*, 24–26.

Rothstein, R.J. (1983). [12] One-step gene disruption in yeast. *Methods in Enzymology* *101*, 202–211.

Ruault, M., Meyer, A.D., Loïodice, I., and Taddei, A. (2011). Clustering heterochromatin: Sir3 promotes telomere clustering independently of silencing in yeast. *J Cell Biol* *192*, 417–431.

Rupp, S., Summers, E., Lo, H.-J., Madhani, H., and Fink, G. (1999). MAP kinase and cAMP filamentation signaling pathways converge on the unusually large promoter of the yeast *FLO11* gene. *The EMBO Journal* *18*, 1257–1269.

Sanborn, A.L., Rao, S.S.P., Huang, S.-C., Durand, N.C., Huntley, M.H., Jewett, A.I., Bochkov, I.D., Chinnappan, D., Cutkosky, A., Li, J., et al. (2015). Chromatin extrusion explains key features of loop and domain formation in wild-type and engineered genomes. *PNAS* *112*, E6456–E6465.

Saner, N., Karschau, J., Natsume, T., Gierliński, M., Retkute, R., Hawkins, M., Nieduszynski, C.A., Blow, J.J., Moura, A.P.S. de, and Tanaka, T.U. (2013). Stochastic association of neighboring replicons creates replication factories in budding yeast. *J Cell Biol* *202*, 1001–1012.

Sanger, F., and Coulson, A.R. (1975). A rapid method for determining sequences in DNA by primed synthesis with DNA polymerase. *J. Mol. Biol.* *94*, 441–448.

Bibliography

Sanger, F., Air, G.M., Barrell, B.G., Brown, N.L., Coulson, A.R., Fiddes, J.C., Hutchison, C.A., Slocombe, P.M., and Smith, M. (1977). Nucleotide sequence of bacteriophage ϕ X174 DNA. *Nature* 265, 687–695.

Santoro, R. (2005). The silence of the ribosomal RNA genes. *Cell. Mol. Life Sci.* 62, 2067–2079.

Schäfer, G., McEvoy, C.R.E., and Patterson, H.-G. (2008). The *Saccharomyces cerevisiae* linker histone Hho1p is essential for chromatin compaction in stationary phase and is displaced by transcription. *Proc. Natl. Acad. Sci. U.S.A.* 105, 14838–14843.

Schardin, M., Cremer, T., Hager, H.D., and Lang, M. (1985). Specific staining of human chromosomes in Chinese hamster x man hybrid cell lines demonstrates interphase chromosome territories. *Hum. Genet.* 71, 281–287.

Schena, M., Shalon, D., Davis, R.W., and Brown, P.O. (1995). Quantitative monitoring of gene expression patterns with a complementary DNA microarray. *Science* 270, 467–470.

Schones, D.E., Cui, K., Cuddapah, S., Roh, T.-Y., Barski, A., Wang, Z., Wei, G., and Zhao, K. (2008). Dynamic regulation of nucleosome positioning in the human genome. *Cell* 132, 887–898.

Schübeler, D., Scalzo, D., Kooperberg, C., van Steensel, B., Delrow, J., and Groudine, M. (2002). Genome-wide DNA replication profile for *Drosophila melanogaster*: a link between transcription and replication timing. *Nat. Genet.* 32, 438–442.

Schwartz, D.C., and Cantor, C.R. (1984). Separation of yeast chromosome-sized DNAs by pulsed field gradient gel electrophoresis. *Cell* 37, 67–75.

Seigneur, M., Bidnenko, V., Ehrlich, S.D., and Michel, B. (1998). RuvAB Acts at Arrested Replication Forks. *Cell* 95, 419–430.

Sexton, T., Yaffe, E., Kenigsberg, E., Bantignies, F., Leblanc, B., Hoichman, M., Parrinello, H., Tanay, A., and Cavalli, G. (2012). Three-dimensional folding and functional organization principles of the *Drosophila* genome. *Cell* 148, 458–472.

Shampay, J., Szostak, J.W., and Blackburn, E.H. (1984). DNA sequences of telomeres maintained in yeast. *Nature* 310, 154–157.

Shinohara, A., Ogawa, H., and Ogawa, T. (1992). Rad51 protein involved in repair and recombination in *S. cerevisiae* is a RecA-like protein. *Cell* 69, 457–470.

Sofueva, S., Yaffe, E., Chan, W.-C., Georgopoulou, D., Rudan, M.V., Mira-Bontenbal, H., Pollard, S.M., Schroth, G.P., Tanay, A., and Hadjur, S. (2013). Cohesin-mediated interactions organize chromosomal domain architecture. *The EMBO Journal* 32, 3119–3129.

Sogo, J.M., Lopes, M., and Foiani, M. (2002). Fork reversal and ssDNA accumulation at stalled replication forks owing to checkpoint defects. *Science* 297, 599–602.

Sonoda, E., Hohegger, H., Saberi, A., Taniguchi, Y., and Takeda, S. (2006). Differential usage of non-homologous end-joining and homologous recombination in double strand break repair. *DNA Repair* 5, 1021–1029.

Bibliography

Spichal, M., Brion, A., Herbert, S., Cournac, A., Marbouty, M., Zimmer, C., Koszul, R., and Fabre, E. (2016). Evidence for actin dual role in regulating chromosome organization and dynamics in yeast. *J Cell Sci* jcs.175745.

Stegmeier, F., Visintin, R., and Amon, A. (2002). Separase, Polo Kinase, the Kinetochore Protein Slk19, and Spo12 Function in a Network that Controls Cdc14 Localization during Early Anaphase. *Cell* 108, 207–220.

Stern, B.M., and Murray, A.W. (2001). Lack of tension at kinetochores activates the spindle checkpoint in budding yeast. *Current Biology* 11, 1462–1467.

Stevenson, J.B., and Gottschling, D.E. (1999). Telomeric chromatin modulates replication timing near chromosome ends. *Genes Dev.* 13, 146–151.

Straight, A.F., Marshall, W.F., Sedat, J.W., and Murray, A.W. (1997). Mitosis in living budding yeast: anaphase A but no metaphase plate. *Science* 277, 574–578.

Strunnikov, A.V., Hogan, E., and Koshland, D. (1995). SMC2, a *Saccharomyces cerevisiae* gene essential for chromosome segregation and condensation, defines a subgroup within the SMC family. *Genes Dev.* 9, 587–599.

Sullivan, M., and Uhlmann, F. (2003). A non-proteolytic function of separase links anaphase onset to mitotic exit. *Nat Cell Biol* 5, 249–254.

Sullivan, M., Higuchi, T., Katis, V.L., and Uhlmann, F. (2004). Cdc14 Phosphatase Induces rDNA Condensation and Resolves Cohesin-Independent Cohesion during Budding Yeast Anaphase. *Cell* 117, 471–482.

Swift, H. (1950). The Constancy of Desoxyribose Nucleic Acid in Plant Nuclei. *Proc Natl Acad Sci U S A* 36, 643–654.

Taddei, A., and Gasser, S.M. (2012). Structure and Function in the Budding Yeast Nucleus. *Genetics* 192, 107–129.

Taddei, A., Hediger, F., Neumann, F.R., and Gasser, S.M. (2004). The Function of Nuclear Architecture: A Genetic Approach.

Taddei, A., Van Houwe, G., Hediger, F., Kalck, V., Cubizolles, F., Schober, H., and Gasser, S.M. (2006). Nuclear pore association confers optimal expression levels for an inducible yeast gene. *Nature* 441, 774–778.

Taddei, A., Schober, H., and Gasser, S.M. (2010). The Budding Yeast Nucleus. *Cold Spring Harb Perspect Biol* 2, a000612.

Takeuchi, Y., Horiuchi, T., and Kobayashi, T. (2003). Transcription-dependent recombination and the role of fork collision in yeast rDNA. *Genes Dev.* 17, 1497–1506.

Terekawa, T., Bisht, S., Eeftens, J., Dekker, C., Haering, C., and Greene, E. (2017). The Condensin Complex Is A Mechanochemical Motor That Translocates Along DNA. *BioRxiv* 137711.

Therizols, P., Fairhead, C., Cabal, G.G., Genovesio, A., Olivo-Marin, J.-C., Dujon, B., and Fabre, E. (2006). Telomere tethering at the nuclear periphery is essential for efficient DNA double strand break repair in subtelomeric region. *J. Cell Biol.* 172, 189–199.

Bibliography

Tittel-Elmer, M., Lengronne, A., Davidson, M.B., Bacal, J., François, P., Hohl, M., Petrini, J.H.J., Pasero, P., and Cobb, J.A. (2012). Cohesin Association to Replication Sites Depends on Rad50 and Promotes Fork Restart. *Molecular Cell* 48, 98–108.

Tjio, J.H., and Levan, A. (1956). THE CHROMOSOME NUMBER OF MAN. *Hereditas* 42, 1–6.

Torres, J.Z., Schnakenberg, S.L., and Zakian, V.A. (2004). *Saccharomyces cerevisiae* Rrm3p DNA helicase promotes genome integrity by preventing replication fork stalling: viability of *rrm3* cells requires the intra-S-phase checkpoint and fork restart activities. *Mol. Cell. Biol.* 24, 3198–3212.

Truong, L.N., Li, Y., Sun, E., Ang, K., Hwang, P.Y.-H., and Wu, X. (2014). Homologous Recombination is a Primary Pathway to Repair DNA Double-Strand Breaks Generated During DNA Rereplication. *J. Biol. Chem.* jbc.M114.576488.

Tuduri, S., Tourrière, H., and Pasero, P. (2010). Defining replication origin efficiency using DNA fiber assays. *Chromosome Res* 18, 91–102.

Ubersax, J.A., Woodbury, E.L., Quang, P.N., Paraz, M., Blethrow, J.D., Shah, K., Shokat, K.M., and Morgan, D.O. (2003). Targets of the cyclin-dependent kinase Cdk1. *Nature* 425, 859–864.

Uhlmann, F. (2016). SMC complexes: from DNA to chromosomes. *Nat Rev Mol Cell Biol* 17, 399–412.

Uhlmann, F., Lottspeich, F., and Nasmyth, K. (1999). Sister-chromatid separation at anaphase onset is promoted by cleavage of the cohesin subunit Scc1. *Nature* 400, 37–42.

Unal, E., Heidinger-Pauli, J.M., and Koshland, D. (2007). DNA double-strand breaks trigger genome-wide sister-chromatid cohesion through Eco1 (Ctf7). *Science* 317, 245–248.

Valton, A.-L., Hassan-Zadeh, V., Lema, I., Boggetto, N., Alberti, P., Saintomé, C., Riou, J.-F., and Prioleau, M.-N. (2014). G4 motifs affect origin positioning and efficiency in two vertebrate replicators. *EMBO J.* 33, 732–746.

Van Bortle, K., and Corces, V.G. (2012). Nuclear organization and genome function. *Annu. Rev. Cell Dev. Biol.* 28, 163–187.

Venkatesh, S., and Workman, J.L. (2015). Histone exchange, chromatin structure and the regulation of transcription. *Nat Rev Mol Cell Biol* 16, 178–189.

Venter, J.C., Adams, M.D., Myers, E.W., Li, P.W., Mural, R.J., Sutton, G.G., Smith, H.O., Yandell, M., Evans, C.A., Holt, R.A., et al. (2001). The Sequence of the Human Genome. *Science* 291, 1304–1351.

Versini, G., Comet, I., Wu, M., Hoopes, L., Schwob, E., and Pasero, P. (2003). The yeast Sgs1 helicase is differentially required for genomic and ribosomal DNA replication. *The EMBO Journal* 22, 1939–1949.

Verstrepen, K.J., Reynolds, T.B., and Fink, G.R. (2004). Origins of variation in the fungal cell surface. *Nat Rev Micro* 2, 533–540.

Bibliography

Verstrepen, K.J., Jansen, A., Lewitter, F., and Fink, G.R. (2005). Intragenic tandem repeats generate functional variability. *Nat Genet* 37, 986–990.

Visintin, R., Prinz, S., and Amon, A. (1997). CDC20 and CDH1: A Family of Substrate-Specific Activators of APC-Dependent Proteolysis. *Science* 278, 460–463.

Visintin, R., Craig, K., Hwang, E.S., Prinz, S., Tyers, M., and Amon, A. (1998). The Phosphatase Cdc14 Triggers Mitotic Exit by Reversal of Cdk-Dependent Phosphorylation. *Molecular Cell* 2, 709–718.

Visintin, R., Hwang, E.S., and Amon, A. (1999). Cfi1 prevents premature exit from mitosis by anchoring Cdc14 phosphatase in the nucleolus. *Nature* 398, 818–823.

Vogelauer, M., Rubbi, L., Lucas, I., Brewer, B.J., and Grunstein, M. (2002). Histone Acetylation Regulates the Time of Replication Origin Firing. *Molecular Cell* 10, 1223–1233.

Walter, J., Schermelleh, L., Cremer, M., Tashiro, S., and Cremer, T. (2003). Chromosome order in HeLa cells changes during mitosis and early G1, but is stably maintained during subsequent interphase stages. *J. Cell Biol.* 160, 685–697.

Wang, B.-D., Eyre, D., Basrai, M., Lichten, M., and Strunnikov, A. (2005). Condensin Binding at Distinct and Specific Chromosomal Sites in the *Saccharomyces cerevisiae* Genome. *Mol. Cell. Biol.* 25, 7216–7225.

Wang, R., Mozziconacci, J., Bancaud, A., and Gadal, O. (2015). Principles of chromatin organization in yeast: relevance of polymer models to describe nuclear organization and dynamics. *Current Opinion in Cell Biology* 34, 54–60.

Wang, R., Kamgoue, A., Normand, C., Léger-Silvestre, I., Mangeat, T., and Gadal, O. (2016). High resolution microscopy reveals the nuclear shape of budding yeast during cell cycle and in various biological states. *J Cell Sci* 129, 4480–4495.

Wang, X., Connelly, J.J., Wang, C.-L., and Sternglanz, R. (2004). Importance of the Sir3 N Terminus and Its Acetylation for Yeast Transcriptional Silencing. *Genetics* 168, 547–551.

Watson, J.D., and Crick, F.H.C. (1953). Molecular Structure of Nucleic Acids: A Structure for Deoxyribose Nucleic Acid. *Nature* 171, 737–738.

Wellinger, R.J., and Zakian, V.A. (2012). Everything You Ever Wanted to Know About *Saccharomyces cerevisiae* Telomeres: Beginning to End. *Genetics* 191, 1073–1105.

Werner-Washburne, M., Braun, E., Johnston, G.C., and Singer, R.A. (1993). Stationary phase in the yeast *Saccharomyces cerevisiae*. *Microbiol. Rev.* 57, 383–401.

Willis, N.A., Chandramouly, G., Huang, B., Kwok, A., Follonier, C., Deng, C., and Scully, R. (2014). BRCA1 controls homologous recombination at Tus/Ter-stalled mammalian replication forks. *Nature advance online publication*.

Winey, M., and Bloom, K. (2012). Mitotic Spindle Form and Function. *Genetics* 190, 1197–1224.

Winey, M., Mamay, C.L., O'Toole, E.T., Mastronarde, D.N., Giddings, T.H., McDonald, K.L., and McIntosh, J.R. (1995). Three-dimensional ultrastructural analysis of the *Saccharomyces cerevisiae* mitotic spindle. *J Cell Biol* 129, 1601–1615.

Bibliography

Wood, V., Gwilliam, R., Rajandream, M.-A., Lyne, M., Lyne, R., Stewart, A., Sgouros, J., Peat, N., Hayles, J., Baker, S., et al. (2002). The genome sequence of *Schizosaccharomyces pombe*. *Nature* *415*, 871–880.

Wyrick, J.J., Aparicio, J.G., Chen, T., Barnett, J.D., Jennings, E.G., Young, R.A., Bell, S.P., and Aparicio, O.M. (2001). Genome-Wide Distribution of ORC and MCM Proteins in *S. cerevisiae*: High-Resolution Mapping of Replication Origins. *Science* *294*, 2357–2360.

Yabuki, N., Terashima, H., and Kitada, K. (2002). Mapping of early firing origins on a replication profile of budding yeast. *Genes Cells* *7*, 781–789.

Yang, C.H., Lambie, E.J., Hardin, J., Craft, J., and Snyder, M. (1989). Higher order structure is present in the yeast nucleus: autoantibody probes demonstrate that the nucleolus lies opposite the spindle pole body. *Chromosoma* *98*, 123–128.

Yang, H., Ren, Q., and Zhang, Z. (2006). Chromosome or chromatin condensation leads to meiosis or apoptosis in stationary yeast (*Saccharomyces cerevisiae*) cells. *FEMS Yeast Research* *6*, 1254–1263.

Yeh, E., Haase, J., Paliulis, L.V., Joglekar, A., Bond, L., Bouck, D., Salmon, E.D., and Bloom, K.S. (2008). Pericentric Chromatin Is Organized into an Intramolecular Loop in Mitosis. *Current Biology* *18*, 81–90.

Yeong, F.M., Lim, H.H., Padmashree, C.G., and Surana, U. (2000). Exit from Mitosis in Budding Yeast: Biphasic Inactivation of the Cdc28-Clb2 Mitotic Kinase and the Role of Cdc20. *Molecular Cell* *5*, 501–511.

Yoder, T.J., Pearson, C.G., Bloom, K., and Davis, T.N. (2003). The *Saccharomyces cerevisiae* Spindle Pole Body Is a Dynamic Structure. *Mol Biol Cell* *14*, 3494–3505.

Yoshida, S., Asakawa, K., and Toh-e, A. (2002). Mitotic Exit Network Controls the Localization of Cdc14 to the Spindle Pole Body in *Saccharomyces cerevisiae*. *Current Biology* *12*, 944–950.

Yu, H. (2002). Regulation of APC–Cdc20 by the spindle checkpoint. *Current Opinion in Cell Biology* *14*, 706–714.

Zeitouni, B., Boeva, V., Janoueix-Lerosey, I., Loeillet, S., Legoix-né, P., Nicolas, A., Delattre, O., and Barillot, E. (2010). SVDetect: a tool to identify genomic structural variations from paired-end and mate-pair sequencing data. *Bioinformatics* *26*, 1895–1896.

Zhou, V.W., Goren, A., and Bernstein, B.E. (2011). Charting histone modifications and the functional organization of mammalian genomes. *Nat Rev Genet* *12*, 7–18.

Zhu, Z., Chung, W.-H., Shim, E.Y., Lee, S.E., and Ira, G. (2008). Sgs1 Helicase and Two Nucleases Dna2 and Exo1 Resect DNA Double-Strand Break Ends. *Cell* *134*, 981–994.

Zimmer, C., and Fabre, E. (2011). Principles of chromosomal organization: lessons from yeast. *The Journal of Cell Biology* *192*, 723–733.

